

# MOLECULARLY IMPRINTED POLYMERS FOR APPLICATIONS IN PROTEOMICS AND DIAGNOSTICS

Magdalena Anna Świtnicka-Plak

2018

A thesis submitted to the Department of Pure and Applied Chemistry,  
in fulfilment of the regulations for the  
Degree of Doctor of Philosophy in Chemistry.

University of Strathclyde

This thesis is the result of the author's original research. It has been composed by the author and has not been previously submitted for examination which has led to the award of a degree.

The copyright of this thesis belongs to the author under the terms of the United Kingdom Copyright Acts as qualified by University of Strathclyde Regulation 3.50. Due acknowledgement must always be made of the use of any material contained in, or derived from, this thesis.

Signed:

Date:

# ACKNOWLEDGEMENTS

Firstly, I would like express my deepest appreciation to Professor Peter Cormack for his supervision, inputs to my works and personal support I received from him.

Special thanks to everyone in the Polymer Group for all their help. There are many that deserve my gratitude for their great help, however I would rather not mention anyone by name to avoid omitting the names of any of these helpful people.

Further appreciation and thanks go to Dr Leonard Berlouis, Lindsay McCulloch and Gavin Bain for their technical support.

The work presented in this Thesis was conducted as a part of a larger project "Robust affinity materials for applications in proteomics and diagnostics" (PEPMIP), co-financed by the European Commission in the 7th Framework Programme. During the course of my PhD, I had a chance to visit and work with PEPMIP partners from the School of Pharmacy at University of Oslo, the Research Department of Neuroscience at Ruhr-Universität Bochum and the Department of Chemistry and Biomedical Sciences at Linnaeus University. I would like to thank everyone who helped make this a useful and rewarding experience.

I would like to thank Strathclyde University and the European Commission for making this project possible to carry out, also financially (Marie Curie Initial Training Network, grant agreement number: 264699). Also, I would like to express my gratitude to everyone from the PEPMIP project for the interesting meetings that we had in Malmö, Odense, Oslo, Bochum, Umeå, Runcorn, Tenerife and here at Strathclyde.

I also thank my husband, parents and the rest of family for supporting me throughout this extended period, for being there when needed, backing me with a good word and for a constant supply of comfort.

# ABSTRACT

Amongst enumerated types of biomarkers are Pro-Gastrin-Releasing Peptide, A $\beta$ -amyloid and  $\alpha$ -Synuclein peptides. ProGRP is reported as a highly specific new biomarker for Small Cell Lung Cancer (SCLC). Aggregates of A $\beta$  and  $\alpha$ -Synuclein peptides are in the group of biomarkers with importance in the diagnosis of Alzheimer's Disease (AD) and Parkinson's Disease (PD), respectively. Therapy and/or drugs work most efficiently in the early stage of AD, PD and SCLC, however in most cases diagnoses are made too late and only after a time when significant progress of pathological change is observed. Therefore, there is a significant demand in the market for cheap and fast diagnostic tools that could allow for the reliable detection of AD, PD and SCLC in their early stages.

Molecularly imprinted polymers (MIPs) are synthetic materials with outstanding affinity and selectivity for a given target molecule. Their low production cost, re-usability and high reproducibility make them attractive candidates for the next generation of separation materials, with potential applications to AD, PD and SCLC.

The purpose of this study was to design, synthesise, characterise and exploit the next generation of MIPs that can enable the selective extractions of targets from native blood or cerebrospinal fluid samples. In this Thesis, a generic synthetic protocol for the synthesis of protein-imprinted polymers was developed. The method allows for the rapid production of peptide imprinted polymers in a convenient microsphere format. In fact, four different formats of MIPs for the peptide-based biomarkers were developed and described. Selected materials were supplied to the PEPMIP partners for the determination of their molecular recognition character and use in proteomics and diagnostics applications. A new, sensitive on-line assay for SCLC has been developed using these materials and good progress made towards a magnetic capture protocol.

# ABBREVIATIONS

A	Alanine
AA	Amino acids
ACN	Acetonitrile
AD	Alzheimer's disease
AIBN	Azobisisobutyronitrile
APM	<i>N</i> -(3-aminopropyl)methacrylamide hydrochloride
APS	Ammonium persulfate
ATR	Attenuated total reflection
BET	Brunauer–Emmett–Teller
BIS	<i>N,N'</i> -methylene <i>bis</i> (acrylamide)
C	BET <i>constant</i>
Cbz	Benzyloxycarbonyl group
CF	Cerebrospinal fluid
CV	Coefficient of variation
D	Aspartic acid
DMSO	Dimethyl sulfoxide
DNA	Deoxyribonucleic acid

DTT	Dithiothreitol
DVB	Divinylbenzene
E	Glutamic acid
EAMA.HCl	<i>N</i> -(2-Aminoethyl) methacrylamide hydrochloride
ESI	Electrospray ionization
EtOH	Ethanol
EVB	Ethylvinylbenzene
F	Phenylalanine
FA	Formic acid
FM	Functional monomer
FT-IR	Fourier-transform infrared
G	Glycine
GRP	Gastrin-releasing peptide
H	Histidine
I	Isoleucine
IAA	Alkylation
IF	Imprinting factor
IUPAC	International Union of Pure and Applied Chemistry
IS	Internal standard
K	Lysine

L	Leucine
LOD	Limit of detection
LOQ	Lower limit of quantification
LCMS	Liquid chromatography–mass spectrometry
LLC	Liquid-liquid chromatography
M	Methionine
MAA	Methacrylic acid
MeOH	Methanol
MDI	Mild cognitive impairment
MIP	Molecularly imprinted polymer
MISPE	Molecularly imprinted solid phase extraction
mLOD	Mass limit of detection
MS	Mass spectrometry
N	Asparagine
NG	Nalgene polyethylene bottle
NIP	Non-imprinted polymer
NTPVU	<i>N</i> -3,5- <i>bis</i> (trifluoromethyl)-phenyl- <i>N'</i> -4-vinylphenylurea
P	Proline
PD	Parkinson's disease

PEPMIP	Robust affinity materials for applications in proteomics and diagnostics
PMP	1,2,2,6,6-Pentamethylpiperidine
PP	Precipitation polymerisation
ProGRP	Pro-Gastrin-Releasing Peptide
PSD	Particle size distribution
p-value	A probability that the achieved result is due to a randomness of the data given the assumptions of performance a statistical test
Q	Glutamine
R	Arginine
S	Serine
SCLC	Small cell lung cancer
SD	Standard deviation
SDS	Sodium dodecyl sulfate
SEM	Scanning electron microscopy
S/N	Signal-to-noise ratio
SNCA	$\alpha$ -Synuclein gene
SPE	Solid phase extraction
SRM	Selected reaction monitoring
T	Threonine



TBA	Tetrabutylammonium
TBZ	Thiabendazole
TEMED	<i>N,N,N',N'</i> -tetramethylethylenediamine
TIC	Total ion current
TSQ	Triple quadrupole
TR-IFMA	Time-resolved immunofluorometric assay
TRIM	Trimethylolpropane trimethacrylate
V	Valine
W	Tryptophan
Y	Tyrosine
Z	Benzyloxycarbonyl group
$\delta$	Solubility parameter
$\theta$	Theta state

# TABLE OF CONTENTS

ACKNOWLEDGEMENTS .....	iii
ABSTRACT .....	iv
ABBREVIATIONS .....	v
TABLE OF CONTENTS .....	x
1. Introduction .....	1
1.1. Molecularly imprinted polymers (MIPs).....	1
1.2. Synthesis of MIPs by the non-covalent approach .....	4
1.2.1. Electrostatic forces .....	10
1.2.2. Van der Waals interactions .....	11
1.2.3. Hydrogen bonds.....	12
1.2.4. Hydrophobic effect .....	13
1.2.5. $\pi$ interactions .....	14
1.3. Synthetic design of MIPs.....	14
1.3.1. Template .....	14
1.3.2. Functional monomers.....	15
1.3.3. Crosslinker.....	17
1.3.4. Solvent.....	18
1.3.5. Initiator .....	20
1.3.6. Epitope and signature peptide imprinting .....	21
1.4. Formats of MIPs.....	26
1.4.1. Macroreticular polymers .....	26
1.4.2. Core-shell polymers .....	31
1.4.3. Magnetic polymers .....	36
1.4.4. Hydrogels .....	38
1.5. Characterisation of MIPs.....	42
1.5.1. Nitrogen sorption porosimetry .....	42

1.5.2.	Microscopy analysis .....	44
1.6.	Aims and scope of work .....	46
1.7.	Bibliography .....	48
2.	Molecularly imprinted polymer microspheres .....	61
2.1	Precipitation polymerisation for the synthesis of peptide imprinted polymer microspheres .....	62
2.1.1	Aim of study .....	62
2.1.2	Experimental section .....	62
2.1.3	Results and discussion .....	68
2.2	Molecularly imprinted polymer microspheres for a $\beta$ -Amyloid target .....	78
2.2.1	$\beta$ -Amyloid and diagnosis of Alzheimer's disease .....	78
2.2.2	Aim of study .....	80
2.2.3	Experimental section .....	81
2.2.4	Results and discussion .....	84
2.3	Molecularly imprinted polymer microspheres for pro-gastrin releasing peptide (ProGRP) target .....	93
2.3.1	ProGRP and diagnosis of small cell lung cancer (SCLC).....	93
2.3.2	Aim of study .....	96
2.3.3	Experimental section .....	97
2.3.4	Results and discussion .....	99
2.4	Molecularly imprinted polymer microspheres for $\alpha$ -Synuclein target .....	118
2.4.1	$\alpha$ -Synuclein and Parkinson's disease .....	118
2.4.2	Aim of study .....	121
2.4.3	Experimental section .....	121
2.4.4	Results and discussion .....	124
2.5	Conclusions and outlook .....	132
2.6	Bibliography .....	134
3.	Core-shell molecularly imprinted polymers.....	138
3.1	Test study: two-step precipitation polymerisation for the synthesis of peptide imprinted core-shell polymer microspheres.....	140

3.1.1 Aim of study .....	140
3.1.2 Experimental section .....	140
3.1.3 Results and discussion .....	147
3.2 Core-shell molecularly imprinted polymer microspheres synthesised by two-step precipitation polymerisation .....	157
3.2.1 Aim of study .....	157
3.2.2 Experimental section .....	158
3.3 Results and discussion.....	168
3.3.1 Synthesis of core-shell molecularly imprinted polymer microspheres for peptide targets .....	168
3.4 Conclusions and outlook.....	179
3.5 Bibliography .....	180
4. Magnetic molecularly imprinted polymer microspheres.....	181
4.1 Magnetic MIP with encapsulated magnetite.....	183
4.1.1 Aim of study .....	183
4.1.2 Experimental section .....	183
4.1.3 Results and discussion .....	187
4.2 Magnetic core-shell MIP with encapsulated magnetite .....	193
4.2.1 Aim of study .....	193
4.2.2 Experimental section .....	194
4.2.3 Results and discussion .....	202
4.3 Magnetic core-shell MIPs with incorporated magnetite .....	210
4.3.1 Aim of study .....	210
4.3.2 Experimental section .....	211
4.3.3 Results and discussion .....	217
4.4 Macroreticular polymers converted into magnetic MIPs for ProGP target ....	227
4.4.1 Aim of study .....	227
4.4.2 Experimental section .....	228
4.4.3 Results and discussion .....	231
4.5 Conclusions and outlook.....	235

4.6 Bibliography .....	236
5. Molecularly imprinted polymer hydrogels.....	238
5.1 Aim of study.....	240
5.2 Experimental section.....	241
5.2.1 Materials.....	241
5.2.2 Synthesis of molecularly imprinted hydrogels for $\alpha$ -Synuclein target .....	241
5.3 Results and discussion.....	246
5.3.1 Synthesis of molecularly imprinted hydrogels for $\alpha$ -Synuclein target .....	246
5.3.2 Molecular recognition of the first generation of hydrogels .....	252
5.4 Conclusions and outlook.....	255
5.5 Bibliography .....	257
6. General conclusions and future work .....	259
Bibliography .....	263
Appendix 1 BET isotherms.....	264
Appendix 2 FT-IR spectra.....	266
Appendix 3 Manuscript .....	267

# 1. Introduction

## 1.1. Molecularly imprinted polymers (MIPs)

Molecularly imprinted polymers (MIPs) are synthetic materials with binding sites that have high affinity and selectivity for a given target molecule. The concept of molecular imprinting reflects binding phenomena in Nature that have fascinated scientists for many decades. The process of molecular imprinting resembles the binding of an antigen by antibodies or the conversion of a substrate to product in an enzymatic reaction.<sup>1</sup> In our daily lives, imprinting concepts can be met on a daily basis, and this includes fingerprints, animal or plant fossil imprints, coins and even sandcastles.

The molecular imprinting mechanism underlying the synthesis of MIPs is relatively straightforward. In a typical imprinting process the following stages can be distinguished: template-monomer(s) assembly, polymerisation and template removal, as illustrated schematically in Figure 1.1. This assembly relates to the self-assembly processes that are central to non-covalent molecular imprinting. The template-monomer assembly is formed through the interactions between the template and functional groups of the monomer(s). Interactions between the template and monomer(s) are chemical in nature and involve either covalent or non-covalent bonds. Pre-polymerisation complexes, dissolved in the solvent, are surrounded by a crosslinking agent. In the next step, the polymerisation process takes place in the presence of initiator. The template molecule becomes trapped in the polymer network. The final step in the imprinting process aims to remove the template from the polymer, and this is usually achieved through a simple washing process. The template extraction reveals cavities that are complementary to the template's shape, size and functional groups. Thereafter, the polymer is capable of recognizing and selectively binding to the template molecule.<sup>1</sup>

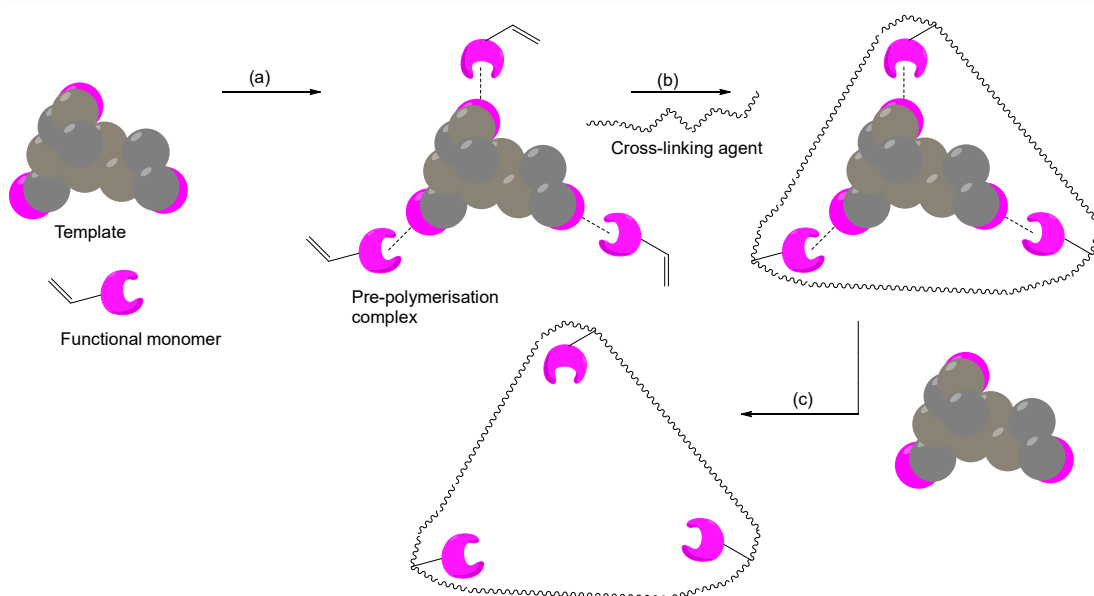


*Figure 1.1 Highly schematic representation of a molecular non-covalent imprinting process, which includes the following stages: (a) assembly, (b) polymerisation and (c) template extraction. Scheme adapted from ref. <sup>2</sup>.*

The idea of molecular imprinting technology is quite old, but it is a rapidly evolving area of science. The concept dates back to the early 1930s.<sup>3</sup> Polyakov, considered as the pioneer in this discipline, synthesised silicas that were capable of binding additives with relatively high capacity.<sup>4</sup> Later on, Dickey, a doctorate student of Pauling, translated Pauling's theories on antibody formation into a molecular imprinting context. He developed the first silica gel with the affinity for dye molecules, methyl-, ethyl-, propyl- or butyl orange.<sup>5</sup> Throughout the subsequent years the topic appeared not to be attractive to the scientific community and only a few groups were working with the idea of molecular imprinting.

However, further studies in the 1970s and the 1980s revolutionised the approach and shed new light on molecular imprinting technology. Wulff introduced an approach in which the assemblies of the template and the functional monomer(s) are created through covalent bonds.<sup>6</sup> These assemblies are formed as a result of chemical modifications of the template which attach it to pendent vinyl groups through covalent bonds: boronate esters, imines, ketals and disulfides.<sup>1</sup> This marked the

beginning of an approach for the synthesis of MIPs known as the “covalent approach”. The method allows for the synthesis of polymers with good binding properties, however the approach has some drawbacks. There is a limited number of compounds that can be used as the template molecule, the selection of functional monomers is narrow and, what is more, the procedure is complicated and takes a lot of time.<sup>7</sup>

In order to overcome the limitations of the “covalent approach”, the group of Mosbach introduced a completely new concept, termed the “non-covalent approach”.<sup>8</sup> In this way, the complexes of the template and the functional monomer(s) are formed through non-covalent interactions. This was a breakthrough in molecular imprinting technology,<sup>9</sup> and has led to hundreds of publications per year on this topic.<sup>10</sup> The detailed description of this method will be introduced in the subsequent section.

The beginning of the 1990s saw a third approach that can be used for the synthesis of MIPs, known as the “semi-covalent approach”.<sup>11</sup> This approach combines advantages from both the covalent and non-covalent approaches. The template is bound to the functional monomer(s) through covalent bonds. Thanks to this, non-specific binding by the MIP is reduced as the amount of the functional monomer(s) used is stoichiometric with respect to the template molecule. Removal of the template from the product is achieved through the cleavage of labile covalent bonds. In the rebinding step, binding to the polymer occurs through non-covalent interactions, and covalent bonds for binding are not important any longer.<sup>1</sup> Further studies on the topic of the semi-covalent approach led to the introduction of a sacrificial spacer to the procedure. Whitcombe and co-workers used a carbonate spacer for the imprinting of cholesterol. Removal of the spacer leaves a defined space that is reserved for the formation of non-covalent bonds during rebinding.<sup>12</sup>

Nowadays, the topic of molecular imprinting is a fast-growing research field; many groups around the world are working on MIPs, employing the concept within different disciplines and trying to better understand the mechanisms of action.



MIPs have found applications as analytical tools. These include: competitive binding assays,<sup>13,14</sup> solid-phase extraction,<sup>15,16</sup> capillary electrochromatography,<sup>17,18</sup> chromatographic stationary phases<sup>19,20</sup>. Also, MIPs can be used in the process of catalysis,<sup>21,22</sup> can be used as sensors<sup>23,24</sup> or as membranes<sup>25,26</sup>, or even they can be used as drug delivery systems<sup>27,28</sup>. MIPs can be applied to the analysis of samples from various sources. In medicine, they are used for the analysis of different types of biological samples: serum,<sup>29</sup> plasma,<sup>30</sup> cerebrospinal fluid<sup>31</sup> and urine<sup>32</sup>. In environmental science, MIPs are applied for the analysis of water samples from different origins: wastewater,<sup>33</sup> lake,<sup>34</sup> pond,<sup>35</sup> sludge,<sup>36</sup> tap, river and well water.<sup>37</sup> Also, MIPs play an important role in the analysis of food samples, such as dairy,<sup>38</sup> poultry,<sup>39</sup> seafood,<sup>40</sup> pork,<sup>41</sup> fruits<sup>42</sup> and vegetables.<sup>43</sup>

## 1.2. Synthesis of MIPs by the non-covalent approach

The non-covalent approach employs electrostatic forces, hydrogen bonds, van der Waals forces,  $\pi$ -interactions or the hydrophobic effect for the formation of template-monomer complexes.<sup>44</sup> A detailed description of these interactions is presented in the next subsections. The non-covalent approach was first reported as the “biochemist’s” method by Mosbach and Arshady at the beginning of the 1980s.<sup>8</sup> Ever since its first disclosure in the open literature, this method has been increasing in popularity amongst researchers.

The non-covalent approach is versatile for MIP synthesis as it is a time-efficient method and is quite simple at the same time. There is a wide range of functional monomers that are capable of forming interactions with almost any kind of template molecule.<sup>44</sup> A typical example of this procedure is shown in Figure 1.2 for the synthesis of a MIP for theophylline. Theophylline is a bronchodilating drug used for the treatment of respiratory diseases such as asthma, emphysema and chronic bronchitis.<sup>45</sup> Methacrylic acid (MAA) is selected as the functional monomer. MAA can be both a hydrogen bond acceptor and donor, but in this example it is a hydrogen bond donor. The assemblies of the theophylline and MAA are formed through hydrogen bonds. The assemblies are copolymerized with an excess of a crosslinking

agent. When the polymerisation is complete, the theophylline is removed through the disruption of hydrogen bonds. This leaves voids and cavities in the polymer network that are complementary to the template molecule and selective to the target molecule.<sup>1</sup>

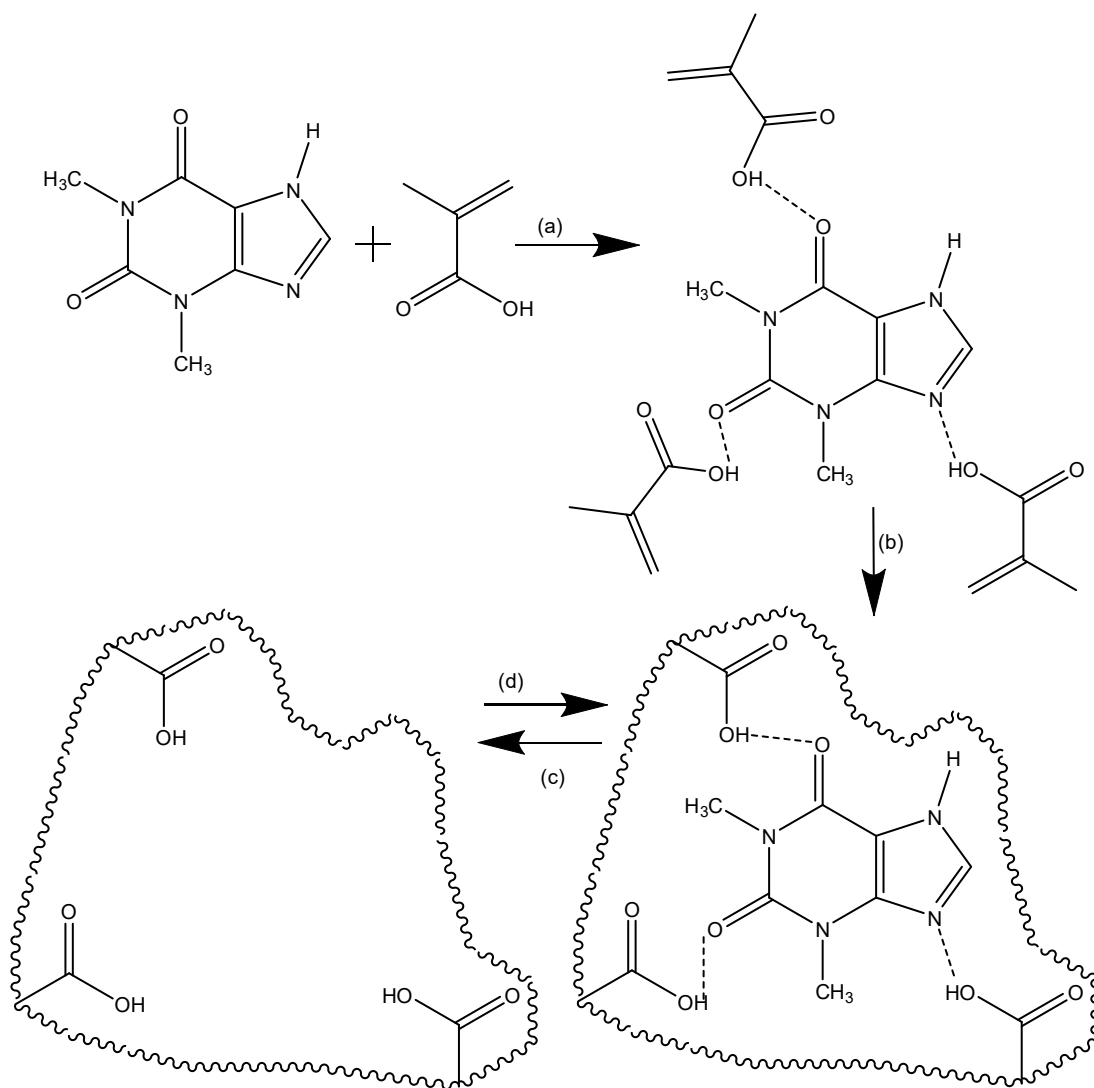


Figure 1.2 Schematic representation of non-covalent imprinting, which includes the following stages: (a) self-assembly of template (theophylline) and functional monomer (methacrylic acid), and the formation of template-monomer complexes through hydrogen bonds; (b) copolymerisation of the complexes formed with an excess of a crosslinking monomer; (c) extraction of the template from the synthesised polymer, thereby revealing a cavity with an affinity for the target molecule; (d) rebinding of the theophylline through non-covalent interactions only. Scheme adapted from ref.<sup>1</sup>.

Another example is shown in Figure 1.3, where a procedure for the synthesis of a MIP for the ProGRP target used in the work reported in Thesis is presented. The protonated amine group of the functional monomer forms electrostatic interactions

with the carboxylate groups of the peptide template. The assemblies formed between the template molecule and the functional monomer are copolymerized with an excess of crosslinking agent. Removal of the template once polymerisation is complete, through the disruption of hydrogen bonds, leaves voids and cavities in the polymer network that are complementary to the template molecule and selective to the target peptide.

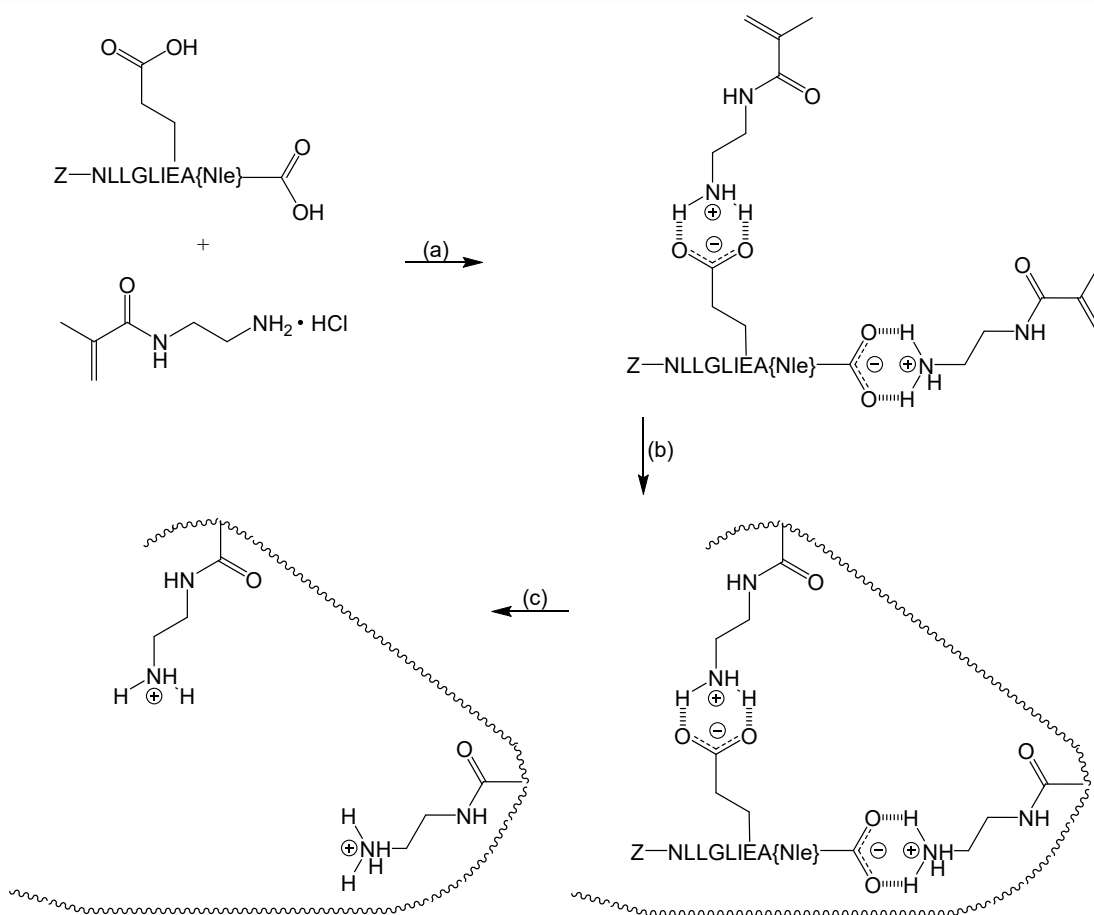


Figure 1.3 Schematic representation of non-covalent imprinting, which includes the following stages: (a) self-assembly of template ( $Z\text{-NLLGLIEA}\{\text{Nle}\}$ ) and functional monomer ( $N$ -(2-aminoethyl) methacrylamide hydrochloride [ $\text{EAMA}\cdot\text{HCl}$ ]), and the formation of template-monomer complexes through hydrogen bonds and electrostatic interactions; (b) copolymerisation of the complexes formed with an excess of a crosslinking monomer; (c) extraction of the template from the synthesised polymer thereby revealing the cavities with the affinity for target molecule.

The formation of template-monomer complexes in the non-covalent approach is governed by Le Chatelier's Principle. Increasing the concentrations of components that form pre-polymerisation complexes may lead to an increasing number of binding sites, which can result in an improved selectivity for the final product.<sup>46</sup> Both the concentrations of functional monomer(s) or template can be increased independent. It is necessary to keep in mind the fact that the amount of the crosslinker should be

kept above a certain level so that the fidelity of the binding sites formed is maintained.<sup>46</sup> Also, keeping an appropriate ratio of functional monomer to template is important as well. Another strategy for driving the equilibrium towards the formation of pre-polymerisation complexes is increasing the concentration of the template, while maintaining an optimum mole ratio of functional monomer(s) to template. However, when the template is added in a significant excess, further addition of this component does not influence the formation of binding sites, as there are no more free binding sites on the functional monomers as all of the functional monomers are complexed to the template.<sup>46</sup> It is worth pointing out one of the drawbacks of this strategy: the lower average affinity and selectivity of the final product. Another important consideration for the non-covalent approach that results from Le Chatelier's Principle is the effect of temperature. When hydrogen bonding interactions are involved, lower temperatures drive the equilibrium towards pre-polymerisation complex formation, thus MIPs prepared under such conditions typically have better selectivity than those synthesised at higher temperatures.<sup>46</sup> The importance of each component that takes part in the synthesis of MIPs is discussed more broadly in later sections.






It is important to bear in mind that the non-covalent approach also has certain drawbacks. An appropriate solvent has to be selected to favour the interactions between the template and functional monomers. Polar protic solvents, especially water, cannot normally be chosen in molecular imprinting involving hydrogen bonding because they disturb formation of the template-monomer complexes.<sup>47</sup> In the example presented in Figure 1.3, acetonitrile was the polar aprotic solvent selected because it stabilises the formation of hydrogen bonds between the functional monomer and template molecule. Also in the non-covalent approach, the functional monomers normally need to be added in excess with respect to the amount of the template molecule in order to favour the formation of template-monomer complexes. Therefore, the amount of the functional monomers used is more than enough for the formation of template-monomer complexes, and non-specific binding sites could be formed as a result of the random incorporation of

surplus functional monomers into the polymer network.<sup>48</sup> What is more, the distribution of the created binding sites is not homogenous in the synthesised polymer. It is believed that the binding sites formed in the non-covalent approach resemble polyclonal antibodies in terms of the spread of affinities.<sup>49</sup>

### 1.2.1. Electrostatic forces

Electrostatic forces, particularly ion-pair interactions, are considered as fundamental non-covalent interactions which play a key role in the non-covalent approach for the synthesis of MIPs.<sup>50</sup> These interactions occur between two oppositely charged ions or molecules that have different charge density. If charge density is asymmetrically distributed within a single molecule, then these different parts also can interact with each other. The electrostatic forces can even be present within molecules that are not charged but their charging is induced by surrounding molecules such as ions or dipoles. Also, some molecules are able to internally redistribute their charges, causing further redistribution of charges in other molecules.<sup>51</sup> A list of electrostatic interactions is presented in Table 1.1. According to Columb's Law, the interactions between two ions are described by the energy  $E$ , which is dependent on either the number of charges in each ion,  $Z$ , or the absolute charge value of the electron,  $e$ . The distance  $r$  between the ionic species and the dielectric constant  $D$  are also taken account. The energy of the ion-dipole and dipole-dipole interactions is additionally dependent on the dipole moment  $\mu$ , and relative orientation  $\theta$  of the dipole to the vector between two interacted species. In the case of ion-induced dipole interactions, the energy  $E$  additionally depends on the polarizability,  $\alpha$ . Dispersion forces are formed as the result of redistribution of the charge within a molecule. This redistribution is caused as the effect of charge compensation during interactions with charges from another molecule.<sup>51</sup>

Table 1.1 List of non-covalent interactions together with their energy,  $E$ , and magnitude. The terms in the equations mean:  $e$ : charge electron value,  $Z$ : number of charges in each molecule;  $\mu$ : dipole moment;  $\alpha$ : polarizability;  $r$ : distance between species;  $D$ : dielectric constant;  $h$ : Planck constant;  $\nu_0$ : frequency.<sup>51</sup> Table adapted from ref. <sup>51</sup>.

	Type of interaction	Equation	Order of magnitude (kJ/mol)
	Ion-ion	$E = \frac{Z_1 Z_2 e^2}{Dr}$	60
	Ion-dipole	$E = \frac{Z_1 e \mu_2 \theta}{Dr^2}$	-8 to +8
	Dipole-dipole	$E = \frac{\mu_1 \mu_2 \theta'}{Dr^3} - \frac{3(\mu_1 r \theta'')(\mu_2 r \theta''')}{Dr^5}$	-2 to +2
	Ion-induced dipole	$E = \frac{Z_1 e^2 \alpha_2}{2D^2 r^4}$	0.2
	Dispersion	$E = \frac{3h\nu_0 \alpha^2}{4r^6}$	0 to 40

As can be seen from Table 1.1, electrostatic interactions are distance-dependent, and ion-pair interactions are the most relevant for selectivity of MIPs. These interactions are considered as the driving force for the rational design of MIPs as their contribution of energy is the highest.<sup>50</sup>

### 1.2.2. Van der Waals interactions

Van der Waals interactions are considered as non-covalent interactions in which ions are not involved. According to the Lennard-Jones potential, van der Waals interactions are dependent on the distance between two atoms which are not bonded together.<sup>52</sup> The energy of these interactions is presented graphically in Figure 1.4. Two types of van der Waals interactions are distinguishable: attractive and repulsive forces. The attractive force of two atoms which are separated arises when these atoms become closer together until their separation is maintained by contact



distance. If this barrier is exceeded, then the energy increases and repulsive force starts to dominate. A typical energy contribution of one pair of atoms is in the range 2 to 4 kJ/mol. This number is quite small, however when two molecules with a large number of atoms come together their energy sum plays a significant role.<sup>52,53</sup>

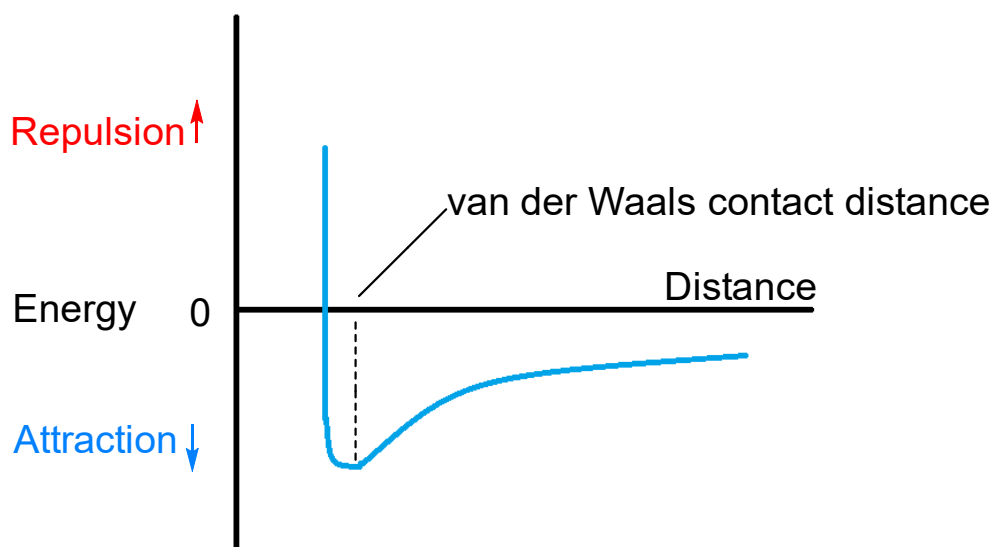


Figure 1.4 Dependence of the distance between two atoms or molecules on the van der Waals energy. Scheme adapted from ref.<sup>53</sup>.

### 1.2.3. Hydrogen bonds

Hydrogen bonds are formed as the result of interactions between hydrogen atoms which are covalently bound to electronegative atoms, and other electronegative atom. A typical structure of hydrogen bond is shown in Figure 1.5. A hydrogen atom shares electrons with an atom designated as hydrogen donor. The energy for

hydrogen bonds lies in the range 4-13 kJ/mol. This bond is about 1 Å shorter than electrostatic interactions.<sup>53</sup>

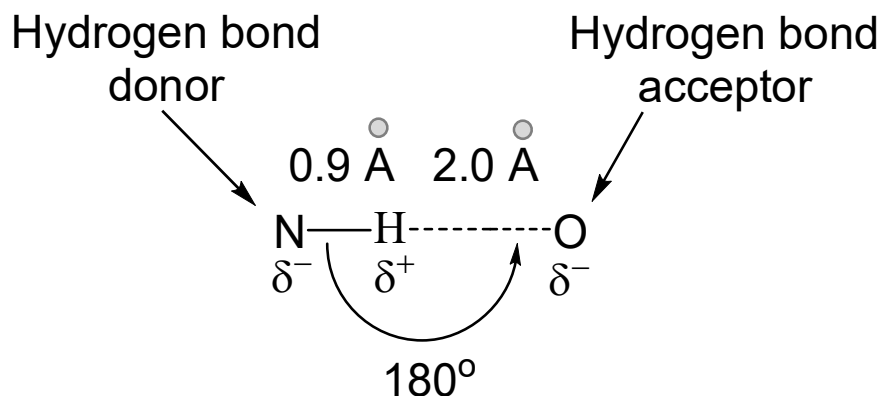


Figure 1.5 Typical hydrogen bond. Scheme adapted from ref.<sup>53</sup>.

#### 1.2.4. Hydrophobic effect

The hydrophobic effect refers to unfavourable interactions that occur when non-polar molecules get into polar solvents. It can be said that this effect describes how bad these interactions are with water. As can be seen in Figure 1.6, when oil droplets get into water, hydrophobic chains are sequestered, avoiding contact with water. Water molecules tend to minimise enthalpically unfavourable interactions with the hydrophobic part of molecules through entropic compensation. It results in the organisation of the water molecules around hydrophobic chains in such way that the hydrophobic surface of the molecule is sheltered. The hydrogen bonds formed between water molecules tend to form away from hydrophobic chains. This is the main principle that underlies the hydrophobic effect.<sup>52,53</sup>

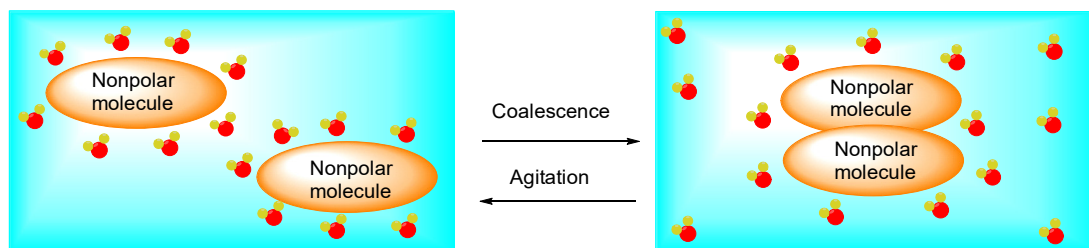


Figure 1.6 Illustration of the hydrophobic effect. When oil (nonpolar molecule) gets into water, two-phases are created. Agitation results in their destruction, however there is a tendency to minimise contact with water, and oil drop is again created.<sup>53</sup> Scheme adapted from ref.<sup>53</sup>.

### 1.2.5. $\pi$ interactions

$\pi$  interactions are classified as very weak non-covalent interactions. They are formed as the result of interactions of a  $\pi$  system with other molecules. A  $\pi$  system is referred to as  $\pi$  bonds, which are covalent chemical bonds which are formed by two  $p$  orbitals that overlap when they are adjacent and aligned. The following  $\pi$  interactions are distinguishable: metal- $\pi$ ,  $\pi$ - $\pi$  stacking, O-H/ $\pi$ , ion- $\pi$ .<sup>54,55</sup>

## 1.3. Synthetic design of MIPs

For the synthesis of an imprinted material that will be able to bind with high selectivity and affinity to a molecule known as the target analyte, an appropriate selection of template, functional monomer(s), crosslinker, porogen and initiator is crucial. This section describes the most important aspects that need to be taken into consideration when the synthesis of MIPs is planned.

### 1.3.1. Template

Template is the most important component in the synthesis of MIPs as it dictates the organisation of the binding sites in the polymer network.

A component chosen as a template should meet the following requirements:

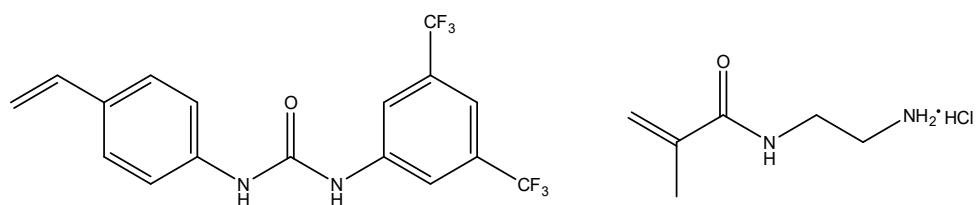
- It should contain functional groups that interact with the functional monomer(s), forming the template-monomer complexes;
- It should not undergo any chemical changes under the polymerisation conditions. The template must be stable under the conditions used for the reaction;
- It should not contain any groups that are involved in the inhibition or retardation of the polymerisation.<sup>56</sup>

A phenomenon known as “template bleeding” may need to be taken into consideration during the selection of the right candidate for the template. MIP washing procedures usually do not allow for the complete removal of all of the template that is used in MIP production. More than 1% of template usually remains in the polymer network, even after extensive washing.<sup>57</sup> Template molecules are physically entrapped in the dense polymer network or may even be covalently bound by the polymer.<sup>57</sup> Application of such a polymer in ultra-trace analysis is limited as the template molecules elute along with the target analyte leading to unreliable results. The use of a template analogue, which is a molecule with a structure similar but not identical to the target analyte, can help to address this problem.<sup>58</sup> The non-covalent approach presented in Figure 1.3 can be given as an example of this strategy. A structural analogue of the ProGRP signature peptide, Z-NLLGLIEA{Nle}, was chosen as the template. The N-terminal end of this peptide is a Z protecting group, and C-terminal lysine is replaced by norleucine. These structural changes lead to differences in molecular weight with respect to target analyte. This strategy helps to reduce or eliminate the risk that the template molecules interfere negatively with the analysis.

### 1.3.2. Functional monomers

An important consideration in the planning of MIP synthesis via a non-covalent imprinting strategy is the proper selection of the functional monomers. The chosen functional monomers should be able to form non-covalent interactions with the template. Through interactions with the template molecules, use of the functional

monomers lead to the creation of voids and cavities with binding sites that are selective to the target analyte. Typically in the non-covalent approach, the mole ratio of the functional monomer to the template molecule is on a level of 4:1. This monomer excess promotes the formation of template interactions, and at the same time this excess is so small that the formation of non-specific binding sites is minimised. It is necessary to keep in mind the reactivity ratios of the functional monomers along with the reactivity ratio of crosslinker if “cocktail polymerisation” is planned. The term “cocktail polymerisation” refers to the synthesis of MIPs containing two or more functional monomers.<sup>56</sup> The chemical structures of the functional monomers used in the work described in this Thesis are shown in Figure 1.7



*N*-3,5-bis(trifluoromethyl)-phenyl-*N'*-4-vinylphenylurea      *N*-(2-Aminoethyl) methacrylamide hydrochloride

Figure 1.7 Chemical structures of functional monomers used in the present work.

*N*-3,5-bis(trifluoromethyl)-phenyl-*N'*-4-vinylphenylurea (NTPVU) belongs to a family of urea-based vinyl monomers that have high binding affinity for oxyanions.<sup>59</sup> This monomer was used for the synthesis of polymer-based artificial receptors by Sellergren and co-workers. Their final products, prepared in the form of irregularly – shaped and sized particles, gave outstanding affinity and selectivity for a  $\beta$ -amyloid target and enrichment of proteotypic peptides.<sup>31,60</sup> The same research group also employed the second monomer shown in Figure 1.7: *N*-(2-aminoethyl) methacrylamide hydrochloride (EAMA.HCl).<sup>61</sup> MIPs were prepared in the form of irregular particles as well. EAMA.HCl was used for the formation of binding sites through hydrogen bonds and electrostatic interactions between cationic amino groups and negatively-charged carboxylate groups in the template molecule.<sup>61</sup>

### 1.3.3. Crosslinker

Crosslinker refers to the crosslinking monomer that plays a role in the polymer's morphology. Through the formation of a highly crosslinked rigid polymer network, stabilisation of the geometry of the imprinted binding sites is achieved along with mechanical stability.<sup>56</sup> In some cases, the crosslinking monomer can even interact with the template molecule, positively influencing the recognition properties of MIP(s), as was reported by Nicholls and others.<sup>62</sup> Therefore, the correct selection of crosslinker is crucial in the rational design of MIPs. In a typical MIP composition, this type of monomer often constitutes 80% or more of the total amount of monomers used, as the amount of crosslinker used must be sufficiently high to form a rigid macroreticular network for binding sites.<sup>56</sup> Also, variations in the content of crosslinker and functional monomer(s) influence the porosity of the final product.<sup>63</sup> The reactivity ratio of crosslinking agent, relative to the other monomers that are planned to be included in the polymerisation, also needs to be taken into consideration.<sup>56</sup> For the polymers described in this Thesis, divinylbenzene-80 (DVB-80) was used mainly as the crosslinker. Figure 1.8 shows the chemical structure of the crosslinker used in this work.

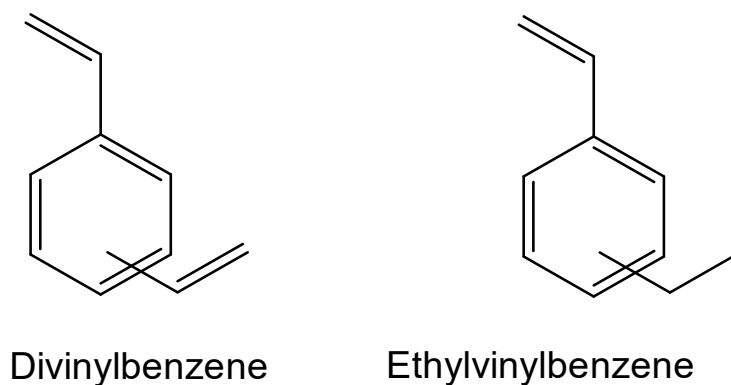


Figure 1.8 Chemical structure of the crosslinking monomer: divinylbenzene (DVB-80), which contains ethylvinylbenzene (EVB) as a major contaminant.

DVB-80 consists of 80% of divinylbenzene (DVB) and 20% of ethylvinylbenzene (EVB). Both DVB and EVB consist of mixture *meta*- and *para*-isomers. In addition, *ortho*- DVB

and EVB isomers are present in negligibly small amounts.<sup>64</sup> DVB has two polymerisable vinyl groups that lead to the formation of non-linear polymer structures. DVB is classified as a multifunctional monomer which is able to form insoluble macroscopic polymer networks in the presence of sufficiently high amounts of porogen.<sup>56</sup>

### 1.3.4. Solvent

Solvent holds multiple functions in the synthesis of MIPs. First of all, it takes part in the creation of the pores in the macroporous polymer network. Due to that, it is sometimes referred as the porogen. The morphology of the polymers, including surface area, pore diameter and pore volume, are solvent-dependent. The next role of solvent in the synthesis of MIPs is to solubilise all the compounds that are used for polymerisation. The solvent brings them into a homogenous phase.<sup>56</sup> Therefore, the polymerisation requires the selection of the solvent in which the monomer(s) used are soluble, but the polymer formed must be insoluble in order to form precipitates. The right selection of the solvent in precipitation polymerisations for the synthesis of high quality polymer microspheres is also very important.

Solvents in polymerisations can be classified as “bad” or “good”.<sup>62</sup> This classification is made on the basis of the thermodynamic Hildebrand ( $\delta$ ) solubility parameter. When a “good” solvent is employed, the formation of the pores is favoured and a polymer network with high surface area is formed. In other words, when a “good” solvent is used, phase separation of polymer occurs late in the polymerisation and leads to the formation of polymer particles with small pores and high surface area. If a thermodynamically “bad” solvent is used than the formation of pores is suppressed and polymers with low surface area are isolated.<sup>56,65</sup>

The theta state is defined as the temperature at which the solvation and association forces for a given polymer molecule are equally strong and the polymer exists in the solution as non-expanded coil.<sup>66</sup> To better understand thermodynamic solubility parameter,  $\theta$  (theta), the solvency characteristics of solvents and the effects of

a polymer in solution should be taken into consideration. The following solubility parameters are distinguished: one- and three-dimensional solubility parameters known as Hildebrand ( $\delta$ ) and Hansen parameters, respectively. The first one defines density of the cohesive energy of solvents and polymers and measure solvency behaviour. In other words, it measures the affinity of a solute for a selected solvent and reflects the overall solvent properties.<sup>67,68</sup> The Hildebrand ( $\delta$ ) solubility parameter is defined as the square root of a cohesive energy density, as is shown in an equation presented below where  $\Delta H_V$  is the molar energy of vaporisation,  $V_m$  is the molar liquid volume,  $R$  and  $T$  correspond with the ideal gas constant,  $\sim 8.31 \text{ J mol}^{-1} \text{ K}^{-1}$ , and temperature.<sup>69</sup>

$$\delta = \sqrt{\frac{\Delta H_V - RT}{V_m}}$$

The cohesive energy density measures the interactions between the molecules in the liquid state. It defines the energy per unit volume of the liquid which is required to move a molecule from the liquid state into a vapour state. The Hildebrand solubility parameter is used to predict liquid-liquid solubility. If the value of Hildebrand solubility parameter is similar for solvent and solute, it would result in good miscibility of the solute molecules in the solvent selected.<sup>69</sup> However, the Hildebrand solubility parameter cannot be used to determine the swelling properties of the polymers in solvent selected as the parameter cannot be determined from vaporisation heats when the substances have high boiling points. Polymer materials are usually decomposed before vaporisation heat can be determined.<sup>70</sup> The second solubility parameter, known as the three-dimensional Hansen solubility parameter extends the Hildebrand solubility parameter and allows for determination of swelling properties of the polymers. In the Hansen solubility parameter, the overall interactions between a solute molecules and solvent are divided into the following forces: dispersion, dipole-dipole and hydrogen bonding interactions.<sup>68</sup> The Hansen solubility parameter ( $\delta$ ) can be described using an equation shown below:

$$\delta^2 = \delta_d^2 + \delta_p^2 + \delta_h^2$$



where  $\delta$  is the sum of the following energies: dispersion ( $\delta_d$ ), dipole-dipole ( $\delta_p$ ) and hydrogen bonding ( $\delta_h$ ) interactions between molecules.<sup>70</sup> These three values can be used in order to predict the behaviour of the polymer chains in the solvent selected. If these three energies are similar for both the polymer and solvent, then the polymer chains will swell in the solvent well and favourable interactions between the solvent and the polymer chains will be increased. This type of solvent is considered as a “good” solvent. On the contrary, a “bad” solvent is one where the interactions between solvent and polymer chains will be reduced and the polymer chains will not swell in the solvent. A theta solvent is a solvent which lies at the border of “good” and “bad” solvents. Proper selection of the porogen in the synthesis of MIPs is crucial, especially in the non-covalent approach. The solvent of choice should not interfere with the formation of interactions between the functional monomer(s) and template molecule.<sup>56</sup> For the synthesis of the MIPs reported in this Thesis, acetonitrile (ACN) was the preferred near-theta solvent in precipitation polymerisations. ACN is a polar, aprotic solvent that stabilises the formation of hydrogen bonds. Low levels of dimethyl sulfoxide (DMSO) were required as co-solvent to improve the solubility of the template and/or the functional monomers.

The solvent also plays an important role in the final stage of MIP preparation. The solvent takes part in the extraction of the template molecules, unreacted and/or residual starting materials such as crosslinker and functional monomer(s) from the formed polymer network structures. Therefore, a properly selected solvent used for the washing step must solubilise all the compounds that are used for polymerisation. When an optimal solvent is used for the washing, the polymer swells and the binding sites become easily accessible, which results in disruption of the interactions between the template molecules and MIP, and finally in template removal. Therefore, the right selection of the solvent in the final stage of MIP preparation is also important.

### 1.3.5. Initiator

An initiator provides a source of radicals for the synthesis of MIPs. In this Thesis, most of the MIPs were prepared via free radical polymerisation, therefore this subsection

is devoted to initiators used in this type of polymerisation. Redox polymerisation is another type of reaction which was used for the synthesis of MIPs in this work, however details of initiation mechanism in this polymerisation is included in 1.4.4 where MIPs in the format of hydrogels are discussed.

In a free radical polymerisation, the initiator undergoes decomposition under the polymerisation conditions and free radicals are generated. The free radicals react with the functional monomer(s) and crosslinker leading to the formation of polymer. It is worth pointing out that if the interactions formed between the functional monomer(s) and the template molecule are driven by hydrogen bonds then lower temperatures for polymerisation are normally preferred. Therefore, under such circumstances initiators which decompose at lower temperatures are desirable for the synthesis of MIPs.<sup>56</sup>

For the synthesis of the polymers described in this Thesis, azobisisobutyronitrile (AIBN) was the initiator of choice. The way in which AIBN undergoes decomposition, and free radicals are generated, is shown in Figure 1.9. In the syntheses described in this Thesis, free radicals were generated thermally, however AIBN can be decomposed by photoinitiation as well. Limé and Irgum successfully employed this initiation system, and were able to produce perfectly monodisperse polydivinylbenzene microspheres.<sup>71</sup>

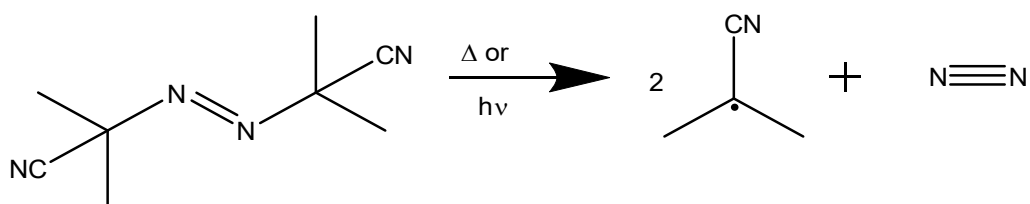


Figure 1.9 Decomposition of azobisisobutyronitrile (AIBN).

### 1.3.6. Epitope and signature peptide imprinting

In the literature, there are many examples of efforts that have been made into the development of protocols for the synthesis of artificially tailored polymer materials

that can mimic antibodies. The low production cost of MIPs, combined with their outstanding affinity and selectivity, reusability and high reproducibility make them an attractive alternative to antibodies. Also, MIPs can be synthesised in either polar or non-polar solvents. What is more, polymer materials of this type are highly stable, both chemically and physically, and are extremely resistant to a range of pH conditions, organic solvents, metal ions and autoclave treatments.<sup>7</sup> On the other hand, antibodies are highly selective as well. However, their stability and reusability are limited. Also, high production costs restricts their use in diagnostics and therapy.

The synthesis of protein-imprinted polymers has always been challenging. Proteins are large and complex molecules with conformational flexibility along their backbone. They are typically insoluble in organic solvents, which makes them even more tricky to imprint.<sup>72</sup> The mobility of large molecules such as proteins are limited within highly crosslinked polymer networks, and this may prevent efficient protein template removal.<sup>73</sup> Also, the conditions that are used for the removal of the protein template from the prepared polymer have to be chosen carefully. There is a risk that the binding sites created in the polymer network can interact with the components that are present in the washing solvent, for instance with sodium dodecyl sulfate (SDS), resulting in creation of polymer sorbents with non-specific binding sites known as artefacts.<sup>74</sup>

In imprinting technology, four approaches have evolved for the synthesis of protein-imprinted polymers. The first one, surface imprinting of proteins, involves immobilisation of the proteins on surfaces such as silica<sup>75</sup> or mica<sup>76</sup>. The second approach uses hydrogels for the creation of imprinted protein cavities. In the third one, the protein is converted into Protein-Coated Micro-Crystals (PCMCs), and in such form are used as the template for the synthesis of MIPs.<sup>77</sup> The fourth one, known as the epitope approach and its derivative, signature peptide imprinting, use part of the protein as the template. In the epitope approach, an oligopeptide, representative of a particular protein with an easy accessible surface, is usually selected as the template molecule.<sup>72</sup> In this section, particular attention will be paid to this approach

and its derivative because templates that were used for synthesis of polymers prepared in PhD thesis were selected on the basis of these rules.

The epitope approach in molecular imprinting largely resembles the mechanism of the immune response to antigens. Antibodies recognize antigens through an antigenic determinant known as the epitope. The epitope is a small part of the antigen that binds to the specific antibody only.<sup>78</sup> In the epitope approach in molecular imprinting, a similar assumption is applied. A part of the target peptide/protein is imprinted which allows for the formation of binding sites that bind the whole peptide/protein.<sup>79</sup> A highly schematic representation of this approach is shown in Figure 1.10. It resembles a typical molecular imprinting process, with a single exception being that the imprinting takes place for a part of the target molecule rather than the whole. The term "epitope approach" in molecular imprinting was introduced by Rachkov and Minoura. A C-terminal tetrapeptide of oxytocin was chosen as the template molecule for synthesis of poly(methacrylic acid-co-ethylene glycol dimethacrylate). The polymer synthesised was able to bind with high selectivity to oxytocin with the C-terminal homology sequence.<sup>79,80</sup> In further work, Rachkov attempted to use the C-terminal octapeptide of angiotensin II for the synthesis of MIPs. However, poor binding of the target peptide to the sorbent was reported.<sup>81</sup> A few years later, a breakthrough in the epitope approach was achieved by Shea and co-workers. Highly specific MIPs for cytochrome C, alcohol dehydrogenase and bovine serum albumin were produced by inclusion of C-terminal nonapeptides in MIP syntheses.<sup>82</sup>

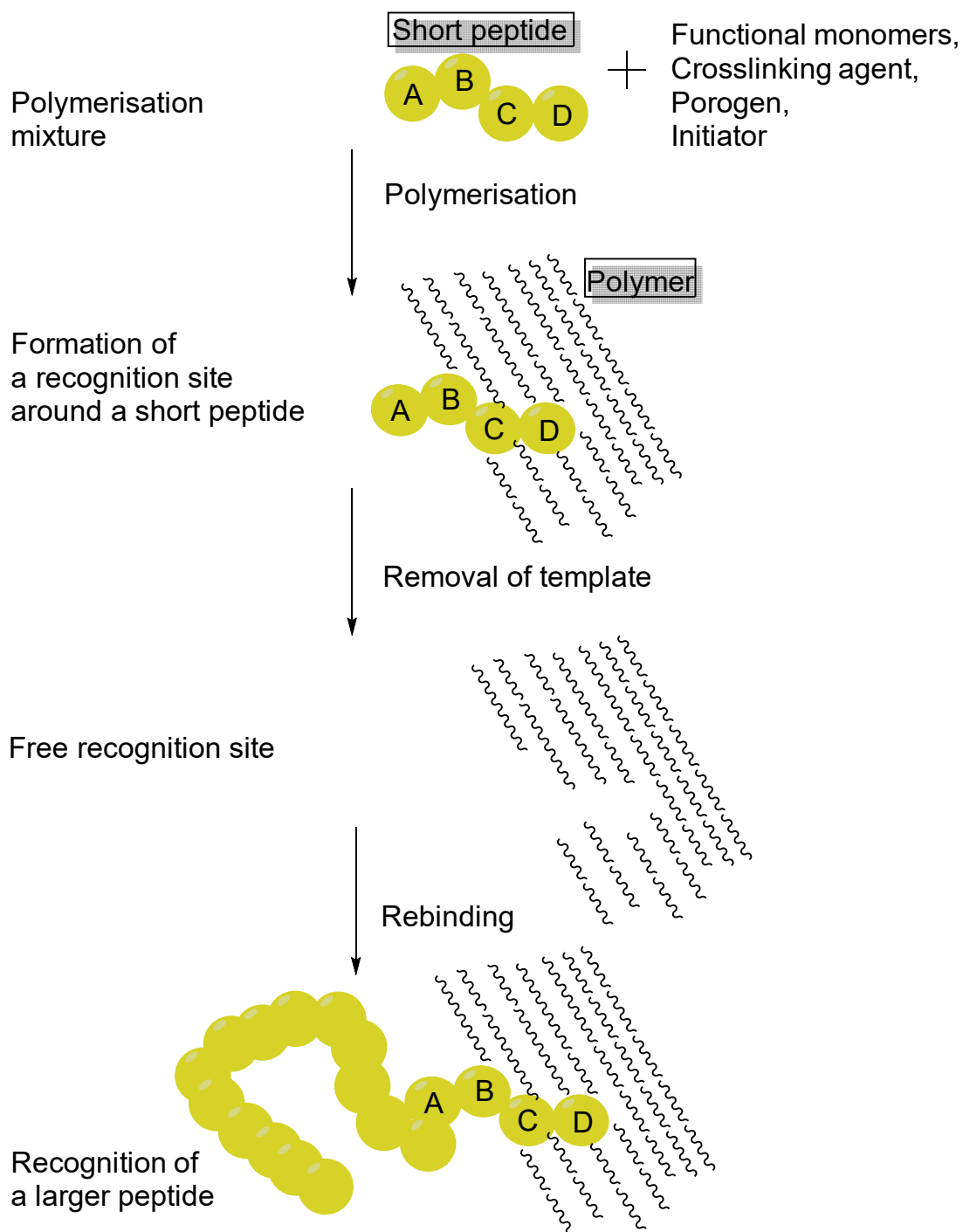


Figure 1.10 Schematic representation of the epitope approach. Scheme adapted from ref.<sup>80</sup>.

The advantages of the epitope approach over other approaches include: reduction of the non-specific interactions between MIPs and proteins, and minimisation of embedding of the proteins in polymer networks. Also, the costs of the synthesis of

polymers are reduced by using this approach as the whole target is not required. What is more, the proteins that will bind to the polymer are properly oriented.<sup>73</sup> Target sites in the proteins are directed towards the binding sites which are present inside the polymer network.

The signature peptide imprinting is another approach for the synthesis of protein-imprinted polymers. This approach largely resembles the epitope approach. Here again, a part of the target peptide/ protein is imprinted. However, in this approach, the selected fragment of amino acids for the imprinting, is generated from the enzymatic digestion of the target peptide/ protein. In the proteomics, serine protease trypsin is used for the cleavage of bonds in the C- terminal ends of lysine and arginine with the exceptions of lysine-proline and arginine-proline sites. This proteolytic digestion of peptide/ protein leads to generation of peptides with the molecular weights which can be analysed by mass spectrometry (MS). The peptides formed after such a digestion are known as the signature peptides and they are used as diagnostic representatives for the analytical analysis by MS.<sup>83,84</sup> When this approach is applied to molecular imprinting, the binding sites formed inside dense polymer network allow for binding to the signature peptide.<sup>61,85</sup> Advantages of this approach include: the whole proteins do not have to be used either for the synthesis of MIPs and/ or for the analysis. It is not important to maintain the native structure of proteins as the whole proteins are not required for the synthesis of MIPs and further for the analysis. The structural variances of proteins do not have an influence on the synthesis of MIPs and analysis, as an unique short sequence of the peptide derived from targeted protein, the signature peptide is imprinted only.<sup>86</sup>

## 1.4. Formats of MIPs

### 1.4.1. Macroreticular polymers

#### 1.4.1.1. *Precipitation polymerisation (PP)*

Near monodisperse and surfactant-free spherical polymer particles in the micron size range can be synthesised by the precipitation polymerisation (PP) method. The PP technique was first reported for the synthesis of polydivinylbenzene in the early 1990s.<sup>87</sup> Highly crosslinked polymer microspheres with uniform size and shape were synthesised as the result of reactions employing three components only: monomer, initiator and solvent.

PP involves the polymerisation of vinyl monomers under dilute solution conditions (the monomer concentration is typically < 5% w/v) in a near- $\theta$  solvent, and in the absence of any added surfactants.<sup>87–89</sup> Polymer microspheres are formed as a result of entropic precipitation of polymer from solution, as presented schematically in Figure 1.11. Two stages are included in this process: nucleation and growth. At the beginning of PP, soluble oligomers form aggregates, which leads to the formation of swollen microgels. Then, microgels undergo internal desolvation and stable nuclei are produced. In the next stage, oligomer radicals react with vinyl groups present on the particle surfaces, and this results in continual growth of microspheres.<sup>90</sup>

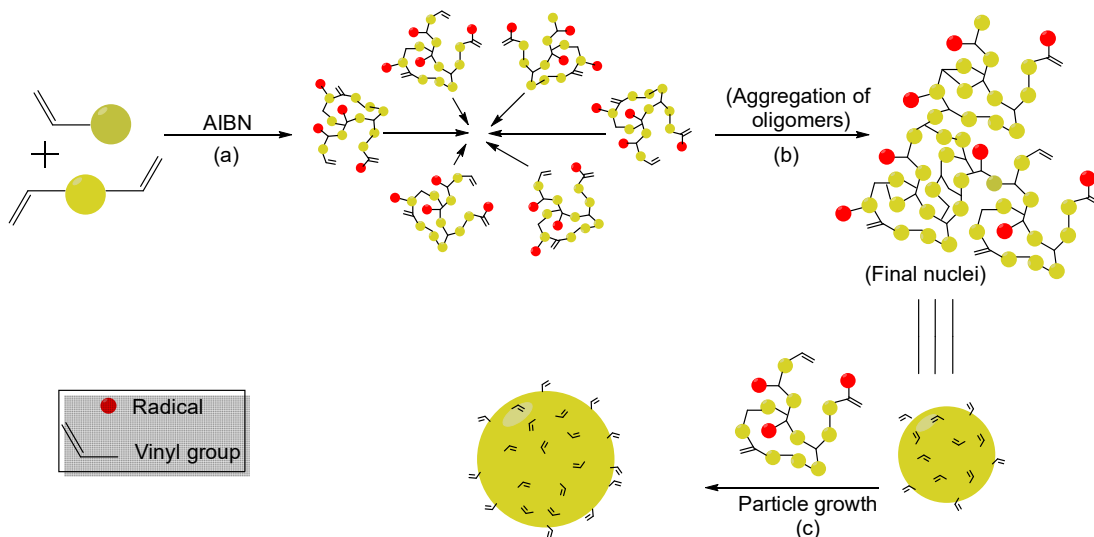


Figure 1.11. Schematic representation of the mechanism of microsphere formation in PP, which includes the following stages: (a and b) the particle nucleation and (c) particle growth. Scheme adapted from ref.<sup>91</sup>.

Polymer microspheres are formed through PP as the result of the conversion of vinyl monomer(s) by free radical polymerisation to product. A schematic representation of the mechanism is shown in Figure 1.12. The mechanism represents steps which are responsible for the conversion of styrene into polystyrene. Three stages can be distinguished: initiation, propagation and termination. The initiation step includes two important reactions: decomposition of the initiator to form two radicals, followed by their attack on monomers. The initiator is 2-2'-azobisisobutyronitrile (AIBN), which can decompose either thermally or photochemically to give cyanoisopropyl radicals and nitrogen. The union of cyanoisopropyl radical species with monomers results in breaking of double bonds and the formation of initiated monomer species. The propagation process involves the sequential addition of monomer units to propagating polymer chains. The termination process occurs by combination: two propagating radical chains combine at their free radical ends.<sup>92</sup>



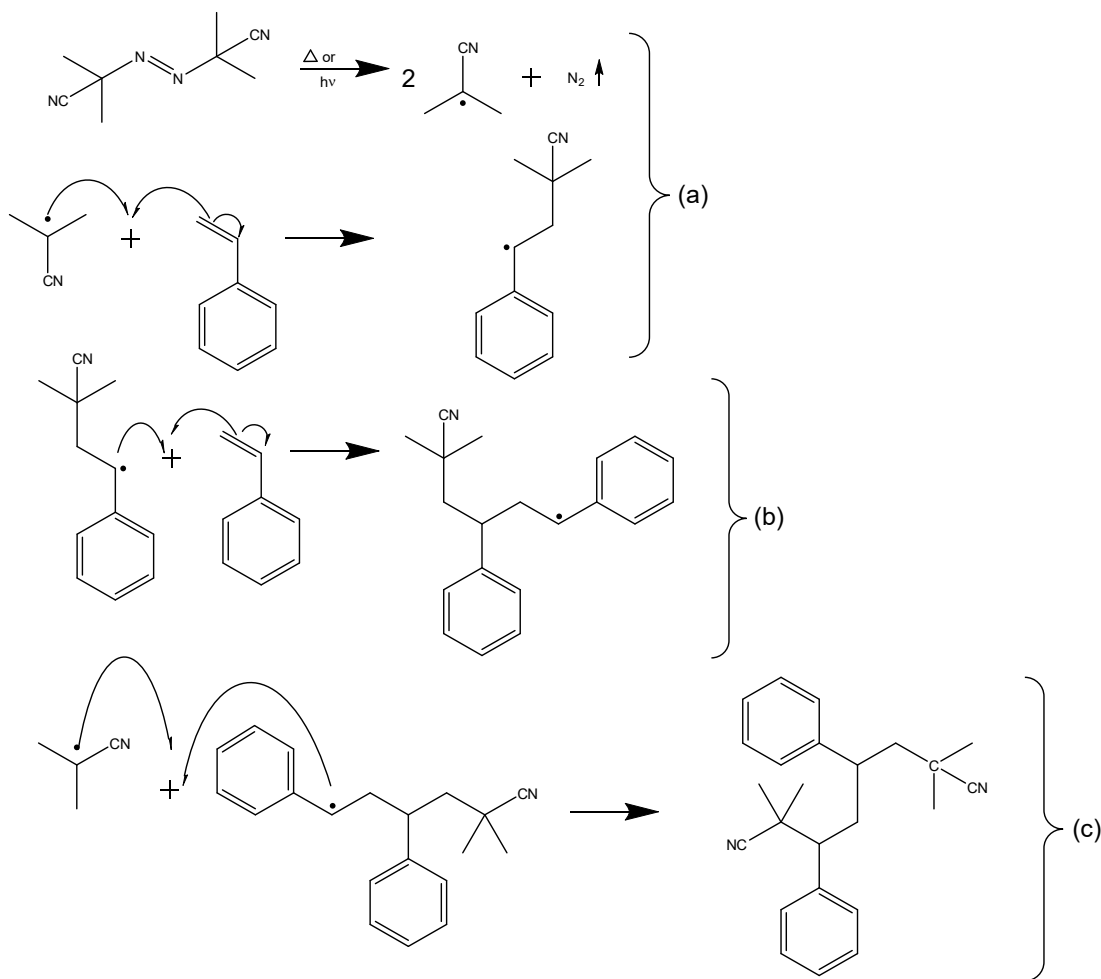


Figure 1.12 Mechanism of free radical polymerisation of styrene, which includes the stages: (a) initiation, (b) propagation and (c) termination by combination of two polymer radicals.

The inclusion of co-solvents such as toluene into the PP medium can significantly improve the porosity and homogeneity of divinylbenzene-based microspheres. In this case, phase separation occurs later.<sup>88</sup> The PP method also proves to be equally effective for the synthesis of copolymer microspheres with narrow particle size distributions.<sup>93</sup> Additionally, the final particle size can be controlled. As was observed for the synthesis of poly(styrene-co-divinylbenzene) microspheres by Choe and others, higher concentrations of divinylbenzene in acetonitrile leads to a smaller size of the final nuclei.<sup>94</sup> However, it is not always true.<sup>88</sup> On the other hand, when the concentration of divinylbenzene increases, the yield of polymerisation rises as well.<sup>94,95</sup> Control over the polymerisation yield of divinylbenzene-based products can also be achieved by changing the reaction time. An extension in polymerisation time

contributes to higher yield. However, it is necessary to keep in mind that sometimes longer syntheses lead to the production of microspheres with broader size distribution. This happens because irreversible agglomerates are formed as a consequence of insufficient toughness of the polymer network at the particle surface.<sup>96</sup> An interesting modification of the PP method was proposed by Yang and co-workers. Instead of the acetonitrile that is typically used as a porogen in the PP of DVB, they used acetic acid as a solvent. This change led to the synthesis of monodisperse divinylbenzene microspheres, while maintaining the crosslinking monomer in very low concentration. For the syntheses with the higher divinylbenzene content, inclusion of co-solvents (methyl ethyl ketone or *n*-heptane) was necessary.<sup>68,97</sup>

#### 1.4.1.2. *Synthesis of macroreticular MIPs*

The main benefits of spherical MIPs over MIPs prepared in the traditional form known as monoliths, are as follows:

- Spherical MIP particulates are less prone to fragmentation and are more physically durable during handling than their irregularly-shaped, crushed counterparts;
- They are packaged more efficiently in analytical columns, giving better flow properties and lower back pressures, thus providing better separation;
- Other characteristics of MIP microspheres are: significantly faster binding kinetics, better accessibility of binding sites, higher binding affinity and specificity to target analytes.<sup>57</sup>

PP is an attractive and relatively simple procedure for producing imprinted polymer microspheres. Highly crosslinked MIPs with rigid pore networks are synthesised in this process. The PP method was applied to the production of MIP microspheres for the first time in the late 1990s.<sup>14</sup> Cormack and Mosbach popularised this method as a microsphere production technique for imprinting. A few years later, the group of Cormack shed new light on the PP method as used for the synthesis of spherical MIPs. The size and porosity of imprinted microspheres can be easily controlled by the

changes in PP conditions. Among these changes are different concentrations of monomers and initiator, and various compositions of solvent, for instance, use of toluene as a co-solvent significantly improves the porosity of the imprinted microspheres.<sup>98</sup> Precise size control of MIP spherical particulates, from around 0.1  $\mu\text{m}$  to 10  $\mu\text{m}$  can also be effectively achieved by changes in the polymerisation conditions. Use of trimethylolpropane trimethacrylate as a crosslinker results in the production of small microspheres in relatively higher yield, whereas divinylbenzene leads to larger microspheres in relatively lower yield.<sup>99</sup>

The advantages of the PP technique for the preparation of MIP microspheres include:

- PP does not require the addition of surfactants or stabilisers. The surfaces of the particles are therefore free from residual additives;
- 0.1-10  $\mu\text{m}$  is the typical size range accessible for the polymer microspheres, and this can be controlled by changing of the PP conditions;
- Reaction yields can in some cases be close to quantitative;
- Near monodisperse microspheres of high quality can be produced in one synthetic step.<sup>100</sup>

In this Thesis, MIPs in the form of microspheres were the desired product format, and PP was chosen as the preferred method for their production.

The PP method has met with great interest from the scientific community. In the literature, there are many examples of successfully implemented PP procedures for the synthesis of MIP microspheres. These include MIPs for targeting the following molecules: propazine,<sup>101</sup> thiabendazole,<sup>102</sup> salicylicazosulfapyridine (sulfasalazine),<sup>27</sup> carbamazepine,<sup>103</sup> (S)-nicotine,<sup>104</sup> 17 $\beta$ -estradiol,<sup>105</sup> theophylline,<sup>98,100,105</sup> bupivacine,<sup>106</sup> caffeic acid,<sup>107</sup> and barbital.<sup>108</sup>

A typical PP procedure for the synthesis of NIPs and MIPs commences with the definition of scale, type of reaction vessel, components, incubation time, and washing solvents. Firstly, the components are added to the reaction vessel: template, co-solvent and porogen, functional monomers, crosslinker, and initiator. If the final

product is a NIP, then addition of template is omitted. Further steps include: removal of oxygen from the reaction solution through nitrogen purging, polymerisation through incubation and finally isolation of insoluble polymer products (Figure 1.13).

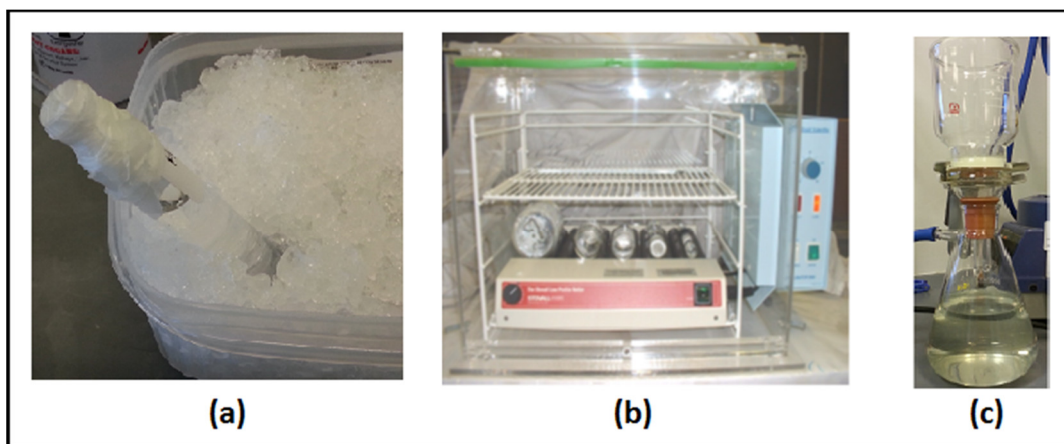


Figure 1.13. Experimental steps in a PP procedure: (a) nitrogen purging, (b) incubation, and (c) product isolation.

Modifications of the PP method have resulted in the development of protocols that allow for the synthesis of MIP microsphere variants: core-shell and grafted spherical particulates. Through the application of a two-step PP procedure, core-shell MIP microspheres can be prepared.<sup>109,110</sup> MIP microspheres with grafted morphology can be synthesised by introduction of a controlled radical polymerisation mechanism into a PP system.<sup>91</sup>

## 1.4.2. Core-shell polymers

### 1.4.2.1. Core-shell particles

Particles with core-shell architecture are formed as the result of merging two materials, often with distinctive properties: the core material is surrounded by the shell material. A highly schematic representation of a particle with core-shell structure is shown in Figure 1.14. The core can be either a single polymer microsphere and/or agglomerates of several polymer microspheres. The shells can also surround the hollow cores with a small particles inside. The shell layer can have distinctive

character as well. The shell can be a continuous layer, as is shown in the Figure 1.14 or multiple shell layers. Also, the shells can be formed as the self-assembly of small microspheres around a big core microspheres. Small microspheres can be incorporated into continuous shell layers and in such a way the complex form can surround the core particles. Depending on synthetic conditions, it is possible to control the physicochemical properties of core and shell, the shell thickness and the size of the core particles.<sup>111</sup>

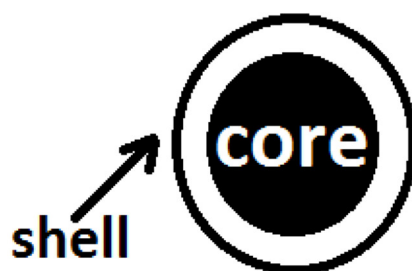


*Figure 1.14 Schematic representation of core-shell particle.*

The concept of core-shell particles was suggested initially by Golay at the Gas Chromatography Symposium at Edinburgh in 1960.<sup>112</sup> A few years later, Horvath and Lipsky produced an ion exchange resin in the form of glass beads coated with poly(styrene-co-divinylbenzene). The coated glass beads were applied for the first time in a liquid-solid chromatography (LSC) system for the separation of ribonucleoside mono-, di-, and triphosphates.<sup>113,114</sup> Outstanding separation was achieved, but the finding did not meet with scientific interest due to the type of used stationary phase. At the same time, Kirkland synthesised the silica core particles with a controlled porosity layer, coated with liquid stationary phase,  $\beta$ ,  $\beta'$ -oxydipropionitrile. The particles were applied in a liquid-liquid chromatography (LLC) system.<sup>115</sup> For the first time, thickness and average pore size were controlled and this material was deemed to be the precursor of the first generation of the core-shell particles.<sup>116</sup> In the early 1970s, the application of the first generation core-shell particles in a LLC system were exploited commercially and a range of the products became available on the market: 37  $\mu\text{m}$  Corasil I and 50  $\mu\text{m}$  Corasil II, 50  $\mu\text{m}$  Zipax,

50  $\mu\text{m}$  Pellicosil. However, extensive studies revealed certain drawbacks with the use of this type of polymer material in a LLC system and this ended the interest in the first generation of core-shell particles.<sup>116</sup> In order to overcome the problems such as poor retention resulting from low specific surface area, the first generation core-shell particles, Zipax were modified through binding functional groups such as tri-functional silanes to their surfaces. The material was commercialised by DuPont under the name Permaphase ETH and OS.<sup>117–119</sup> Further improvements in the core-shell technology resulted in the synthesis of core-shell particles with an average particle size of 7  $\mu\text{m}$ , known as the Poroshell 300, and considered as the second generation of core-shell particles. The particles were significantly distinct from the previous generation due to the synthetic approach used for their preparation. The particles were prepared by the spray-drying method, where silica core particles were suspended in silica sol. After the spraying and drying steps, the silica core particles were coated with thin layer of silica from the sol. Improved mass transfer was observed, compared with the previous generation of particles, but the core particles were usually unevenly or partially coated with the shell layers. Also, apart from the shell layers formed on the silica cores particles, a fraction of newly porous microspheres from the sol were formed during the spraying process. There was the tendency to form particles with broad particle size distribution.<sup>120,121</sup> Therefore, the method for the synthesis of the second generation particles was modified further through the application of coacervation method. This method again had a certain drawback and the need towards further improvement of the core-shell particles still existed.<sup>122</sup> The third generation of core-shell particles, silica based, met with high scientific interest. The particles with core-shell morphology are expected to be bigger than their non-core-shell counterparts and their size can be easily controlled. Therefore, one of the advantages of core-shell particles as packing materials is the separation operates under relatively low back pressure and fast flow rate at the same time.<sup>6</sup> The core-shell particles form solid cores and porous shells. Thanks to this, high surface area is provided for the separation.<sup>7</sup> The particles with high surface area usually have small pore volumes which helps significantly to reduce the diffusion path

lengths which contributes to rapid mass transfer.<sup>124</sup> In addition, the shell thickness influences the mass transfer. When the shell thickness is decreased, fast mass transfer is observed and it contributes to an improvement in column efficiency and elution time.<sup>111,125–127</sup>

#### 1.4.2.2. Synthesis of core-shell MIPs by two-step PP

Core-shell particles can be prepared by different methods. In the following, the main focus is on core-shell microspheres prepared by PP, as it was the main synthetic method used for the synthesis of the MIP core-shell variants in the work presented here. In 2000, Li and Stöver demonstrated that PP can be used effectively for the synthesis of core-shell polymer microspheres. PP opens the possibility to synthesise core-shell particles in two ways: either by a two-step batch mode or semi-batch *in situ* mode. In the two-step method, the crosslinked core polymer microspheres are firstly prepared by a typical PP. Then, these core particles are used as the seed particles in a subsequent polymerisation for the preparation of the core-shell polymers. The semi-batch *in situ* mode involves the synthesis of the polymer cores and shells in a single reaction vessel using two sequential reaction periods. Co-monomer(s) and/or crosslinker which form the polymer shell are added to the polymerisation vessel after a certain polymerisation time.<sup>93</sup> It is worth pointing out that particles with narrow particle size distribution (PSD) should be maintained during the whole synthesis. Therefore, the addition of crosslinker in the second stage of the PP when the shell layer is formed is a key requirement. The crosslinker contributes to formation of a solvent-swollen gel layer on the surface of the polymer cores. The layer sterically stabilises the core-shell particles and inhibits homocoagulation, thus it prevents the formation of particles with broad PSD.<sup>128</sup> The size of the core and the thickness of the shell can be tuned through changing the reaction conditions, *e.g.*, inclusion of the co-solvent and/or co-monomer(s).<sup>93</sup> The introduction of co-solvents, such as toluene into the PP medium can significantly improve the porosity and homogeneity of divinylbenzene-based microspheres.<sup>88</sup> The final particle size of the polymer cores can be controlled through changing the concentration of the

crosslinking agent. Higher concentrations of divinylbenzene in acetonitrile leads to a smaller size of the final nuclei.<sup>94</sup> Further exploration of the PP procedure as a synthetic method for the preparation of core-shell particles was reported by Huang and others. They successfully proved the use of wide range of co-monomers incorporated into the polymer shell layers. These include co-monomers with the following functional groups: ester, hydroxyl, chloromethyl, carboxylic acid, amide, cyano and glycidyl groups.<sup>129</sup> The formation of a new fraction of particles besides the core-shell particles, also known as secondary nucleation, is probably the main problem to deal with during PP. Two competing reactions can be distinguished in the second step of the PP. When oligomer radicals react with residual double bonds present on the surfaces of the polymer cores, then shell layers are formed. When soluble active radicals reacts themselves or with soluble oligomers, then new particles known as the secondary particles are initiated. The capture of soluble oligomers from solution is dependent on the content of residual double bonds and degree of crosslinking in the solvent-swollen gel layer. When the number of residual double bonds and the degree of crosslinking are high, the soluble oligomers are captured effectively and then secondary nucleation is minimised. Therefore, secondary nucleation is favoured when a large quantity of co-monomer is added in the second step of the PP.<sup>128</sup> In 2011, Barahona and others used two-step PP for the first time for the synthesis of core-shell MIPs. Non-imprinted poly(DVB-80) microspheres, preformed in the first step of PP, were successfully used as the seed particles for the synthesis of imprinted poly(DVB-80-co-MAA) core-shell microspheres for a thiabendazole (TBZ) target. The MIPs in the micron-sized range were applicable as a stationary phase in liquid chromatography.<sup>110</sup> Another example of successfully prepared core-shell MIPs are polymers for the bisphenol A target. Wang and others used non-imprinted poly(DVB-80) core particles as the seeds for the synthesis of core-shell MIPs. The composition of the solvent used for the synthesis of core-shell MIPs were optimised by manipulation of the ratio of toluene to acetonitrile. The use of toluene in the concentration range between 15% - 30%



allowed for exclusion of secondary nucleation and/or agglomeration of the particles.<sup>130</sup>

### 1.4.3. Magnetic polymers

#### 1.4.3.1. *Magnetic particles*

Magnetic particles are a class of particles that can be manipulated using magnetic fields. Magnetic particles possess their magnetic properties thanks to components included in their structure such as iron, nickel and cobalt.<sup>131</sup>

Magnetite and maghemite include iron in their structures and possess strong magnetic properties, therefore both can be used as the magnetic components for the synthesis of superparamagnetic particles. The co-precipitation of FeCl<sub>3</sub> and FeCl<sub>2</sub> under basic condition (at a pH between 8 and 14) results in the formation of either magnetite, Fe<sub>3</sub>O<sub>4</sub>, or maghemite, γFe<sub>2</sub>O<sub>3</sub>. The synthesis of magnetite as shown in the first equation in Figure 1.15 requires anaerobic conditions in contrast to maghemite. However, the magnetite is not very stable and can be easily transformed to maghemite under oxidizing conditions, as shown in the second equation in Figure 1.15.<sup>132,133</sup>

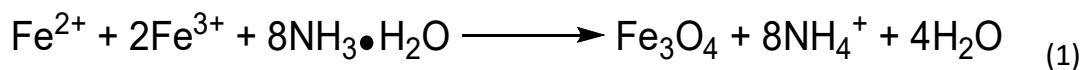


Figure 1.15 Synthesis reactions of magnetite (1) and maghemite (2).

### 1.4.3.2. *Synthesis of magnetic MIPs*

Magnetic MIPs are desirable because they can be localised using magnet. This would allow simplification of separation science applications since magnetic capture can be used to localise the MIPs.

The magnetic MIPs can be prepared either by encapsulation of magnetic nanoparticles within the polymer network<sup>134–136</sup> or by the growth of magnetic particles within and on the surfaces of the polymer network in a post-polymerisation magnetisation step.<sup>137</sup> The synthesis of magnetic MIPs usually consists of four steps. The first two steps include preparation of magnetic particles, during which their synthesis and functionalisation take place. These two steps can be skipped if commercially available magnetic particles with desirable functional groups are used. Magnetic particles are widely commercially available and can be easily purchased with different functional groups. In the third step, functionalised magnetic particles are added into the reaction vessel together with template, functional monomer(s) and crosslinker. These magnetic particles are used as the seed particles for the synthesis of magnetic MIPs. Growth of the MIPs takes place on the surfaces of the functionalised magnetic particles, and magnetic particles are encapsulated inside MIPs. In the last step, the template molecule is extracted and the magnetic MIPs are ready for further characterisation.<sup>138</sup>

Magnetic molecularly imprinted polymers were prepared for the first time by Mosbach and Ansell in the late 1990s. They used suspension polymerisation for the incorporation of iron oxide particles into poly(MAA-co-TRIM) MIP and corresponding NIP. Such a prepared MIP was used successfully for radioligand assay for the binding of the  $\beta$ -blocker (*S*)-propranolol.<sup>139</sup> In the literature, there are many examples of magnetic MIPs used for the detection of compounds in biological or environmental samples prepared by different polymerisation methods. These include: core-shell vinyl-modified silica coated magnetic MIPs and polyethylene glycol-modified MIP particles for herbicide residues<sup>140,141</sup>, nanocomposites with amino-modified magnetic

particles for (*S*)-propranolol synthesised by surface-initiated RAFT polymerisation<sup>142</sup>, acrylamide-based magnetic MIPs for sulfonamide drugs<sup>143</sup> and others.<sup>144,145,146</sup>

#### 1.4.4. Hydrogels

Hydrogels are defined as polymer materials with three-dimensional network structures which are swellable in water. They can absorb and retain water, in some cases up to thousands of times of their dry weight.<sup>147,148</sup> The synthesis of hydrogels involves phase transition from the liquid state to the gel state at the gel point, at which stage the three-dimensional network structures have started to form. During the gel formation, phase separation can occur and voids or macropores filled with water are created. Depending on the type of bonds involved in the formation of the three-dimensional network structure, the following types of hydrogels can be distinguished: permanent, known as chemical, and reversible known, as physical. The first type, the chemically crosslinked hydrogels involve the formation of network structures by covalent interactions, while the second type, the physically crosslinked hydrogels include the creation of three-dimensional network structures by non-covalent interactions such as ionic and hydrogen bonds, hydrophobic effects and/or molecular entanglements.<sup>149</sup> The gel-like structure is formed when hydrophilic regions present in the polymer network absorb water from an aqueous environment and become hydrated.

This type of polymer material, a hydrogel, is composed mostly of water. The water molecules absorbed in hydrogels are classified according to their occurrence within the polymer network. The following type of water molecules are distinguishable: primary and secondary bound water, free and truly free water. Primary water occurs in the most polar regions and is bound to the polymer network by hydrogen bindings and ionic interactions. As these regions became hydrated with the primary water, the hydrogel network swells and hydrophobic groups became exposed. The secondary water is bound to the hydrophobic groups of the polymer network thanks to the occurrence of hydrophobic effect. The primary and secondary bound water are also known as the total bound water. The remaining water which surrounds the polymer

backbone, and which is not bound through the interactions mentioned above, is classified as free water. The free water molecules usually fill the pores and voids within the polymer network. The truly free water does not adhere in any way to the polymer backbone and is localised mainly in the centre of the pores and voids within the polymer network.<sup>149</sup>

Hydrogels are heterogenous materials; they are composed of regions with high crosslink density which are hardly swellable in water, and regions with low crosslink density, with high swellability in water. The crosslink degree in hydrogels is very low, and typically reaches 3% (w/w).<sup>147</sup> The chemically crosslinked hydrogels can be prepared by either redox polymerisation,  $\gamma$ - radiation, small molecule crosslinking, or condensation reaction.<sup>149</sup>

#### 1.4.4.1. *Redox polymerisation for the synthesis of hydrogels*

Hydrogels can be prepared by different methods. In the Thesis work, the main focus was on the hydrogels prepared by the redox polymerisation. Redox polymerisation is one of the method for the synthesis of the chemically crosslinked hydrogels. Low-molecular weight monomer, *e.g.*, acrylamide, polymerises in the presence of crosslinking agent, *e.g.*, *N,N'*-methylene bis(acrylamide) (BIS). The reaction is initiated by a redox initiator, *e.g.*, ammonium persulfate (APS), and a catalyst, *e.g.*, *N,N,N',N'*-tetramethylethylenediamine (TEMED). The rate of formation of free radicals from APS is accelerated by TEMED, as it promotes decomposition of APS to form radicals followed by their association to monomers. TEMED decreases the activation energy required for polymerisation by almost three times and hence allows the synthesis to proceed at low temperatures.<sup>150</sup> The decomposition of APS is shown in Figure 1.16.

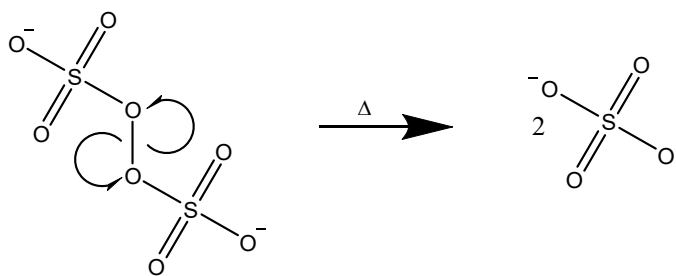


Figure 1.16 Decomposition of APS.<sup>150,151</sup>

Polyacrylamide-based hydrogels are formed by the free radical copolymerisation of acrylamide and BIS.<sup>152</sup>

#### 1.4.4.2. MIPs hydrogels

The Hjertén method is a well-known technique for the synthesis of molecularly imprinted hydrogels.<sup>153</sup> The method involves the synthesis of typical polyacrylamide-based hydrogels in the presence of protein targets. Acrylamide and BIS were used solely by Hjertén as the monomers in the formation of three-dimensional imprinted gel network structures. In this method, apart from acrylamide, other functional monomer(s) were not included in the polymerisation solution. Proteins (ribonuclease, haemoglobin, lysozyme, myoglobin and human growth factor) were imprinted in the polyacrylamide-based hydrogels. The hydrogels showed preferential recognition for their targets.<sup>153</sup> In addition to this, a further study performed by Hjertén revealed that this type of polymer material could be perfectly used for the discrimination between the structural variances of the same proteins: iron-free and iron-containing transferrin, and for the discrimination of the same proteins which came from different species such as human and bovine haemoglobin.<sup>154,155</sup>

More than 20 years have passed since the Hjertén method was first disclosed, and the mechanism of imprinting is still unknown. It would seem that hydrogen bonds were involved mainly in the process of imprinting, but the molecular recognition took place in aqueous solution, in an environment which is normally unfavourable for the formation of hydrogen bonds between target proteins and hydrogels as the water molecules compete with target molecules for the binding sites present in the

hydrogels. Therefore, it could be concluded that the sheer number of weak electrostatic interactions formed between the surface of the proteins and gels played a role in the selectivity. According to Hjérten, the properties of this type of gel are mainly dependent on degree of crosslinking, pH and ionic strength.<sup>153</sup> Further modification of the Hjérten method involved inclusion of functional monomers: acrylic acid and/or *N,N*-dimethyl-aminopropylacrylamide into hydrogel network(s)<sup>156</sup>. Lysozyme imprinted hydrogels were grafted on silica beads and exhibited high selective recognition for the target protein. This type of hydrogel was successfully used as the polymer film in a quartz crystal microbalance sensor for the recognition of lysozyme.<sup>156</sup> Ou and others used lysozyme again for the synthesis of imprinted polyacrylamide-based hydrogels. In their study, methacrylic acid was used as the functional monomer and 2-(dimethylamino)ethyl methacrylate. However, discrimination between the proteins tested (albumin and lysozyme) were not observed. In addition, the problem was template removal as 25% of the lysozyme remained entrapped in the hydrogels.<sup>157</sup> On the other hand, another study showed high selectivity for the haemoglobin by polyacrylamide-based imprinted hydrogels.<sup>158,159</sup> In addition, mechanical stability of the polyacrylamide-based imprinted hydrogels were improved by the entrapment of the gel network structure into porous chitosan beads.<sup>158,159</sup> The problem with the template removal from the gel network structure was studied extensively by Hawkins and others. The combination of surfactant, sodium dodecyl sulfate and acetic acid allowed for the extraction of 90% of the template from the imprinted hydrogels.<sup>160</sup>

As is outlined above, there were some successfully reported imprinted polyacrylamide-based hydrogels, however this type of polymer material still suffers from some limitations. Low crosslink degrees, which typically reached 3% (w/w) for this type of polymer materials, contributes to rapid loss of imprinted properties and the stability of hydrogels is highly affected by the changes in the environment.<sup>161,162,163</sup> Also, hydrogel-based imprinted polymers suffer from low mechanical robustness. Another problem discussed already is lack of complete extraction of the template from the imprinted gel network structure.

## 1.5. Characterisation of MIPs

Determination of the physical properties of MIPs, especially for the imprinted materials which would be potentially used in disease diagnosis, is important. Therefore, MIPs prepared together with their non-imprinted counterparts are normally characterised using a range of techniques including Optical Microscopy, Scanning Electron Microscopy (SEM), Nitrogen Sorption Porosimetry and Fourier-Transform Infrared (FT-IR) Spectroscopy. The main methods used in the current work are summarised here.

### 1.5.1. Nitrogen sorption porosimetry

Specific surface area and porosity are important features in the characterisation of polymers. The specific surface area defines the area which is exposed by one gram of solid. The term porosity is used to determine the ratio of volume of all interstices known as the pores in the polymer material to the volume of total polymer sample. High specific surface area usually corresponds to a polymer material with porous morphology. These properties are relevant in the characterisation of MIP morphology as they allow me to assess the possibility of the transportation of the analytes to the polymer phase. High specific surface area and big pores with narrow pore size distribution are desirable in the morphology of MIPs. They are related to better accessibility of the binding sites and permeability of MIPs, and therefore would be related with better recognition properties.<sup>161</sup>

The specific surface area and porosity can be determined using a nitrogen sorption method. The solid surface of the analysed sample is exposed to nitrogen which fills the pores and can form one or more layers on the surfaces of the analysed material. During this process, gas molecules are not restricted to cover the specific sites and are free to occupy the whole surface. This physical adsorption of gas molecules forms non-disruptive structural changes between the sites of analysed solid and the gas. Therefore, the method allows me to reuse the analysed samples as the process of physical adsorption does not affect the structure of material analysed. The

adsorption of gas molecules on the analysed sample is reversible and it permits observation both adsorption and desorption processes. The adsorption forces involved in this process are mainly dispersion forces, but other interactions are observed, such as: ion-dipole, ion-induced dipole, dipole-dipole and quadrupole interactions.<sup>164</sup> When the nitrogen gas molecules formed on the surface of the analysed solid sample form two or more layers, then the Brunauer, Emmet and Teller (BET) equation is used in order to calculate the specific surface area. BET equation is as follows<sup>165</sup>:

$$\frac{1}{V\left[\left(\frac{P_0}{P}\right) - 1\right]} = \frac{1}{V_m C} + \frac{C - 1}{V_m C} \left(\frac{P}{P_0}\right)$$

where,  $P_0$  and  $P$  correspond to the equilibrium and saturation pressures of the adsorbed gas at adsorption temperature,  $V$  and  $V_m$  represent the quantity of the adsorbed gas and the quantity of adsorbed gas on the monolayer surface, respectively.  $C$  stands for the BET *constant*, which equals  $\exp\left(\frac{E_1 - E_L}{RT}\right)$ , where  $E_1$  and  $E_L$  are energy of the adsorption in the first and the second and further layers.<sup>165</sup> The  $C$  value can define the strength of interactions between the gas molecules and the molecules of analysed samples. If the  $C$  value is less than 20, it indicates only weak adsorption interactions. If the value is more or equal to 20, but less than 100, it indicates only strong interactions between adsorbent and adsorbate.  $R$  and  $T$  are the gas constant and temperature of the gas.<sup>165</sup>

Important information which can be derived from the porosity analysis is the type of pores in the analysed material. IUPAC classifies pores according to their widths. The following types of materials can be distinguished: microporous, where the pore width is less than 2 nm, mesoporous structure with the pore width between 2 nm and 50 nm, and macroporous material with the pore width more than 50 nm.<sup>165</sup>



### 1.5.2. Microscopy analysis

Determination of the size and shape of newly synthesised polymers is important. Polymer microspheres with narrow particle size distributions are desirable for off-line and on-line Molecularly Imprinted Solid-Phase Extraction (MISPE).

In order to compare the polydispersities of the microspheres, statistical analysis was performed in R framework.<sup>166</sup> For this comparison, we used Welch's t-test<sup>167</sup>, which assumes different degrees of variation for each of the compared groups. The coefficient of variation (CV) measures the dispersity of the polymer microspheres in the analysed sample. It is expressed in percentages and given by:

$$CV = \frac{SD}{\bar{D}} \times 100\%$$

where  $SD$  and  $\bar{D}$  denote standard deviation and arithmetic mean, respectively. Depending on the CV value, the dispersity of the microspheres can be classified as follows:

- monodisperse if  $CV \leq 3.04\%$ ;
- quasi monodisperse if  $3.04\% < CV < 16\%$ ;
- polydisperse if  $CV \geq 16\%$ .<sup>168</sup>

The SD defines how closely a particle size distribution is grouped around the  $\bar{D}$  value. SD is given by the following formula:

$$SD = \sqrt{\frac{1}{n} \sum_{i=1}^n (D_i - \bar{D})^2}$$

where  $D_i$  is a diameter of a single microsphere and  $\bar{D}$  represents the arithmetic mean diameter of  $n$  repeat diameter measurements of microspheres.<sup>168</sup>

In order to check if two or more populations of microspheres have the same arithmetic mean diameter, the value of Welch's  $t$  statistic can be calculated using the following equation:

$$t' = \frac{\overline{D}_1 - \overline{D}_2}{\sqrt{\frac{S_1^2}{N_1} + \frac{S_2^2}{N_2}}}$$

where  $\overline{D}_1$  and  $\overline{D}_2$  are arithmetic mean diameters for the first and second compared population of microspheres.  $S_1$  and  $S_2$  are variances for the first and second compared populations of microspheres.  $N_1$  and  $N_2$  are the size of the first and second populations of microspheres. The degrees of freedom ( $\nu$ ) in Welch's  $t$ -test is calculated using a Welch–Satterthwaite equation<sup>169</sup>:

$$\nu \approx \frac{\frac{S_1^2}{N_1} + \frac{S_2^2}{N_2}}{\frac{S_1^4}{N_1^2 \times \nu_1} + \frac{S_2^4}{N_2^2 \times \nu_2}}$$

where  $\nu_1 = N_1 - 1$  and  $\nu_2 = N_2 - 1$  are the degrees of freedom associated with the first and the second variance, respectively.  $S_1$  and  $S_2$  are variances for the first and second compared population of microspheres.  $N_1$  and  $N_2$  are the size of the first and second population of microspheres.<sup>169</sup>

After the values of  $\nu$  and  $t$  are calculated for both statistical samples using the presented formulas, one checks the two-sided probability of the null hypothesis in the  $t$ -distribution parameterized using the determined values. This probability is abbreviated as a  $p$ -value in tables/ plots.

## 1.6. Aims and scope of work

The design, synthesis, characterisation and exploitation of MIPs for peptide targets was main goal of the Thesis. The synthesis of protein-imprinted polymers has always been challenging. Proteins are large and complex molecules with conformational flexibility along their backbone. They are typically insoluble in organic solvents, which makes them even more tricky to imprint.<sup>72</sup> The mobility of large molecules such, as proteins, are limited within highly crosslinked polymer networks, and this may prevent efficient protein template removal.<sup>73</sup> Also, the conditions that are used for the removal of the protein template from the prepared polymer have to be chosen carefully. There is a risk that the binding sites created in the polymer network can interact with the components that are present in the washing solvent, for instance with sodium dodecyl sulfate (SDS), resulting in creation of polymer sorbents with non-specific binding sites known as artefacts.<sup>74</sup>

*Robust Affinity Materials for Applications in Proteomics and Diagnostics* (PEPMIP) was a collaborative research project, involving twelve European partner institutions within Germany, Sweden, Norway, Denmark and the UK. The research work in PEPMIP was concentrated on creating robust materials for applications in proteomics and diagnostics, with particular focus on artificial receptors developed by various molecular imprinting techniques.<sup>170</sup>

An objective in the project was to design, synthesise, characterise and deliver optimised imprinted materials which can enable selective extractions of biomarker targets from native blood or cerebrospinal fluid samples.

Accordingly, the aims of the work presented in this Thesis were as follows:

- Design of MIPs for  $\beta$ -Amyloid, ProGRP and  $\alpha$ -Synuclein targets;
- Design of core-shell MIP variants for  $\beta$ -Amyloid and ProGRP targets;
- Design of magnetic MIP variants for  $\beta$ -Amyloid and ProGRP targets;
- Design of hydrogel MIP variants for  $\alpha$ -Synuclein target;

- Synthesis of polymer macroreticular materials for  $\beta$ -Amyloid, ProGRP and  $\alpha$ -Synuclein targets;
- Synthesis of core-shell variants for  $\beta$ -Amyloid and ProGRP targets;
- Synthesis of magnetic variants for  $\beta$ -Amyloid and ProGRP targets;
- Synthesis of hydrogel MIP variants for  $\alpha$ -Synuclein target;
- Characterisation of materials produced;
- Delivery of the next generation of materials to the PEPMIP partners for evaluation of molecular recognition and exploitation in new bioanalytical methods.

## 1.7. Bibliography

- 1 P. A. G. Cormack, in *Encyclopedia of Supramolecular Chemistry*, eds. J. L. Atwood and J. W. Steed, Taylor & Francis, 2004.
- 2 F. Puoci, G. Cirillo, M. Curcio, F. Iemma, O. I. Parisi, U. G. Spizzirri and N. Picci, in *Biopolymers*, ed. M. Elnashar, InTech, 2010, p. 548.
- 3 M. V. Polyakov, *Zhur. Fiz. Khim.*, 1931, **2**, 799–805.
- 4 M. Resmini, K. Flavin and D. Carboni, *Top. Curr. Chem.*, 2012, **325**, 307–342.
- 5 F. Dickey, H, *J. Phys. Chem.*, 1955, **59**, 695–707.
- 6 G. Wulff and A. Sarhan, *Angew. Chem. Int. Ed.*, 1972, **11**, 341–344.
- 7 H. Zhang, L. Ye and K. Mosbach, *J. Mol. Recog.*, 2006, **19**, 248–259.
- 8 R. Arshady and K. Mosbach, *Macromol. Chem. Phys.*, 1981, **182**, 687–692.
- 9 A. Cameron, H. S. Andersson, L. I. Andersson, R. J. Ansell, N. Kirsch, I. A. Nicholls, J. O'Mahony and M. J. Whitcombe, *J. Mol. Recog.*, 2006, **19**, 106–80.
- 10 P. A. G. Cormack and K. Mosbach, *React. Funct. Polym.*, 1999, **41**, 115–124.
- 11 B. Sellergren and L. Andersson, *J. Org. Chem.*, 1990, **55**, 3381–3383.
- 12 M. J. Whitcombe, M. E. Rodriguez, P. Villar and E. N. Vulfson, *J. Am. Chem. Soc.*, 1995, **117**, 7105–7111.
- 13 G. Vlatakis, L. I. Andersson, R. Muller and K. Mosbach, *Nature*, 1993, **361**, 645–647.
- 14 L. Ye, P. A. G. Cormack and K. Mosbach, *Anal. Commun.*, 1999, **46**, 35–38.
- 15 A. Beltran, R. M. Marcé, P. A. G. Cormack, D. C. Sherrington and F. Borrull, *J. Sep. Sci.*, 2008, **31**, 2868–2874.

- 16 N. Harun, R. A. Anderson and P. A. G. Cormack, *Anal. Bioanal. Chem.*, 2010, **396**, 2449–2459.
- 17 C.-H. Hsu, Y.-J. Cheng, B. Singco and H.-Y. Huang, *J. Chromatogr. A*, 2011, **1218**, 350–358.
- 18 B.-Y. Huang, Y.-C. Chen, G.-R. Wang and C.-Y. Liu, *J. Chromatogr. A*, 2011, **1218**, 849–855.
- 19 M. Kempe and K. Mosbach, *J. Chromatogr. A*, 1995, **691**, 317–323.
- 20 E. Turiel, J. L. Tadeo, P. A. G. Cormack and A. Martín-Esteban, *Analyst*, 2005, **130**, 1601–1607.
- 21 X.-C. Liu and K. Mosbach, *Macromol. Rapid. Commun.*, 1998, **19**, 671–674.
- 22 M. Tada, T. Sasaki, T. Shido and Y. Iwasawa, *Phys. Chem. Chem. Phys.*, 2002, **4**, 5899–5909.
- 23 A. Gräfe, K. Haupt and G. J. Mohr, *Anal. Chim. Acta*, 2006, **565**, 42–47.
- 24 T. Alizadeh and F. Rezaloo, *Sens. Actuators B Chem.*, 2013, **176**, 28–37.
- 25 M. Zayats, M. Lahav, A. B. Kharitonov and I. Willner, *Tetrahedron*, 2002, **58**, 815–824.
- 26 G. Ciardelli, C. Borrelli, D. Silvestri, C. Cristallini, N. Barbani and P. Giusti, *Biosen. & Bioelec.*, 2006, **21**, 2329–2338.
- 27 F. Puoci, F. Iemma, R. Muzzalupo, U. G. Spizzirri, S. Trombino, R. Cassano and N. Picci, *Macromol. Biosci.*, 2004, **4**, 22–26.
- 28 G. Cirillo, O. I. Parisi, M. Curcio, F. Puoci, F. Iemma, U. G. Spizzirri and N. Picci, *J. Pharm. Pharmacol.*, 2010, **62**, 577–582.
- 29 M. T. Jafari, B. Rezaei and B. Zaker, *Anal. Chem.*, 2009, **81**, 3585–3591.

- 
- 30 M. Lasáková, D. Thiébaud, P. Jandera and V. Pichon, *J. Sep. Sci.*, 2009, **32**, 1036–1042.
- 31 J. L. Urraca, C. S. A. Aureliano, E. Schillinger, H. Esselmann, J. Wiltfang and B. Sellergren, *J. Am. Chem. Soc.*, 2011, **133**, 9220–9223.
- 32 H. Yan, K. H. Row and G. Yang, *Talanta*, 2008, **75**, 227–232.
- 33 M. K.-Y. Li, N.-Y. Lei, C. Gong, Y. Yu, K.-H. Lam, M. H.-W. Lam, H. Yu and P. K.-S. Lam, *Anal. Chim. Acta*, 2009, **633**, 197–203.
- 34 J. Fan, Y. Wei, J. Wang, C. Wu and H. Shi, *Anal. Chim. Acta*, 2009, **639**, 42–50.
- 35 H. Sun and F. Qiao, *J. Chromatogr. A*, 2008, **1212**, 1–9.
- 36 L. Núñez, E. Turiel, A. Martín-Esteban and J. L. Tadeo, *J. Sep. Sci.*, 2008, **31**, 2492–2499.
- 37 O. Zamora, E. E. Paniagua, C. Cacho, L. E. Vera-Avila and C. Perez-Conde, *Anal. Bioanal. Chem.*, 2009, **393**, 1745–1753.
- 38 H. Yan, M. Tian and K. H. Row, *J. Sep. Sci.*, 2008, **31**, 3015–3020.
- 39 T. Jing, X.-D. Gao, P. Wang, Y. Wang, Y.-F. Lin, X.-Z. Hu, Q.-L. Hao, Y.-K. Zhou and S.-R. Mei, *Anal. Bioanal. Chem.*, 2009, **393**, 2009–2018.
- 40 C. Long, Z. Mai, Y. Yang, B. Zhu, X. Xu, L. Lu and X. Zou, *J. Chromatogr. A*, 2009, **1216**, 2275–2281.
- 41 S. Wang, L. Liu, G. Fang, C. Zhang and J. He, *J. Sep. Sci.*, 2009, **32**, 1333–1339.
- 42 C. Cacho, L. Schweitz, E. Turiel and C. Pérez-Conde, *J. Chromatogr. A*, 2008, **1179**, 216–223.
- 43 L. A. Pereira and S. Rath, *Anal. Bioanal. Chem.*, 2009, **393**, 1063–1072.
- 44 K. Mosbach and O. Ramström, *Nat. Biotech.*, 1996, **14**, 163–170.

- 45 www.webmd.com, *Drugs & Medications Theophylline*, 2014.
- 46 D. A. Spivak, *Adv. Drug Deliv. Rev.*, 2005, **57**, 1779–1794.
- 47 K. Haupt and K. Mosbach, *Trends. Biotech.*, 1998, **16**, 468–475.
- 48 G. Wulff and K. Knorr, *Bioseparation*, 2001, **10**, 257–276.
- 49 B. Sellergren, *J. Chromatogr. A*, 2001, **906**, 227–252.
- 50 J. O’Mahony, A. Molinelli, K. Nolan, M. R. Smyth and B. Mizaikoff, *Biosens. Bioelectron.*, 2005, **20**, 1884–93.
- 51 K. E. van Holde, W. C. Johnson and P. S. Ho, *Principles of Physical Biochemistry*, Pearson Prentice Hall, Upper Saddle River, New Jersey, 2nd edn., 2006.
- 52 J. N. Israelachvili, *Intramolecular and Surface Forces*, Elsevier Inc., San Diego, California, 3rd edn., 2011.
- 53 M. J. Berg, L. J. Tymoczko and L. Stryer, *Biochemistry*, W.H. Freeman and Company, 5th edn., 2002.
- 54 E. A. Meyer, R. K. Castellano and F. Diederich, *Angew. Chem. Int. Ed.*, 2003, **42**, 1210–1250.
- 55 H. Harold, L. E. Craine and J. Hart, D., *Chemia Organiczna Krótki Kurs*, Wydawnictwo Lekarskie PZWL, Warszawa, 1999.
- 56 P. A. G. Cormack and A. Z. Elorza, *J. Chromatogr. B*, 2004, **804**, 173–182.
- 57 B. Sellergren, Ed., *Molecularly Imprinted Polymers—Man-Made Mimics of Antibodies and Their Application in Analytical Chemistry*, Elsevier, Amsterdam, 2001.
- 58 L. I. Andersson, A. Paprica and T. Arvidsson, *Chromatographia*, 1997, **46**, 57–62.



- 59 A. J. Hall, P. Manesiotis, M. Emgenbroich, M. Quaglia, E. De Lorenzi and B. Sellergren, *J. Org. Chem.*, 2005, **70**, 1732–1736.
- 60 S. Helling, S. Shinde, F. Brosseron, A. Schnabel, T. Müller, H. E. Meyer, K. Marcus and B. Sellergren, *Anal. Chem.*, 2011, **83**, 1862–1865.
- 61 A. A. Qader, J. Urraca, S. B. Torsetnes, F. Tønnesen, L. Reubsæet and B. Sellergren, *J. Chromatogr. A*, 2014, **1370**, 56–62.
- 62 G. D. Olsson, B. C. G. Karlsson, S. Shoravi, J. G. Wiklander and I. A. Nicholls, *J. Mol. Recogn.*, 2012, **25**, 69–73.
- 63 L. Schweitz, L. I. Andersson and S. Nilsson, *Analyst*, 2002, **127**, 22–28.
- 64 D. A. Vadim and M. P. Tsyurupa, *Hypercrosslinked Polymeric Networks and Adsorbing Materials: Synthesis, Properties, Structure, and Applications*, Elsevier, 2011.
- 65 D. C. Sherrington, *Chem. Commun.*, 1998, 2275–2286.
- 66 B. Dietrich, H. Cherdrón, M. Rehahn, H. Ritter and B. Voit, *Polymer Synthesis: Theory and Practice*, Springer Heidelberg New York Dordrecht London, 5th edn., 2013.
- 67 E. C. C. Goh and H. D. H. Stöver, *Macromolecules*, 2002, **35**, 9983–9989.
- 68 Q. Yan, T. Zhao, Y. Bai, F. Zhang and W. Yang, *J. Phys. Chem. B*, 2009, **113**, 3008–3014.
- 69 G. T. Dee and B. B. Sauer, in *Computational Studies, Nanotechnology, and Solution Thermodynamics of Polymer Systems*, eds. M. D. Dadmun, W. A. Van Hook, D. W. Noid, B. Melnichenko, Yuri and B. G. Sumpter, Springer US, Wilmington, 2002, pp. 29–36.
- 70 M. Belmares, M. Blanco, W. A. Goddard, R. B. Ross, G. Caldwell, S. Chou, J.

- Pham, P. M. Olofson and C. Thomas, *J. Comput. Chem.*, 2004, **25**, 1814–1826.
- 71 F. Limé and K. Irgum, *Macromolecules*, 2009, **42**, 4436–4442.
- 72 K. Haupt, A. V Linares, M. Bompart and B. Tse Sum Bui, *Top. Curr. Chem.*, 2012, **325**, 1–28.
- 73 L. Chen, S. Xu and J. Li, *Chem. Soc. Rev.*, 2011, **40**, 2922–2942.
- 74 E. Verheyen, J. P. Schillemans, M. van Wijk, M.-A. Demeniex, W. E. Hennink and C. F. van Nostrum, *Biomaterials*, 2011, **32**, 3008–3020.
- 75 T. Shiomi, M. Matsui, F. Mizukami and K. Sakaguchi, *Biomaterials*, 2005, **26**, 5564–5571.
- 76 H. Shi, W. Tsai, M. D. Garrison, S. Ferrari and B. D. Ratner, *Nature*, 1999, **398**, 593–597.
- 77 M. H. Coyle, PhD Thesis, University of Strathclyde, 2010.
- 78 H. Lodish, A. Berk, P. Matsudaira, C. A. Kaiser and M. Krieger, *Molecular Cell Biology*, W. H. Freeman Publishers, 5th edn., 2003.
- 79 A. Rachkov and N. Minoura, *J. Chromatogr. A*, 2000, **889**, 111–118.
- 80 A. Rachkov and N. Minoura, *Biochim. Biophys. Acta*, 2001, **1544**, 255–266.
- 81 A. Rachkov, M. Hu, E. Bulgarevich, T. Matsumoto and N. Minoura, *Anal. Chem.*, 2004, **504**, 191–197.
- 82 H. Nishino, C.-S. Huang and K. J. Shea, *Angew. Chem. Int. Ed.*, 2006, **45**, 2392–2396.
- 83 J. V Olsen, S. Ong and M. Mann, *Mol. Cell. Proteomics*, 2004, **3**, 608–614.
- 84 A. J. Link and J. LaBaer, *Proteomics : a Cold Spring Harbor Laboratory course manual*, Cold Spring Harbor Laboratory Press, New York, 2009.

- 85 C. Rossetti, M. A. Switnicka-Plak, T. G. Halvorsen, P. A. G. Cormack, B. Sellergren and L. Reubsaet, *Sci. Rep.*, 2017, **7**, 1–11.
- 86 M. Geng, J. Ji and F. E. Regnier, *J. Chromatogr. A*, 2000, **870**, 295–313.
- 87 K. Li and H. D. H. Stöver, *J. Polym. Sci. Part A Polym. Chem.*, 1993, **31**, 3257–3263.
- 88 W.-H. Li and H. D. H. Stöver, *J. Polym. Sci. Part A Polym. Chem.*, 1997, **36**, 1543–1551.
- 89 J. S. Downey, G. Mclsaac, R. S. Frank and H. D. H. Stöver, *Macromolecules*, 2001, **34**, 4534–4541.
- 90 J. S. Downey, R. S. Frank, W. Li and H. D. H. Stöver, *Macromolecules*, 1999, **32**, 2838–2844.
- 91 H. Zhang, *Eur. Polym. J.*, 2013, **49**, 579–600.
- 92 J. M. G. Cowie and V. Arrighi, *Polymers: Chemistry and Physics of Modern Materials, Third Edition*, CRC Press, Taylor and Francis Group, 3rd edn., 2007.
- 93 W. Li and H. D. H. Stöver, *Macromolecules*, 2000, **33**, 4354–4360.
- 94 S. E. Shim, S. Yang, H. H. Choi and S. Choe, *J. Polym. Sci. Part A Polym. Chem.*, 2004, **42**, 835–845.
- 95 J. M. Jin, S. Yang, S.-T. Han and S. Choe, *J. Ind. Eng. Chem*, 2006, **12**, 268–274.
- 96 R. Perrier-Cornet, V. Héroguez, A. Thienpont, O. Babot and T. Toupance, *J. Chromatogr. A*, 2008, **1179**, 2–8.
- 97 Q. Yan, Y. Bai, Z. Meng and W. Yang, *J. Phys. Chem. B*, 2008, **112**, 6914–6922.
- 98 J. Wang, P. A. G. Cormack, D. C. Sherrington and E. Khoshdel, *Angew. Chem. Int. Ed.*, 2003, **42**, 5336–5338.

- 99 K. Yoshimatsu, K. Reimhult, A. Krozer, K. Mosbach, K. Sode and L. Ye, *Anal. Chim. Acta*, 2007, **584**, 112–121.
- 100 J. Wang, P. A. G. Cormack, D. C. Sherrington and E. Khoshdel, *Pure Appl. Chem.*, 2007, **79**, 1505–1519.
- 101 C. Cacho, E. Turiel, A. Martín-Esteban, C. Pérez-Conde and C. Cámara, *J. Chromatogr. B*, 2004, **802**, 347–353.
- 102 E. Turiel, J. L. Tadeo, P. A. G. Cormack and A. Martín-Esteban, *Analyst*, 2005, **130**, 1601–1607.
- 103 A. Beltran, R. M. Marcé, P. A. G. Cormack and F. Borrull, *J. Chromatogr. A*, 2009, **1216**, 2248–2253.
- 104 H. Sambe, K. Hoshina, R. Moaddel, I. W. Wainer and J. Haginaka, *J. Chromatogr. A*, 2006, **1134**, 88–94.
- 105 L. Ye, P. A. G. Cormack and K. Mosbach, *Anal. Chim. Acta*, 2001, **435**, 187–196.
- 106 J. Oxelbark, C. Legido-Quigley, C. S. A. Aureliano, M.-M. Titirici, E. Schillinger, B. Sellergren, J. Courtois, K. Irgum, L. Dambies, P. A. G. Cormack, D. C. Sherrington and E. De Lorenzi, *J. Chromatogr. A*, 2007, **1160**, 215–226.
- 107 A. Valero-Navarro, M. Gómez-Romero, J. F. Fernández-Sánchez, P. A. G. Cormack, A. Segura-Carretero and A. Fernández-Gutiérrez, *J. Chromatogr. A*, 2011, **1218**, 7289–7296.
- 108 A. Beltran, F. Borrull, P. A. G. Cormack and R. M. Marcé, *J. Chromatogr. A*, 2011, **1218**, 4612–4618.
- 109 F. Barahona, E. Turiel, P. A. G. Cormack and A. Martín-Esteban, *J. Sep. Sci.*, 2009, **48**, 1058–1066.
- 110 F. Barahona, E. Turiel, P. A. G. Cormack and A. Martín-Esteban, *J. Sep. Sci.*,

- 2011, **34**, 217–24.
- 111 R. Hayes, A. Ahmed, T. Edge and H. Zhang, *J. Chromatogr. A*, 2014, 36–52.
- 112 M. J. E. Golay, in *Gas Chromatography 1960, Edinburgh*, ed. R. P. W. Scott, Butterworths, London, 1960, p. 138.
- 113 C. G. Horvath, B. A. Preiss and S. R. Lipsky, *Anal. Chem.*, 1967, **39**, 1422–1428.
- 114 C. G. Horvath and S. R. Lipsky, *J. Chromatogr. Sci.*, 1969, 109–116.
- 115 J. J. Kirkland, *Anal. Chem.*, 1969, **41**, 218–220.
- 116 G. Guiochon and F. Gritti, *J. Chromatogr. A*, 2011, 1915–1938.
- 117 J. J. Kirkland and J. J. DeStefano, *J. Chromatogr. Sci.*, 1970, **8**, 309–314.
- 118 J. J. Kirkland, *J. Chromatogr. Sci.*, 1971, **9**, 206–214.
- 119 DuPont Instruments, *PERMAPHASE Liquid Chromatographic Packings with new chemically-bonded stationary phases*, 1970.
- 120 J. J. Kirkland, *Anal. Chem.*, 1992, **890**, 1239–1245.
- 121 WO 2015/002711 A1, 2015, 1–25.
- 122 J. J. Kirkland, F. A. Truszkowski, C. H. Dilks and G. S. Engel, *J. Chromatogr. A*, 2000, **890**, 3–13.
- 123 R. W. Brice, X. Zhang and L. A. Colón, *J. Sep. Sci.*, 2009, **32**, 2723–2731.
- 124 N. Wu and A. M. Clausen, *J. Sep. Sci.*, 2007, **30**, 1167–1182.
- 125 J. J. DeStefano, S. A. Schuster, J. M. Lawhorn and J. J. Kirkland, *J. Chromatogr. A*, 2012, **1258**, 76–83.
- 126 L. E. Blue and J. W. Jorgenson, *J. Chromatogr. A*, 2011, **1218**, 7989–7995.

- 127 J. O. Omamogho, J. P. Hanrahan, J. Tobin and J. D. Glennon, *J. Chromatogr. A*, 2011, **1218**, 1942–1953.
- 128 F. Bai, X. Yang, Y. Zhao and W. Huang, *Polym. Int.*, 2005, **54**, 168–174.
- 129 F. Bai, X. Yang and W. Huang, *J. Appl. Polym. Sci.*, 2006, **100**, 1776–1784.
- 130 Y. Wang, Q. Liu, F. Rong and D. Fu, *Appl. Surf. Sci.*, 2011, **257**, 6704–6710.
- 131 A. Aseri, S. K. Garg, A. Nayak, S. K. Trivedi and J. Ahsan, *Int. J. Pharm. Sci. Rev. Res.*, 2015, **31**, 119–131.
- 132 S. Laurent, D. Forge, M. Port, A. Roch, C. Robic, L. Vander Elst and R. N. Muller, *Chem. Rev.*, 2008, **108**, 2064–2110.
- 133 R. Massart, *IEEE*, 1981, **17**, 1247–1248.
- 134 L. Li, X. He, L. Chen and Y. Zhang, *Chem. Asian J.*, 2009, **4**, 286–293.
- 135 N. Sankarakumar and Y. W. Tong, *RSC Adv.*, 2013, **3**, 1519–1527.
- 136 C. J. Tan and Y. W. Tong, *Anal. Chem.*, 2007, **79**, 299–306.
- 137 S. K. Suh, K. Yuet, D. K. Hwang, K. W. Bong, P. S. Doyle and T. A. Hatton, *J. Am. Chem. Soc.*, 2012, **134**, 7337–7343.
- 138 L. Chen and B. Li, *Anal. Methods*, 2012, **4**, 2613–2621.
- 139 R. J. Ansell and K. Mosbach, *Analyst*, 1998, **123**, 1611–6.
- 140 S. S. Miao, M. S. Wu, H. G. Zuo, C. Jiang, S. F. Jin, Y. C. Lu and H. Yang, *J. Agric. Food Chem.*, 2015, **63**, 3634–3645.
- 141 Y. Hu, R. Liu, Y. Zhang and G. Li, *Talanta*, 2009, **79**, 576–82.
- 142 C. Gonzato, M. Courty, P. Pasetto and K. Haupt, *Adv. Funct. Mater.*, 2011, **21**, 3947–3953.

- 
- 143 L. Chen, Y. K. Lee, Y. Manmana, K. S. Tay, V. S. Lee and N. A. Rahman, *e-Polymers*, 2015, **15**, 141–150.
- 144 M. Gümüşderelioglu, A. S. Kahraman and A. Tuncel, *Polym. Bull.*, 2012, **69**, 323–335.
- 145 H. Macková, V. Proks, D. Horák, J. Kučka and M. Trchová, *J. Polym. Sci. Part A Polym. Chem.*, 2011, **49**, 4820–4829.
- 146 C. Rodriguez, E. Castro, A. Martin, J. R. Marín, J. Berganza and J. M. Cuevas, *Micro Nano Lett.*, 2011, **6**, 349–352.
- 147 J. M. Rosiak and F. Yoshii, *NIM B*, 1999, **151**, 56–64.
- 148 R. Barbucci, *Hydrogels Biological Properties and Applications*, Springer-Verlag, Milan, 2009.
- 149 M. Ebara, Y. Kotsuchibashu, R. Narain, N. Idota, Y.-J. Kim, J. M. Hoffman, K. Uto and T. Aoyagi, *Smart Biomaterials*, Springer Japan, 1st edn., 2014.
- 150 B. Strachota, L. Matejka, A. Zhigunov, R. Konefał, J. Spevacek, J. Dybal and R. Puffr, *Soft Matter*, 2015, **11**, 9291–9306.
- 151 G. Xinqiu, Q. Kunyuan and F. Xinde, *Chin. J. Pol. Sci.*, 1989, **7**, 165–173.
- 152 S. Zhang, Z. Shi, H. Xu, X. Ma, J. Yin and M. Tian, *Soft Matter*, 2016, **12**, 2575–2582.
- 153 S. Hjertén, J.-L. Liao, K. Nakazato, Y. Wang, G. Zamaratskaia and H.-X. Zhang, *Chromatographia*, 1997, **44**, 227–234.
- 154 A. Takátsy, Á. Végvári, S. Hjertén and F. Kilár, *Electrophoresis*, 2007, **28**, 2345–2350.
- 155 A. Takátsy, A. Kilár, F. Kilár and S. Hjertén, *J. Sep. Sci.*, 2006, **29**, 2802–2809.

- 156 K. Hirayama, Y. Sakai and K. Kameoka, *J. Appl. Polym. Sci.*, 2001, **81**, 3378–3387.
- 157 S. H. Ou, M. C. Wu, T. C. Chou and C. C. Liu, *Anal. Chim. Acta*, 2004, **504**, 163–166.
- 158 T. Y. Guo, Y. Q. Xia, G. J. Hao, M. D. Song and B. H. Zhang, *Biomaterials*, 2004, **25**, 5905–5912.
- 159 T.-Y. Guo, Y.-Q. Xia, J. Wang, M.-D. Song and B.-H. Zhang, *Biomaterials*, 2005, **26**, 5737–5745.
- 160 D. M. Hawkins, D. Stevenson and S. M. Reddy, *Anal. Chim. Acta*, 2005, **542**, 61–65.
- 161 M. Yan and O. Ramström, Eds., *Molecularly Imprinted Materials: Science and Technology*, Taylor & Francis Group Ltd, LLC, New York, 2004.
- 162 N. W. Turner, C. W. Jeans, K. R. Brain, C. J. Allender, V. Hlady and D. W. Britt, *Biotechnol Prog.*, 2006, **22**, 1474–1489.
- 163 A. Bossi, F. Bonini, A. P. F. Turner and S. A. Piletsky, *Biosens. Bioelectron.*, 2007, **22**, 1131–1137.
- 164 S. Lowell and J. E. Shields, *Powder Surface Area and Porosity*, Chapman & Hall, London, 3rd edn., 1991.
- 165 J. Rouquerol, D. Avnir, C. W. Fairbridge, D. H. Everett, J. H. Haynes, N. Pernicone, J. D. F. Ramsay, K. S. W. Swing and K. K. Unger, *Pure Appl. Chem.*, 1994, **66**, 1739–1758.
- 166 *R A Lang. Environ. Stat. Comput.*, 2015, 55, 275–286.
- 167 B. L. Welch, *Biometrika*, 1947, **34**, 28–35.
- 168 J. C. De La Vega, P. Elischer, T. Schneider and U. O. Häfeli, *Nanomedicine*, 2013,



**8**, 265–285.

169 B. L. Welch, *Biometrika*, 1938, 29, 350–362.

170 [www.pepmip.eu](http://www.pepmip.eu), *Robust Affinity Materials for Applications in Proteomics and Diagnostics (PEPMIP)*, 2016.

## 2. Molecularly imprinted polymer microspheres

The synthesis of MIPs in a spherical particulate format was the main interest in the Thesis work. The main benefits of spherical MIPs over MIP particulates obtained via the crushing and grinding of MIP monoliths are as follows:

- Spherical MIP particulates are less prone to fragmentation and are more physically durable during handling than their irregularly-shaped, crushed counterparts;
- They pack more efficiently in analytical columns, giving better flow properties and lower back pressures, thus providing better separation;
- Other characteristics of MIP microspheres are: significantly faster binding kinetics, better accessibility of binding sites, higher binding affinity and specificity to target analytes.<sup>1</sup>

In separation science, the highest column efficiency is normally achieved when small particles are used as stationary phase, which in practical terms means particles with diameters as low as  $\sim 1.7 \mu\text{m}$ .<sup>2</sup> Small particles improve significantly the mass transfer inside the chromatography column and the diffusion within particles is reduced.<sup>3</sup> This comes from van Deemter equation which describes relationship between a height equivalent to a theoretical plate,  $H$  and a mobile phase velocity,  $\mu$ .<sup>4</sup> This equation is as follows<sup>5</sup>:

$$H = A + \frac{B}{\mu} + C\mu$$

where  $A$ ,  $B$  and  $C$  denote an eddy diffusion, a longitudinal diffusion, and resistance to a mass transfer, respectively.<sup>5</sup> In this equation,  $H$ , the length needed by one

theoretical plate, is inversely proportional to particle size.<sup>4</sup> Therefore, small and uniform particles were desirable to produce and deliver to PEPMIP partners, however these particles could not be too small as small particles contribute to high backpressure.<sup>6</sup>

## 2.1 Precipitation polymerisation for the synthesis of peptide imprinted polymer microspheres

### 2.1.1 Aim of study

In our test studies for the design and synthesis of polymer macroreticular materials for peptide imprinting, we hypothesize that

- Precipitation polymerisation (PP) is a useful synthesis method for the preparation of high-quality, MIP microspheres. Near monodisperse and surfactant-free spherical polymer particles in the micron size range can be synthesised by the precipitation polymerisation method;
- *N*-(2-Aminoethyl)methacrylamide hydrochloride and *N*-3,5-*bis*(trifluoromethyl)-phenyl-*N'*-4-vinylphenylurea are functional monomers which could be copolymerized by the PP and further involved in the formation of non-covalent interactions with peptide templates for the synthesis of molecularly imprinted polymer microspheres.

Based on this, the aims of the work presented in this section were as follows:

- Identification of the PP conditions that can be used for the synthesis of MIPs;
- Design and synthesis of non-imprinted polymer materials as controls;
- Characterisation of materials produced.

### 2.1.2 Experimental section

#### 2.1.2.1 *Materials*

*N*-(2-Aminoethyl)methacrylamide hydrochloride (EAMA.HCl, purity  $\geq 98\%$ ) was purchased from Polysciences Inc. (Niles, IL, USA). *N*-3,5-*bis*(trifluoromethyl)-phenyl-

*N'*-4-vinylphenylurea (NTPVU, purity >95%) is not commercially available and was kindly donated by Dortmund University. 2,2'-Azobisisobutyronitrile (AIBN, purity 98%) was purchased from BDH Lab. Supplies (UAE). Divinylbenzene-80 (DVB-80, 80% DVB isomers and 20% ethylvinylbenzene isomers), 1,2,2,6,6-pentamethylpiperidine (PMP, purity >99%), tetrabutylammonium hydroxide solution (TBA.HO, 1.0 M in methanol, 25% ≤ purity <50%) and hydrochloric acid (37 wt. % in H<sub>2</sub>O) were all purchased from Sigma-Aldrich (St. Louis, MI, USA). DVB-80 was purified by filtration through a short plug of neutral aluminium oxide prior to use. AIBN was recrystallized from acetone at low temperature. All other chemicals used (acetonitrile [ACN], methanol and dimethyl sulfoxide [DMSO, purity ≥99.9%]) were of analytical grade.

#### 2.1.2.2 *Synthesis and characterisation of non-imprinted polymers*

The first prepared polymers were synthesised by typical PP as described elsewhere.<sup>7</sup> The PP method has been presented and discussed in detail in Chapter 1. In this experimental section, a detailed description of the methods used for characterisation of the synthetic polymers described in the Thesis is presented. The same characterisation methodology was applied to all other materials prepared by PP.

Solubility tests for EAMA.HCl (functional monomer) were performed. Different mole ratios of EAMA.HCl and DVB-80 (crosslinker), together with different combinations of ACN (PP solvent) and DMSO (PP co-solvent) were tested as presented in Table 2.1. In the first test performed, 123 mg of EAMA.HCl was added into a borosilicate Kimax tube and an attempt was made to dissolve in 0.25 mL of DMSO. In order to improve the solubility of EAMA.HCl, the tubes with the solutions tested were either shaken, for a few minutes and/or placed in a heated oil bath (~70 °C). When EAMA.HCl dissolved in DMSO, 24.75 mL of ACN was added to the solution. The tests were evaluated if the solutions were homogeneous, cloudy or turbid.

Table 2.1 Solubility tests for EAMA.HCl.

Test	EAMA.HCl/DVB (mole ratio)	EAMA.HCl (mmol)	ACN/DMSO (v/v)
1	1/5	0.747	99/1
2	1/5	0.747	96/4
3	0.1/5	0.074	99/1
4	0.1/5	0.074	96/4

The feed compositions of the tested materials is shown in Table 2.2. Polymers were synthesised on a 0.5 g monomer scale, with a monomer and initiator concentration of 2% w/v (with respect to the solvent) and 2 mol% (with respect to the total number of polymerisable double bonds), respectively. Polymers were prepared in either borosilicate glass Kimax culture tubes or Nalgene polyethylene bottles. In Table 2.2, when the letter B appears at the end of the polymer's name then this means that these polymers were prepared in Nalgene polyethylene bottles, whereas the others were synthesised in borosilicate glass Kimax culture tubes.

Table 2.2 Compositions of the tested polymers.

Polymer code	Functional Monomer (mmol)	DVB-80 (mmol)	Solvent (mL)	AIBN (mol%) <sup>a</sup>	Other components (mmol)
MAS1	-	3.060	ACN (20)	2	-
MAS2	EAMA.HCl (0.07)	3.73	ACN (24) DMSO (1)	2	-
MAS3	EAMA.HCl (0.07) NTPVU (0.007)	3.73	ACN (24) DMSO (1)	2	TBA.HO (0.007)
MAS3(B) <sup>b</sup>	EAMA.HCl (0.07) NTPVU (0.007)	3.73	ACN (24) DMSO (1)	2	TBA.HO (0.007)
MAS4	EAMA.HCl (0.07)	3.73	ACN (24) DMSO (1)	2	PMP (0.006)
MAS4(B) <sup>b</sup>	EAMA.HCl (0.07)	3.73	ACN (24) DMSO (1)	2	PMP (0.006)

<sup>a</sup> Relative to the number of moles of polymerisable double bonds.

<sup>b</sup> B letter in the polymer name means that these polymers were prepared in Nalgene polyethylene bottles, *e.g.*, MAS3(B).

The synthesis of the polymer with code MAS3 can serve as a cognate example of the PP. Firstly, DMSO (1 mL) was added into a borosilicate glass Kimax tube. Thereafter, TBA.HO (7.43  $\mu$ L, 0.007 mmol) was added followed by the functional monomer EAMA.HCl (12.3 mg, 0.07 mmol), solvent ACN (24 mL), crosslinker DVB-80 (0.49 g, 0.53 mL, 3.73 mmol) and initiator AIBN (22.3 mg, 0.2 mmol). The solution was then ultrasonicated for 10 minutes at ambient temperature and sparged with oxygen-free nitrogen gas for 10 minutes at ice-bath temperature, to remove dissolved molecular oxygen. Thereafter, the reaction vessel was sealed under nitrogen and transferred to a Stuart Scientific S160 incubator equipped with a Stovall low-profile roller. The incubator temperature was ramped from ambient to 60 °C over a period of around two hours and then maintained at 60 °C for a further 22 hours to yield a milky suspension of polymer microspheres. An illustration of the methodology used for the synthesis and characterisation of the polymers synthesised in the present work is shown in Figure 2.1.

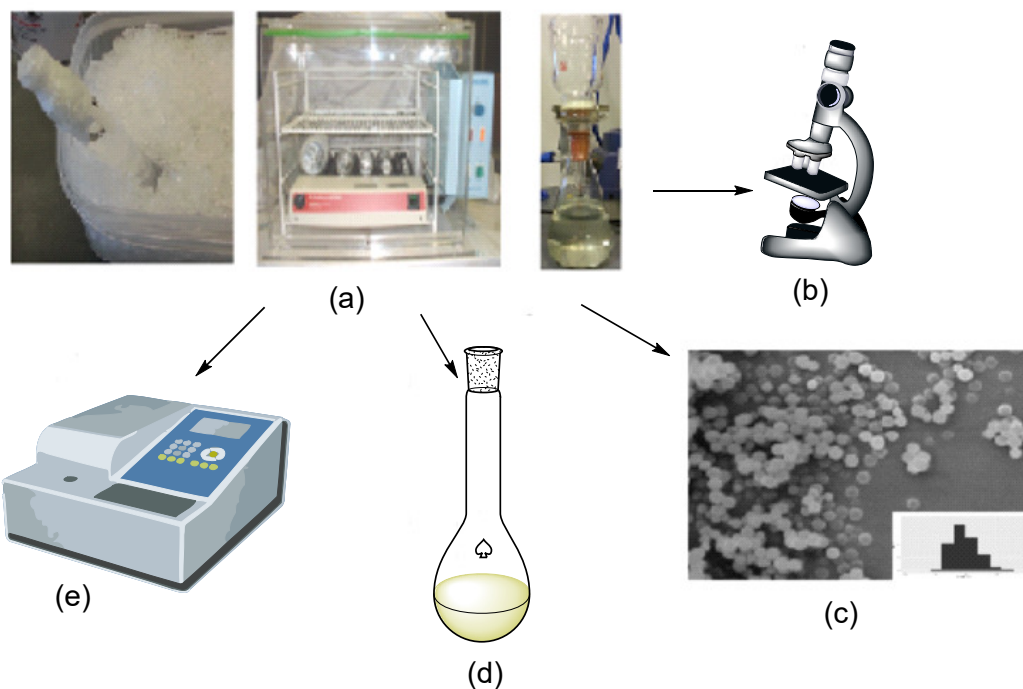


Figure 2.1 Work flow of the methods used in the present work: (a) precipitation polymerisation (b) optical microscope (c) SEM together with image analysis (d) nitrogen sorption analysis (e) FT-IR spectroscopic analysis.

After the polymerisation, a few drops were collected from the polymerisation mixture, and were applied onto a glass microscope slide and examined by an Olympus Vanox optical microscope. Polymer microspheres were observed and recorded in terms of size, dispersity and their aggregation (if any).

Finally, the polymer microspheres were isolated from the reaction mixture by filtration on a 0.45  $\mu\text{m}$  nylon membrane filter using a Vacuumbrand Vacuum System (2.0 mbar), and washed sequentially with ACN (50 mL) and MeOH (50 mL). The isolated product was transferred into a pre-weighed vial and dried overnight in a Townson & Mercer vacuum oven (60 mbar) at 70  $^{\circ}\text{C}$ . The yield of the synthesised material was checked gravimetrically. The yield of MAS3 was 28%.

Polymer microspheres were imaged by scanning electron microscopy (SEM) using a Cambridge Instruments Stereoscan 90. The sample preparation procedure for microscopic analysis involved the following steps: adhesion of a conducting carbon tab on an aluminium pin stub with 12 mm diameter placed on a holder, application of small amount of polymer, and coating the sample surface with a mixture of platinum-palladium nanoparticles. The sputter coating system included Polar SC500A Sputter Coater Fison Instrument connected to an argon cylinder. 4 min was set as the platinum-palladium deposition time, and 20 mA as the current density. After coating, the samples were placed inside the SEM chamber and a vacuum was applied. During the microscopic analysis, the magnification values and working distances ranged from:  $\times 372$  to  $\times 6010$ , and between 18 nm to 20 mm, respectively.

Image analysis of SEM micrographs was done by Image Processing and Analysis software written in Java known as Image J.<sup>8</sup> The particle size distribution of the polymer microspheres was evaluated for these polymers, where their microsphere shape was clearly distinguishable. The polymer microspheres were divided horizontally into two equally projected areas. 100 was the population of microspheres for the determination of particle size distribution. Plotting was done using 'ggplot2' package in R framework.<sup>9</sup>

Micromeritics Accelerated Surface Area and Porosimetry, ASAP 2010 and ASAP 2020 Analyzers, volumetric adsorption systems were used for the evaluation of porosity and specific surface area of the synthesised polymers. The amount of gas adsorbed into the analysed sample was measured before and after adsorption at constant temperature. According to standard procedures, 0.2-0.3 g was the recommended amount of material for this analysis. Prior to use, samples were dried overnight in a vacuum oven (60 mbar) at 70 °C. Also, the clean sample tubes were dried overnight in an oven at 100 °C before the dried sample was transferred into the sample tube. The mass of the sample tube was measured before use. When an ASAP 2020 Analyzer was used, the sample tube was sealed with a seal frit. In the degassing step, the sample attached to the degassing port under the vacuum (0.002-0.01 mbar) was



heated to 100 °C overnight, and from 100 °C to 150 °C over 24 to 72 h, when ASAP 2000 and ASAP2020 were used, respectively. After the degassing step the sample tube was transferred from the degassing port to the analyser port. The sample tube together with the analysed polymer was weighed again. The dry weight of the polymer was calculated and the obtained value was entered into the analysis data. When an ASAP 2020 Analyzer was used, a glass rod was additionally placed inside the sample tube to minimise the volume of free space. During the analysis, the sample tube was immersed in the analysis Dewar with the liquid nitrogen at approx. 77.4 K. An adsorption equilibrium time was 5 s for each point. Brunauer-Emmett-Teller (BET) theory was applied for the determination of the morphology parameters of polymers.

Structural determination of the chemical compositions of the synthesised polymers was evaluated using a Shimadzu IRAffinity-1 FT-IR Spectrophotometer or an Agilent 5500a FT-IR Spectrophotometer. During analysis, a small amount of sample was applied directly into diamond cell and scanned in ATR mode in the ranges of 4000-650  $\text{cm}^{-1}$  or 4000–700  $\text{cm}^{-1}$  for Shimadzu spectrometer and Agilent spectrometer, respectively.

### 2.1.3 Results and discussion

#### *2.1.3.1 Synthesis of polymer microspheres and characterisation of the polymers*

MAS1 was the first polymer synthesised. A representation of the chemical structure of MAS1 is shown in Figure 2.2. MAS1 microspheres with narrow size distribution were formed in moderate yield (Table 2.3). The isolated yield of MAS1 is typical for the polymerisation of divinylbenzene under such precipitation polymerisation conditions. It can be seen from the SEM image in Figure 2.3 that the polymer microspheres had regular spherical shapes. The particle size distribution analysis (Figure 2.3) revealed that the diameters of these microspheres ranged from 1.2  $\mu\text{m}$  to 1.8  $\mu\text{m}$ , with an average diameter of 1.45  $\mu\text{m}$ . The FT-IR spectrum of MAS1 together with assignments of FT-IR peaks is presented in Figure 2.4. The following characteristic peaks were observed: aromatic C-H stretches at 3018  $\text{cm}^{-1}$  and

3007  $\text{cm}^{-1}$ , aliphatic C-H stretches at 2916  $\text{cm}^{-1}$ , aromatic C=C stretches at 1627  $\text{cm}^{-1}$ , 1600  $\text{cm}^{-1}$  and 1510  $\text{cm}^{-1}$ , alkene stretches at 987  $\text{cm}^{-1}$  and 902  $\text{cm}^{-1}$ , and three stretches at 829  $\text{cm}^{-1}$ , 794  $\text{cm}^{-1}$  and 709  $\text{cm}^{-1}$ , corresponding to *para*- and *meta*-disubstituted benzene rings.

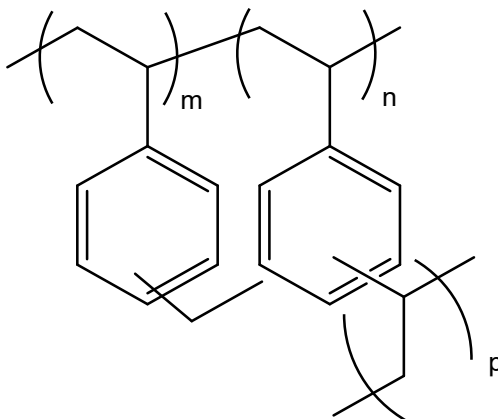


Figure 2.2 Chemical structure of MAS1 poly(DVB-80).

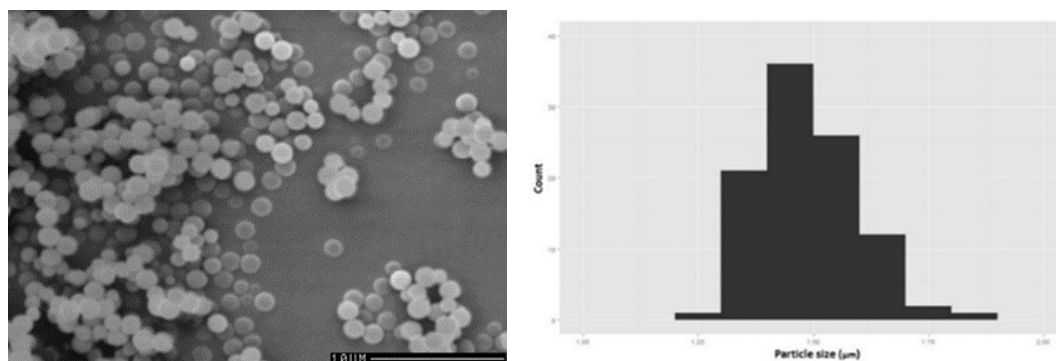
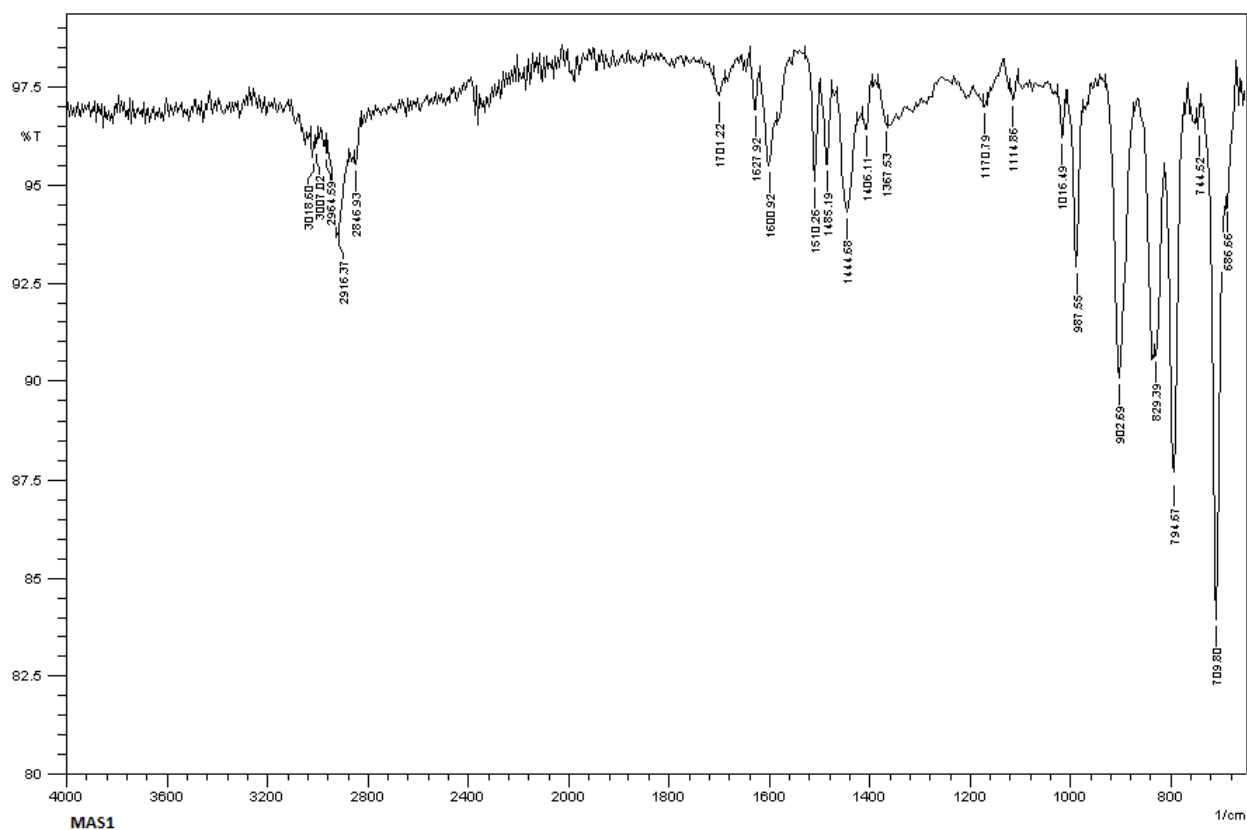


Figure 2.3 SEM image (left) and particle size distribution (right) of MAS1 ( $d = 1.45 \mu\text{m} \pm 0.10 \mu\text{m}$ );  $\times 2940$  magnification for SEM image (scale = 10  $\mu\text{m}$ ).



Approximate stretching frequency (cm <sup>-1</sup> )	Group
3018 and 3007	Aromatic C-H
2916	Aliphatic C-H
1627, 1600 and 1510	Aromatic C=C
987 and 902	Aliphatic C=C
829	<i>para</i> -di- substituted benzene
794 and 709	<i>meta</i> -di- substituted benzene

Figure 2.4 FT-IR spectrum of MAS1 and assignments of FT-IR peaks.

MAS2 was the next polymer prepared, where DVB-80 was copolymerised with EAMA.HCl; the chemical structure of the product is shown in Figure 2.5. EAMA.HCl was the functional monomer planned to be used in the synthesis of MIPs for peptide targets. EAMA.HCl contains a cationic moiety which would be able to form non-covalent interactions with negatively-charged carboxylic groups of certain amino

acids. This monomer was used for the synthesis of polymer-based artificial receptors by Sellaergren and co-workers. Their final products, prepared in the form of irregular particles, gave outstanding affinity and selectivity for the ProGRP target.<sup>10</sup> During the synthesis of MAS2, a problem with the solubility of EAMA.HCl arose in the initial stage. The use of EAMA.HCl in the same 0.1:5 molar ratio of EAMA.HCl: DVB as used in the previous published work resulted in monomer insolubility.<sup>10</sup> The problem was overcome by manipulation of the monomer feed ratios. In the fourth solubility test performed (Table 2.2), an amount of EAMA.HCl ten times smaller (0.049% w/v) than that used in the earlier work proved sufficient. EAMA.HCl (0.07 mmol) dissolved completely in the following solvent: 4% of DMSO and 96% of ACN. Additionally, at the end of the polymerisation, it was observed that the final product adhered to the reaction vial. The yield of MAS2 was lower than for MAS1 (Table 2.3). The polymer particles were in the form of nearly regular microspheres, as can be seen in the SEM image in Figure 2.6. Their size distribution was broader than for MAS1 (Table 2.4). The average diameter of MAS2 microspheres reached almost 4  $\mu\text{m}$ . The FT-IR data is not shown here, but the FT-IR spectrum of the MAS2 showed the peaks typically associated with poly(DVB-80) only. Peaks associated with the presence of EAMA.HCl were not observed, as the amount of added EAMA.HCl was relatively small (0.016 mol%).

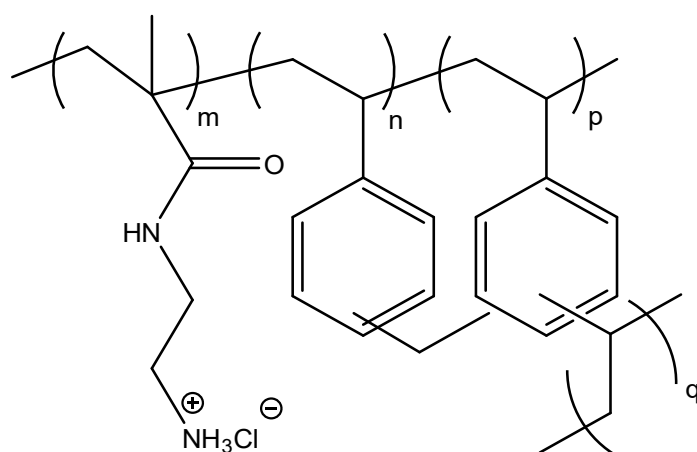


Figure 2.5 Chemical structure of MAS2 poly(EAMA.HCl-co-DVB-80).

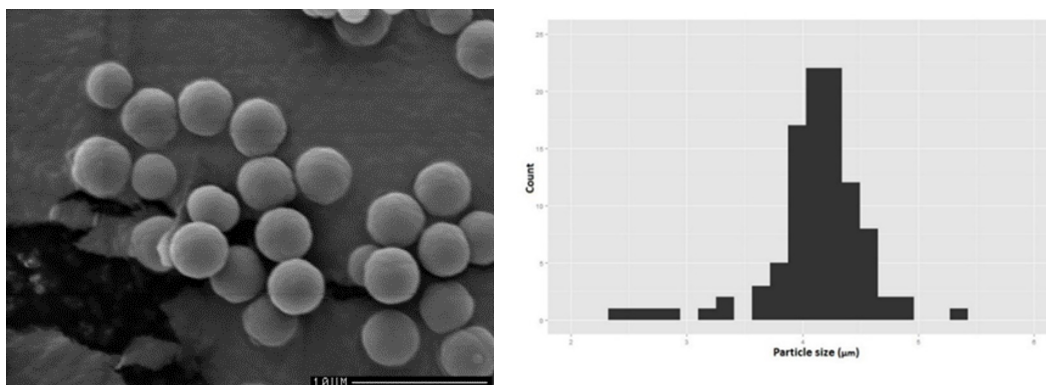


Figure 2.6 SEM image (left) and particle size distributions (right) of MAS2 ( $d = 4.12 \mu\text{m} \pm 0.43 \mu\text{m}$ );  $\times 3020$  magnification for SEM image (scale =  $10 \mu\text{m}$ ).

Poly(EAMA.HCl-co-DVB-80) was also synthesised in the presence of PMP. It was planned to be use PMP in the synthesis of MIPs for peptide targets as its role is activate the functional monomer, EAMA.HCl. PMP was used to bring the polymerisation components into an appropriate ionization states for non-covalent interactions. Two parallel polymerisations were carried out in a borosilicate glass Kimax tube (MAS4) and a plastic Nalgene polyethylene bottle (MAS4(B)). After polymerisation, particles of MAS4(B) were freely suspended in the porogen, while MAS4 stuck to sides of the reaction vessel. The yield of MAS4 was higher than for MAS4(B) (Table 2.3). Both products were in the form of polydisperse microspheres (Figure 2.7 and Figure 2.8). It is worth pointing out that the particle size analysis revealed that the average diameter of microspheres in MAS4 was about half that of MAS4(B) (Table 2.4). The FT-IR data are not shown here, for the same reason as for MAS2.

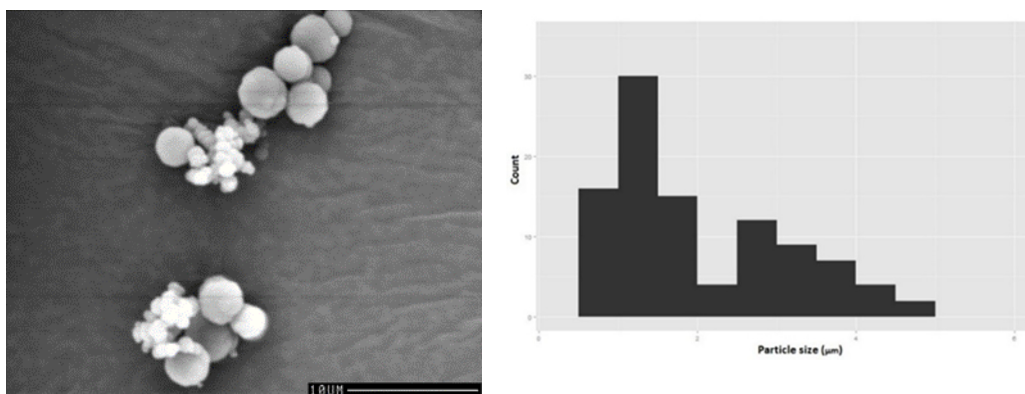


Figure 2.7 SEM image (left) and particle size distribution (right) of MAS4 ( $d = 1.99 \mu\text{m} \pm 1.12 \mu\text{m}$ );  $\times 3020$  magnification for SEM image (scale =  $10 \mu\text{m}$ ).

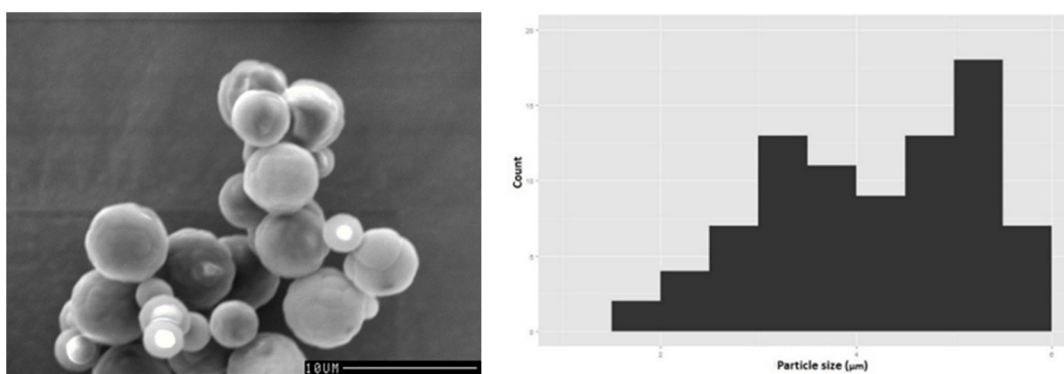


Figure 2.8 SEM image (left) and particle size distribution (right) of MAS4(B) ( $d = 4.48 \mu\text{m} \pm 1.24 \mu\text{m}$ );  $\times 3090$  magnification for SEM image (scale =  $10 \mu\text{m}$ ).

Copolymerisations of EAMA.HCl with NTPVU were performed in the presence of TBA.HO. The NTPVU was planned to be used in the synthesis of MIPs for peptide targets as it belongs to a family of urea-based vinyl monomers that have high binding affinity for oxyanions.<sup>11</sup> This monomer was used for the synthesis of polymer-based artificial receptors by Sellergren and co-workers. Their final products, prepared in the form of irregular particles, gave outstanding affinity and selectivity for  $\beta$ -Amyloid targets and the enrichment of proteotypic peptides.<sup>12,13</sup> TBA.HO was also used in the synthesis of MIPs for peptide targets, as its role was to activate the template molecule. TBA.HO was used to bring the template into an appropriate ionization states for non-covalent interactions. The reactions were carried out in two different reaction vessels: a borosilicate glass Kimax tube (MAS3) and plastic Nalgene polyethylene bottle (MAS3(B)). A representation of the chemical structures of MAS3

and MAS3(B) is shown in Figure 2.9. During the copolymerisations, a similar observation as for the MAS4 and MAS4(B) pair was noted. The polymer prepared in the borosilicate Kimax tube adhered to the reaction vessel, while the MAS3(B) polymer particles were freely suspended in the porogen. The yield of MAS3(B) was significantly lower than that of MAS3 (Table 2.3). The polymer microspheres produced were not narrow in their size distribution (Figure 2.10, Figure 2.11 and Table 2.4 ). The MAS3(B) microspheres were considerably larger than MAS3. The particle size distribution analysis was performed for MAS3(B) (Figure 2.11) only, as it was not possible to distinguish the exact shapes of the MAS3 microparticles. The FT-IR spectroscopic data is not shown here for the same reason as for MAS2. However, the theoretical (predicted) compositions of the polymers produced could be determined when the concentrations and relative reactivity of the monomers used in the polymerisations are taken into consideration. In the Polymer Handbook, there is no data for NTPVU and EAMA.HCl. Instead, data for monomers with similar chemical structures are available and these data can be used. The same approach was applied for DVB-80, where the reactivity ratios values of styrene were taken. The data for the reactivity of EVB was also not available in the Polymer Handbook.<sup>14</sup> Therefore, the reactivity of *meta*-EVB and *para*-EVB were assessed on the basis of the stability of the monomer radicals formed upon radical attack on the vinyl groups, with *para*-EVB being predicted to be more reactive than *meta*-DVB. Reactivities of *para*-DVB and *meta*-DVB were evaluated in respect to the number of resonance forms. *ortho*-DVB and EVB were not taken into consideration as these isomers are present in negligibly small amounts. In fact, it is not present at all as it is converted to naphthalene during manufacturing.<sup>15</sup> Therefore, with the above assumptions, relative monomer reactivity falls in the following order: *para*-DVB > *meta*-DVB > *para*-EVB > NTPVU > *meta*-EVB > EAMA.HCl.

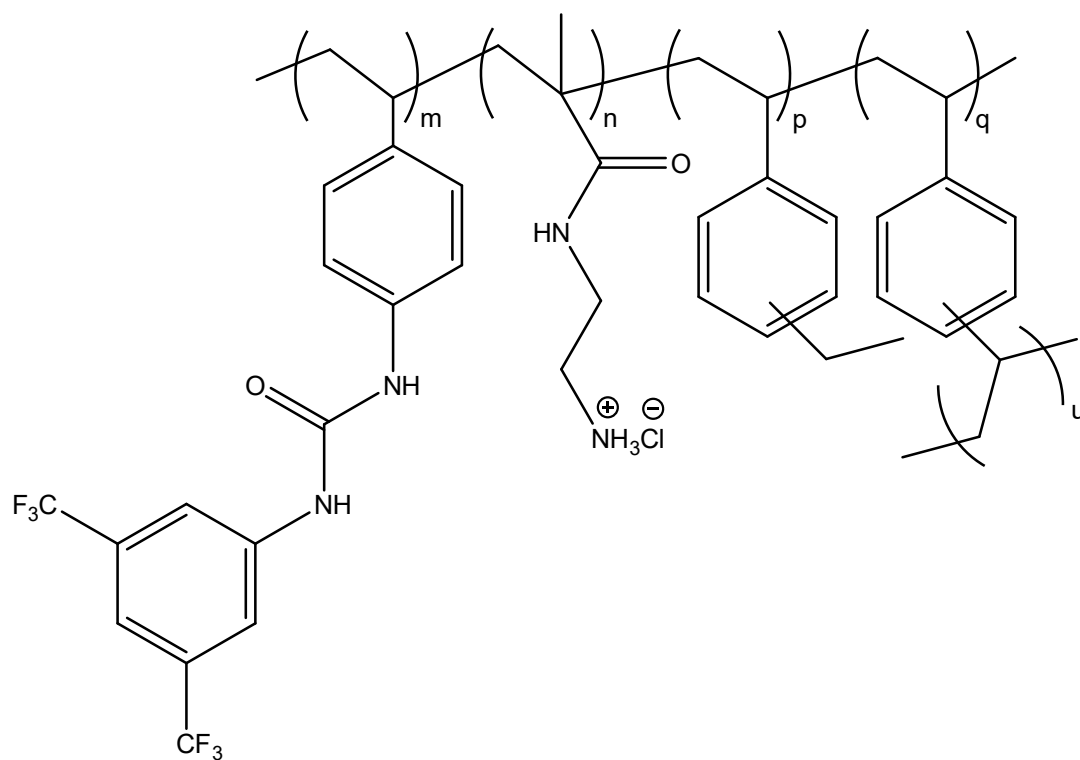


Figure 2.9 Chemical structure of MAS3 and MAS3(B) poly(NTPVU-co-EAMA.HCl-co-DVB-80).

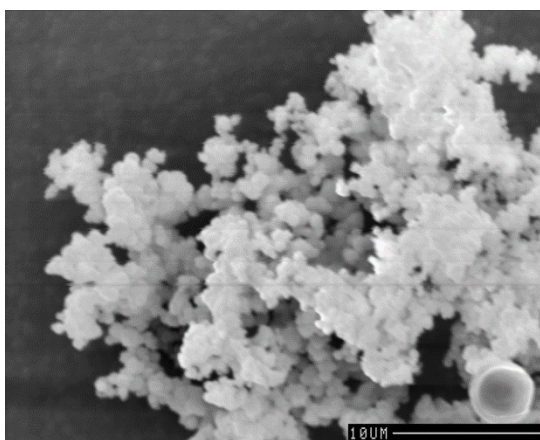


Figure 2.10 SEM image of MAS3;  $\times 3020$  magnification (scale = 10  $\mu\text{m}$ ).



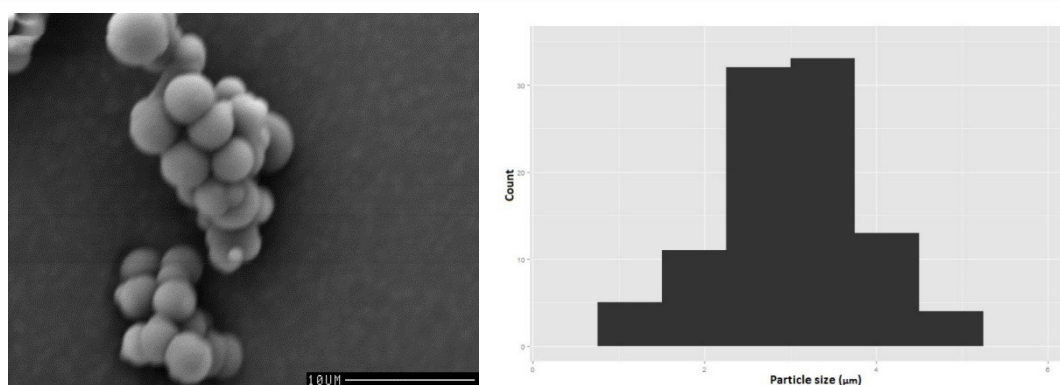


Figure 2.11 SEM image (left) and particle size distribution (right) of MAS3(B) ( $d = 2.99 \mu\text{m} \pm 0.91 \mu\text{m}$ );  $\times 3020$  magnification for SEM image (scale =  $10 \mu\text{m}$ ).

Table 2.3 Effect of PP feed compositions and type of reaction vessel on the yield of the polymer products.

Polymer code	Polymer name	Vessel type: Kimax tube or NG bottle	Yield (%)
MAS1	poly(DVB-80)	Kimax	29
MAS2	poly(EAMA.HCl-co-DVB-80)	Kimax	24
MAS3	poly(NTPVU-co-EAMA.HCl-co-DVB-80) <sup>a</sup>	Kimax	28
MAS3(B)	poly(NTPVU-co-EAMA.HCl-co-DVB-80) <sup>a</sup>	NG	4
MAS4	poly(EAMA.HCl-co-DVB-80) <sup>b</sup>	Kimax	22
MAS4(B)	poly(EAMA.HCl-co-DVB-80) <sup>b</sup>	NG	19

a and b superscripts mean that in these polymerisations the following components were also included: TBA.HO and PMP, for a and b, respectively.

NG refers to Nalgene polyethylene bottle.

Table 2.4 Microscopic characterisation of morphology of polymer microspheres.

Polymer code	Optical microscopy observation			Bead average diameter in $\mu\text{m}$ ( $\pm\text{SD}$ ) <sup>a</sup>
	Dispersity	Bead size ( $\mu\text{m}$ )	Aggregation	
MAS1	Narrow PSD <sup>c</sup>	1-2	None	1.45 (0.10)
MAS2	Narrow PSD <sup>c</sup>	3-4	None	4.12 (0.43)
MAS3	Polydisperse	Beads? <sup>d</sup>	Chemical	approx. 1
MAS3(B) <sup>b</sup>	Polydisperse	Beads? <sup>d</sup>	None	2.99 (0.91)
MAS4	Polydisperse	2-3	Physical	1.99 (1.12)
MAS4(B) <sup>b</sup>	Polydisperse	3-4	Physical	4.48 (1.24)

a A population of 100 microspheres from SEM image was measured for the determination of bead av. diameters.

b B letter in the polymer name means that these polymers were prepared in Nalgene polyethylene bottles, e.g., MAS3(B).

c PSD = Particle Size Distribution.

d Beads? indicates uncertainty whether the observed structures were microspheres.

### 2.1.3.2 Selection of the precipitation polymerisation conditions

A series of non-imprinted polymers were prepared in order to design the conditions for the synthesis of MIPs for peptide targets. For success, precipitation polymerisations must involve the polymerisation of monomers in dilute solution (typically < 5% w/v monomer in solvent) in a near- $\Theta$  solvent, therefore DVB-80 was selected as crosslinker, the porogen was acetonitrile and the monomer concentration was fixed at 2% w/v. A small volume of DMSO was required to promote solubility of EAMA.HCl and keep all components in solution prior to polymerisation, but use of DMSO was kept to a minimum. The solubility tests performed helped to determine the amount of DMSO needed to turn all the PP components successfully into a homogenous state. High crosslinker levels were used to ensure good yields of mechanically robust polymer microspheres with well-developed and permanent porous morphology. 2,2'-Azobisisobutyronitrile (AIBN) was the initiator of choice and free radicals were generated thermally. The duration of polymerisation was 24h as it was compatible with the half-life of AIBN at 60 °C which is around 10 h.<sup>16</sup> *N*-(2-Aminoethyl)methacrylamide hydrochloride and *N*-3,5-bis(trifluoromethyl)-

phenyl-*N'*-4-vinylphenylurea were selected as functional monomers. PMP and TBA.HO were used to bring the various functional groups into appropriate ionization states for non-covalent interactions. The mole ratio of DVB to *N*-3,5-*bis*(trifluoromethyl)-phenyl-*N'*-4-vinylphenylurea was set at 1:0.01. The mole ratio of EAMA.HCl to DVB was set at 0.1:5, while in earlier work the mole ratio of EAMA.HCl to DVB used was 1:5.<sup>40</sup> Such a change to the mole ratio of crosslinker: EAMA.HCl and use such of a small amount of *N*-3,5-*bis*(trifluoromethyl)-phenyl-*N'*-4-vinylphenylurea in the polymer networks would also help further to minimise the formation of non-specific binding in synthesis of the molecularly imprinted polymers. With this study, PP conditions have been identified for further synthesis of MIPs where EAMA.HCl and/or the NTPVU are used as the functional monomer(s).

## 2.2 Molecularly imprinted polymer microspheres for a $\beta$ -Amyloid target

### 2.2.1 $\beta$ -Amyloid and diagnosis of Alzheimer's disease

Alzheimer's disease (AD) is a neurodegenerative disorder, first reported by Alois Alzheimer at the beginning of the 20th century.<sup>17</sup> The disease results in functional problems such as speech deterioration, ability to make decisions, judgement, attention span and other symptoms that are associated with the impairment of memory and cognitive functions. Nowadays, the early detection of AD is still challenging, and in fact there is no straightforward and cheap diagnosis tool that can detect the disorder before irreversible changes appear in the brain.<sup>18</sup>

The underlying mechanism for AD development is based on the formation of protein agglomerates: insoluble A $\beta$  peptide and neurofibrillary tangles are deposited inside and outside of neurons. The high accumulation causes healthy neurons to lose their function, and as a consequence contributes to the loss of brain cell function and communication, and finally leads to their death.<sup>19</sup> The aggregates of A $\beta$  peptide are in the group of biomarkers that have particular importance in the early diagnosis of AD, as their presence can be reported before pathophysiological changes are

observed. The graph presented in Figure 2.12 shows the stages of the disease along with biomarker occurrence.<sup>20</sup>

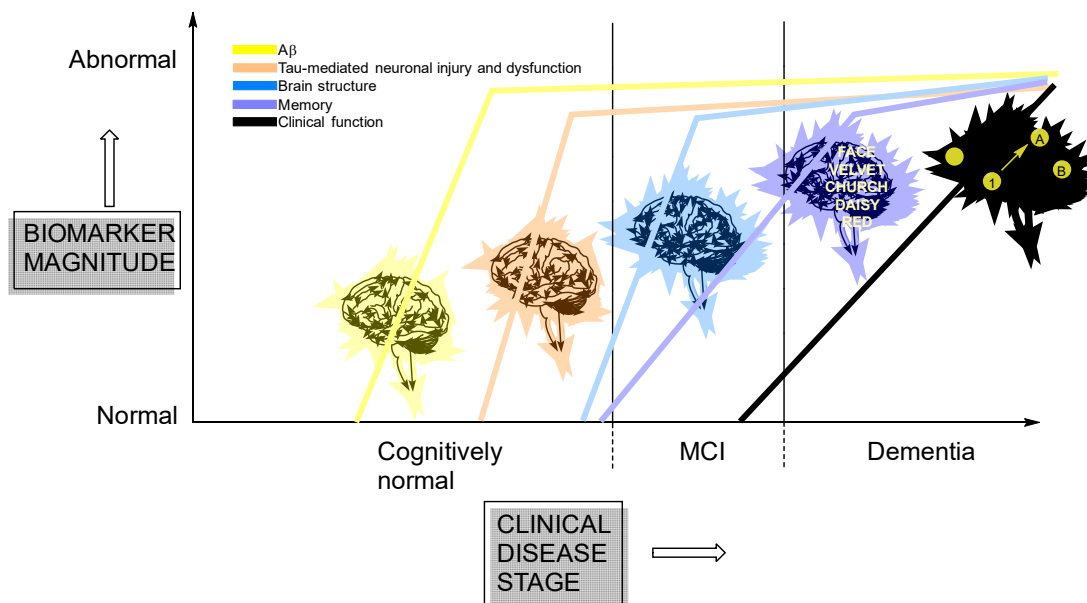


Figure 2.12 Biomarkers that help to predict AD. MCI refers to Mild Cognitive Impairment.

Scheme adapted from ref.<sup>20</sup>.

The A $\beta$  peptide exists in two forms, A $\beta$ 40 and A $\beta$ 42, which comprise 40 and 42 amino acid residues, respectively (Figure 2.13). Each of these isoforms consist of a highly hydrophobic C-terminal domain, and a structure of  $\beta$ -strands that is formed by 28 residues.<sup>21</sup> The peptide occurs in very low concentrations in cerebrospinal fluid, reaching a few hundred pg/mL only. Analytical methods which are currently available do not allow for its precise quantification and detection. The difficulties in identification of the A $\beta$  peptides arise from the fact that its isoforms self-polymerise, forming more complex units. Another challenge arises due to the occurrence of other proteins in the analysed samples, such as albumin and  $\alpha$ -2-macroglobulin that mask the peptide and hinder its detection.<sup>12,22</sup>

**$\beta$ -Amyloid**

	<u>10</u>	<u>20</u>	<u>30</u>	<u>40</u>
A $\beta$ 42	DAEFRHDSGY	EVHHQKLVFF	AEDVGSNKGA	IIGLMVGGVV <b>IA</b>
A $\beta$ 40	DAEFRHDSGY	EVHHQKLVFF	AEDVGSNKGA	IIGLMVGGVV

Figure 2.13 Sequences of amino acids (AAs) of  $\beta$ -Amyloid isoforms: A $\beta$ 42 and A $\beta$ 40. The AAs that are underlined represent a distinct part of the isoforms. The AAs in bold are selected as a target analyte for the synthesis of MIPs. Scheme adapted from ref.<sup>23</sup>.

Therapy and/or drugs work most efficiently in the early stage of the disease, however in most cases AD is detected too late when the brain starts to degenerate and significant disease progress is observed.

### 2.2.2 Aim of study

In our design and synthesis studies of polymer materials for a  $\beta$ -Amyloid target, we hypothesize that

- MIPs as the synthetic materials have binding sites that have high affinity and selectivity for a given target molecule;
- use of spherical MIPs is desirable since they are more robust and suited to be packed in solid-phase extraction cartridges or analytical columns, resulting in lower back pressures. Microspheres have also rapid binding kinetics and consequently good binding affinity for the target analyte, due to the improved accessibility of binding sites;
- PP conditions are successfully identified for the synthesis of spherical non-imprinted poly(EAMA.HCl-co-DVB-80) and poly(NTPVU-co-EAMA.HCl-co-DVB-80) in the micron size range. These reaction conditions would be implemented for the synthesis of imprinted polymers;

- $\beta$ -Amyloid is considered as a biomarker which is highly sensitive and specific for Alzheimer's Disease.

Based on this, the aims of the work presented in this section were as follows:

- Design and synthesis of polymer materials for a  $\beta$ -Amyloid target;
- Characterisation of materials produced;
- Delivery of the first generation materials to the PEPMIP partners for evaluation of molecular recognition. An objective was to deliver optimised imprinted materials which can enable the selective extractions of biomarker target from native blood or cerebrospinal fluid samples.

The molecular recognition work discussed in the Results and discussion section was performed by Dr Roberto Boi from Essen University.

## 2.2.3 Experimental section

### 2.2.3.1 *Materials*

The peptide template Ac-GGVVIA-OH (>95% purity), was purchased from LifeTein, *N*-(2-aminoethyl)methacrylamide hydrochloride (EAMA.HCl, purity  $\geq 98\%$ ) was purchased from Polysciences Inc. (Niles, IL, USA), *N*-3,5-*bis*(trifluoromethyl)-phenyl-*N'*-4-vinylphenylurea (NTPVU, purity >95%) is not commercially available and was kindly donated by Dortmund University, 2,2'-Azobisisobutyronitrile (AIBN, purity 98%) was purchased from BDH Lab. Supplies (UAE). Divinylbenzene-80 (DVB-80, 80% DVB isomers and 20% ethylvinylbenzene isomers), 1,2,2,6,6-pentamethylpiperidine (PMP, purity >99%), tetrabutylammonium hydroxide solution (TBA.HO, 1.0 M in methanol, 25%  $\leq$  purity <50%) and hydrochloric acid (37 wt. % in H<sub>2</sub>O) were all purchased from Sigma-Aldrich (St. Louis, MI, USA). DVB-80 was purified by filtration through a short plug of neutral aluminium oxide prior to use. AIBN was recrystallized

from acetone at low temperature. All other chemicals used (acetonitrile [ACN], methanol and dimethyl sulfoxide [DMSO, purity  $\geq 99.9\%$ ]) were of analytical grade.

#### *2.2.3.2 Synthesis and characterisation of molecularly imprinted polymer microspheres for $\beta$ -Amyloid target*

MIPs and their corresponding NIPs were synthesised by a typical PP procedure as described elsewhere.<sup>7</sup> The PP method has been presented and discussed in detail in Chapter 1. The methods used for the characterisation of MIPs are presented in 2.1.2.2.

A series of MIPs and their corresponding non-imprinted counterparts were prepared. The monomer feed compositions of the first generation materials is shown Table 2.5. Each MIP was prepared as one part of a pair together with the corresponding non-imprinted counterpart, with the exception of polymer MAS5. Polymers were synthesised mainly on a 0.5 g monomer scale, with a monomer and initiator concentrations of 2% w/v (with respect to the solvent) and 2 mol% (respect to the total number of polymerisable double bonds), respectively. Some polymers were also formulated on a 1 g monomer scale by increasing the monomer and initiator concentrations to 3% w/v and 4 mol% (MAS8 and MAS9) or by doubling of the amount of all reagents used (MAS10 and MAS11). 24 hours was the precipitation polymerisation time, but the last MIP and NIP pairs (MAS12 and MAS13) had a polymerisation time of 48 hours.

Table 2.5 Feed compositions for Ac-GGVVIA-OH imprinted polymers and their corresponding NIPs.

Polymer code	Template (mmol)	Functional Monomer (mmol)	DVB-80 (mmol)	Solvent (mL)	AIBN (mol%)	TBA.HO (mmol)
MAS5	0.07	EAMA.HCl (0.07) NTPVU (0.007)	3.71	ACN (24) DMSO (1)	2	0.007
MAS6	-	EAMA.HCl (0.07) NTPVU (0.007)	3.71	ACN (24) DMSO (1)	2	0.007
MAS7	0.07	EAMA.HCl (0.07) NTPVU (0.07)	3.71	ACN (24) DMSO (1)	2	0.007
MAS8	-	EAMA.HCl (0.1) NTPVU (0.01)	7.43	ACN (24) DMSO (1)	3	0.01
MAS9	0.01	EAMA.HCl (0.1) NTPVU (0.01)	7.43	ACN (24) DMSO (1)	3	0.01
MAS10	-	EAMA.HCl (0.1) NTPVU (0.01)	7.43	ACN (48) DMSO (2)	2	0.01
MAS11	0.01	EAMA.HCl (0.1) NTPVU (0.01)	7.43	ACN (48) DMSO (2)	2	0.01
MAS12	-	EAMA.HCl (0.07) NTPVU (0.007)	3.71	ACN (24) DMSO (1)	2	0.007
MAS13	0.07	EAMA.HCl (0.07) NTPVU (0.007)	3.71	ACN(24) DMSO (1)	2	0.007

The synthesis of the MIP with polymer code MAS5 can be serve as an illustrative example of the PP. Firstly, the template, Ac-GGVVIA-OH (4.2 mg, 0.07 mmol) was added into a borosilicate glass Kimax tube. Thereafter, DMSO (1 mL) was added (to dissolve the template) followed by TBA.HO (7.43  $\mu$ L, 0.007 mmol), the functional monomer *N*-3,5-*bis*(trifluoromethyl)-phenyl-*N'*-4-vinylphenylurea (2.5 mg, 0.007 mmol) and the functional monomer EAMA.HCl (12.3 mg, 0.07 mmol). ACN (24 mL) was then added followed by DVB-80 (0.49 g, 0.53 mL, 3.73 mmol) and AIBN (22.3 mg, 0.2 mmol). (For the synthesis of the corresponding NIP, the template was omitted from the synthetic protocols). The solution was then ultrasonicated for 10 minutes at ambient temperature and sparged with oxygen-free nitrogen gas for 10 minutes at ice-bath temperature, to remove dissolved molecular oxygen.



Thereafter, the reaction vessel was sealed under nitrogen and transferred to a Stuart Scientific S160 incubator equipped with a Stovall low-profile roller. The incubator temperature was ramped from ambient to 60 °C over a period of around two hours and then maintained at 60 °C for a further 22 hours to yield milky suspensions of polymer microspheres.

Finally, the polymer microspheres were isolated from the reaction medium by vacuum filtration on a 0.45 µm nylon membrane filter using a Vacuumbrand Vacuum System (2.0 mbar), washed sequentially with ACN (50 mL), MeOH/0.1 M aq. HCl (90/10, v/v, 50 mL) and MeOH (50 mL). The isolated product was transferred into pre-weighed vial and dried overnight in a Townson & Mercer vacuum oven (60 mbar) at 70 °C. The yield of the synthesised material was checked gravimetrically. The yield of MAS5 was 30%.

SEM together with image analysis, optical microscopy, FT-IR and nitrogen porosimetry analysis were performed. These analyses are introduced and discussed in detail in the 2.1.2.2 experimental section.

The first generation of MIPs and their corresponding NIPs were selected and delivered to Essen University. The molecular recognition of polymers were evaluated by Dr Roberto Boi.

## 2.2.4 Results and discussion

### 2.2.4.1 *Synthesis of MIPs and their corresponding NIPs*

Identification of the most promising PP conditions, aimed at giving porous products with narrow PSDs of diameters around 2-3 µm, in good yield, was achieved in the course of adjustment of reaction variables. MAS5 was the first MIP synthesised. This polymer was not prepared in a pair with a non-imprinted counterpart as was the case for the later syntheses. MAS5 was produced in moderate yield (Table 2.6). A change in the reaction vessel from a Kimax tube to a Nalgene polyethylene bottle, while keeping the same PP conditions, resulted in significant decreases in yield (MAS6 and

MAS7). However, the polymerisation yields increased considerably when the concentrations of monomers and initiator were raised to 4% w/v and 3 mol% (MAS8 and MAS9), presumably because of higher polymerisation rates. The same effect was observed when the polymers were prepared in 50 mL Kimax tubes on a one gram monomer scale, and the concentrations of monomers and initiator were kept at 2% w/v and 2 mol%, respectively (MAS10 and MAS11). Again, this was due to high level of crosslinker in the monomer feed. The extension of the polymerisation time from 24 h to 48 h, while keeping the concentrations of monomers and initiator at 2% w/v and 2 mol%, also resulted in good yields (MAS12 and MAS13). In this case, it was again expected as the longer polymerisation time contributes to higher yield. The isolated yields of the polymers (40-50%) were typical for the polymerisation of divinylbenzenes under such precipitation polymerisation conditions. This study provided a good indication of which PP conditions should be applied for further synthesis where peptide templates are used, together with EAMA.HCl and/or NTPVU used as the functional monomer(s).

Table 2.6 Effect of monomer and initiator concentrations, reaction time and scale, and type of reaction vessel used on the yield of the non-imprinted and Ac-GGVVIA-OH imprinted polymers.

Polymer code	Monomer conc. (% w/v) <sup>a</sup>	Initiator conc. (mol %) <sup>b</sup>	Incubation time (h)	Monomer scale (g)	Kimax or NG*	Yield (%)
MAS5	2	2	24	0.5	Kimax	30
MAS6	2	2	24	0.5	NG	25
MAS7	2	2	24	0.5	NG	6
MAS8	4	3	24	1	Kimax	46
MAS9	4	3	24	1	Kimax	48
MAS10	2	2	24	1	Kimax	42
MAS11	2	2	24	1	Kimax	36
MAS12	2	2	48	0.5	Kimax	62
MAS13	2	2	48	0.5	Kimax	58

a with respect to the solvent.

b with respect to the total number of polymerisable double bonds.

\*NG refers to Nalgene polyethylene bottles.

#### 2.2.4.2 Characterisation

The SEM micrographs show that the MIPs and NIPs produced are spherical in nature (example of SEM shown in Figure 2.14). Discrete particles in the micron-sized range had been produced, although the microspheres were polydisperse (possibly as a consequence of the presence of DMSO as a co-solvent). The quality of the particles was not ideal as the particles overlap or combine with each other into larger and irregular agglomerates. The SEM observations would suggest that the aggregation of particles was due to chemical bonds formed between the beads. Nevertheless, the particles were suitable for packing into trap columns. The microscopic analysis clearly

shows that the NIPs were of higher quality than the MIPs, suggesting a template effect.

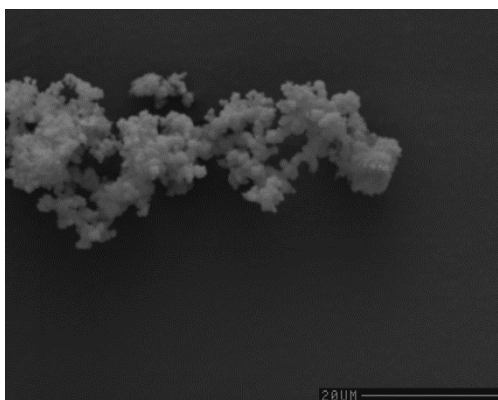


Figure 2.14 SEM image of MAS13;  $\times 1560$  magnification (scale = 20  $\mu\text{m}$ ).

Table 2.7 Microscopic characterisation of polymer microsphere morphology.

Polymer code	Optical microscopy observation			Bead average diameter in $\mu\text{m}^a$
	Dispersity	Bead size ( $\mu\text{m}$ )	Aggregation	
MAS5	Polydisperse	Beads? <sup>b</sup>	Chemical	approx. 1
MAS6	Polydisperse	1-2	Chemical	approx. 1
MAS7	Polydisperse	2-3	Chemical	approx. 1
MAS8	Polydisperse	1-2	Chemical	approx. 1
MAS9	Polydisperse	1-2	Chemical	approx. 1
MAS10	Polydisperse	Beads? <sup>b</sup>	Chemical	approx. 1
MAS11	Polydisperse	Beads? <sup>b</sup>	Chemical	approx. 1
MAS12	Polydisperse	1-2	Chemical	approx. 1
MAS13	Polydisperse	1-2	Chemical	approx. 1

<sup>a</sup> SEM microscopy observation.

<sup>b</sup> Beads? indicates uncertainty whether the observed structures were microspheres.

Nitrogen sorption analysis was performed only on those polymers which were delivered to PEPMIP partners.

The nitrogen sorption data, shown in Table 2.8, revealed that the MIPs and NIPs were macroreticular; this was important to establish in view of the need for analyte to

access the molecularly imprinted binding sites during MISPE. The NIPs were not identical to the MIPs in respect of their porous morphologies, again suggestive of the idea that the presence of template during polymerisation influences the polymerisation outcome.

Table 2.8 Nitrogen sorption analysis data for the non-imprinted and imprinted polymers for the Ac-GGVVIA-OH target.

Polymer code	BET C value	Specific surface area (m <sup>2</sup> /g)		Specific pore volume (cm <sup>3</sup> /g) <sup>a</sup>	Average pore diameter (nm) <sup>b</sup>
		BET	Langmuir		
MAS8	-20	63	77	n/a	n/a
MAS9	-342	322	435	0.154	3.12
MAS10	-41	106	142	0.013	1.67
MAS11	-178	278	373	0.115	3.10
MAS12	-177	621	835	0.115	2.15
MAS13	-218	392	529	0.167	2.99

<sup>a</sup> BJH cumulative adsorption pore volume of pores between 1.7 and 300 nm.

<sup>b</sup> Determined by equation: 4 pore volume/BET surface area.

n/a Not available.

In the nitrogen sorption analysis, the gradient of the BET plot is used in order to calculate the BET C value. BET C values describe how strong interactions are between absorbed nitrogen molecules and the tested solid. High BET C values are related with strong interaction between the nitrogen molecules and the solid. BET C values for NIPs and MIPs were negative, indicating that the data for the tested samples did not fit to BET a isotherm (Table 2.8). Negative BET C values mean that the nitrogen was absorbed in a single layer onto the surface of the solid rather than absorbed in several distinct layers. The interactions between nitrogen molecules were stronger than the interactions between the nitrogen molecules and the analysed materials. The change in sorption mode implies that the Langmuir isotherm should be used to describe the specific surface area of the tested polymers for the analysis porosimetry data. The porosimetry analysis shows that the average pore size reached a maximum of 3.12 nm (Table 2.8, MAS9). Tested polymers were highly crosslinked as poly(DVB-80)

constituted more than 97% of the whole polymer network structure. Such high crosslinking levels usually results in small pore size. High specific surface areas coupled with the average pore diameters of  $\sim 2$  nm, indicated that the materials tested were microporous.<sup>24</sup> These conclusions are supported by the analysis of nitrogen sorption isotherms (examples of obtained isotherms are shown in Appendix 1); a type I isotherm was generated (MAS8, MAS10, MAS11, MAS12 and MAS13). This isotherm is formed when a single layer of nitrogen molecules is absorbed on the solid and is typical for materials with microporous structures. In addition to the presence of micropores, there is a small percentage of mesopores within the materials tested (*i.e.*, pores  $> 2$  nm but  $< 50$  nm). The nitrogen sorption isotherm resembles a type II isotherm, characteristic for non-porous or macroporous solids with pore width more than 50 nm was also generated (MAS9). The first rise, known as “round knee”, was observed in the isotherm and such a rise indicates an approximate location of the monolayer formation.<sup>24</sup> There is also in the middle of the isotherm a low slope region which shows that the first few multilayers are formed. In the isotherm type II, the adsorption and desorption paths must be exactly the same.<sup>24</sup> In the case of the isotherm generated during the nitrogen sorption analysis of MIPs and NIPs, the desorption path was not exactly the same as the adsorption path. It indicated some divergence from the type II isotherm. This divergence, and the data from the nitrogen sorption analysis (3.12 nm average pore diameter) would suggest that part of material tested was mesoporous in nature.<sup>24</sup>

Unsurprisingly, given the high levels of DVB-80 used in the monomer feeds, the FT-IR spectra of the polymers (example of obtained spectra is shown in Appendix 2) were consistent with the formation of polydivinylbenzenes.

#### 2.2.4.3 Selection of the template

The epitope approach<sup>25–28</sup> was used for the design of MIPs, and precipitation polymerisation was the polymerisation method of choice since it delivers products directly in an appropriate format for packing into trap columns. A sequence of six amino acids (GGVVIA, shown in Figure 2.13), corresponding to the C- terminal

sequence of A $\beta$ 42-Amyloid peptide, was selected as the target analyte for the absolute quantification of A $\beta$ 42 in serum matrices. A close structural analogue of the hexapeptide was used as template for the synthesis of MIPs, rather than using the GGVVIA as template, to avoid the possibility of template bleeding interfering with the quantification of the biomarker. The template used was Ac-GGVVIA, where the N-terminus of the C- terminal of the A $\beta$ 42 peptide has been acetylated.

#### 2.2.4.4 Selection of functional and crosslinking monomers

*N*-(2-Aminoethyl)methacrylamide hydrochloride and *N*-3,5-*bis*(trifluoromethyl)-phenyl-*N'*-4-vinylphenylurea were selected as functional monomers since the carboxylic acid group in the C-terminus of the template was targeted *via* a non-covalent molecular imprinting approach. Indeed, both monomers have been shown to be useful for the targeting of oxy-anions.<sup>10,12,29</sup> TBA.HO was used to bring the various functional groups into appropriate ionization states for non-covalent interaction and to promote template solubility. Figure 2.15 shows a schematic representation of the Ac-GGVVIA-imprinted binding sites. For success, precipitation polymerisations must involve the polymerisation of monomers in dilute solution (typically < 5% w/v monomer in solvent) in a near- $\Theta$  solvent, therefore DVB-80 was selected as crosslinker, the porogen was acetonitrile and the monomer concentration was fixed at 2% w/v. A small volume of DMSO was required to promote solubility of

template and keep all components in solution prior to polymerisation, but use of DMSO was kept to a minimum.

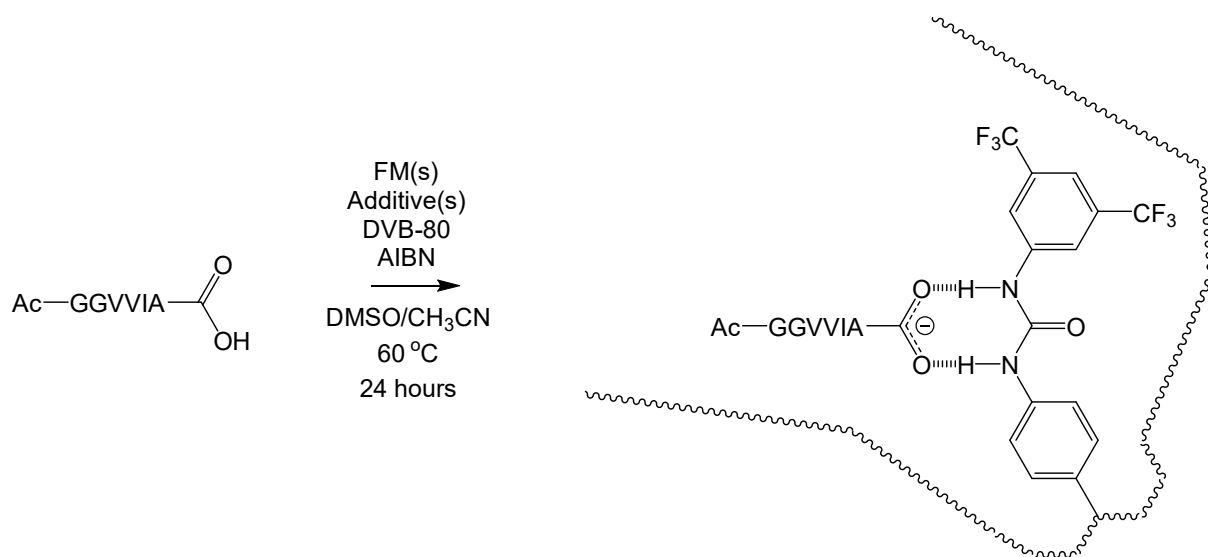


*Figure 2.15 Schematic representation of the non-covalent molecular imprinting of Ac-GGVVIA, a structural analogue of the  $\beta$ -Amyloid C-terminal hexapeptide. The carboxylic acid group in the C-terminus of Ac-GGVVIA is drawn explicitly for emphasis, since this functional group is involved in the self-assembly of the Ac-GGVVIA with functional monomers. The complexed synthetic receptor (right hand side) depicts a molecularly imprinted binding site formed upon the free radical copolymerisation of a 1:1 molecular complex of Ac-GGVVIA and N-3,5-bis(trifluoromethyl)-phenyl-N'-4-vinylphenylurea with N-(2-aminoethyl)methacrylamide hydrochloride and crosslinker (DVB-80).*

#### 2.2.4.5 Selection of the mole ratio of template: functional monomer(s): crosslinker

An important consideration in the molecular imprinting design process was the ratio of template to functional monomers to crosslinker. High crosslinker levels were used to ensure good yields of mechanically robust polymer microspheres with well-developed and permanent porous morphology. Initially, the same mole ratio of template to EAMA.HCl, 1:100 as reported in earlier work was planned to be used.<sup>30</sup> However, difficulties arose with the solubility of the functional monomer, EAMA.HCl,



in the PP solvent and it was not possible to use the same ratio of EAMA.HCl to template as in the earlier work. In the PP procedures used for the synthesis of MIPs for  $\beta$ -Amyloid target, the amount of EAMA.HCl used was ten times smaller than in the original procedure. The mole ratio of template to EAMA.HCl was set at 1:10; thus whilst an excess of functional monomer is used to promote template-functional monomer self-assembly, very large excesses of functional monomer are avoided to minimise the possibility of non-specific binding events arising from the random incorporation of excess EAMA.HCl into the polymer networks. The mole ratio of template to *N*-3,5-*bis*(trifluoromethyl)-phenyl-*N'*-4-vinylphenylurea was set at 1:1. This ratio was set at such a level as there was only one binding site in the template, the carboxylic acid group at the C-terminus. Additionally, such mole a ratio contributes to minimisation of the formation of non-specific binding sites.

Selected polymers targeting the  $\beta$ -Amyloid target, and their corresponding NIPs, were sent to a PEPMIP partner (Essen University) for off-line Molecularly Imprinted Solid-Phase Extraction (MISPE). Information on the molecular recognition was invaluable in respect of the further optimisation of synthetic protocols.

#### *2.2.4.6 Molecular recognition of the first generation of MIPs*

The molecular recognition work was performed by Dr Roberto Boi from Essen University. The polymers were tested using SPE coupled with Western Blotting and MALDI-TOF analyses. This subsection contains feedback received from Dr Boi after the testing of the first generation of MIPs for the A $\beta$ -Amyloid target.

During the SPE procedure, leakage of the polymers was observed. The polymers were present in almost every collected fraction. In some of the fractions, even though these, there was no visual sign of polymer particles, their presence was detected in Western Blotting as a massive interference or in MALDI as an absence of signal. The problem during testing could have been caused by the particles being too small. The polymer microspheres with particle diameters reaching at maximum  $\sim 2 \mu\text{m}$  were isolated. The SPE results did not show any specificity towards the A $\beta$  42 target peptide. Furthermore, frits or C8 filters that were used in the SPE procedure were

unfavorable for A $\beta$  enrichment. The flow was blocked through a SPE tube and the C8 filter could also be involved in the binding of A $\beta$  peptides. During testing, it was observed that the A $\beta$  peptide stuck to everything (non-specific bindings). The peptide adhered to almost every surface, including SPE tubes which are even a little hydrophobic in nature. A highly hydrophobic nature and susceptibility to aggregation were the main challenges in the analytical chemistry procedures applied to this biomarker.

Based on the feedback received, a focus of further research was on the preparation of a second generation of polymer microspheres for the  $\beta$ -Amyloid target, with mean diameters exceeding 2  $\mu\text{m}$ .

## 2.3 Molecularly imprinted polymer microspheres for pro-gastrin releasing peptide (ProGRP) target

### 2.3.1 ProGRP and diagnosis of small cell lung cancer (SCLC)

According to the WHO, lung cancer is the most frequent cancer. It has been estimated that 1.8 million new cases are diagnosed every year, and this accounts for almost 13% of the total diagnosed cancers. The disease contributes to 1.59 million deaths yearly, which is 19.4% of the total.<sup>31</sup>

3,4-Benzopyrene, occurring in cigarette smoke, is considered as the main agent causing lung cancer. The carcinogen causes mutation in DNA binding domains. Guanine is substituted by thymine resulting in inactivation of the p53 gene, blocking of the binding of specific target DNA sequences and activation of adjacent genes. It causes dysfunctions of protein p53 that is responsible for the cell cycle control in normally functioning organisms, and finally leads to lung abnormalities.<sup>32</sup> In patients suffering from the disease, enormous secretions of neuropeptides, hormones and cytoplasmic neurosecretory granules is reported. Among these are gastrin-releasing peptide (GRP), which is released into bloodstream, and its precursor pro-gastrin-releasing peptide (ProGRP).<sup>33</sup> The two-minute half-life of GRP makes it impossible to test its level, however ProGRP is more stable and reported as a highly specific new

biomarker for Small Cell Lung Cancer (SCLS).<sup>34</sup> ProGRP occurs physiologically in blood in very low concentration: from 2 to 50 pg/mL. Concentrations above this limit indicate an early stage of SCLC.<sup>35</sup> There are three isoforms of ProGRP (Figure 2.16), with the following number of amino acids: 148 (Isoform 1), 141 (Isoform 2) and 138 (Isoform 3). These isoforms have 120 amino acids which are homologous sequences, and the isoforms differ only in terms of the amino acids at the C-terminal ends.

**Pro-Gastrin-Releasing Peptide**

		<u>10</u>	<u>20</u>	<u>30</u>	<u>40</u>	<u>50</u>
Isoform 1	MRGRELPLVL	LALVLCLAPR	GRAVPLPAGG	GTVLTKMYPR	GNHWAVGHLM	
		<u>60</u>	<u>70</u>	<u>80</u>	<u>90</u>	<u>100</u>
	GKKSTGESSS	VSERGSLKQQ	LREYIRWEEA	<b>ARNLLGLIEA</b>	<b>KENRNHQPPQ</b>	
		<u>110</u>	<u>120</u>	<u>130</u>	<u>140</u>	
	PKALGNQQPS	WSEDSSNFK	<u>DVGSKGKVGR</u>	<u>LSAPGSQREG</u>	<u>RNPQLNQQ</u>	
		<u>10</u>	<u>20</u>	<u>30</u>	<u>40</u>	<u>50</u>
Isoform 2	MRGRELPLVL	LALVLCLAPR	GRAVPLPAGG	GTVLTKMYPR	GNHWAVGHLM	
		<u>60</u>	<u>70</u>	<u>80</u>	<u>90</u>	<u>100</u>
	GKKSTGESSS	VSERGSLKQQ	LREYIRWEEA	<b>ARNLLGLIEA</b>	<b>KENRNHQPPQ</b>	
		<u>110</u>	<u>120</u>	<u>130</u>	<u>140</u>	
	PKALGNQQPS	WSEDSSNFK	<u>DVGSKGKGSQ</u>	<u>REGRNPQLNQ</u>	<u>Q</u>	
		<u>10</u>	<u>20</u>	<u>30</u>	<u>40</u>	<u>50</u>
Isoform 3	MRGRELPLVL	LALVLCLAPR	GRAVPLPAGG	GTVLTKMYPR	GNHWAVGHLM	
		<u>60</u>	<u>70</u>	<u>80</u>	<u>90</u>	<u>100</u>
	GKKSTGESSS	VSERGSLKQQ	LREYIRWEEA	<b>ARNLLGLIEA</b>	<b>KENRNHQPPQ</b>	
		<u>110</u>	<u>120</u>	<u>130</u>		
	PKALGNQQPS	WSEDSSNFK	<u>DLVDSLLQVL</u>	<u>NVKEGTPS</u>		

Figure 2.16 Sequences of amino acids (AAs) of ProGRP isoforms. The AAs which are underlined represent distinct part of the isoforms.<sup>36</sup> The sequences of nine AAs shown in bold is the signature peptide selected as target analyte for ProGRP assay. Scheme adapted from ref.<sup>23</sup>.

Nowadays, the early detection of SCLC is still challenging. In fact, there is no straightforward and cheap diagnosis tool that can detect the cancer in the early stage when therapy and/or drugs work most efficiently. In most cases, SCLC is detected too late when significant disease progress is observed. Currently, there are only a few products available on the market for quantification of ProGRP from blood. Amongst

these are antibody-based immunoassays offered by Roche, Abbott Diagnostics and Fujirebio Diagnostics, Inc. These tests are highly sensitive, but they are expensive and this prevents their use in the routine diagnosis of SCLC.

### 2.3.2 Aim of study

In our design and synthesis studies of polymer materials for the ProGRP target, we hypothesize that

- the conditions for the synthesis of MIPs for  $\beta$ -Amyloid target had been successfully identified, it is believed that this synthetic approach could be implemented for the synthesis of other peptide-based MIPs;
- ProGRP is considered as a biomarker which is highly sensitive and specific for Small Cell Lung Cancer.

Based on this, the aims of the work presented in this section were as follows:

- Design and synthesis of polymer macroreticular materials for ProGRP target;
- Characterisation of materials produced;
- Delivery of the first generation materials to the PEPMIP partners for evaluation of molecular recognition. An objective was to deliver optimised imprinted materials which can enable selective extractions of biomarker target from native blood or cerebrospinal fluid samples.

Most of the ProGRP analytical work presented in the Thesis was performed by Cecilia Rossetti, a PhD student from Oslo University. However, a secondment at Oslo University by the author of this Thesis enabled the author to participate in and contribute to this body of work. Much of the work presented in the Results and discussion subsection had been published in a co-authored paper<sup>37</sup> in Scientific Reports (Appendix 3).

### 2.3.3 Experimental section

#### 2.3.3.1 *Materials*

The peptide template Z-NLLGLIEA{Nle} (purity 96.58%), was purchased from LifeTein, *N*-(2-aminoethyl)methacrylamide hydrochloride (EAMA.HCl, purity  $\geq 98\%$ ) was purchased from Polysciences Inc. (Niles, IL, USA), *N*-3,5-*bis*(trifluoromethyl)-phenyl-*N'*-4-vinylphenylurea (NTPVU, purity  $> 95\%$ ) is not commercially available and was kindly donated by Dortmund University. 2,2'-Azobisisobutyronitrile (AIBN, purity 98%) was purchased from BDH Lab. Supplies (UAE). Divinylbenzene-80 (DVB-80, 80% DVB isomers and 20% ethylvinylbenzene isomers), 1,2,2,6,6-pentamethylpiperidine (PMP, purity  $> 99\%$ ), tetrabutylammonium hydroxide solution (TBA.HO, 1.0 M in methanol,  $25\% \leq$  purity  $< 50\%$ ) and hydrochloric acid (37 wt. % in H<sub>2</sub>O) were all purchased from Sigma-Aldrich (St. Louis, MI, USA). DVB-80 was purified by filtration through a short plug of neutral aluminium oxide prior to use. AIBN was recrystallized from acetone at low temperature. All other chemicals used (acetonitrile [ACN], methanol and dimethyl sulfoxide [DMSO, purity  $\geq 99.9\%$ ]) were of analytical grade.

#### 2.3.3.2 *Synthesis and characterisation of molecularly imprinted polymer microspheres for ProGRP target*

MIPs and their corresponding NIPs were synthesised by typical a PP procedure as described elsewhere.<sup>7</sup> The PP method has been presented and discussed in details in Chapter 1. The methods used for the characterisation of MIPs are presented in 2.1.2.2.

A series of MIPs and their corresponding non-imprinted counterparts were prepared. The feed compositions of the first generation materials is shown in Table 2.9. Eight distinct pairs of polymers were synthesized: four MIPs (MAS17, MAS19, MAS21 and MAS23) and four corresponding non-imprinted polymers (NIPs) (MAS16, MAS18, MAS20 and MAS22). Polymers were produced on a 0.5 g monomer scale with a monomer and initiator concentration of 2% w/v (with respect to the solvent) and

2 mol% (with respect to the total number of polymerisable double bonds), respectively.

Table 2.9 PP conditions for Z-NLLGLIEA{Nle} imprinted polymers and their corresponding NIPs.

Polymer code	Template (mmol)	Functional Monomer (mmol)	DVB-80 (mmol)	Solvent (mL)	AIBN (mol%)	PMP and/ or TBA.HO (mmol)
MAS16	-	EAMA.HCl (0.07)	3.73	ACN (24) DMSO (1)	2	PMP (0.006)
MAS17	0.007	EAMA.HCl (0.07)	3.73	ACN (24) DMSO (1)	2	PMP (0.006)
MAS18	-	NTPVU (0.01)	3.73	ACN (24) DMSO (1)	2	TBA.HO (0.01)
MAS19	0.007	NTPVU (0.01)	3.73	ACN (24) DMSO (1)	2	TBA.HO (0.01)
MAS20	-	EAMA.HCl (0.07)	3.73	ACN (24) DMSO (1)	2	PMP (0.01)
MAS21	0.007	EAMA.HCl (0.07)	3.73	ACN (24) DMSO (1)	2	PMP (0.01)
MAS22	-	EAMA.HCl (0.07) NTPVU (0.01)	3.73	ACN (24) DMSO (1)	2	PMP (0.01) TBA.HO (0.01)
MAS23	0.007	EAMA.HCl (0.07) NTPVU (0.01)	3.73	ACN (24) DMSO (1)	2	PMP (0.01) TBA.HO (0.01)

The synthesis of the MIP with polymer code MAS23 can serve as an illustrative example of the PP procedure. Firstly, the template, Z-NLLGLIEA{Nle} (8.2 mg, 0.007 mmol) was added into a borosilicate glass Kimax tube. Thereafter, DMSO (1 mL) was added (to dissolve the template), followed by PMP (1.9 mg, 0.01 mmol), the functional monomer EAMA.HCl (12.3 mg, 0.07 mmol), TBA.HO (3.93 mg, 0.01 mmol) and the functional monomer *N*-3,5-*bis*(trifluoromethyl)-phenyl-*N'*-4-vinylphenylurea (5.25 mg, 0.01 mmol). ACN (24 mL) was then added followed by DVB-80 (0.49 g, 0.53 mL, 3.73 mmol) and AIBN (22.3 mg, 0.2 mmol). (For the synthesis of the corresponding NIP, the template was omitted from the synthetic protocol). The solution was then ultrasonicated for 10 minutes at ambient temperature and

sparged with oxygen-free nitrogen gas for 10 minutes at ice-bath temperature, to remove dissolved molecular oxygen. Thereafter, the reaction vessel was sealed under nitrogen and transferred to a Stuart Scientific S160 incubator equipped with a Stovall low-profile roller. The incubator temperature was ramped from ambient to 60 °C over a period of around two hours and then maintained at 60 °C for a further 22 hours to yield milky suspensions of polymer microspheres.

Finally, the polymer microspheres were isolated from the reaction media by vacuum filtration on a 0.45 µm nylon membrane filter using a Vacuumbrand Vacuum System (2.0 mbar), washed sequentially with ACN (50 mL), MeOH/0.1 M aq. HCl (90/10, v/v, 50 mL) and MeOH (50 mL). The isolated product was transferred into a pre-weighed vial and dried overnight in a Townson & Mercer vacuum oven (60 mbar) at 70 °C. The yield of the synthesised material was checked gravimetrically. The yield of MAS23 was 52%.

SEM together with image analysis, optical microscopy, FT-IR spectroscopy and nitrogen sorption analysis were performed. These analyses are introduced and discussed in detail in the 2.1.2.2 experimental section.

The first generation of MIPs and their corresponding NIPs were selected and delivered to Oslo University. The molecular recognition of polymers were tested by Cecilia Rossetti, a PhD student within the PEPMIP project. The secondment at Oslo University allowed the author of the Thesis to participate in this piece of work.

## 2.3.4 Results and discussion

### 2.3.4.1 *Synthesis of MIPs and their corresponding NIPs*

The non-imprinted and imprinted polymers for the Z-NLLGLIEA{Nle} target were prepared in good yields; the average yield of particles was 47% (Table 2.10). The yields of products were variable and depended upon the polymerisation conditions. The yields of isolated MIPs were lower than for the corresponding NIPs: MAS18 and



MAS19, and MAS20 and MAS21. In the case of other pairs of polymers, the yield of MIPs was similar to the NIPs.

Table 2.10 Effect of polymer compositions on the yield of the polymer products.

Polymer code	Polymer name	Yield (%)
MAS16	poly(EAMA.HCl-co-DVB-80)	54
MAS17	poly(EAMA.HCl-co-DVB-80)	47
MAS18	poly(NTPVU-co-DVB-80)	49
MAS19	poly(NTPVU-co-DVB-80)	34
MAS20	poly(EAMA.HCl-co-DVB-80)	54
MAS21	poly(EAMA.HCl-co-DVB-80)	41
MAS22	poly(NTPVU-co-EAMA.HCl-co-DVB-80)	49
MAS23	poly(NTPVU-co-EAMA.HCl-co-DVB-80)	52

#### 2.3.4.2 Characterisation

The SEM micrographs of the MIP and NIP microspheres (example of SEMs shown in Figure 2.17) revealed that discrete particles in the micron-sized range suitable for packing into trap columns had been produced, although the microspheres were polydisperse (possibly as a consequence of the presence of DMSO as a co-solvent). Particles overlap or combine with each other into larger and irregular agglomerates. The NIP marked MAS18 was determined to be imprinted of narrowly distributed microspheres only. The particle size distribution analysis was performed for the NIPs only, with the exception of MAS22 where EAMA.HCl was copolymerised with the NTPVU. The microscopic analysis clearly shows that the NIPs were of higher quality than the MIPs, suggesting a template effect (example of SEMs shown in Figure 2.17).

Table 2.11 Microscopic characterisation of polymer microsphere morphology.

Polymer code	Optical microscopy observation			Bead average diameter ( $\mu\text{m}$ ) ( $\pm\text{SD}$ ) <sup>a</sup>
	Dispersity	Bead size ( $\mu\text{m}$ )	Aggregation	
MAS16	Polydisperse	3-5	Physical	4.99 (0.83)
MAS17	Polydisperse	2-5	Chemical	approx. 1
MAS18	Narrow PSD <sup>b</sup>	2-3	Physical	1.99 (0.47)
MAS19	Polydisperse	1	Physical	approx. 1
MAS20	Polydisperse	4-5	Physical	4.94 (0.65)
MAS21	Polydisperse	1-5	Chemical	approx. 1
MAS22	Polydisperse	Beads? <sup>c</sup>	Chemical	> 20
MAS23	Polydisperse	Beads? <sup>c</sup>	Chemical	approx. 1

<sup>a</sup> A population of 100 microspheres from SEM image was measured for the determination of bead av. diameters.

<sup>b</sup> PSD = Particle Size Distribution.

<sup>c</sup> Beads? indicates uncertainty whether the observed structures were microspheres.

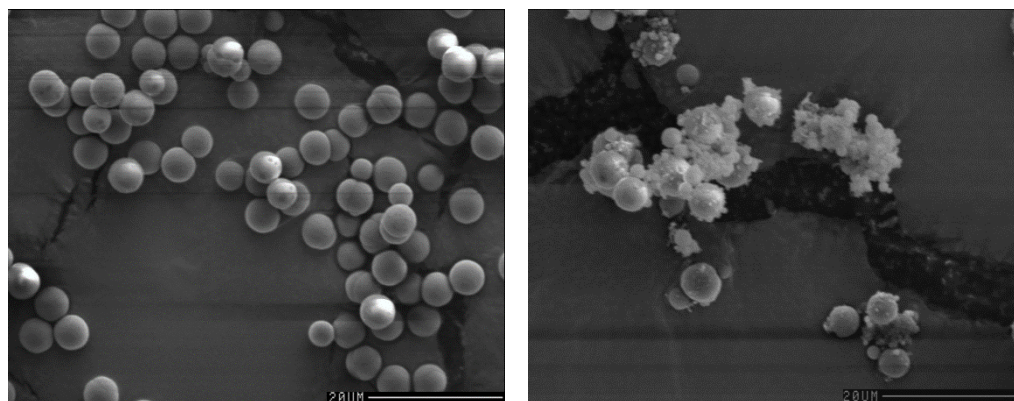


Figure 2.17 SEMs image of MAS20 non-imprinted polymer (left) and MAS21 imprinted polymer (right) (magnifications:  $\times 1500$  and  $\times 1560$  for left and right, respectively; scale =  $20 \mu\text{m}$ ).

The nitrogen sorption analysis required 0.2-0.3 g amount of material. In the case of a few samples, it was not possible to perform nitrogen sorption analysis as there was insufficient material to accomplish this analysis satisfactorily (MAS17). Even though, an attempt was made to perform this analysis with smaller amount of the material.

The nitrogen sorption data, shown in Table 2.12, revealed that the MIPs and NIPs were macroporous; this was important to establish in view of the need for analyte to access molecularly imprinted binding sites during MISPE. The NIPs were not identical to the MIPs in respect of their porous morphologies, again suggestive of the idea that the presence of template during polymerisation influences the polymerisation outcomes.

Table 2.12 Nitrogen sorption analysis data for the non-imprinted and imprinted polymers for the Z-NLLGLIEA{Nle} target.

Polymer code	BET C value	Specific surface area (m <sup>2</sup> /g)		Specific pore volume (cm <sup>3</sup> /g) <sup>a</sup>	Average pore diameter (nm) <sup>b</sup>
		BET	Langmuir		
MAS16	-136	273	364	0.028	1.96
MAS17	-83(±3)	23 (±10)	38(±7)	n/a	n/a
MAS18	-135	371	496	0.042	2.02
MAS19	-104	324	433	0.087	2.75
MAS20	-163	221	297	0.036	2.10
MAS21	-149(±26)	31(±20)	42(±2)	n/a	n/a
MAS22	-127	307	410	0.026	1.96
MAS23	-195	349	468	0.083	2.34

<sup>a</sup> BJH cumulative adsorption pore volume of pores between 1.7 and 300 nm.

<sup>b</sup> Determined by equation: 4 pore volume/BET surface area.

n/a Not available.

The BET C values for the NIPs and MIPs were negative, indicating that the data for the tested samples did not fit to the BET isotherm as the nitrogen molecules were sorbed in a single layer onto the surface of the solids. (Table 2.12). This change in sorption mode implies that the Langmuir isotherm should be used to describe the specific surface area of the tested polymers for the analysis. The analysis shows that the average pore size reached a maximum of 2.75 nm (Table 2.12, MAS19). The tested polymers were highly crosslinked as poly(DVB-80) constituted more than 97% of the whole polymer network structure and such high crosslinking level usually results in small pore size. High specific surface areas coupled with the average pore diameters

of ~2 nm, indicated that the materials tested were microporous.<sup>24</sup> These conclusions are supported by the analysis of nitrogen sorption isotherms. A type I isotherm was generated (MAS16, MAS18, MAS20, MAS22, MAS22 and MAS23). This isotherm is formed when a single layer of nitrogen molecules is absorbed on the solid and is typical for materials with microporous structure. In addition to the presence of micropores, there can be a small percentage of mesopores within the materials tested (*i.e.*, pores > 2 nm and < 50 nm). The nitrogen sorption isotherm which resembles type II isotherm, characteristic for non-porous or macroporous solids with pore width more than 50 nm was also generated (MAS19). In this isotherm generated during the analysis, some divergence was observed: the desorption path was not exactly the same as the adsorption path. This divergence indicated the presence of mesoporous in the polymer network structures.<sup>24</sup> The nitrogen sorption isotherms of MAS17 and MA21 do not resemble any known isotherms (MAS21 isotherm shown in Appendix 1). A sharp initial region, which is related with very strong adsorption, followed by a gradual decrease and sharp rise in nitrogen adsorption were observed. The gradual decrease in adsorption could be related to insufficient drying of the samples.<sup>24</sup> The nitrogen sorption analysis together with drying procedure was repeated three times, however the same nitrogen sorption isotherms were obtained. It could be due to insufficient amount of the materials used for this analysis.

Unsurprisingly, given the high levels of DVB-80 used in the monomer feeds, the FT-IR spectra of the polymers (spectra not shown) were consistent with the formation of polydivinylbenzenes.

#### 2.3.4.3 *Selection of the template*

Signature peptide imprinting<sup>10,37</sup> was used for the design of MIPs, and precipitation polymerisation was the polymerisation method of choice since it delivers products directly in an appropriate format for packing into trap columns. A sequence of nine amino acids (NLLGLIEAK, shown in Figure 2.16), corresponding to the signature peptide of ProGRP, was selected as the target analyte for the absolute quantification of ProGRP in serum matrices. A close structural analogue of the signature peptide

was used as template for the synthesis of MIPs, rather than using the signature peptide as template, to avoid the possibility of template bleeding interfering with the quantification of the biomarker. The template used was Z-NLLGLIEA{Nle}; in effect, the N-terminus of the signature peptide has been protected with a benzyloxycarbonyl group (Cbz; Z) to enhance the solubility of the template in the porogenic solvents used for the precipitation polymerisations, and the C-terminal lysine has been replaced by norleucine (Nle).<sup>38</sup> This strategy helps to eliminate intramolecular competition caused by the lysine which interfere negatively with the analysis.<sup>37</sup>

#### 2.3.4.4 Selection of the functional and crosslinking monomers

*N*-(2-Aminoethyl)methacrylamide hydrochloride and *N*-3,5-bis(aminoethylmethyl)-phenyl-*N'*-4-vinylphenylurea were selected as functional monomers since the carboxylic acid groups in the glutamic acid (E) residue and C-terminus of the template were targeted *via* a non-covalent molecular imprinting approach. Indeed, both monomers have been shown to be useful for the targeting of oxy-anions.<sup>20,39,40</sup> PMP and TBA.HO were used to bring the various functional groups into appropriate ionization states for non-covalent interactions and to promote template solubility. Figure 2.18, Figure 2.19 and Figure 2.20 show schematic representations of the Z-NLLGLIEA{Nle}-imprinted binding sites in MIPs MAS17 and MAS21, MAS19 and MAS23, respectively. For success, precipitation polymerisations must involve the polymerisation of monomers in dilute solution (typically < 5% w/v monomer in solvent) in a near- $\Theta$  solvent, therefore DVB-80 was selected as crosslinker, the porogen was acetonitrile and the monomer concentration was fixed at 2% w/v. A small volume of DMSO was required to promote solubility of template and keep all components in solution prior to polymerisation, but use of DMSO was kept to a minimum.

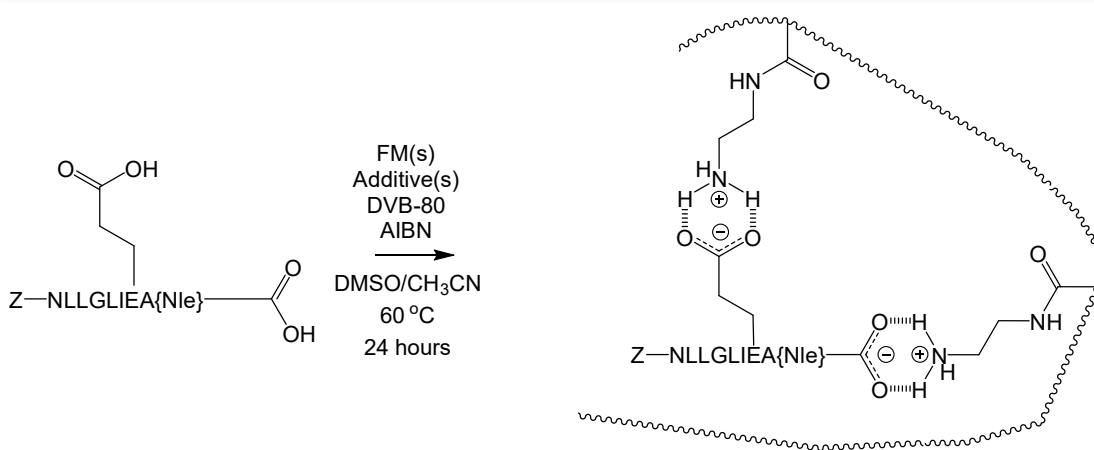


Figure 2.18 Schematic representation of the non-covalent molecular imprinting of Z-NLLGLIEA{Nle}, a structural analogue of the ProGRP signature peptide. The carboxylic acid groups in the glutamic acid (E) residue and C-terminus of Z-NLLGLIEA{Nle} are drawn explicitly for emphasis, since these functional groups are involved in the self-assembly of the Z-NLLGLIEA{Nle} with functional monomers (FMs). The complexed synthetic receptor (right hand side) depicts a molecularly imprinted binding site formed upon the free radical copolymerisation of a 1:2 molecular complex of Z-NLLGLIEA{Nle} and N-(2-aminoethyl)methacrylamide hydrochloride with crosslinker (DVB-80).

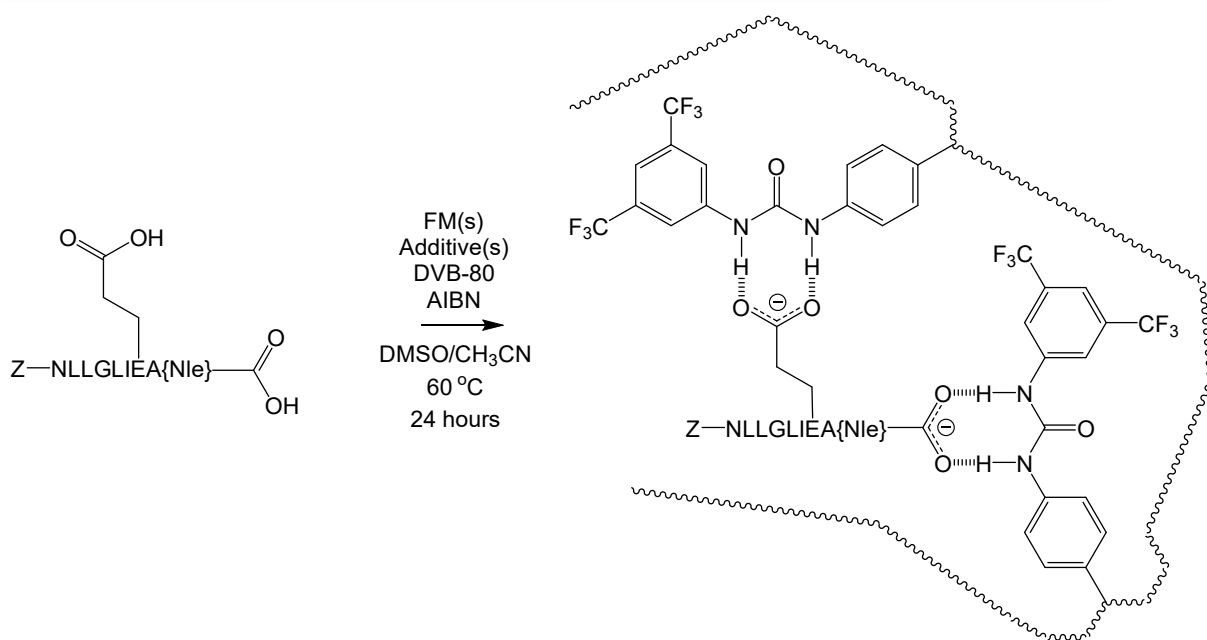


Figure 2.19 Schematic representation of the non-covalent molecular imprinting of  $Z\text{-NLLGLIEA}\{Nle\}$ , a structural analogue of the ProGRP signature peptide. The carboxylic acid groups in the glutamic acid (E) residue and C-terminus of  $Z\text{-NLLGLIEA}\{Nle\}$  are drawn explicitly for emphasis, since these functional groups are involved in the self-assembly of the  $Z\text{-NLLGLIEA}\{Nle\}$  with functional monomers (FMs). The complexed synthetic receptor (right hand side) depicts a molecularly imprinted binding site formed upon the free radical copolymerisation of a 1:2 molecular complex of  $Z\text{-NLLGLIEA}\{Nle\}$  and  $N\text{-3,5-bis(trifluoromethyl)-phenyl-N'-4-vinylphenylurea}$  with crosslinker (DVB-80).

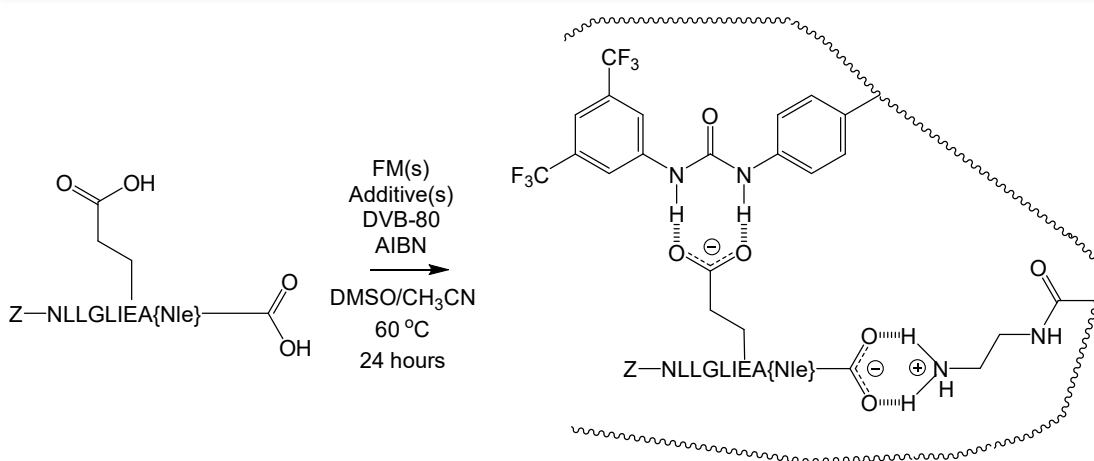


Figure 2.20 Schematic representation of the non-covalent molecular imprinting of Z-NLLGLIEA{Nle}, a structural analogue of the ProGRP signature peptide. The carboxylic acid groups in the glutamic acid (E) residue and C-terminus of Z-NLLGLIEA{Nle} are drawn explicitly for emphasis, since these functional groups are involved in the self-assembly of the Z-NLLGLIEA{Nle} with functional monomers (FMs). The complexed synthetic receptor (right hand side) depicts a molecularly imprinted binding site formed upon the free radical copolymerisation of a 1:1:1 molecular complex of Z-NLLGLIEA{Nle}, N-(2-aminoethyl)methacrylamide hydrochloride and N-3,5-bis(trifluoromethyl)-phenyl-N'-4-vinylphenylurea with crosslinker (DVB-80).

#### 2.3.4.5 Selection of the mole ratio of template: functional monomer(s): crosslinker

An important consideration in the molecular imprinting design process was the ratio of template to functional monomers to crosslinker. High crosslinker levels were used to ensure good yields of mechanically robust polymer microspheres with well-developed and permanent porous morphology. The mole ratio of template to EAMA.HCl was set at 1:10; thus, whilst an excess of functional monomer is used to promote template-functional monomer self-assembly, very large excesses of functional monomer are avoided to minimise the possibility of non-specific binding events arising from the random incorporation of excess EAMA.HCl into the polymer networks. In earlier work, the mole ratio of template to EAMA.HCl used was 1:100.<sup>30</sup> The isolated yields of the polymers (40-50%) are typical for the polymerisation of



divinylbenzenes under such precipitation polymerisation conditions. The mole ratio of template to *N*-3,5-*bis*(trifluoromethyl)-phenyl-*N'*-4-vinylphenylurea was set at 1:2. This ratio was set at such a level as those were two sites in the template, the carboxylic acid group in the side chain of glutamic acid (E) and the carboxylic acid group at the C-terminus which are able to form oxyanions. Additionally, such a mole ratio contributed to minimisation of the formation of non-specific binding sites.

All prepared polymers targeting the ProGRP target, and their corresponding NIPs, were sent to a PEPMIP partners (Oslo University) for off-line Molecularly Imprinted Solid-Phase Extraction (MISPE) and G&T Septech for packing into capillary columns. Information on molecular recognition was invaluable in respect of the further optimisation of synthetic protocols.

#### *2.3.4.6 Molecular recognition of the first generation of MIPs*

The molecular recognition characteristics were interrogated together with Cecilia Rossetti, a PhD student from Oslo University. The results presented in the subsections were achieved collaboratively and are included in a co-authored paper<sup>37</sup> (Appendix 3). In this paper, the design, synthesis and analytical use of MIPs for SCLC diagnostics is presented. The synthetic receptors targeted a signature peptide derived from ProGRP, a blood-based biomarker for SCLC, and were used for on-line enrichment in bottom-up proteomics with quantification by mass spectrometry. The analytical work presented below was performed by Cecilia Rossetti, a PhD student from Oslo University.

##### *2.3.4.6.1 Peptide retention on MIP and corresponding NIP by direct injection of ProGRP isoform 1*

MIP A (MAS21), MIP B (MAS23), NIP A (MAS20) and NIP B (MAS22) polymers were packed into stainless steel columns and evaluated for peptide retention by direct injection of protein digests containing the target peptide NLLGLIEAK. Thus, ProGRP isoform 1 was trypsinated and loaded on the MIP and NIP columns which were, at this stage, used as analytical columns coupled directly with the ESI source of

the MS detector (Figure 2.21). The SRM transitions corresponding to the ProGRP peptides (LSAPGSQR and the target peptide NLLGLIEAK) were acquired from the moment of the injection to the end of the gradient. No retention was seen for the signature peptide of isoform 1 of ProGRP (LSAPGSQR) on both MIP (MAS23) and NIP (MAS22) columns. The target peptide, NLLGLIEAK, was retained longer on the MIP (19.05 minutes), and this was reassuring given the intention to use the MIP as a trap column in a later part of the study.

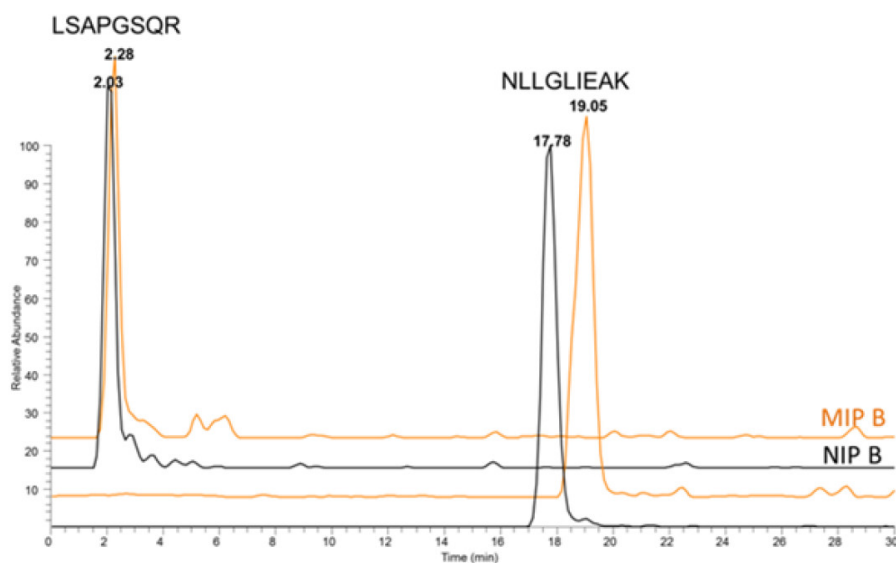


Figure 2.21 MS/MS Chromatograms of 10 nM digested ProGRP isoform 1 obtained by using MIP B (orange, MAS23) and NIP B (black, MAS22) coupled directly to the MS detector, without analytical column.

#### 2.3.4.6.2 Effect of the loading pH

The optimal pH to promote non-covalent interactions between the target peptide and the binding sites of the MIPs was assessed by testing MIP A (MAS21) and B (MAS23) solely. Figure 2.22 shows the retention time and the intensities obtained on both MIPs upon loading the heavy labeled target peptide NLLGLIEA[K-<sup>13</sup>C<sub>6</sub> <sup>15</sup>N<sub>2</sub>] at three different pH values (3.0, 7.6 and 8.6). Loading with 20 mM FA (pH 3.0) for 10 minutes gave peptide high intensity and retention times above 27 minutes on both MIPs. Upon increasing the pH of the loading solution using 50 mM ammonium

bicarbonate buffer adjusted to pH 7.6 and pH 8.6, the retention time of the peptide rises until 29.5 minutes, but a drop in signal intensity is observed simultaneously for both MIPs. The increase in peptide retention at higher pH can be rationalized as the progressive strengthening of the interactions between the positively charged EAMA residues in both polymers (pKa 9.6) and the negative charges of the glutamic acid residue (pKa 4.2) and the C-terminal carboxylic acid (pKa 2.2) of the peptide. At pH 3.0, only 10% of the glutamic acid residues are charged while for pH > 6.2 more than 99% of them are available to establish ionic interactions with the FMs. Likewise, 90% of the C-terminal carboxylic acid is charged at pH 3.0 contributing to the peptide retention which increases at higher pH.

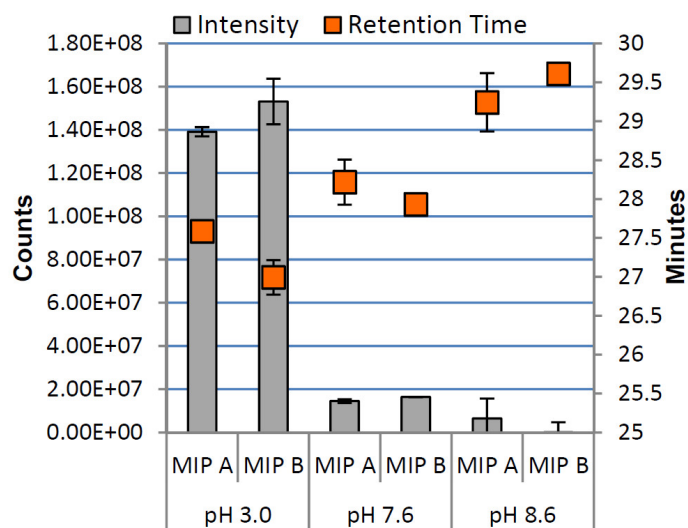


Figure 2.22 Effect of loading pH on retention times and peak areas of NLLGLIEA[K-<sup>13</sup>C<sub>6</sub>-<sup>15</sup>N<sub>2</sub>] (5 nM) extracted on both MIPs. MIP A and MIP B correspond to the polymer with the codes: MAS21 and MAS23.

In addition to these interactions, a combined effect of the peptide negative charges (pI 6.44) is feasible when the pH is basic. The drop in signal intensities can be ascribed to incomplete positive ionization of the peptide in the MS detector when the pH is > 7. This was confirmed by direct injection in the TSQ analyzer of the peptide solutions (1 nM) with three different pH values (3.0, 7.6 and 8.6) (Figure 2.23). Since the increase in retention time at higher pH was of less significance than the increase in

signal intensity at low pH, 20 mM FA was used for the loading of the samples on the columns.

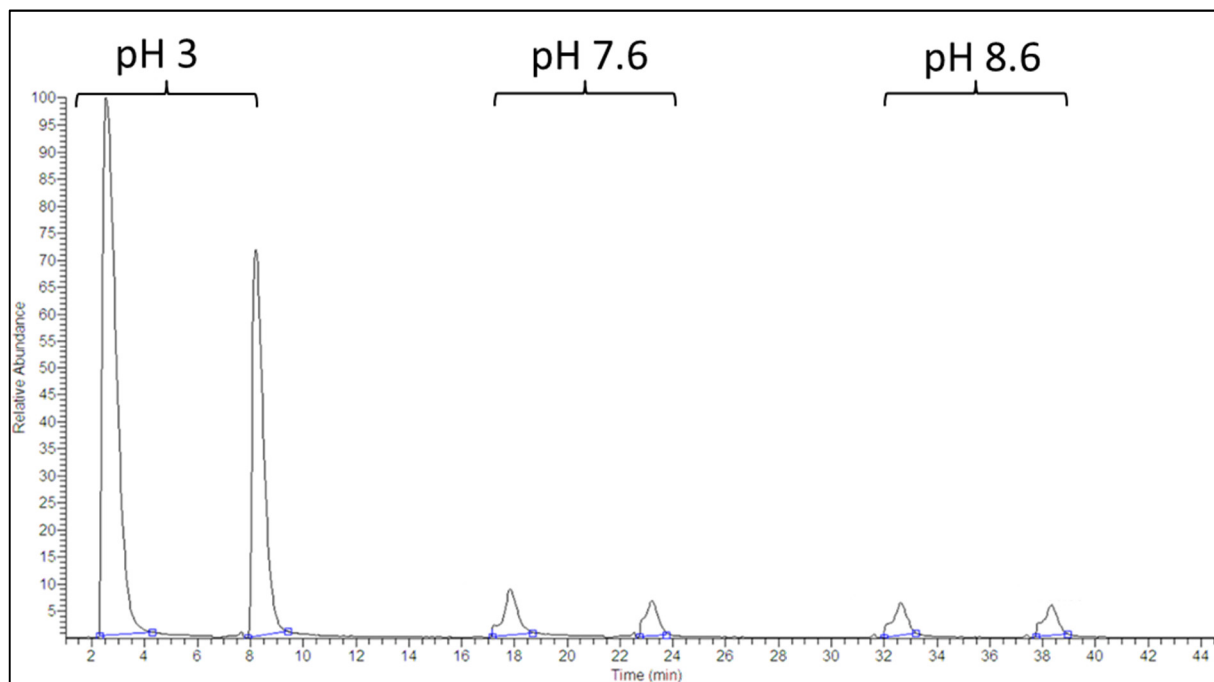


Figure 2.23 Direct MS infusion TIC chromatogram of 1 nM NLLGLIEA[K-<sup>13</sup>C<sub>6</sub><sup>15</sup>N<sub>2</sub>] prepared at different pH values and injected at different time points.

#### 2.3.4.6.3 Evaluation of MIP/NIP pairs and MIP selection

The imprinting effects were evaluated by comparison of the NLLGLIEAK retention times on the two MIP/NIP pairs. Retention times of NLLGLIEA[K-<sup>13</sup>C<sub>6</sub><sup>15</sup>N<sub>2</sub>] were recorded upon its loading onto all the columns with 10 column volumes of 20 mM FA and subsequent isocratic elution directed to the MS detector, using small ACN increments (Figure 2.24). The differences in NLLGLIEA[K-<sup>13</sup>C<sub>6</sub><sup>15</sup>N<sub>2</sub>] retention of the MIP/NIP pairs appears to be highest when EAMA.HCl was used as sole functional monomer (MIP A, MAS21). Any significant differences in peptide retention among the polymer batches can be ascribed uniquely to differences in the polymer structure of the binding sites, since the columns were checked for complete packing by optical control of the transversal section of the cartridges (Figure 2.25 D), and measurement

of backpressures gave similar results for all columns (7 PSI for MIP A, MAS21 and NIP A, MAS20 and 10 PSI for MIP B, MAS23 and NIP B, MAS22).

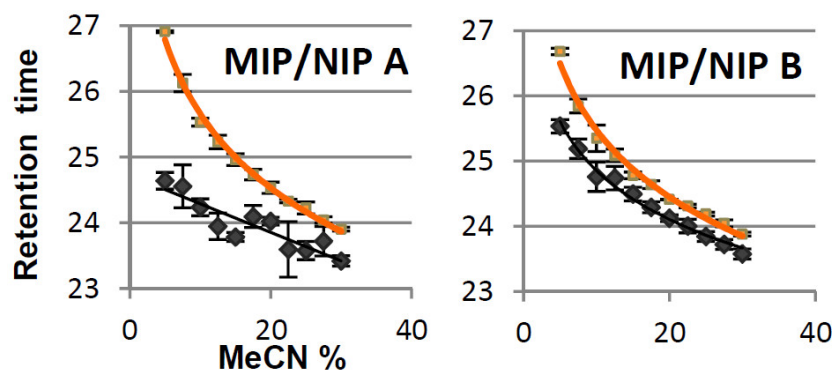


Figure 2.24 Differences in retention times of  $LLGLIEA[K_{13}C_6 \text{ }^{15}N_2]$  (1 nM) on the MIPs (orange) and corresponding NIPs (black) for both polymer pairs (A and B).

The MIP A, MAS21 column was selected as trap column for further automatization and coupled with the analytical column. The MIP A, MAS21, also showed longer analyte retention, which is desirable for highly specific enrichment of the peptide when it is in the presence of many different interferences occurring in complex matrices such as serum samples. Additionally, MIP A, MAS21, showed a higher imprinting factor (IF) than MIP B, MAS23 (Table 2.13).

Table 2.13 Retention factors and imprinting factors of the two polymerisation protocols.

	Retention factor, $k'$	Imprinting factor, IF
<b>MIP A (MAS21)</b>	14.36	1.11
<b>NIP A (MAS20)</b>	12.91	
<b>MIP B (MAS23)</b>	13.41	1.00
<b>NIP B (MAS22)</b>	13.43	

#### 2.3.4.6.4 Coupling of MIP columns with the analytical column and method optimisation

The arrangement of the 6-port valve when the sample is loaded onto the MIP column and subsequent valve switching is shown in Figure 2.25 A and B, respectively.

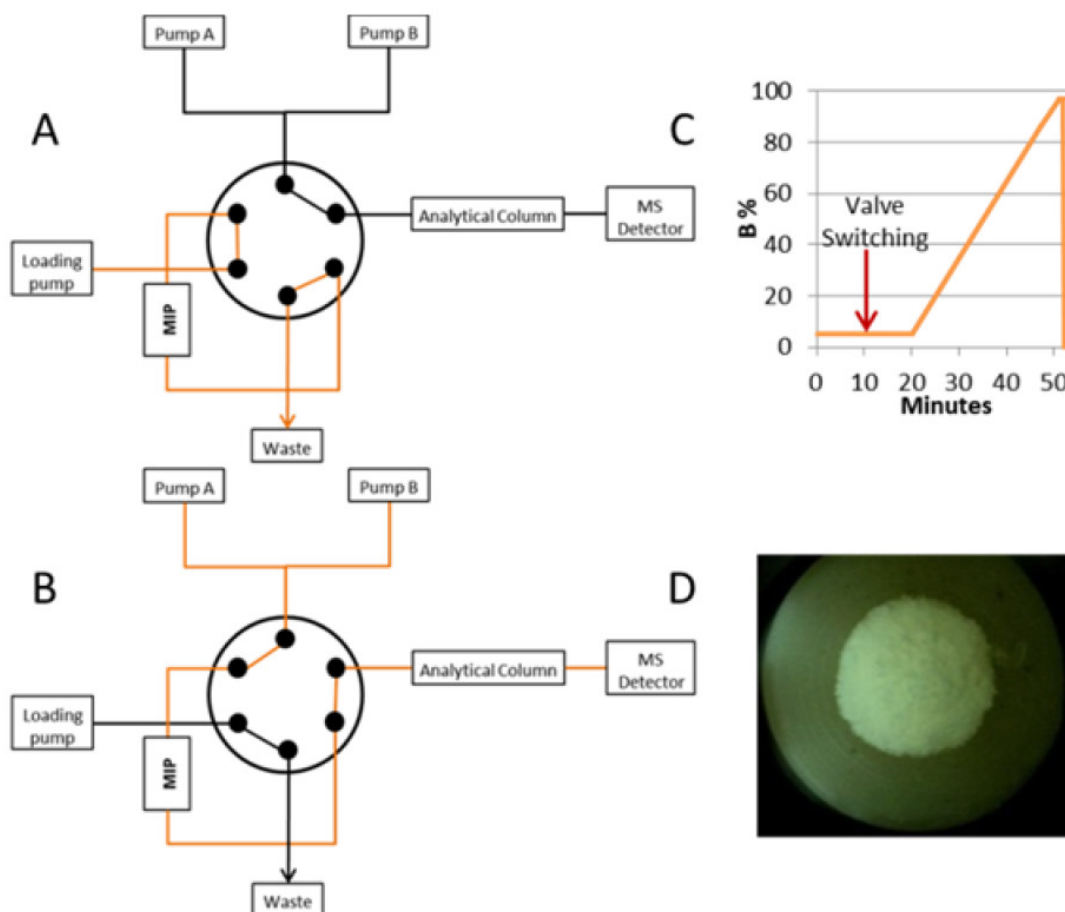


Figure 2.25 Schematic representation of on-line extraction using a 6-port-valve: (A) loading of the sample on MIP column, (B) forward flushing of the MIP column to the analytical column, (C) analytical gradient applied for NLLGLIEAK determination, (D) transversal section of the MIP A after packing in trap column.

Optimisation of wash and loading duration (Figure 2.26 A and B) provided 10 minutes for loading and 5 minutes for washing, whilst keeping the flow constant at 30  $\mu\text{L}/\text{min}$ . The capacity of the columns determined the serum volume to be extracted (Figure 2.26 C). The extraction of 50  $\mu\text{L}$  of serum performed remarkably well in terms

of peptide signal intensity (for comparison, the present gold standard method of TR-IFMA requires 100  $\mu\text{L}$ ) and was judged to be optimal. This result was very promising indeed for the management of clinical samples, often available in very limited volumes only. Increasing the injection volume from 5 to 30  $\mu\text{L}$  allowed a linear increase in the peptide signal intensity (Figure 2.26 D), demonstrating the suitability of the extraction of 50  $\mu\text{L}$  of serum. In order to minimise the sample complexity before the extraction, depletion of the high abundant proteins, such as serum albumin, was decided to be performed by protein precipitation. This step was optimised by testing different ACN volumes for the protein precipitation of ProGRP isoform 1 spiked samples. The highest peptide recovery was achieved using a 0.75:1 ratio of ACN: serum (v/v) and 1:40 trypsin to substrate ratio, without reduction/alkylation (Figure 2.26 E and F). The enzyme to protein ratios shown in the figure are based on the amount of serum albumin expected to be left in the sample after protein precipitation. Such amounts range between 1% and 10% in earlier studies which investigated protein precipitation with different acetonitrile concentrations.<sup>39,40</sup> Accordingly, a depletion of at least 90% of serum albumin with 50% of acetonitrile as precipitant agent can be assumed.

The extraction into the on-line system and the chromatographic run were complete within 50 minutes. The overall outcome was an automated and cost-effective method with remarkably low sample volume consumption.

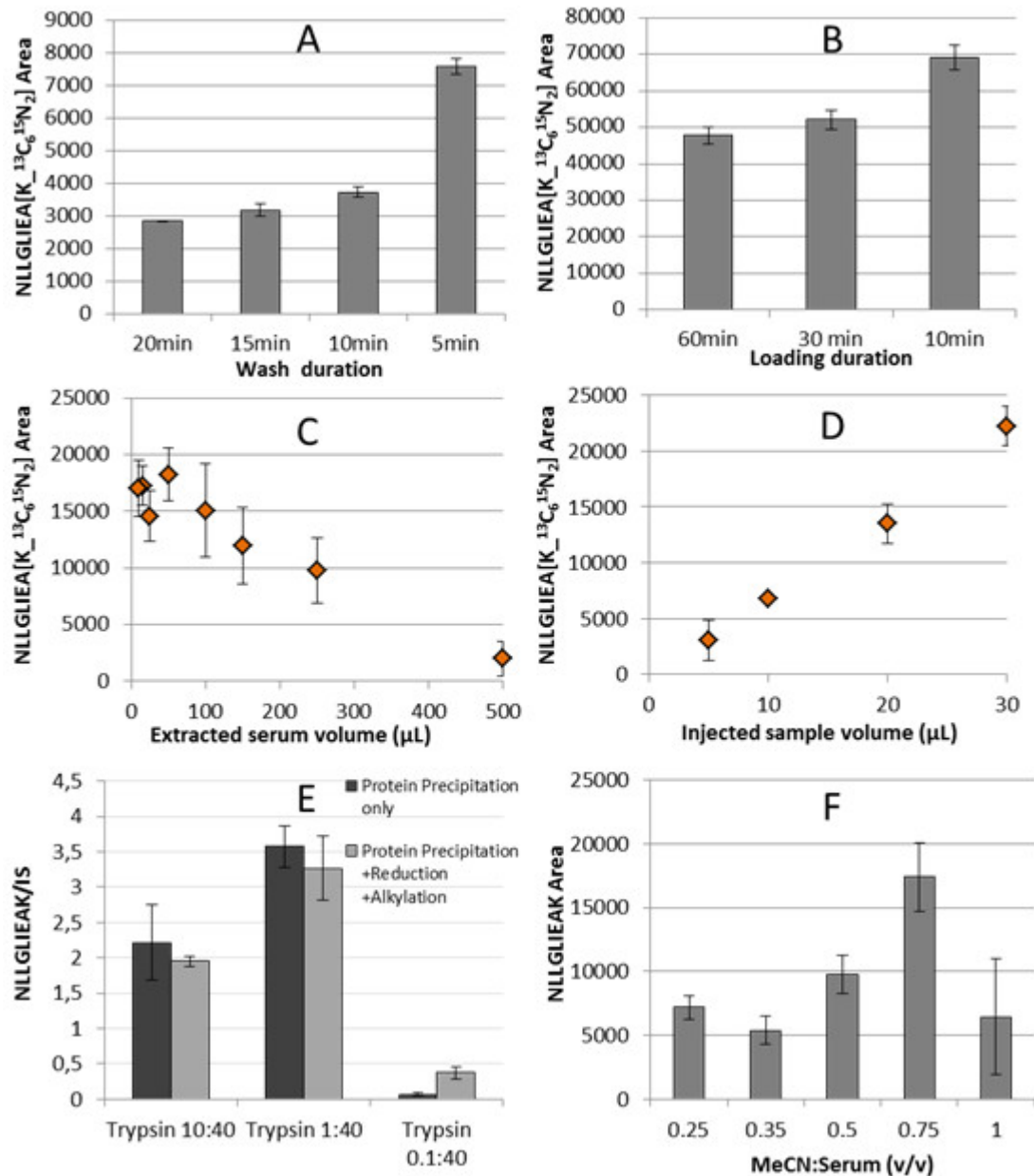


Figure 2.26 Extraction optimisation (A-D) by using 1 nM NLLGLIEA[K-<sup>13</sup>C<sub>6</sub><sup>15</sup>N<sub>2</sub>]: (A) duration of the wash step (5% ACN) on MIP A column; (B) duration of the loading step (20 mM FA) on MIP A column; (C) capacity evaluation by extraction of different serum volumes; (D) injection volume evaluation by extraction of 50 μL of serum. Sample pretreatment optimisation (E-F) by using 37 nM ProGRP isoform 1 spiked serum samples: (E) evaluation of trypsin amount and reduction (DTT) and alkylation (IAA) after protein precipitation (PP) on spiked serum; (F) optimisation of the ACN: Serum ratio (v/v) in protein precipitation step. MIP A corresponds with the polymer MAS21.



## 2.3.4.6.5 Linearity, LOD and LOQ

The linearity of the method was explored over 3 orders of magnitude of ProGRP levels. The regression curve obtained (Figure 2.27) upon plotting the ratio of the area of the signature peptide NLLGLIEAK to the area of the IS NLLGLIEA[K-<sup>13</sup>C<sub>6</sub><sup>15</sup>N<sub>2</sub>] had an acceptable correlation value ( $R^2 > 0.97$ ).

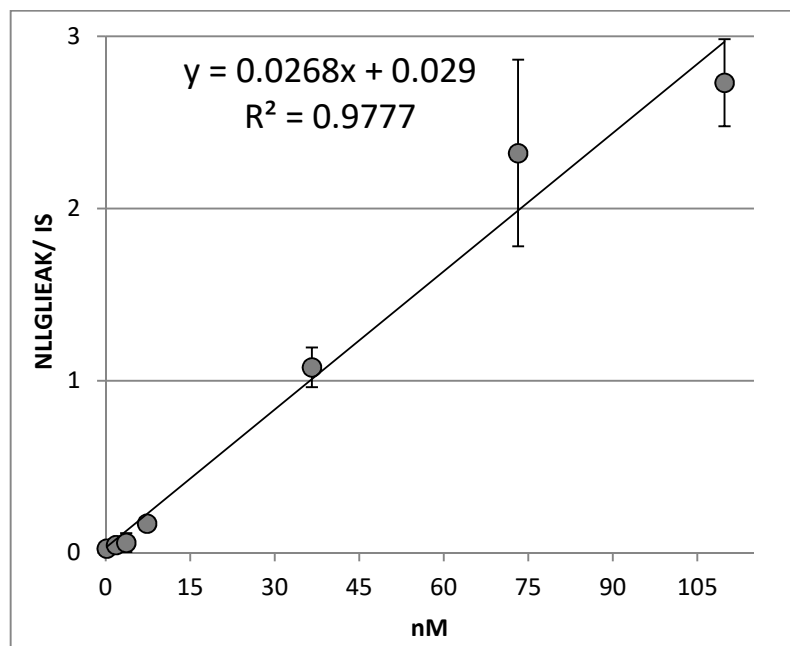


Figure 2.27 Calibration curve obtained by plotting the ratio of the area of the signature peptide NLLGLIEAK to the area of the internal standard (IS) for different ProGRP isoform 1 concentrations in serum.

From the signal-to-noise ratio (S/N) of the lowest concentration of the curve, the limit of detection (LOD) was estimated to be 17.2 pM (S/N=3) corresponding to a lower limit of quantification (LOQ) of 57.3 pM (S/N=10). The mass limit of detection (mLOD) on column was estimated to be 425 amol.

The detection limit of this new method is therefore substantially lower than the limit achieved previously by a MIP-based extraction<sup>38</sup> (625 pM) but is still higher compared to immunocapture LC-MS<sup>38</sup> (1 pM) and TR-IFMA methods. In the case of extended disease, clinically relevant concentrations of ProGRP are above the LOD achieved with

this method.<sup>41</sup> However, the method is not able to discriminate healthy donors close to the reference limit of 7.6 pM.

#### 2.3.4.6.6 Analysis of patient samples and benchmarking with other methods

Two serum samples from patients suffering from SCLC were analyzed to demonstrate the applicability of the method to determine ProGRP at clinically relevant concentrations (Figure 2.28). The monitoring of selected transitions together with retention times of NLLGLIEAK along with the co-elution of the IS allowed correct peak identification.

From the calibration curve, the ProGRP concentrations were calculated for both samples and values reported in Table 2.14 together with the ProGRP concentrations determined previously for these samples by the immunocapture LC-MS and TR-IFMA methods.<sup>42</sup> Good accordance among ProGRP values is demonstrated. These results demonstrate very clearly the suitability of the method for the extraction and quantification of ProGRP present in clinical serum samples.

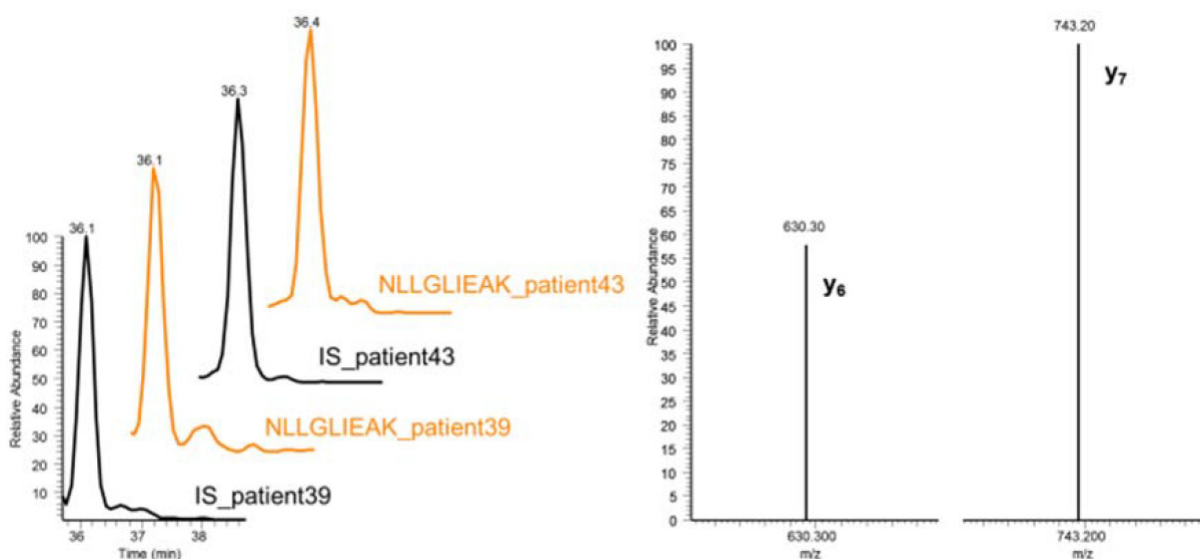


Figure 2.28 Analysis of patient serum samples: chromatograms of NLLGLIEAK (orange) and the Internal Standard (IS) NLLGLIEA[K-<sup>13</sup>C<sub>6</sub>-<sup>15</sup>N<sub>2</sub>] (black) (left side) and corresponding ion spectra for selected reaction monitored (fragments y<sub>6</sub> and y<sub>7</sub>) for NLLGLIEAK determination (right side).

Table 2.14 Table Benchmark of ProGRP concentrations in patient samples measured by the three analytical methods.

	MISPE-LCMS (pM)	Immuno-LCMS (pM) <sup>43</sup>	TR-IFMA (pM) <sup>43</sup>
<b>Patient_S39</b>	2402	922	2425
<b>Patient_S43</b>	1029	918	1899

The automated method we have developed is devoid of labile and expensive biological receptors. The method was successfully applied for ProGRP analysis in SCLC patient serum and we believe that it can help to satisfy the strong demand for improved technologies in terms of diagnostic sensitivity and specificity and in terms of analytical automation and speed. Additionally it allows effective analysis of scarce samples, which is a particular requirement and challenge in clinical analysis. This study employs MIPs targeting one prototypic peptide for ProGRP. However, given the programmable nature of the imprinting technique, materials targeting other sequence motifs can be generated relatively easily, thereby extending the method to encompass other relevant biomarkers.

## 2.4 Molecularly imprinted polymer microspheres for $\alpha$ -Synuclein target

### 2.4.1 $\alpha$ -Synuclein and Parkinson's disease

Parkinson's disease (PD) is the second most common neurodegenerative disorder, first reported by James Parkinson in 1817.<sup>44</sup> The disease results in movement related symptoms such as tremor, muscular rigidity, slowness of movement and postural instability, and non-movement functional problems such behavioural dysfunctions, *i.e.* depression, dementia and psychosis, autonomic dysfunctions, *i.e.* gastric, cardiovascular and respiratory dysfunctions, sleep-related, sensory and sensorimotor dysfunctions.<sup>45,46</sup> The disease mainly affects men, about 1% of individuals who reach

the age of 65, and even 5% of the population who are aged 85 or above are affected by PD.<sup>44,47</sup>

There is no simple answer to the origin of PD, however it is believed that genetic and environment factors, and interactions between them, contributes to the development of the disease.<sup>48</sup> Amongst them are aggregates of  $\alpha$ -Synuclein in the Lewy bodies and neurites, considered as the main source of PD.  $\alpha$ -Synuclein is a 140 amino acids long protein (SNCA-140aa, Figure 2.29), which normally occurs in the presynaptic terminals of the central nervous system.<sup>49</sup> However, the physiological functions of the peptide still needs to be better elucidated.<sup>50</sup> Amongst the functions currently identified are: the control of biogenesis, cytoskeletal components, synaptic proteins, neurotransmitter release and neuronal survival.<sup>51</sup> Mutations in the  $\alpha$ -Synuclein (SNCA) gene (point mutations, duplications, triplications and polymorphism) are thought to underpin in the pathogenesis of PD. Apart from SNCA-140aa, three more isoforms with 98, 112 and 126 amino acid residues are identified as the result of the alternative splicing of the gene SNCA (Figure 2.29).<sup>44,52</sup> The mechanism of expression of proteins such as  $\alpha$ -Synuclein as the biomarker for the detection of PD from the blood or cerebrospinal samples is still under investigation.

Nowadays, the early detection of PD is still challenging and, in fact, similarly to AD, there is no straightforward and cheap diagnosis tool that can detect the disorder before irreversible changes appear in the brain. Therapy and/or drugs work most efficiently in the early stage of the disease, however in most cases PD, similarly to AD and SCLC, is detected too late when significant disease progress is observed. The method for the synthesis of MIPs for peptide-based targets, successfully developed in this Thesis work, could be implemented for the synthesis of materials for detecting PD in its early stage.

**$\alpha$ -Synuclein**

	<u>10</u>	<u>20</u>	<u>30</u>	<u>40</u>	<u>50</u>
Isoform 1	MDVFMKGLSK	AKEGVVAAAE	KTKQGVAEAA	GKTKEGVLYV	GSKTKEGVVH
	<u>60</u>	<u>70</u>	<u>80</u>	<u>90</u>	<u>100</u>
	GVATVAEKT	EQVTNVGGAV	VTGVTAVAQK	TVEGAGSIAA	ATGFVKKDQL
	<u>110</u>	<u>120</u>	<u>130</u>	<u>140</u>	
	GKNEEGAPQE	GILEDMPVDP	DNEAYEMPSE	<b>EGYQDYPEA</b>	
Isoform 2	<u>10</u>	<u>20</u>	<u>30</u>	<u>40</u>	<u>50</u>
	MDVFMKGLSK	AKEGVVAAAE	KTKQGVAEAA	GKTKEGVLYV	-----
	<u>60</u>	<u>70</u>	<u>80</u>	<u>90</u>	<u>100</u>
	---VAEKT	EQVTNVGGAV	VTGVTAVAQK	TVEGAGSIAA	ATGFVKKDQL
	<u>110</u>	<u>120</u>	<u>130</u>	<u>140</u>	
	GKNEEGAPQE	GILEDMPVDP	DNEAYEMPSE	<b>EGYQDYPEA</b>	
Isoform 3	<u>10</u>	<u>20</u>	<u>30</u>	<u>40</u>	<u>50</u>
	MDVFMKGLSK	AKEGVVAAAE	KTKQGVAEAA	GKTKEGVLYV	GSKTKEGVVH
	<u>60</u>	<u>70</u>	<u>80</u>	<u>90</u>	<u>100</u>
	GVATVAEKT	EQVTNVGGAV	VTGVTAVAQK	TVEGAGSIAA	ATGFVKKDQL
	<u>110</u>	<u>120</u>	<u>130</u>	<u>140</u>	
	GK-----	-----	-----	<b>EGYQDYPEA</b>	
Isoform 4	<u>10</u>	<u>20</u>	<u>30</u>	<u>40</u>	<u>50</u>
	MDVFMKGLSK	AKEGVVAAAE	KTKQGVAEAA	GKTKEGVLYV	-----
	<u>60</u>	<u>70</u>	<u>80</u>	<u>90</u>	<u>100</u>
	---VAEKT	EQVTNVGGAV	VTGVTAVAQK	TVEGAGSIAA	ATGFVKKDQL
	<u>110</u>	<u>120</u>	<u>130</u>	<u>140</u>	
	GK-----	-----	-----	<b>EGYQDYPEA</b>	

Figure 2.29 Sequences of amino acids (AAs) of  $\alpha$ -Synuclein isoforms. The AAs which are underlined represent distinct parts of the isoforms. The AAs in bold are target analytes. Scheme adapted from ref.<sup>23</sup>.

## 2.4.2 Aim of study

In our design and synthesis studies of polymer materials for  $\alpha$ -Synuclein target, we hypothesize that

- the method developed for the synthesis of MIP microspheres for  $\beta$ -Amyloid and ProGRP targets could be further extended for the synthesis of other MIPs targeting peptides;
- $\alpha$ -Synuclein is considered as a biomarker which is highly sensitive and specific for Parkinson's Disease.

Based on this, the aims of the work presented in this section were as follows:

- Design and synthesis of polymer materials for  $\alpha$ -Synuclein target;
- Characterisation of the materials produced;
- Delivery of the first generation materials to the PEPMIP partners for evaluation of the molecular recognition. An objective in the project was to deliver optimised imprinted materials which can enable selective extractions of biomarker target from native blood or cerebrospinal fluid samples.

The molecular recognition work discussed in the Results and discussion section was performed by Prabal Subedi, a PhD student from Ruhr-Universität Bochum, Germany. A secondment at Ruhr-Universität Bochum allowed the author of this Thesis to participate in, and contribute to, a portion of this work.

## 2.4.3 Experimental section

### 2.4.3.1 *Materials*

The peptide templates Ac-DYEPEA (>95% purity) and Ac-EGYQDYEPEA (>95% purity) were purchased from ChinaPeptides, *N*-(2-aminoethyl)methacrylamide hydrochloride (EAMA.HCl, purity  $\geq$ 98%) was purchased from Polysciences Inc. (Niles, IL, USA), and 2,2'-azobisisobutyronitrile (AIBN, purity 98%) was purchased from BDH Lab. Supplies (UAE). Divinylbenzene-80 (DVB-80, 80% DVB isomers and 20% ethylvinylbenzene isomers), 1,2,2,6,6-pentamethylpiperidine (PMP, purity >99%)

and hydrochloric acid (37 wt. % in H<sub>2</sub>O) were all purchased from Sigma-Aldrich (St. Louis, MI, USA). DVB-80 was purified by filtration through a short plug of neutral aluminium oxide prior to use. AIBN was recrystallized from acetone at low temperature. All other chemicals used (acetonitrile [ACN], methanol and dimethyl sulfoxide [DMSO, purity ≥99.9%]) were of analytical grade.

#### *2.4.3.2 Synthesis and characterisation of molecularly imprinted polymer microspheres for $\alpha$ -Synuclein target*

MIPs and their corresponding NIPs were synthesised by a typical PP protocol as described elsewhere.<sup>7</sup> The PP method has been presented and discussed in detail in Chapter 1. The methods used for the characterisation of MIPs are presented in 2.1.2.2.

A series of MIPs and their corresponding non-imprinted counterparts were prepared. The feed compositions of the first generation materials is shown in Table 2.15. Eight distinct pair of polymers were synthesized: four MIPs (MAS25, MAS26, MAS40 and MAS42) and four corresponding non-imprinted polymers (NIPs) (MAS24, MAS27, MAS39 and MAS41). Two of the MIPs were imprinted with the shorter template (Ac-DYEPEA; MAS26 and MAS42) and other two were imprinted with the longer template: Ac-EGYQDYEPEA (MAS25 and MAS40). Polymers were produced on a 0.5 g monomer scale with a monomer and initiator concentration of 1.89% w/v and 2% w/v (with respect to the solvent), and 2 mol% (with respect to the total number of polymerisable double bonds), respectively. Some of polymers were also formulated on a 1 g monomer scale by doubling of the amount of all reagents used (MAS39 and MAS40). 24 hours was the precipitation polymerisation time, but the last MIP and NIP pair (MAS41 and MAS42) had a polymerisation time of 48 hours.

Table 2.15 PP conditions for Ac-EGYQDYEPEA and Ac-DYEPEA imprinted polymers and their corresponding NIPs.

Polymer code	Template (mmol)	EAMA.HCl (mmol)	DVB-80 (mmol)	Solvent (mL)	AIBN (mol%)	PMP (mmol)
MAS24	-	0.07	3.73	ACN (24) DMSO (2.5)	2	0.025
MAS25	Ac-EGYQDYEPEA (0.006)	0.07	3.73	ACN (24) DMSO (2.5)	2	0.025
MAS26	Ac-DYEPEA (0.006)	0.07	3.73	ACN (23) DMSO (2)	2	0.025
MAS27	-	0.07	3.73	ACN (23) DMSO (2)	2	0.025
MAS39	-	0.07	3.73	ACN (48) DMSO (5)	2	0.025
MAS40	Ac-EGYQDYEPEA (0.006)	0.07	3.73	ACN (48) DMSO (5)	2	0.025
MAS41	-	0.07	3.73	ACN (24) DMSO (1)	2	0.025
MAS42	Ac-DYEPEA (0.006)	0.07	3.73	ACN (24) DMSO (1)	2	0.025

The synthesis of the MIP with the polymer code MAS25 can serve as an illustrative example of the PP procedure. The reaction vessel, a borosilicate glass Kimax tube, was immersed in a heated oil bath (~70 °C) during addition of reaction components. Firstly, the template, Ac-EGYQDYEPEA (4.85 mg, 0.006 mmol) was added into the reaction vessel. Thereafter, DMSO (2.5 mL) was added (to dissolve the template), followed by PMP (4.5 μL, 0.025 mmol). The functional monomer EAMA.HCl (12.3 mg, 0.07 mmol) was then added followed by DVB-80 (0.49 g, 0.53 mL, 3.73 mmol) and AIBN (22.3 mg, 0.2 mmol). (For the synthesis of the corresponding NIP, the template was omitted from the synthetic protocol). The solution was then ultrasonicated for 10 minutes at ambient temperature and sparged with oxygen-free nitrogen gas for 10 minutes at ice-bath temperature, to remove dissolved molecular oxygen. Thereafter, the reaction vessel was sealed under nitrogen and transferred to a Stuart Scientific S160 incubator equipped with a Stovall low-profile roller. The incubator



temperature was ramped from ambient to 60 °C over a period of around two hours and then maintained at 60 °C for a further 22 hours to yield a milky suspension of polymer.

Finally, the polymer microspheres were isolated from the reaction mixture by vacuum filtration on a 0.45 µm nylon membrane filter using a Vacuumbrand Vacuum System (2.0 mbar), washed sequentially with ACN (50 mL), MeOH/0.1 M aq. HCl (90/10, v/v, 50 mL) and MeOH (50 mL). The isolated product was transferred into a pre-weighed vial and dried overnight in a Townson & Mercer vacuum oven (60 mbar) at 70 °C. The yield of the synthesised material was checked gravimetrically. The yield of MAS25 was 23%.

SEM together with image analysis, optical microscopy, FT-IR spectroscopy and nitrogen sorption analysis were performed. These analyses are introduced and discussed in detail in the 2.1.2.2 experimental section.

The first generation of MIPs and their corresponding NIPs were delivered to Ruhr-Universität Bochum, Germany. The molecular recognition of polymers were tested by Prabal Subedi, a PhD student within the PEPMIP project.

## 2.4.4 Results and discussion

### 2.4.4.1 *Synthesis of MIPs and their corresponding NIPs*

The synthesis procedure used for the production of polymer microspheres for the  $\alpha$ -Synuclein targets was analogous to the methodology used for the synthesis of polymer microspheres for the  $\beta$ -Amyloid and ProGRP targets. An initial problem with the solubility of FMs and/or templates was addressed by keeping the reaction vessel in a heated oil bath (~70 °C) while the components were being added slowly. The non-imprinted and imprinted polymers for the  $\alpha$ -Synuclein target were prepared in good yields; the average yield of particles was 47% (Table 2.16). The polymerisation yields increased considerably when the amount of all reagents used was doubled (MAS39 and MAS40). This was expected as the rate of a free radical polymerisation

is directly proportional to the monomer concentration and directly proportion to the square of the initiator concentration. The extension of the polymerisation time from 24 h to 48 h, while keeping the concentrations of monomers and initiator at 2% w/v and 2 mol%, also resulted in good yields (MAS41 and MAS42). In this case, it was again expected as the longer polymerisation time contributes to higher yield. These results help to support the belief that the adjustment of reaction variables would help in identification of the PP conditions, aimed at giving porous products with narrow PSDs and microsphere diameters around  $\sim 1\text{-}2\ \mu\text{m}$ .

Table 2.16 Effect of monomer and initiator concentrations, reaction time and scale on the yield of the non-imprinted and imprinted polymers for the  $\alpha$ -Synuclein target.

Polymer code	Monomer conc. (% w/v) <sup>a</sup>	Initiator conc. (mol%) <sup>b</sup>	Incubation time (h)	Monomer scale (g)	Yield (%)
MAS24	1.89	2	24	0.5	28
MAS25	1.89	2	24	0.5	23
MAS26	2	2	24	0.5	25
MAS27	2	2	24	0.5	23
MAS39	1.89	2	24	1	77
MAS40	1.89	2	24	1	68
MAS41	2	2	48	0.5	63
MAS42	2	2	48	0.5	68

a with respect to the solvent.

b with respect to the total number of polymerisable double bonds.

#### 2.4.4.2 Characterisation

The SEM micrographs show that the MIPs and NIPs produced are spherical in nature (SEM example shown in Figure 2.30). Discrete particles in the micron-sized range were produced, although the microspheres are polydisperse (possibly as a consequence of the presence of DMSO as a co-solvent). The quality of particles was not ideal as the particles overlap or combine with each other into larger and irregular agglomerates. The SEM observations would suggest that the aggregation of particles was due to chemical bonds formed between the beads. Nevertheless, the particles

were suitable for packing into trap columns. The microscopic analysis clearly shows that the NIPs were of higher quality than the MIPs, suggesting a template effect.

Table 2.17 Microscopic characterisation of polymer microsphere morphology.

Polymer code	Optical microscopy observation			Bead average diameter in $\mu\text{m}^a$
	Dispersity	Bead size ( $\mu\text{m}$ )	Aggregation	
MAS24	Polydisperse	1-2	Chemical	approx. 1
MAS25	Polydisperse	1-2	Chemical	approx. 1
MAS26	Polydisperse	1-2	Chemical	approx. 1
MAS27	Polydisperse	1-2	Chemical	approx. 1
MAS39	Polydisperse	1-2	Chemical	approx. 1
MAS40	Polydisperse	1-2	Chemical	approx. 1
MAS41	Polydisperse	1-8	Chemical	approx. 1
MAS42	Polydisperse	1-2	Chemical	approx. 1

<sup>a</sup> SEM microscopy observation.

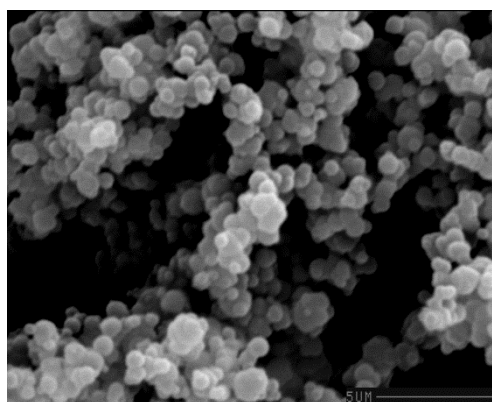


Figure 2.30 SEM image of MAS24;  $\times 5420$  magnification (scale =  $5 \mu\text{m}$ ).

The nitrogen sorption data, shown in Table 2.18, revealed that the MIPs and NIPs were macroporous; this was important to establish in view of the need for analyte to access molecularly imprinted binding sites during MISPE. The NIPs were not identical to the MIPs in respect of their porous morphologies, again suggestive of the

idea that the presence of template during polymerisation influences the polymerisation outcomes.

Table 2.18 Nitrogen sorption analysis data for the non-imprinted and imprinted polymers for the  $\alpha$ -Synuclein target.

Polymer code	BET C value	Specific surface area (m <sup>2</sup> /g)		Specific pore volume (cm <sup>3</sup> /g) <sup>a</sup>	Average pore diameter (nm) <sup>b</sup>
		BET	Langmuir		
MAS24	-127	418	559	0.31	2.9
MAS25	-45	209	273	n/a	n/a
MAS26	-31	56	71	n/a	n/a
MAS27	186	44	61	0.04	3.8
MAS39	-66	195	330	0.11	2.4
MAS40	-93	478	618	0.20	1.7
MAS41	n/a	n/a	n/a	n/a	n/a
MAS42	-42	115	154	0.03	0.9

<sup>a</sup> BJH cumulative adsorption pore volume of pores between 1.7 and 300 nm.

<sup>b</sup> Determined by equation: 4 pore volume/BET surface area.

n/a not available.

Table 2.18 shows that the polymer with code MAS27 follows the BET isotherm and the nitrogen molecules were absorbed in several layers as the BET C value is high and positive. The BET C values for the rest of MIPs and NIPs are negative, indicating that the data for the tested samples did not fit to a BET isotherm as the nitrogen molecules were absorbed in a single layer onto the surface of the solids. Therefore, the Langmuir isotherm should be used to describe the specific surface area of the tested polymers for the analysis. The analysis shows that the average pore size reached a maximum of 3.8 nm (MAS27). The polymers were highly crosslinked as poly(DVB-80) constituted more than 97% of the whole polymer network structure and such a high crosslinking level usually results in small pore sizes. High specific surface areas, coupled with the average pore diameters of ~2 nm, indicated that the materials tested were microporous.<sup>24</sup> These conclusions can be supported by the analysis of nitrogen sorption isotherms. A type I isotherm was generated (MAS25,

MAS26, MAS27 and MAS40). This isotherm is obtained when a single layer of nitrogen molecules is absorbed on the solid and is typical for materials with microporous structure. In addition to the presence of micropores, there can be a small percentage of mesopores within the materials tested (*i.e.*, pores > 2 nm and < 50 nm). A nitrogen sorption isotherm which resembles a type II isotherm, characteristic for non-porous or macroporous solids with pore width more than 50 nm, was also generated (MAS24 and MAS39). In this isotherm generated during the analysis some divergence was observed; the desorption path was not exactly the same as the sorption path. This divergence indicated the presence of mesoporous in the polymer network structures.<sup>24</sup> The specific surface area increased considerably when the amount of all reagents used were doubled (Table 2.18). This was observed for the following pairs of MIPs and NIPs: MAS25 and MAS40, and MAS24 and MAS39, respectively. The extension of the polymerisation time from 24 h to 48 h, while keeping the concentrations of monomers and initiator at 2 % w/v and 2 mol%, also resulted in an increase in the specific surface area from 71 m<sup>2</sup>/g to 154 m<sup>2</sup>/g for MAS26 and MAS42, respectively. The same effect was observed when the concentration of monomers was raised from 1.89 % w/v to 2 % w/v (MAS24 and MAS27).

#### 2.4.4.3 Selection of the template

The epitope approach<sup>25–28</sup> and the synthetic method successfully developed for MIPs targeting  $\beta$ -Amyloid and ProGRP were implemented for the design of MIPs for  $\alpha$ -Synuclein. Precipitation polymerisation was again the polymerisation method of choice since it delivers products directly in an appropriate format for packing into trap columns. A sequence of six and ten amino acids (DYEPEA and EGYQDYEPEA, Figure 2.31 and Figure 2.32) corresponding to the C-terminal sequence of  $\alpha$ -Synuclein, were selected as the target analytes for the absolute quantification of  $\alpha$ -Synuclein in serum matrices. Close structural analogues of the signature peptides were used as templates for the synthesis of MIPs, rather than using the DYEPEA or EGYQDYEPEA as templates, to avoid the possibility of template bleeding interfering

with the quantification of the biomarkers. The templates used were Ac-DYEPEA and Ac-EGYQDYEPEA, where the N-termini of the peptides have been acetylated.

#### 2.4.4.4 Selection of the functional and crosslinking monomers

*N*-(2-Aminoethyl)methacrylamide hydrochloride was selected as functional monomer since the carboxylic acid groups in the glutamic acid (E) and aspartic acid (D) residues, and C-terminus of the templates were targeted *via* a non-covalent molecular imprinting approach. Indeed, this functional monomer has been shown to be useful for the targeting of oxy-anions.<sup>20,39,40</sup> PMP was used to bring the various functional groups into appropriate ionization states for non-covalent interaction and to promote template solubility. Figure 2.31 and Figure 2.32 show schematic representations of the imprinted binding sites in MIP MAS25 and MAS26, respectively. For success, precipitation polymerisations must involve the polymerisation of monomers in dilute solution (typically < 5% w/v monomer in solvent) in a near- $\theta$  solvent, therefore DVB-80 was selected as crosslinker, the porogen was acetonitrile and the monomer concentrations were fixed at 1.89% w/v and 2% w/v for the imprinting of Ac-EGYQDYEPEA-OH and Ac-DYEPEA, respectively. A small volume of DMSO was added to promote solubility of templates and keep all components in solution prior to polymerisation, but use of DMSO was kept to a minimum. For the imprinting of Ac-EGYQDYEPEA-OH, it was required to increase the level of DMSO from 4% (v/v) to 10% (v/v). This solubility issue shows that the template used was rather polar in nature.

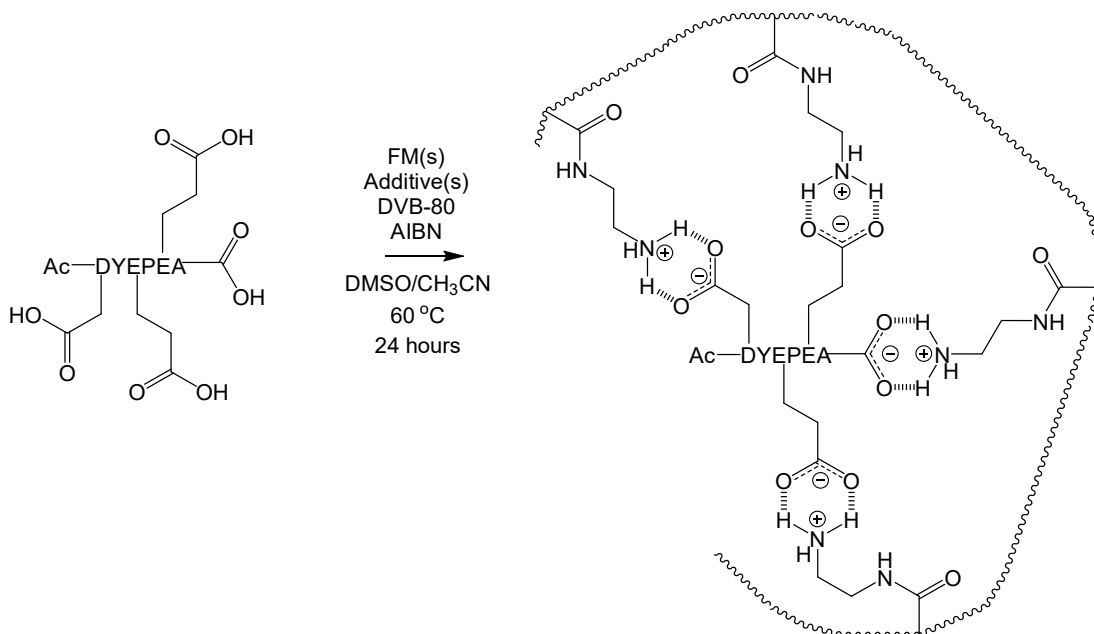


Figure 2.31 Schematic representation of the non-covalent molecular imprinting of a structural analogue of the  $\alpha$ -Synuclein epitope peptide. The carboxylic acid groups in the glutamic acid (E) residues and C-terminus of Ac-DYEPEA are drawn explicitly for emphasis, since these functional groups are involved in the self-assembly of the Ac-DYEPEA with functional monomers (FM). The complexed synthetic receptor (right hand side) depicts a molecularly imprinted binding site formed upon the free radical copolymerisation of a 1:3 molecular complex of Ac-DYEPEA and N-(2-aminoethyl)methacrylamide hydrochloride.

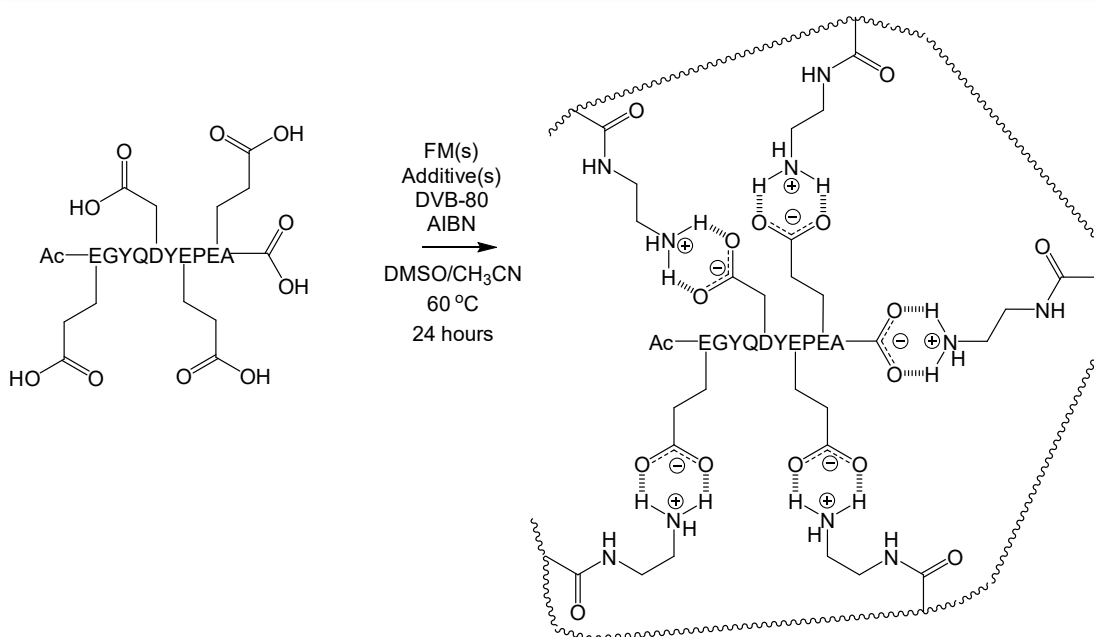


Figure 2.32 Schematic representation of the non-covalent molecular imprinting of a structural analogue of the  $\alpha$ -Synuclein epitope peptide. The carboxylic acid groups in the glutamic acid (E) and aspartic acid (D) residues, and C-terminus of Ac-EGYQDYEEPA are drawn explicitly for emphasis, since these functional groups are involved in the self-assembly of the Ac-EGYQDYEEPA with functional monomers. The complexed synthetic receptor (right hand side) depicts a molecularly imprinted binding site formed upon the free radical copolymerisation of a 1:5 molecular complex of Ac-EGYQDYEEPA and *N*-(2-aminoethyl)methacrylamide hydrochloride.

#### 2.4.4.5 Selection of the mole ratio of template: functional monomer(s): crosslinker

An important consideration in the molecular imprinting design process was the ratio of template to functional monomers to crosslinker. High crosslinker levels were used to ensure good yields of mechanically robust polymer microspheres with well-developed and permanent porous morphology. The mole ratio of template to EAMA.HCl was set at 1:10; thus whilst an excess of functional monomer is used to promote template-functional monomer self-assembly, very large excesses of functional monomer are avoided to minimise the possibility of non-specific binding events arising from the random incorporation of excess EAMA.HCl into the polymer



networks. In earlier work, the mole ratio of template to EAMA.HCl used was 1:100.<sup>30</sup> The isolated yields of the polymers (23-77%) are typical for the polymerisation of divinylbenzenes under such precipitation polymerisation conditions.

All prepared polymers targeting the  $\alpha$ -Synuclein target, and their corresponding NIPs, were sent to a PEPMIP partner (Ruhr University Bochum) for off-line Molecularly Imprinted Solid-Phase Extraction (MISPE) and G&T Septech, Norway, for packing into capillary columns.

#### 2.4.4.6 *Molecular recognition of the first generation of MIPs*

The molecular recognition characteristics were interrogated by Prabal Subedi, a PhD student from Ruhr University Bochum, Germany. For this work, all polymers were packed into stainless steel columns, however there was a problem of column regeneration and at the time of writing no molecular recognition data was available.

## 2.5 Conclusions and outlook

The scope of the work presented in this chapter spans the design, synthesis and characterisation of the first generation of polymer materials targeting  $\beta$ -Amyloid, ProGRP and  $\alpha$ -Synuclein targets. The synthesised polymers have been produced in a microsphere format *via* precipitation polymerisation. Selected polymers were supplied to PEPMIP partners for testing and evaluation. Although not all materials have been tested in full, prepared MIPs, especially those for the ProGRP target, show a promising degree of imprinting-related selectivity. However, it can be stated that some areas ought to be investigated in order to optimise the MIPs. First of all, a focus of further research would be on the preparation of polymer microspheres with mean diameters exceeding 2  $\mu\text{m}$  as microspheres with sizes approx. 1  $\mu\text{m}$  were too small as they caused problems with material handling. Another area of interest that would require further investigation is the particle size distribution. Monodisperse microspheres can be well packed in in solid-phase extraction cartridges or analytical columns, resulting in better efficiencies than cartridges and columns packed with polydisperse microspheres. Therefore, efforts should be invested in the synthesis of

materials with narrow PSDs. Also, the mean pore diameters of the microspheres produced reached a maximum of 3 nm only. There was a possibility that the pores of the microspheres were too small to allow for entry of target analytes. Therefore, more effort should be invested in the synthesis of MIPs with bigger pores.

Overall, the successful synthesis and characterisation of the first generation of MIPs can be considered a promising achievement, encouraging us to synthesise MIPs with different formats: magnetic and core-shell MIPs.

---

## 2.6 Bibliography

- 1 B. Sellergren, Ed., *Molecularly Imprinted Polymers—Man-Made Mimics of Antibodies and Their Application in Analytical Chemistry*, Elsevier, Amsterdam, 2001.
- 2 L. Nováková, D. Solichová and P. Solich, *J. Sep. Sci.*, 2006, **29**, 2433–2443.
- 3 O. H. Ismail, M. Catani, L. Pasti, A. Cavazzini, A. Ciogli, C. Villani, D. Kotoni, F. Gasparrini and D. S. Bell, *J. Chromatogr. A*, 2016, **1454**, 86–92.
- 4 [www.restek.com](http://www.restek.com), *How do small particle size columns increase sample throughput*, 2018.
- 5 J. J. van Deemter, F. J. Zuiderweg and A. Klinkenberg, *Chem. Eng. Sci.*, 1956, **6**, 271–289.
- 6 K. Broeckhoven and G. Desmet, *Trends in Anal. Chem.*, 2014, **63**, 65–75.
- 7 J. Wang, P. A. G. Cormack, D. C. Sherrington and E. Khoshdel, *Angew. Chem. Int. Ed.*, 2003, **42**, 5336–5338.
- 8 [www.imagej.net](http://www.imagej.net), *Image J*, 2018.
- 9 *R A Lang. Environ. Stat. Comput.*, 2015, 55, 275–286.
- 10 A. A. Qader, J. Urraca, S. B. Torsetnes, F. Tønnesen, L. Reubsæet and B. Sellergren, *J. Chromatogr. A*, 2014, **1370**, 56–62.
- 11 A. J. Hall, P. Manesiotis, M. Emgenbroich, M. Quaglia, E. De Lorenzi and B. Sellergren, *J. Org. Chem.*, 2005, **70**, 1732–1736.
- 12 J. L. Urraca, C. S. A. Aureliano, E. Schillinger, H. Esselmann, J. Wiltfang and B. Sellergren, *J. Am. Chem. Soc.*, 2011, **133**, 9220–9223.
- 13 S. Helling, S. Shinde, F. Brosseron, A. Schnabel, T. Müller, H. E. Meyer, K.

- Marcus and B. Sellergren, *Anal. Chem.*, 2011, **83**, 1862–1865.
- 14 E. A. G. J. Brandrup, E. H. Immergut, *Polymer Handbook*, 2003.
- 15 D. A. Vadim and M. P. Tsyurupa, *Hypercrosslinked Polymeric Networks and Adsorbing Materials: Synthesis, Properties, Structure, and Applications*, Elsevier, 2011.
- 16 [www.polymerdatabase.com](http://www.polymerdatabase.com), *Polymer Properties Database*, 2018.
- 17 [www.alz.org](http://www.alz.org), *Advancing Alzheimer's Research Worldwide*, 2014.
- 18 S. Gauthier, *Clinical Diagnosis and management of Alzheimer's Disease*, M. Duntitz, London, 1996.
- 19 [www.memory.ucsf.edu](http://www.memory.ucsf.edu), *UCSF Memory and Aging Center*, 2014.
- 20 [www.adni.loni.usc.edu](http://www.adni.loni.usc.edu), *Sharing Alzheimer's Research Data with the World*, 2014.
- 21 D. Whitford, *Proteins Structure And Function*, John Wiley & Sons, Ltd, West Sussex, 2005.
- 22 T. A. Lanz and J. B. Schachter, *J. Neurosci. Meth.*, 2008, **169**, 16–22.
- 23 A. A. Qader, PhD Thesis, Technical University of Dortmund, 2014.
- 24 S. Lowell and J. E. Shields, *Powder Surface Area and Porosity*, Chapman & Hall, London, 3rd edn., 1991.
- 25 A. Rachkov and N. Minoura, *Biochim. Biophys. Acta*, 2001, **1544**, 255–266.
- 26 A. Rachkov and N. Minoura, *J. Chromatogr. A*, 2000, **889**, 111–118.
- 27 A. Rachkov, M. Hu, E. Bulgarevich, T. Matsumoto and N. Minoura, *Anal. Chem.*, 2004, **504**, 191–197.

- 28 H. Nishino, C.-S. Huang and K. J. Shea, *Angew. Chem. Int. Ed.*, 2006, **45**, 2392–2396.
- 29 P. Manesiotis, A. J. Hall, J. Courtois, K. Irgum and B. Sellergren, *Angew. Chem. Int. Ed. Engl.*, 2005, **44**, 3902–6.
- 30 A. A. Qader, J. Urraca, S. B. Torsetnes, F. Tønnesen, L. Reubsæet and B. Sellergren, *Pers. Commun.*, 2013, 1–38.
- 31 [www.globocan.iarc.fr](http://www.globocan.iarc.fr), *International Agency for Research on Cancer, World Health Organization*, 2014.
- 32 H. Lodish, A. Berk, P. Matsudaira, C. A. Kaiser and M. Krieger, *Molecular Cell Biology*, W. H. Freeman Publishers, 5th edn., 2003.
- 33 M. Harmsma, B. Schutte and F. C. S. Ramaekers, *Biochim. Biophys. Acta*, 2013, **1836**, 255–272.
- 34 C. Deakin, *Biomed. Sci.*, 2009, **1**, 13–15.
- 35 R. Molina, X. Filella and J. M. Augé, *EJCMO*, 2009, **1**, 1–8.
- 36 [www.ncbi.nlm.nih.gov](http://www.ncbi.nlm.nih.gov), *National Center for Biotechnology Information*, 2016.
- 37 C. Rossetti, M. A. Switnicka-Plak, T. G. Halvorsen, P. A. G. Cormack, B. Sellergren and L. Reubsæet, *Sci. Rep.*, 2017, **7**, 1–11.
- 38 C. Rossetti, A. A. Qader, T. G. Halvorsen, B. Sellergren and L. Reubsæet, *Anal. Chem.*, 2014, **86**, 12291–12298.
- 39 C. Polson, P. Sarkar, B. Incedon, V. Raguvaran and R. Grant, *J. Chromatogr. B*, 2003, **785**, 263–275.
- 40 R. Kay, C. Barton, L. Ratcliffe, B. Matharoo-Ball, P. Brown, J. Roberts, P. Teale and C. Creaser, *Rapid Commun. Mass Spectrom.*, 2008, **22**, 3255–3260.

- 41 K. Aoyagi, Y. Miyake, K. Urakami, T. Kashiwakuma, A. Hasegawa, T. Kodama and K. Yamaguchi, *Clin. Chem.*, 1995, **41**, 537–543.
- 42 G. Jura and W. D. Harkins, *J. Am. Chem. Soc.*, 1944, **66**, 1356–1362.
- 43 S. B. Torsetnes, M. N. Broughton, E. Paus, T. G. Halvorsen and L. Reubsæet, *Anal. Bioanal. Chem.*, 2014, **406**, 2733–2738.
- 44 A. Wood-Kaczmar, S. Gandhi and N. W. Wood, *Trends Mol. Med.*, 2006, **12**, 521–528.
- 45 R. F. Pfeiffer and I. Bodis-Wollner, Eds., *Parkinson's Disease and Nonmotor Dysfunction*, Human Press Inc., Totowa, New Jersey, 2005.
- 46 [www.parkinsons.org.uk](http://www.parkinsons.org.uk), 2014.
- 47 G. F. Wooten, L. J. Currie, V. E. Bovbjerg, J. K. Lee and J. Patrie, *J Neurol Neurosurg Psychiatry*, 2004, **75**, 637–639.
- 48 M. S. Okun, H. H. Fernandez, D. G. Grosset and K. A. Grosset, *Parkinson's Disease: Clinician's Desk Reference*, Manson Publishing, 2009.
- 49 V. M. Y. Lee and J. Q. Trojanowski, *Neuron*, 2006, **52**, 33–38.
- 50 V. Ruipérez, F. Darios and B. Davletov, *Prog. Lipid Res.*, 2010, **49**, 420–428.
- 51 A. Bellucci, M. Zaltieri, L. Navarria, J. Grigoletto, C. Missale and P. Spano, *Brain Res.*, 2012, **1476**, 183–202.
- 52 M. Bungeroth, S. Appenzeller, A. Regulín, W. Völker, I. Lorenzen, J. Grötzinger, M. Pendziwiat and G. Kuhlenbäumer, *Neurobiol. Aging*, 2014, **35**, 1913–1919.

### 3. Core-shell molecularly imprinted polymers

The synthesis of MIPs in a core-shell format is the focus of the work presented in this Chapter. Through the synthesis of core-shell particles, better control of particle size and particle morphology can be anticipated. Core-shell MIP microspheres are expected to be bigger, have narrower particle size distributions and binding sites that are more easily accessible compared to non-core-shell MIP counterparts. Additionally, less template is required for their synthesis, making the overall process less expensive.

Core-shell particles can be prepared by different methods. In this work, the main focus was on core-shell microspheres prepared by PP, as it was the main synthetic method for the synthesis of the core-shell MIP variants. In 2000, Li and Stöver demonstrated for the first time that the PP can be effectively used for the synthesis of the core-shell polymer microspheres. PP opens the possibility to synthesise the core-shell particles in two ways: either by a two-step batch mode or semi-batch *in situ*. In the two-step method, crosslinked core polymer microspheres are firstly prepared by typical PP.<sup>1</sup> Then, these core particles are used as the seed particles in a subsequent second polymerisation for the synthesis of core-shell polymers. The semi-batch *in situ* method involves the synthesis of the polymer cores and shells in a single reaction involving two successive reaction periods. Co-monomer(s) and/or crosslinker which form the polymer shell are added to the polymerisation solution after a certain polymerisation time.<sup>2</sup> The crosslinker forms a solvent-swollen gel layer on the surface of the polymer cores. This layer sterically stabilises the core-shell particles and prevents homocoagulation, thus it prevents the formation of particles with broad particle size distribution.<sup>3</sup> Therefore, particles with narrow particle size distribution are maintained during the whole synthesis. The size of the core and the

thickness of the shell of the core-shell microspheres can be tuned through changing of the reaction conditions, *e.g.*, inclusion of co-solvent and/or co-monomer(s).<sup>2</sup> The introduction of co-solvents, such as toluene, into the PP medium can significantly improve the porosity and homogeneity of divinylbenzene-based microspheres.<sup>4</sup> The final particle size of the polymer core can be controlled through changing of the concentration of the crosslinking agent. Higher concentrations of divinylbenzene in acetonitrile leads to a smaller size of the final nuclei.<sup>5</sup> Further exploitation of the PP procedure as the synthetic method for the preparation of core-shell particles was studied by Huang and others. They demonstrated the use of wide range of co-monomers incorporated into the polymer shell layers. These included co-monomers with functional groups such as: ester, hydroxyl, chloromethyl, carboxylic acid, amide, cyano and glycidyl groups.<sup>6</sup> The formation of a new fraction of particles besides the core-shell particles, also known as secondary nucleation, is the main problem to deal with during the PP. Two competing reactions can be distinguished in the second step of the PP. When co-monomer radicals react with residual double bonds present on the surfaces of the polymer cores, then core-shell layers are formed. When soluble active radicals react with themselves or with soluble oligomers, then new particles known as secondary particles, (nuclei) are initiated. The capture of soluble polymer radicals from solution is dependent on the content of residual double bonds and degree of crosslinking in the solvent-swollen gel layer. When the number of residual double bonds and the degree of crosslinking are high, the soluble polymer radicals are captured effectively and the secondary nucleation is minimised.<sup>3</sup> In 2011, Barahona and others used two-step PP for the first time for the synthesis of core-shell MIPs. Non-imprinted poly(DVB-80) microspheres, preformed in the first step of PP, were successfully used as the seed particles for the synthesis of imprinted poly(DVB-80-co-MAA) core-shell microspheres for a thiabendazole (TBZ) target. MIP microspheres in the micron-sized range were applied as the stationary phase in liquid chromatography.<sup>7</sup> Another example of core-shell MIPs are polymers for bisphenol A target. Wang and others used non-imprinted poly(DVB-80) core particles as the seeds for the synthesis of core-shell MIPs. The composition of the solvent used for



the synthesis of the core-shell MIPs was optimised by manipulation of the ratio of toluene to acetonitrile. The use of toluene in concentrations between 15% and 30% allowed for exclusion of secondary nucleation and/or agglomeration of the particles.<sup>8</sup>

### 3.1 Test study: two-step precipitation polymerisation for the synthesis of peptide imprinted core-shell polymer microspheres

#### 3.1.1 Aim of study

In our test studies for the design and synthesis of core-shell materials for peptide imprinting, we hypothesize that

- Two-step PP can be a useful synthesis method for the preparation of high-quality core-shell polymer microspheres. Near monodisperse and surfactant-free core-shell spherical polymer particles in the micron size range can be synthesised by the two-step PP method;
- Preformed poly(DVB-80) and/or poly(DVB-55) can be used as the seed particles for the synthesis of core-shell particles.

Based on this, the aims of the work presented in this section were as follows:

- Identification of the PP conditions that can be used for the synthesis of core and core-shell microspheres;
- Characterisation of the materials produced.

#### 3.1.2 Experimental section

##### 3.1.2.1 Materials

*N*-(2-Aminoethyl)methacrylamide hydrochloride (EAMA.HCl, purity  $\geq 98\%$ ) was purchased from Polysciences Inc. (Niles, IL, USA). *N*-3,5-*bis*(trifluoromethyl)-phenyl-*N'*-4-vinylphenylurea (NTPVU, purity  $> 95\%$ ) is not commercially available and was kindly donated by Dortmund University. 2-2'-Azobisisobutyronitrile (AIBN, 98% purity) was purchased from BDH Lab. Supplies. Divinylbenzene-80 (DVB-80, 80% DVB isomers and 20% ethyl vinylbenzene isomers), divinylbenzene-55 (DVB-55, 55% DVB

isomers and 45% ethyl vinylbenzene isomers), 1,2,2,6,6-pentamethylpiperidine (PMP, purity >99%), tetrabutylammonium hydroxide solution (TBA.HO, 1.0 M in methanol, 25% ≤ purity <50%), acetonitrile (ACN), methanol (MeOH), tetrahydrofuran (THF) and toluene (Tol) were all purchased from Sigma-Aldrich (St. Louis, MI, USA). AIBN was recrystallized from cold acetone before use. DVB-80 and DVB-55 were purified by filtration through a short plug of neutral aluminium oxide prior to use. All other chemicals used (ACN, MeOH, THF and Tol) were of analytical grade.

#### *3.1.2.2 Synthesis and characterisation of core and core-shell non-imprinted polymers*

The core-shell particles were synthesised as described elsewhere by Stover.<sup>2</sup> The core and core-shell particles were prepared in two separate and successive reactions. The first step included the synthesis of crosslinked core particles by typical PP as described elsewhere.<sup>1</sup> The preformed core particles were then used as the seed microspheres for the synthesis of core-shell particles, and the core-shell particles were prepared in the second PP.

#### *3.1.2.3 Core polymers*

The first step in our synthetic design for the synthesis of core-shell MIPs included identification of the conditions for the synthesis of the core particles which could be used further as the seed particles for the synthesis of core-shell particles. A series of polymers was prepared with the feed compositions shown in Table 3.1. Polymers were synthesised either on a 1 g or a 2 g monomer scale. The monomer concentrations were 1.9%, 2%, 4% and 4.8% w/v (with respect to the solvent). The initiator concentrations were 0.8 mol% or 2 mol%, relative to the number of moles of polymerisable double bonds. Polymers were synthesised either in plastic (polyethylene) Nalgene bottles or borosilicate glass Kimax tubes. 72 h was the precipitation polymerisation time.

Table 3.1 List of PP conditions tested for the synthesis of core particles. The scale relates to the mass of the cores.

Polymer code	Components (mmol)	Monomer conc. (% w/v)	Initiator conc. (mol%)	Solvent (v/v)	Scale (g)	Kimax/ NG	Yield (%)
MAS52	DVB-55 (15.25)	1.9	0.8	ACN	2	NG	36
MAS53	DVB-55 (15.25)	4.8	0.8	ACN	2	NG	49
MAS54	DVB-55 (15.25)	4	2	ACN	2	NG	57
MAS55	DVB-80 (15.32)	4	2	ACN	2	NG	67
MAS56	DVB-55 (7.63)	1.9	0.8	ACN	1	Kimax	45
MAS57	DVB-55 (15.25)	4.8	0.8	ACN	2	Kimax	56
MAS58	DVB-55 (15.25)	4	2	ACN	2	Kimax	68
MAS59	DVB-80 (15.32)	4	2	ACN	2	Kimax	68
MAS62	DVB-55 (7.63)	2	2	ACN/Tol (80/20)	1	Kimax	66
MAS63	DVB-55 (15.25)	4	2	ACN/THF (60/40)	2	Kimax	70
MAS64	DVB-55 (7.63)	2	2	ACN/Tol (60/40)	1	Kimax	70
MAS65	MAA (2.70), DVB-55 (13.48)	4	2	ACN	2	Kimax	53
MAS66	MAA (2.71), DVB-80 (13.53)	4	2	ACN	2	Kimax	64
MAS68	DVB-80 (7.66)	2	2	ACN/Tol (60/40)	1	Kimax	60

The synthesis of the core particles with the polymer code MAS59 can serve as an example of the procedure used for the synthesis of core particles. DVB-80 (2.189 mL, 15.32 mmol) was dissolved in ACN (50 mL). Then, AIBN (90 mg, 0.55 mmol) was added into the monomer solution. The solution was then ultrasonicated for 10 minutes at ambient temperature and sparged with oxygen-free nitrogen gas for 10 minutes at ice-bath temperature, to remove dissolved molecular oxygen. Thereafter, the reaction vessel was sealed under nitrogen and transferred to a Stuart Scientific S160 incubator equipped with a Stovall low-profile roller. The incubator temperature was

ramped from ambient to 60 °C over a period of around two hours and then maintained at 60 °C for a further 70 hours to yield a milky suspension of polymer microspheres.

The insoluble polymer product was isolated from the reaction medium by vacuum filtration on a 0.45 µm nylon membrane filter using using Vacuumbrand Vacuum System (2.0 mbar), washed with ACN (50 mL) and MeOH (50 mL). The polymer was dried overnight in a Townson & Mercer vacuum oven (60 mbar) at 70 °C. The yield of the synthesised material was checked gravimetrically. The yield of MAS59 was 68%.

During the isolation of MAS62, MAS63, MAS64 and MAS68, toluene (50 mL) or THF (50 mL) were additionally used for the washing step, as these solvents were included in the polymerisation solutions.

SEM together with image analysis were performed. These analyses are introduced and discussed in detail in the 2.1.2.2 experimental section.

#### *3.1.2.4 Core-shell polymers*

The second step in the synthetic design for the synthesis of core-shell MIPs was focused on identification of the PP conditions for the synthesis of polymer shells. A series of core-shell polymers was prepared with the feed compositions shown in Table 3.2. 2:1 w/w and 5:1 w/w were the ratios of core particles to monomer. Polymers were produced on 0.3 g and 0.6 g monomer scales, with a monomer and initiator concentrations of 4 w/v and 2% w/v (with respect to the solvent), and 2 mol% (with respect to the total number of polymerisable double bonds), respectively. 24 hours was the precipitation polymerisation time.

Table 3.2 List of PP conditions tested for the synthesis of core-shell particles. The scale relates to the mass of cores and shells.

Polymer code	Core	Shell description	Monomer conc. (% w/v)	Initiator conc. (mol%)	Solvent (v/v)	Scale (g)	Yield (shell) (%)
MAS72	MAS59	100% DVB-80 2:1 Core: Shell	4	2	ACN	0.6	6
MAS73	MAS59	100% DVB-80 5:1 Core: Shell	4	2	ACN	0.6	0
MAS74	MAS64	100% DVB-55 2:1 Core: Shell	2	2	ACN/Tol (60/40)	0.3	0
MAS75	MAS64	100% DVB-55 5:1 Core: Shell	2	2	ACN/Tol (60/40)	0.3	0

The synthesis of the core-shell particles with polymer code MAS72 can serve as an example of a two-step PP for the synthesis of core-shell polymers. Firstly, MAS59 (0.4 g) core particles was placed into a borosilicate Kimax culture tube. Then ACN (14.1 mL) was added into the polymerisation mixture, followed by the addition of DVB-80 (0.2 g, 0.22 mL, 1.52 mmol) and AIBN (9 mg, 0.054 mmol). The mixture was then ultrasonicated for 10 minutes at ambient temperature and sparged with oxygen-free nitrogen gas for 10 minutes at ice-bath temperature, to remove dissolved molecular oxygen. Thereafter, the reaction vessel was sealed under nitrogen and transferred to a Stuart Scientific S160 incubator equipped with a Stovall low-profile roller. The incubator temperature was ramped from ambient to 60 °C over a period of around two hours and then maintained at 60 °C for a further 22 hours to yield a milky suspension of polymer microspheres.

The insoluble polymer product was isolated from the reaction medium by vacuum filtration on a 0.45 µm nylon membrane filter using using a Vacuumbrand Vacuum System (2.0 mbar), and washed with ACN (50 mL) and MeOH (50 mL). The polymer was dried overnight in a Townson & Mercer vacuum oven (60 mbar) at 70 °C prior to characterisation. The yield of the synthesised materials was checked gravimetrically. The yield of MAS72 was 6%.

SEM together with image analysis were performed. These analyses are introduced and discussed in detail in the 2.1.2.2 experimental section.

#### *3.1.2.5 Reproducibility of core polymer: MAS59*

The conditions used for the synthesis of the MAS59 core particles with a 4 % w/v concentration of DVB-80 (with respect to the solvent) and 2 mol% concentration of AIBN (with respect to the total number of polymerisable double bonds) were reproduced. Polymers were produced on 1 g, 2 g and 10 g monomer scales. Polymers were synthesised in borosilicate glass Kimax tubes. 72 hours was the precipitation polymerisation time.

Polymers were characterised by the same methods as the MAS59 core particles presented in the previous subsection (3.1.2.3).

#### *3.1.2.6 Synthesis of non-imprinted core-shell polymers*

In the next step, the functional monomers (EAMA.HCl and NTPVU) were included in the synthesis of the core-shell particles. Two non-imprinted core-shell polymers were prepared: MAS80, where two functional monomers were polymerised together, and the polymer with code MAS81 where only EAMA.HCl was used (Table 3.3). The polymer particles with the code MAS76, the synthesis of which was reported in the previous subsection (3.1.2.5), were used as the cores. 0.4 g of MAS76 was used as the core particles for each polymer prepared, and the core-shell polymers were produced on a 0.6 g scale. A 2:1 w/w ratio of core particles to monomer was used for the synthesis of the non-imprinted core-shell particles. The shell for MAS80 included 97% of DVB-80, 2.5% of EAMA.HCl and 0.5% of NTPVU, which corresponds to a mole ratio of NTPVU: EAMA.HCl: DVB-80 of 0.01:0.1:5. The mole ratio of template: NTPVU: EAMA.HCl for the synthesis of the shell in MAS81 was set at 1:1:10. These molar ratios were the same as used in the previous syntheses presented in Chapter 2, for the synthesis of macroreticular polymers. The shell for MAS81 included 97.5% of DVB-80 and 2.5% of EAMA.HCl, which corresponds to a mole ratio of EAMA.HCl: DVB-80 of 0.1:5. The mole ratio of template: EAMA.HCl for the synthesis of the shell in MAS81

was set at 1:10. These molar ratios were again the same as in the previous syntheses presented in Chapter 2, for the synthesis of macroreticular polymers. The initiator concentrations were 4 mol% or 2 mol%, relative to the number of moles of polymerisable double bonds. 24 hours was the precipitation polymerisation time.

Table 3.3 PP conditions tested for the synthesis of non-imprinted core-shell particles.

Polymer code	Core	Shell description (2:1 Core: Shell)	Monomer conc. (% w/v)	Initiator conc. (mol%)	Yield (%)
MAS80	MAS76	97% DVB-80, 2.5% EAMA.HCl, 0.5 % NTPVU	4	2	0
MAS81	MAS76	97.5% DVB-80, 2.5% EAMA.HCl	4	2	0

The synthesis of the polymer with code MAS80 can serve as an example of the PP procedure for the synthesis of core-shell polymers. Firstly, DMSO (0.3 mL) was added into a borosilicate Kimax tube, followed by TBA.OH (2.9  $\mu$ L, 0.0029 mmol), the functional monomer NTPVU (1 mg, 0.028 mmol) and the functional monomer EAMA.HCl (5 mg, 0.028 mmol). ACN (14.1 mL) was then added followed by DVB-80 (0.2 g, 0.21 mL, 1.52 mmol), AIBN (9 mg, 0.054 mmol) and MAS94 (0.4 g). The mixture was then ultrasonicated for 10 minutes at ambient temperature and sparged with oxygen-free nitrogen gas for 10 minutes at ice-bath temperature, to remove dissolved molecular oxygen. Thereafter, the reaction vessel was sealed under nitrogen and transferred to a Stuart Scientific S160 incubator equipped with a Stovall low-profile roller. The incubator temperature was ramped from ambient to 60 °C over a period of around two hours and then maintained at 60 °C for a further 22 hours to yield a milky suspension of polymer microspheres.

Finally, the polymer microspheres were isolated from the reaction medium by filtration on a 0.45  $\mu$ m nylon membrane filter using a Vacuumbrand Vacuum System (2.0 mbar), washed sequentially with ACN (50 mL) and MeOH (50 mL). The isolated product was transferred into a pre-weighed vial and dried overnight in a Townson & Mercer vacuum oven (60 mbar) at 70 °C. The yield of the synthesised

materials was checked gravimetrically. The yield of MAS80 was 0% due to operation in small scale.

SEM together with image analysis and optical microscopy were performed. These analyses are introduced and discussed in detail in the 2.1.2.2 experimental section.

### 3.1.3 Results and discussion

#### *3.1.3.1 Synthesis and characterisation of core polymers*

Sixteen (16) different conditions were screened in order to identify the PP conditions that can be used for the synthesis of core particles and used further for the synthesis of core-shell MIPs. The starting point in the selection of the conditions tested was implementation of the conditions reported elsewhere by Stöver, where highly crosslinked polymer microspheres with uniform size and shape were synthesised.<sup>2</sup> Applied PP conditions which were used for the synthesis of MAS52 and MAS53 included: use of DVB-55 as the crosslinker and ACN as a near-theta solvent. The monomer scale was set at 2 g, the monomer concentrations were 1.9% or 4.8% w/v (with respect to the solvent) and the initiator concentration was 0.8 mol% (relative to the number of polymerisable double bonds). Also, almost the same PP conditions as in the Stöver procedure were used for the further PP conditions tested: MAS56 and MAS57. Amongst the differences were the type of reaction vessel used. MAS56 and MAS57 were prepared in borosilicate glass Kimax tubes as opposed to MAS52 and MAS53 which were synthesised in plastic (polyethylene) Nalgene bottles. Also, MAS56 was prepared on a 1 g monomer scale. Further PP conditions tested were selected based on the experience gained in the Cormack Polymer Group. DVB-80 and DVB-55 were both evaluated as crosslinkers. Also, methacrylic acid (MAA) was included as the co-monomer in several syntheses with the mole ratio of MAA: DVB-80 and MAA: DVB-55 kept at level 1:5. Acetonitrile was the near-theta solvent



used, however toluene or THF were also included as co-solvents in some syntheses. Crosslinkers and co-monomer were polymerised thermally with AIBN as initiator.

Sixteen (16) core particle products were prepared in good yields (50-60%, Table 3.4), typical for the polymerisation of divinylbenzenes under such precipitation polymerisation conditions. It was observed that particles prepared in plastic Nalgene polyethylene bottles were freely suspended in the porogen, while the products prepared in glass Kimax culture tubes stuck to the reaction vessels. These observations were associated with the hydrophobic properties of the materials prepared. This could be due to interactions of the polar groups in the polymers with polar groups present on the glass Kimax tubes. Amongst the products prepared, two were selected for further synthesis of core-shell polymers. Two selected products (MAS59 and MAS64) were in the form of polymer microspheres with narrow particle size distributions. The SEMs and particle size distributions of MAS59 and MAS64 are shown in Figure 3.1 and Figure 3.2. The average particle diameter in each case was 4.81  $\mu\text{m}$  (MAS59) and 8.82  $\mu\text{m}$  (MAS64) (Table 3.5). The particles produced were highly regular in size and shape. Although the polymer microspheres formed were not monodisperse, as CV values reached 15.87% and 4.72% for MAS59 and MAS64, respectively, their particle size distributions were relatively narrow which make them useful as the core particles for the synthesis of core-shell polymers.

Table 3.4 Effect of the PP feed and type of reaction vessel on the yield of the polymer core products. The scale relates to the mass of the cores.

Polymer code	Polymer name	Monomer conc. (% w/v)	Initiator conc. (mol%)	Solvent (v/v)	Scale (g)	Kimax /NG	Yield (%)
MAS52	poly(DVB-55)	1.9	0.8	ACN	2	NG	36
MAS53	poly(DVB-55)	4.8	0.8	ACN	2	NG	49
MAS54	poly(DVB-55)	4	2	ACN	2	NG	57
MAS55	poly(DVB-80)	4	2	ACN	2	NG	67
MAS56	poly(DVB-55)	1.9	0.8	ACN	1	Kimax	45
MAS57	poly(DVB-55)	4.8	0.8	ACN	2	Kimax	56
MAS58	poly(DVB-55)	4	2	ACN	2	Kimax	68
MAS59	poly(DVB-80)	4	2	ACN	2	Kimax	68
MAS62	poly(DVB-55)	2	2	ACN/Tol (80/20)	1	Kimax	66
MAS63	poly(DVB-55)	4	2	ACN/THF (60/40)	2	Kimax	70
MAS64	poly(DVB-55)	2	2	ACN/Tol (60/40)	1	Kimax	70
MAS65	poly(MAA-co-DVB-55)	4	2	ACN	2	Kimax	53
MAS66	poly(MAA-co-DVB-80)	4	2	ACN	2	Kimax	64
MAS68	poly(DVB-80)	2	2	ACN/Tol (60/40)	1	Kimax	60

NG refers to Nalgene polyethylene bottles.

Table 3.5 Microscopic characterisation of polymer cores.

Polymer code	Optical microscopy observation			Bead average diameter in $\mu\text{m}$ ( $\pm\text{SD}$ ) <sup>b</sup>
	Dispersity (CV%) <sup>a</sup>	Bead size ( $\mu\text{m}$ )	Aggregation	
MAS52	Quasi monodisperse (7.52)	2-3	none	2.27 (0.17)
MAS53	Polydisperse	1-5	Chemical	1-5
MAS54	Polydisperse (21.06)	3-4	none	3.41 (0.74)
MAS55	Polydisperse (27)	3-5	none	3.60 (0.97)
MAS56	Polydisperse	1-5	Chemical	1-5
MAS57	Polydisperse	1-5	Chemical	1-5
MAS58	Polydisperse (20)	3-5	Chemical	4.34 (0.90)
MAS59	Quasi monodisperse (15.87)	4-5	none	4.81 (0.76)
MAS62	Polydisperse (27)	6-8	Chemical	7.24 (2.00)
MAS63	Polydisperse	5-6	Chemical	5-6
MAS64	Quasi monodisperse (4.72)	8-9	none	8.82 (0.41)
MAS65	Polydisperse (49)	2-3	none	4.91 (2.41)
MAS66	Quasi monodisperse (9.5)	1-2	none	2.18 (0.20)
MAS68	Polydisperse (33)	6-7	none	6.65 (2.25)

<sup>a</sup> CV% values come from calculations made using SEM images.

<sup>b</sup> A population of 100 microspheres from SEM image was measured for the determination of bead av. diameter.

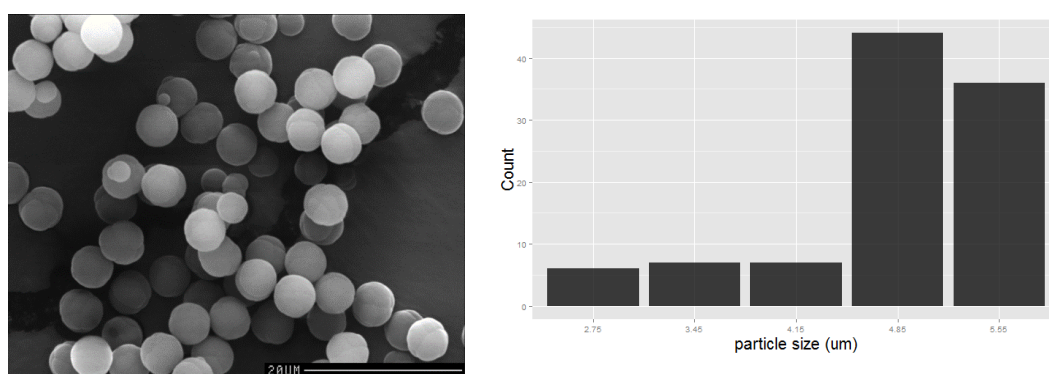


Figure 3.1 SEM and particle size distribution of MAS59 ( $d = 4.81 \mu\text{m} \pm 0.76$ );  $\times 1900$  magnification for SEM image (scale =  $20 \mu\text{m}$ ).

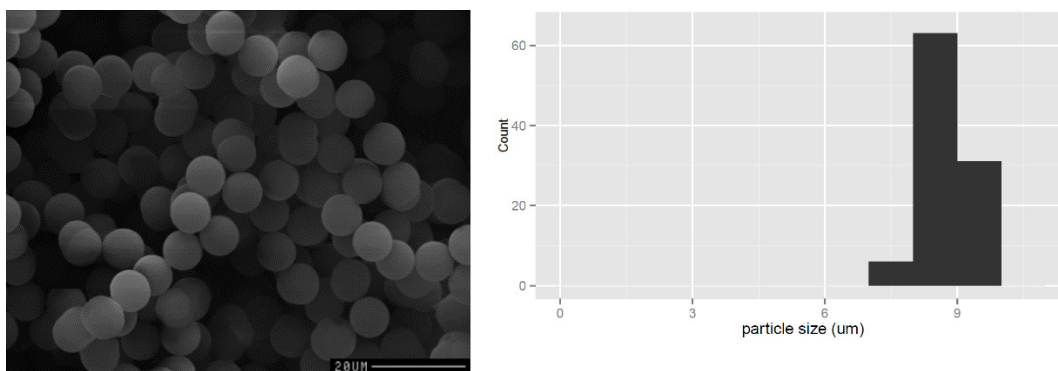


Figure 3.2 SEM and particle size distribution of MAS64 ( $d = 8.82 \mu\text{m} \pm 0.41$ );  $\times 1110$  magnification for SEM image (scale =  $20 \mu\text{m}$ ).

### 3.1.3.2 Synthesis and characterisation of core-shell polymers

Two ratios of core particles to monomer (2:1 and 5:1 w/w) were selected for the synthesis of the core-shell particles. These ratios were selected based on the experience gained in the Cormack Polymer Group. Such ratios were predicted to result in shells of  $0.5\text{-}1 \mu\text{m}$  thickness. The PP conditions used for the synthesis of core-shell polymers were almost identical to those used for the synthesis of the polymer cores (MAS59 and MAS64). The monomer and initiator concentrations were 4% w/v and 2% w/v and 2 mol%. Amongst the differences were: scale of monomer = 0.3 g and 0.6 g, and polymerisation time = 24 hours. Four (4) core-shell polymers were synthesised (Table 3.6). Unfortunately, there was no observable difference in mass between the starting material (core polymer) and the products (putative core-shell polymer), however this was probably due to the low scale of operation and loss of material during product work-up rather than to polymerisation failure. The particle size distribution analysis revealed that the putative core-shell product of MAS72 had a higher mean particle diameter than the starting material (MAS59) and suggested that the mean shell thickness was  $0.1 \mu\text{m}$  (PSD shown in Figure 3.3). Secondary nucleation, which is the nucleation and growth of new particles as the result of reactions in which soluble active radicals react with themselves or with soluble oligomers, was not observed for the core-shell polymers where MAS59 was used as the core (SEM in Figure 3.3), unlike for the other two core-shell polymers, where MAS64 was used as the core (SEMs not shown). Also, we observed a statistically

significant difference in particle size distributions between the MAS59 and MAS72 polymer populations (p-value = 0.01328, Welch's t-test). This statistically significant difference was not observed for the MAS59 and MAS73 polymer populations (p-value = 0.9677, Welch's t-test). This observation implies that the polymer population of MAS72 was different from the polymer population of MAS59, suggesting again that the mean shell thickness was 0.1  $\mu\text{m}$ , which cannot be said for MAS73. Therefore the conditions used for the synthesis of core-shell polymer MAS72, where a 2:1 w/w ratio of core particles to monomer was used, and was further exploited for the synthesis of core-shell MIPs.

Table 3.6 Microscopic characterisation of core-shell polymer morphology.

Polymer code	Optical microscopy observation			Bead average diameter in $\mu\text{m}$ ( $\pm\text{SD}$ ) <sup>b</sup>
	Dispersity (CV%) <sup>a</sup>	Bead size ( $\mu\text{m}$ )	Aggregation	
MAS72	Quasi monodisperse (15.33)	approx. 5	none	5.08 ( $\pm 0.78$ )
MAS73	Quasi monodisperse (15.01)	approx.5	none	4.81 ( $\pm 0.72$ )
MAS74	Quasi monodisperse (10.85)	8-10	Chemical	8.81 ( $\pm 0.95$ )
MAS75	Polydisperse (31.75)	7-10	Chemical	7.08 ( $\pm 2.25$ )

a CV% values come from calculations made using SEM images .

b A population of 100 microspheres from SEM image was measured for the determination of bead av. diameter.

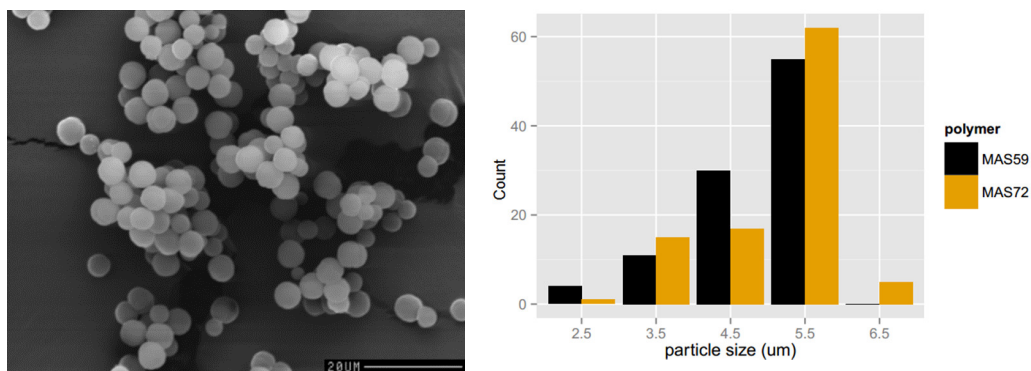


Figure 3.3 SEM of MAS72, core-shells and comparison of particle size distributions of MAS72 ( $n = 100$ ;  $d = 5.08 \mu\text{m} \pm 0.78$ ,  $CV = 15.33\%$ ) and MAS59, cores ( $n = 100$ ;  $d = 4.81 \mu\text{m} \pm 0.76$ ,  $CV = 15.87\%$ );  $\times 1180$  magnification for SEM image (scale =  $20 \mu\text{m}$ ).

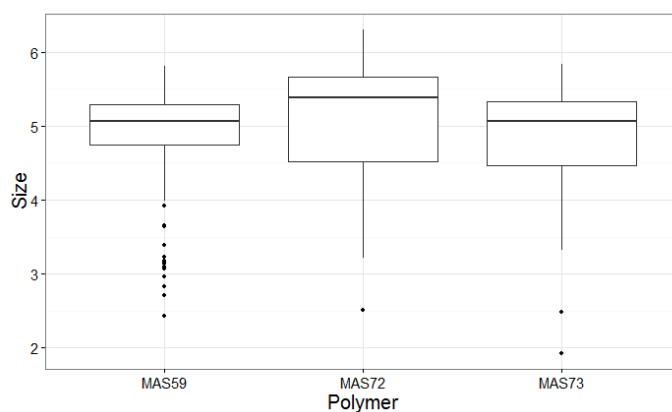


Figure 3.4 Box-plots showing distributions of the particle sizes of MAS59, MAS72 and MAS73.

### 3.1.3.3 Synthesis and characterisation of reproduced core polymer: MAS59

Particles of MAS59 were highly regular in size and shape. Although the polymer microspheres formed were not monodisperse, as the CV value was 15.87% then the particle size distribution of microspheres was relatively narrow which makes them useful as the core particles for the synthesis of core-shell polymers. Therefore, it was required to prepare more material for the synthesis of MIPs. MAS59 was successfully reproduced in the second batch: MAS76 (Table 3.7). However, further attempts failed in terms of reproducibility. The SEMs revealed that the polymer microspheres formed agglomerates with shapes that were not possible to distinguish, and/or the polymer microspheres with broad particle size distributions were formed (SEMs not shown).

However, the reproducibility issue is not new in polymer science. After many unsuccessful attempts, good quality polymer microspheres with narrow particle size distributions were formed with mean particle diameter values from 1.99  $\mu\text{m}$  to 2.26  $\mu\text{m}$ . The mean particle diameter was not exactly the same as MAS59, although they were synthesised on a 10 g monomer scale and their particle size distributions were relatively narrow which make them useful as the core particles for the synthesis of core-shell polymers. The CV values for these polymer microspheres were in the range from 1.4% to 14.06%, which classified them as monodisperse and quasi monodisperse particles. The core polymers MAS91, MAS94, MAS105 and MAS109 were further selected for the synthesis of core-shell MIPs.

Table 3.7 Microscopic characterisation and yield of reproduced polymer core particles. The scale relates to the mass of the cores.

Polymer code	Optical microscopy observation			Bead average diameter in $\mu\text{m}$ ( $\pm\text{SD}$ ) <sup>b</sup>	Scale (g)	Yield (%)
	Dispersity (%CV) <sup>a</sup>	Bead size ( $\mu\text{m}$ )	Aggregation			
MAS59	Quasi monodisperse (15.87)	4-5	none	4.81 (0.76)	2	68
MAS76	Polydisperse (19.91)	4-5	none	4.44 (0.89)	2	61
MAS83	Quasi monodisperse (15.97)	3-5	none	2.97 (0.47)	2	78
MAS84	Polydisperse	3-5	Chemical	n/a	2	75
MAS85	Polydisperse (18.73)	3-4	none	3.92 (0.74)	2	85
MAS86	Polydisperse	3-5	Chemical	n/a	2	85
MAS87	Polydisperse (17.33)	2-3	none	2.84 (0.49)	2	91
MAS88	Polydisperse	3-5	Chemical	n/a	2	81
MAS91	Monodisperse (1.49)	2-3	none	1.99 (0.29)	10	71
MAS93	Polydisperse (23.83)	2-3	none	2.77 (0.66)	1	76
MAS94	Quasi monodisperse (14.06)	2-3	none	2.26 (0.31)	10	80
MAS95	Quasi monodisperse (11.21)	2-3	none	2.41 (0.27)	1	87
MAS105	Quasi monodisperse (10.52)	2-3	none	3.05 (0.23)	10	61
MAS109	Quasi monodisperse (6.85)	1-2	none	1.87 (0.12)	10	70

<sup>a</sup> CV% values come from calculations made using SEM images .

<sup>b</sup> A population of 100 microspheres from SEM image was measured for the determination of bead av. diameters.

n/a not available.

#### 3.1.3.4 Synthesis and characterisation of non-imprinted polymers

For the synthesis of polymer shells where functional monomers were included, 2:1 w/w ratios of core particles to monomer were selected. This ratio was expected to result in shells of 0.1  $\mu\text{m}$  in thickness, as it was observed for MAS72 (Figure 3.3). The PP conditions for the synthesis of MAS80 and MAS81 were almost identical to those used for the synthesis of the polymer cores: MAS76. The monomer and initiator concentrations were 4 % w/v and 2% w/v and 2 mol%. Amongst the differences were:



scale of monomers = 0.6 g, and polymerisation time = 24 hours. Unfortunately, there was no observable difference in mass between the starting material (core polymer) and the product (putative core-shell polymer), however this was probably due to the low scale of operation and loss of material during product work-up rather than to polymerisation failure (Table 3.8). The particle size distribution analysis revealed that the putative core-shell product of MAS80 had a higher mean particle diameter than the starting material (MAS76) and suggested that the mean shell thickness was 0.1  $\mu\text{m}$  (PSD in Figure 3.5). Although the core-shell polymers formed were not monodisperse, as the CV values were 18.99% and 14.06% for MAS80 and MAS81, respectively, their particle size distributions were relatively narrow. Secondary nucleation, which is the nucleation and growth of new particles as the result of reactions in which soluble active radicals react with themselves or with soluble oligomers, was not observed for both non-imprinted core-shell polymers (SEM shown in Figure 3.5). It is suggested that the same molar ratio of functional monomer(s): DVB-80 as used in the previous syntheses presented in Chapter 2 for the syntheses of macroreticular polymers does not result in secondary nucleation. Therefore, the conditions used for the synthesis of core-shell polymer MAS80 and MAS81 were exploited further for the synthesis of core-shell MIPs.

Table 3.8 Effect of the PP feed conditions on the yield of non-imprinted core-shell polymers.

Polymer code	Core	Shell description (2:1 Core: Shell)	Monomer conc. (% w/v)	Initiator conc. (mol%)	Yield (%)
MAS80	MAS76	97% DVB-80, 2.5% EAMA.HCl, 0.5% NTPVU	4	2	0
MAS81	MAS76	97.5% DVB-80, 2.5% EAMA.HCl	4	2	0

Table 3.9 Microscopic characterisation of non-imprinted core-shell particles.

Polymer code	Optical microscopy observation			Bead average diameter in $\mu\text{m}$ ( $\pm\text{SD}$ ) <sup>b</sup>
	Dispersity (%CV) <sup>a</sup>	Bead size ( $\mu\text{m}$ )	Aggregation	
MAS80	Polydisperse (18.99)	approx. 5	none	4.65 ( $\pm 0.88$ )
MAS81	Quasi monodisperse (14.06)	approx. 5	none	4.68 ( $\pm 0.65$ )

<sup>a</sup> CV% values come from calculations made using SEM images .

<sup>b</sup> A population of 100 microspheres from SEM image was measured for the determination of bead av. diameters.

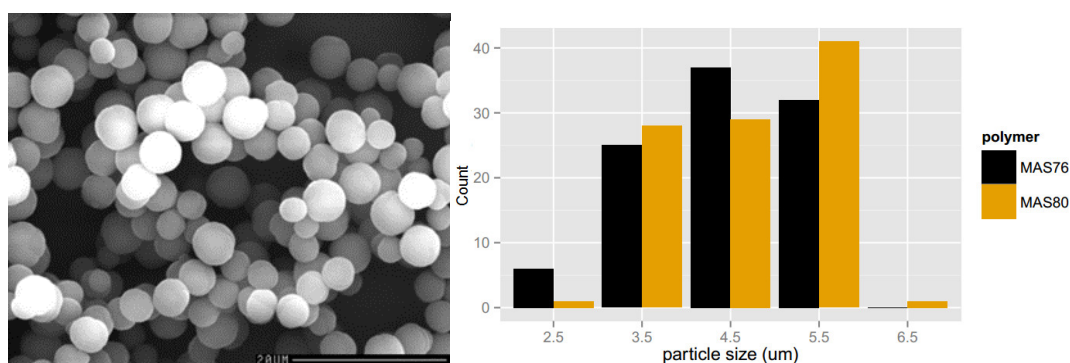


Figure 3.5 SEM of MAS80, core-shells and comparison of particle size distributions of MAS80 ( $n = 100$ ;  $d = 4.65 \mu\text{m} \pm 0.88$ ,  $CV = 18.99\%$ ) and MAS76, cores ( $n = 100$ ;  $d = 4.44 \mu\text{m} \pm 0.89$ ,  $CV = 19.91\%$ );  $\times 1910$  magnification for SEM image (scale =  $20 \mu\text{m}$ ).

## 3.2 Core-shell molecularly imprinted polymer microspheres synthesised by two-step precipitation polymerisation

### 3.2.1 Aim of study

In our studies on the synthesis of core-shell polymers for peptide imprinting, we hypothesize that

- Two-step PP can be a useful synthetic method for the preparation of high-quality core-shell microspheres. Near monodisperse and surfactant-free core-shell spherical polymer particles in the micron size range can be synthesised by the two-step PP method;

- Preformed poly(DVB-80) microspheres can be used as the seed particles for the synthesis of core-shell MIPs;
- Conditions identified in the test study can be implemented for the synthesis of core-shell MIPs.

Based on this, the aims of the work presented in this section were as follows:

- Synthesis of core-shell molecularly imprinted polymers for  $\beta$ -Amyloid and ProGRP targets;
- Characterisation of materials produced;
- Delivery of the next generation materials to the PEPMIP partners for evaluation of molecular recognition.

### 3.2.2 Experimental section

#### 3.2.2.1 Materials

The peptide templates: Ac-GGVVIA-OH (>95% purity) and Z-NLLGLIEA{Nle} (purity 96.58%) were purchased from LifeTein, *N*-(2-aminoethyl)methacrylamide hydrochloride (EAMA.HCl, purity  $\geq 98\%$ ) was purchased from Polysciences Inc. (Niles, IL, USA), *N*-3,5-*bis*(trifluoromethyl)-phenyl-*N'*-4-vinylphenylurea (NTPVU, purity >95%) is not commercially available and was kindly donated by Dortmund University, 2,2'-azobisisobutyronitrile (AIBN, purity 98%) was purchased from BDH Lab. Supplies (UAE). Divinylbenzene-80 (DVB-80, 80% DVB isomers and 20% ethylvinylbenzene isomers), 1,2,2,6,6-pentamethylpiperidine (PMP, purity >99%), tetrabutylammonium hydroxide solution (TBA.HO, 1.0 M in methanol, 25%  $\leq$  purity < 50%) and hydrochloric acid (37 wt. % in H<sub>2</sub>O) were all purchased from Sigma-Aldrich (St. Louis, MI, USA). DVB-80 was purified by filtration through a short plug of neutral aluminium oxide prior to use. AIBN was recrystallized from acetone at low

temperature. All other chemicals used (acetonitrile [ACN], methanol and dimethyl sulfoxide [DMSO, purity  $\geq 99.9\%$ ]) were of analytical grade.

### *3.2.2.2 Synthesis of core-shell molecularly imprinted polymer microspheres for peptide targets*

The core-shell MIPs and their corresponding NIPs were synthesised by two-step PP as described elsewhere.<sup>2</sup> The core and core-shell particles were prepared in two separate and successive reactions. The first step included the synthesis of crosslinked core particles by typical PP as described elsewhere.<sup>1</sup> The synthesis of the core particles have been described already in the previous subsections (3.1.2.5 and 3.1.3.3). The core polymers: MAS91, MAS94, MAS105 and MAS109 were selected for the synthesis of the core-shell materials. These preformed core particles were used as the seed microspheres for the synthesis of core-shell particles, which were prepared in the second PP reaction.

### *Synthesis of core-shell MIPs with the same concentration of T and FMs as in the previous syntheses reported in Chapter 2*

Initially, two core-shell MIPs and their corresponding non-imprinted counterparts were prepared. The feed compositions of the first generation of core-shell materials is shown in Table 3.10. MAS100 and MAS101, and MAS102 and MAS103 are pairs of MIPs and NIPs for the Z-NLLGLIEA{Nle} and Ac-GGVVIA-OH targets, respectively. The polymer particles with the code MAS94, the synthesis of which was reported in the previous subsections (3.1.2.5 and 3.1.3.3), were used as the cores. 1 g of MAS94 was used as the core particles for each prepared polymer, and the core-shell polymers were produced on a 1.5 g scale. A 2:1 w/w ratio of core particles to monomer was used for the synthesis of the core-shell particles. The shells for the MIP and NIP for the Z-NLLGLIEA{Nle} target included 97.5% of DVB-80 and 2.5% of EAMA.HCl, which corresponds to a mole ratio of EAMA.HCl: DVB-80 of 0.1:5. The mole ratio of template: EAMA.HCl for the synthesis of the shell in MAS100 was set at 1:10. These molar ratios were the same as used in the previous syntheses presented in

Chapter 2, for the synthesis of macroreticular polymers. The shells for the MIP and NIP for the Ac-GGVVIA-OH target included 97% of DVB-80, 2.5% of EAMA.HCl and 0.5% of the NTPVU, which corresponds to a mole ratio of NTPVU: EAMA.HCl: DVB-80 of 0.01:0.1:5. The mole ratio of template: NTPVU: EAMA.HCl for the synthesis of the shell in MAS102 was set at 1:1:10. These molar ratios were the same as used in the previous syntheses presented in Chapter 2, for the synthesis of macroreticular polymers. The conditions identified in the test studies presented in the previous subsections (3.1.2.6 and 3.1.3.4), for the synthesis of particle cores and shells by the two-step PP were applied. The monomer and initiator concentrations were 4% w/v (with respect to the solvent) and 2 mol% (with respect to the total number of polymerisable double bonds), respectively. 24 h was the polymerisation time.

Table 3.10 Feed composition of core-shell MIPs and their corresponding NIPs.

Polymer code	Core	Shell description (2:1 Core: Shell)	Template	Monomer conc. (% w/v)	Initiator conc. (mol%)	Yield (shell) (%)
MAS100	MAS94	97.5% DVB-80 2.5% EAMA.HCl	Z-NLLGLIEA{Nle}	4	2	24
MAS101	MAS94	97.5% DVB-80 2.5% EAMA.HCl	-	4	2	0
MAS102	MAS94	97% DVB-80 2.5% EAMA.HCl 0.5% NTPVU	Ac-GGVVIA-OH	4	2	7
MAS103	MAS94	97% DVB-80 2.5% EAMA.HCl 0.5% NTPVU	-	4	2	16

The synthesis of the MIP with polymer code MAS100 can serve as an example of the PP procedure for the synthesis of core-shell MIPs. Firstly, the template, Z-NLLGLIEA{Nle} (8.2 mg, 0.007 mmol) was added into a borosilicate Kimax tube. Thereafter, DMSO (0.75 mL) was added (to dissolve the template), followed by PMP (1.82  $\mu$ L, 0.01 mmol) and the functional monomer EAMA.HCl (12.3 mg, 0.07 mmol). ACN (36.75 mL) was then added followed by DVB-80 (0.49 g, 0.53 mL, 3.73 mmol), AIBN (22.3 mg, 0.2 mmol) and 1 g of MAS94. (For the synthesis of the corresponding

NIP, the template was omitted from the synthetic protocols). The mixture was then ultrasonicated for 10 minutes at ambient temperature and sparged with oxygen-free nitrogen gas for 10 minutes at ice-bath temperature, to remove dissolved molecular oxygen. Thereafter, the reaction vessel was sealed under nitrogen and transferred to a Stuart Scientific S160 incubator equipped with a Stovall low-profile roller. The incubator temperature was ramped from ambient to 60 °C over a period of around two hours and then maintained at 60 °C for a further 22 hours to yield a milky suspension of polymer microspheres.

A few drops were collected from the reaction mixture and applied onto a microscope slide and examined by an Olympus Vanox optical microscope. Polymer microspheres were controlled in terms of size, dispersity and their aggregation (if any) by the optical microscopy analysis.

Finally, the polymer microspheres were isolated from the reaction medium by filtration on 0.45 µm nylon membrane filters using a Vacuumbrand Vacuum System (2.0 mbar), washed sequentially with ACN (50 mL), MeOH/0.1 M aq. HCl (90/10, v/v, 50 mL) and MeOH (50 mL). The isolated product was transferred into a pre-weighed vial and dried overnight in a Townson & Mercer vacuum oven (60 mbar) at 70 °C. The yield of the synthesised materials was checked gravimetrically. The yield of MAS100 was 24%.

*Synthesis of core-shell MIPs with a 5-fold reduction in the concentration of T and FMs in comparison with the previous syntheses reported in Chapter 2*

In a further study, three more core-shell MIPs and their corresponding non-imprinted counterparts were prepared. In this study, the concentration of template and functional monomer(s) was reduced five-fold. The feed compositions of these materials is shown in Table 3.11. MAS112 and MAS113, MAS114 and MAS115 are pairs of MIPs and NIPs for the Z-NLLGLIEA{Nle} target. MAS114 and MAS115 are the MIP and NIP for the Ac-GGVVIA-OH target. The polymer particles with code MAS105, the synthesis of which was reported in the previous subsections (3.1.2.5 and 3.1.3.3),

were used as the cores. 1 g of MAS105 was used as the core particles for each polymer prepared, and the core-shell polymers were produced on a 1.5 g scale. A 2:1 w/w ratio of core particles to monomer scale was used for the synthesis of the core-shell particles. The shells for the first MIP and NIP pair for the Z-NLLGLIEA{Nle} target included 99.5% of DVB-80 and 0.5% of EAMA.HCl, which corresponds to a mole ratio of EAMA.HCl: DVB-80 of 0.02:5. Along with the reduction of EAMA.HCl, the amount of template was also reduced five-fold, but the mole ratio of template: EAMA.HCl for the synthesis of the shell in MAS112 was kept at 1:10. The shells for the second MIP and NIP pair for the Z-NLLGLIEA{Nle} target included 99.3% of DVB-80 and 0.5% of EAMA.HCl and 0.2% of NTPVU, which corresponds to a mole ratio of NTPVU: EAMA.HCl: DVB-80 of 0.002:0.02:5. Along with the reduction of functional monomers, the amount of template was again reduced five-fold, but the mole ratio of template: NTPVU: EAMA.HCl for the synthesis of the shell in MAS114 was kept at 1:2:10. The shells for the MIP and NIP pair for the Ac-GGVVIA-OH target included 99.4% of DVB-80 and 0.5% of EAMA.HCl and 0.1% of NTPVU, which corresponds to a mole ratio of NTPVU: EAMA.HCl: DVB-80 of 0.001:0.02:5. Along with the reduction of functional monomers, the amount of template was again reduced five-fold, but the mole ratio of template: NTPVU: EAMA.HCl for the synthesis of the shell in MAS116 was kept at 1:1:10. The conditions identified in the test studies presented in the previous subsections (3.1.2.6 and 3.1.3.4), for the synthesis of particle cores and shells by the two-step PP, were applied. The monomer and initiator concentration were 4% w/v (with respect to the solvent) and 2 mol% (with respect to the total number of polymerisable double bonds), respectively. 24 h was the polymerisation time.

Table 3.11 Feed composition of core-shell MIPs and their corresponding NIPs.

Polymer code	Core	Shell description (2:1 Core: Shell)	Template	Monomer conc. (% w/v)	Initiator conc. (mol%)	Yield (shell) (%)
MAS112	MAS105	99.5% DVB-80 0.5% EAMA.HCl	Z-NLLGLIEA{Nle}	4	2	11
MAS113	MAS105	99.5% DVB-80 0.5% EAMA.HCl	-	4	2	15
MAS114	MAS105	99.3% DVB-80 0.5% EAMA.HCl 0.2% NTPVU	Z-NLLGLIEA{Nle}	4	2	14
MAS115	MAS105	99.3% DVB-80 0.5% EAMA.HCl 0.2% NTPVU	-	4	2	15
MAS116	MAS105	99.4% DVB-80 0.5% EAMA.HCl 0.1% NTPVU	Ac-GGVVIA-OH	4	2	11
MAS117	MAS105	99.4% DVB-80 0.5% EAMA.HCl 0.1% NTPVU	-	4	2	27

*Synthesis of core-shell MIPs with a 5-fold reduction in the concentration of T and FMs and where addition of T and FMs was timed 1.5 h after the polymerisation started*

In a yet further study, three more core-shell MIPs and their corresponding non-imprinted counterparts were prepared. The concentration of template and functional monomer(s) was again reduced five-fold. This time, the addition of template and functional monomer(s) was timed 1.5 h after the polymerisation started. The feed compositions of these materials is shown in Table 3.12. MAS119 and MAS120, MAS121 and MAS122 are the pairs of MIPs and NIPs for the Z-NLLGLIEA{Nle} target. MAS123 and MAS124 are the MIP and NIP for the Ac-GGVVIA-OH target. The polymer particles with the code MAS91, the synthesis of which was reported in the previous subsections (3.1.2.5 and 3.1.3.3), were used as the cores. 1 g of MAS91 was used as the core particles for each polymer prepared, and the core-shell polymers were produced on a 1.5 g scale. A 2:1 w/w ratio of core particles to monomer was used for



the synthesis of the core-shell particles. The shells for the first pair of MIP and NIP for the Z-NLLGLIEA{Nle} target included 99.5% of DVB-80 and 0.5% of EAMA.HCl, which corresponds to a mole ratio of EAMA.HCl: DVB-80 of 0.02:5. Along with the reduction of EAMA.HCl, the amount of template was also reduced five-fold, but the mole ratio of template: EAMA.HCl for the synthesis of the shell in MAS120 was kept at 1:10. The shells for the second pair of MIP and NIP for the Z-NLLGLIEA{Nle} target included 99.3% of DVB-80 and 0.5% of EAMA.HCl and 0.2% of NTPVU, which corresponds to a mole ratio of NTPVU: EAMA.HCl: DVB-80 of 0.002:0.02:5. Along with the reduction of functional monomers, the amount of template was again reduced five-fold, but the mole ratio of template: NTPVU: EAMA.HCl for the synthesis of the shell in MAS121 was kept at 1:2:10. The shells for MIP and NIP pair for the Ac-GGVVIA-OH target included 99.4% of DVB-80 and 0.5% of EAMA.HCl and 0.1% of NTPVU, which corresponds to a mole ratio of NTPVU: EAMA.HCl: DVB-80 of 0.001:0.02:5. Along with the reduction of functional monomers, the amount of template was again reduced five-fold, but the mole ratio of template: NTPVU: EAMA.HCl for the synthesis of the shell in MAS123 was kept at 1:1:10. The conditions identified in the test studies, presented in the previous subsections (3.1.2.6 and 3.1.3.4) for the synthesis of particle cores and shells by the two-step PP, were applied. The monomer and initiator concentration were 4% w/v (with respect to the solvent) and 2 mol% (with respect to the total number of polymerisable double bonds), respectively. 24 h was the polymerisation time.

Table 3.12 Feed composition of core-shell MIPs and their corresponding NIPs.

Polymer code	Core	Shell description (2:1 Core: Shell)	Template	Monomer conc. (% w/v)	Initiator conc. (mol%)	Yield (shell) (%)
MAS119	MAS91	99.5% DVB-80 0.5% EAMA.HCl	-	4	2	3
MAS120	MAS91	99.5% DVB-80 0.5% EAMA.HCl	Z-NLLGLIEA{Nle}	4	2	8
MAS121	MAS91	99.3% DVB-80 0.5% EAMA.HCl 0.2% NTPVU	Z-NLLGLIEA{Nle}	4	2	1
MAS122	MAS91	99.3% DVB-80 0.5% EAMA.HCl 0.2% NTPVU	-	4	2	2
MAS123	MAS91	99.4% DVB-80 0.5% EAMA.HCl 0.1% NTPVU	Ac-GGVVIA-OH	4	2	5
MAS124	MAS91	99.4% DVB-80 0.5% EAMA.HCl 0.1% NTPVU	-	4	2	0

The synthesis of the MIP with polymer code MAS120 can serve as an example of the PP procedure for the synthesis of core-shell MIPs by delayed addition of template and functional monomer(s). Firstly, MAS91 (1 g) core particles were placed into a borosilicate Kimax culture tube. Then, ACN (36.75 mL) was added into the vessel, followed by the addition of DVB-80 (0.49 g, 0.53 mL, 3.73 mmol) and AIBN (22.3 mg, 0.2 mmol). The mixture was then ultrasonicated for 10 minutes at ambient temperature and sparged with oxygen-free nitrogen gas for 10 minutes at ice-bath temperature, to remove dissolved molecular oxygen. Thereafter, the reaction vessel was sealed under nitrogen and transferred to a Stuart Scientific S160 incubator equipped with a Stovall low-profile roller. The incubator temperature was ramped from ambient to 60 °C over a period of one and a half hours (1h 30 min). In the meantime, a solution of template and functional monomer was prepared. The template, Z-NLLGLIEA{Nle} (1.6 mg, 0.0014 mmol) was added into a small vial. (For the synthesis of the corresponding NIP, the template was omitted from the synthetic

protocol). Thereafter, DMSO (0.75 mL) was added (to dissolve the template), followed by PMP (0.33  $\mu$ L, 0.002  $\mu$ mol) in DMSO and the functional monomer EAMA.HCl (2.30 mg, 0.014 mmol). In order to measure such a small amount of PMP, PMP (2  $\mu$ L, 0.012  $\mu$ mol) was dissolved in 12  $\mu$ L of DMSO and 2.31  $\mu$ L of this solution was transferred into the vial. The solution was shaken to ensure that all components added were dissolved. When the temperature in the incubator reached 60 °C after one and half hour, the solution of template and functional monomer was transferred into the borosilicate Kimax culture tube. The borosilicate Kimax culture tube was shaken gently and placed back into the incubator. The temperature was maintained at 60 °C for a further 24 hours to yield a milky suspension of polymer microspheres.

After 24 h, a few drops were collected from the reaction mixture, and applied onto a microscope slide and examined by an Olympus Vanox optical microscope. Polymer microspheres were controlled in terms of size, dispersity and their aggregation (if any) by the optical microscopy analysis.

Finally, the polymer microspheres were isolated from the reaction medium by filtration on a 0.45  $\mu$ m nylon membrane filter using a Vacuumbrand Vacuum System (2.0 mbar), washed sequentially with ACN (50 mL), MeOH/0.1 M aq. HCl (90/10, v/v, 50 mL) and MeOH (50 mL). The isolated product was transferred into a pre-weighed vial and dried overnight in a Townson & Mercer vacuum oven (60 mbar) at 70 °C. The yield of the synthesised materials was checked gravimetrically. The yield of MAS120 was 8%.

In another follow-up study, one more core-shell MIP and its corresponding non-imprinted counterpart were prepared. The concentration of template and the functional monomer, EAMA.HCl, was again reduced five-fold. The concentration of the second functional monomer, NTPVU, was the same as used for the synthesis of the imprinted shell for the Ac-GGVVIA-OH target. This time, the addition of template and functional monomer(s) was again timed 1.5 h after the polymerisation started. The feed compositions of these materials is shown in Table 3.13. The polymer particles with the code MAS109, the synthesis of which was reported in the previous

subsections (3.1.2.5 and 3.1.3.3), were used as the cores. 1 g of MAS91 was used as the core particles for each polymer prepared, and the core-shell polymers were produced on a 1.5 g scale. A 2:1 w/w ratio of core particles to monomer was used for the synthesis of the core-shell particles. The shells for the MIP and NIP for the Z-NLLGLIEA{Nle} target included 99.4% of DVB-80 and 0.5% of EAMA.HCl and 0.1% of NTPVU, which corresponds to a mole ratio of NTPVU: EAMA.HCl: DVB-80 of 0.001:0.02:5. Along with the reduction of functional monomers, the amount of template was again reduced five-fold, but the mole ratio of template: NTPVU: EAMA.HCl for the synthesis of the shell in MAS121 was kept at 1:1:10. The conditions identified in the test studies presented in the previous subsection (3.1.2.6 and 3.1.3.4), for the synthesis of particle cores and particle shells by the two-step PP, were applied. The monomer and initiator concentration were 4% w/v (with respect to the solvent) and 2 mol% (with respect to the total number of polymerisable double bonds), respectively. 24 h was the polymerisation time.

Table 3.13 Feed composition of core-shell MIPs and their corresponding NIPs.

Polymer code	Core	Shell description (2:1 Core: Shell)	Template	Monomer conc. (% w/v)	Initiator conc. (mol%)	Yield (shell) (%)
MAS129	MAS109	99.4% DVB-80 0.5% EAMA.HCl 0.1% NTPVU	Z-NLLGLIEA{Nle}	4	2	15
MAS130	MAS109	99.4% DVB-80 0.5% EAMA.HCl 0.1% NTPVU	-	4	2	19

SEM together with image analysis were performed. These analyses are introduced and discussed in detail in the 2.1.2.2 experimental section.

### 3.3 Results and discussion

#### 3.3.1 Synthesis of core-shell molecularly imprinted polymer microspheres for peptide targets

The studies presented in this section involved the design and the synthesis of core-shell MIPs and the corresponding NIPs for Z-NLLGLIEA{Nle} and Ac-GGVVIA-OH targets. Two-step PP was the synthetic method used. The conditions identified in the test studies, as presented in the previous subsections (3.1.2.6 and 3.1.3.4) for the synthesis of particle cores and particle shells by the two-step PP, were implemented. The core particles (MAS91, MAS94, MAS105 and MAS109) reported in the previous subsections (3.1.2.5 and 3.1.3.3) were selected for the synthesis of core-shell MIPs. The selected polymer microspheres were of good quality, with narrow particle size distributions and mean particle diameters  $\sim 2 \mu\text{m}$ . These particles were prepared with DVB-80 and AIBN concentrations set at 4% w/v (with respect to the solvent) and 2 mol% (with respect to the total number of polymerisable double bonds), respectively. 72 h was the polymerisation time used for the synthesis of the core particles. A 2:1 w/w ratio of core particles to monomer was used for the synthesis of the core-shell particles. Such a ratio allowed for the synthesis of core-shell microspheres with a shell thickness  $\sim 0.1 \mu\text{m}$ . The conditions used for the synthesis of the core-shell particles was almost the same as used for the synthesis of the core particles. The monomer and initiator concentrations were 4 % w/v (with respect to the solvent), and 2 mol% (with respect to the total number of polymerisable double bonds), respectively. Amongst the differences was the polymerisation time, which was reduced from 72 h to 24 h. It was expected that the shorter polymerisation time would minimise the likelihood of secondary nucleation.

The first pairs of MIPs and NIPs were prepared with the same concentration of template and functional monomer(s) as used in the previous syntheses reported in Chapter 2. The yields of core-shell products were low (12% on average, Table 3.14). Secondary nucleation was observed for all MIPs (MAS100 and MAS102) and the NIP

where the NTPVU was used as one of the functional monomers (example of SEM shown in Figure 3.6). The addition of template or functional monomer: NTPVU resulted in the synthesis of new particles formed beside core-shell microspheres. Secondary nucleation was not observed for the core-shell NIP, MAS101. The particle size distribution analysis revealed core-shell NIP particles with 0.1  $\mu\text{m}$  shell thickness (SEM and PSD shown in Figure 3.7). The black and orange bars represent the fraction of particles which are part of the cores and core-shells, respectively. The fraction of core-shell particles is shifted significantly towards bigger sizes. This analysis clearly shows that the core-shell particles are bigger than their core particles. These studies showed that the presence of the NTPVU and templates, either Z-NLLGLIEA{Nle} and Ac-GGVVIA-OH, contributed to secondary nucleation, therefore the conditions used for the synthesis of the core-shell particles required to be revised.

Table 3.14 Effect of shell compositions on the yield of MIPs and NIPs.

Polymer code	Core	Shell description (2:1 Core: Shell)	Template	Yield (shell) (%)
MAS100	MAS94	97.5% DVB-80 2.5% EAMA.HCl	Z-NLLGLIEA{Nle}	24
MAS101	MAS94	97.5% DVB-80 2.5% EAMA.HCl	-	0
MAS102	MAS94	97% DVB-80 2.5% EAMA.HCl 0.5% NTPVU	Ac-GGVVIA-OH	7
MAS103	MAS94	97% DVB-80 2.5% EAMA.HCl 0.5% NTPVU	-	16

Table 3.15 Microscopic characterisation of core-shell MIPs and their corresponding NIPs.

Polymer code	Optical microscopy observation			Bead average diameter in $\mu\text{m}$ ( $\pm\text{SD}$ ) <sup>b</sup>
	Dispersity (CV%) <sup>a</sup>	Bead size ( $\mu\text{m}$ )	Aggregation	
MAS100	Polydisperse	1-3	Chemical	0.5-3
MAS101	Quasi monodisperse (8.01)	2-3	none	2.40 (0.19)
MAS102	Polydisperse	1-3	Chemical	0.5-3
MAS103	Polydisperse	1-3	Chemical	0.5-3

a CV% values come from calculations made using SEM images .

b A population of 100 microspheres from SEM image was measured for the determination of bead av. diameters.

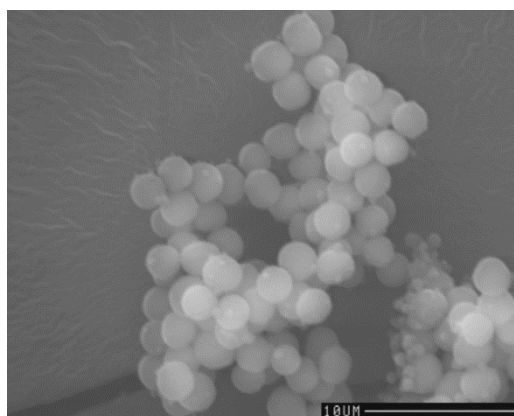


Figure 3.6 SEM of MAS100;  $\times 3200$  magnification (scale =  $10 \mu\text{m}$ ).

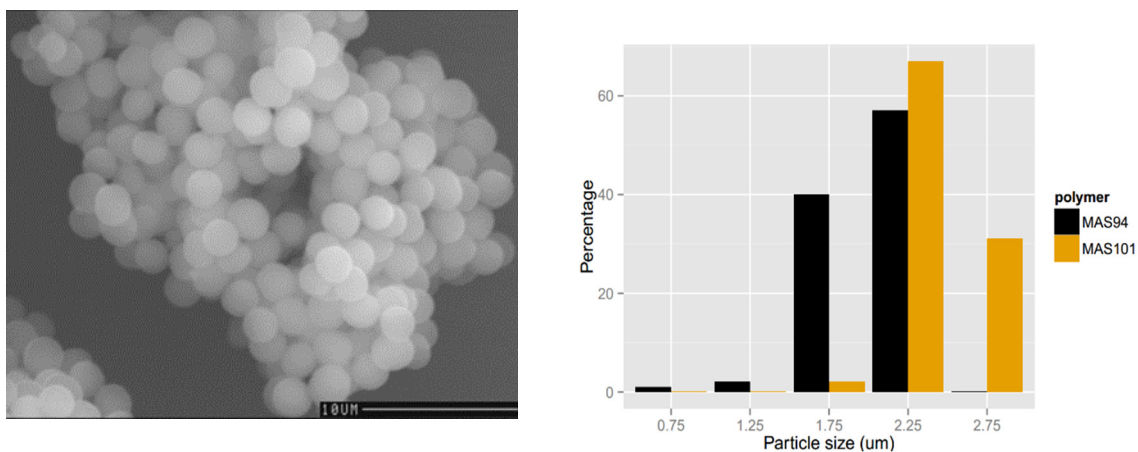


Figure 3.7 SEM of MAS101, core-shells and comparison of particle size distributions of MAS101 ( $n = 100$ ;  $d = 2.40 \mu\text{m} \pm 0.19$ ,  $CV = 8.01\%$ ) and MAS94, cores ( $n = 100$ ;  $d = 2.41 \mu\text{m} \pm 0.27$ ,  $CV = 11.21\%$ );  $\times 3200$  magnification for SEM image (scale =  $10 \mu\text{m}$ ).

The next three pairs of MIPs and NIPs were prepared with five-fold reduced concentrations of template and functional monomers(s) (Table 3.16). Secondary nucleation was still observed for all of the imprinted products (MAS112 and MAS114, SEMs not shown). What is more, the nucleation and growth of new particles was also observed for the non-imprinted product, MAS115, where the urea functional monomer was used in a “cocktail” polymerisation. This effect was not observed for the core-shell NIP where EAMA.HCl was used as the sole functional monomer (SEM and PSD not shown). These observations were exactly the same as observed for the first two pairs of MIPs and NIPs. The reduction of concentrations of template and functional monomer(s) did not help to overcome the secondary nucleation problem, therefore the conditions used for the synthesis of polymer shells were again required to be revised. In a yet further study, delayed addition of template and monomer(s) was taken into consideration.



Table 3.16 Effect of shell compositions on the yield of MIPs and NIPs.

Polymer code	Core	Shell description (2:1 Core: Shell)	Template	Yield (%) (shell)
MAS112	MAS105	99.5% DVB-80, 0.5% EAMA.HCl	Z-NLLGLIEA{Nle}	11
MAS113	MAS105	99.5% DVB-80, 0.5% EAMA.HCl	-	15
MAS114	MAS105	99.3% DVB-80, 0.5% EAMA.HCl, 0.2% NTPVU	Z-NLLGLIEA{Nle}	14
MAS115	MAS105	99.3% DVB-80, 0.5% EAMA.HCl, 0.2% NTPVU	-	15
MAS116	MAS105	99.4% DVB-80, 0.5% EAMA.HCl, 0.1% NTPVU	Ac-GGVVIA-OH	11
MAS117	MAS105	99.4% DVB-80, 0.5% EAMA.HCl, 0.1% NTPVU	-	27

Table 3.17 Microscopic characterisation of core-shell MIPs and their corresponding NIPs.

Polymer code	Optical microscopy observation			SEM average diameter in $\mu\text{m}$ ( $\pm\text{SD}$ ) <sup>b</sup>
	Dispersity (CV%) <sup>a</sup>	Bead size ( $\mu\text{m}$ )	Aggregation	
MAS112	Polydisperse	1-3	Chemical	1-3
MAS113	Polydisperse (18.01)	2-3	none	3.15 (0.57)
MAS114	Polydisperse	1-3	Chemical	1-3
MAS115	Polydisperse	1-3	Chemical	1-3
MAS116	Polydisperse	1-3	Chemical	1-3
MAS117	Polydisperse	1-3	Chemical	1-3

<sup>a</sup> CV% values come from calculations made using SEM images.

<sup>b</sup> A population of 100 microspheres from SEM image was measured for the determination of bead av. diameters. The particle size distribution analysis was performed for MAS113 only, as it was not possible to distinguish the exact shapes of the other microparticles.

The next three pairs of MIPs and NIPs were prepared again with five-fold reduced concentrations of template and functional monomers(s) (Table 3.18). This time, however, addition of template and functional monomer(s) was timed 1.5 h after the polymerisations had started. These changes in the polymerisations helped to overcome the secondary nucleation problem (Table 3.19). Schematic representations of binding sites in successfully prepared core-shell MIPs for the ProGRP and  $\beta$ -Amyloid targets are shown in Figure 3.8 and Figure 3.9, respectively. There were still doubts if the secondary nucleation was observed in MAS121 and MAS122. Therefore, these syntheses were repeated with a decreased 0.1% concentration of NTPVU in the shell. This concentration of NTPVU was the same as for the synthesis of the imprinted shell for the Ac-GGVVIA-OH target where SEM showed no sign of secondary nucleation. SEM analysis confirmed that such a reduction in the concentration of the NTPVU in the polymer shell helped to completely overcome the problem with the secondary nucleation (SEM shown in Figure 3.11). A schematic representation of a binding site in the core-shell MIP for the ProGRP target prepared via a “cocktail” polymerisation is shown in Figure 3.10.

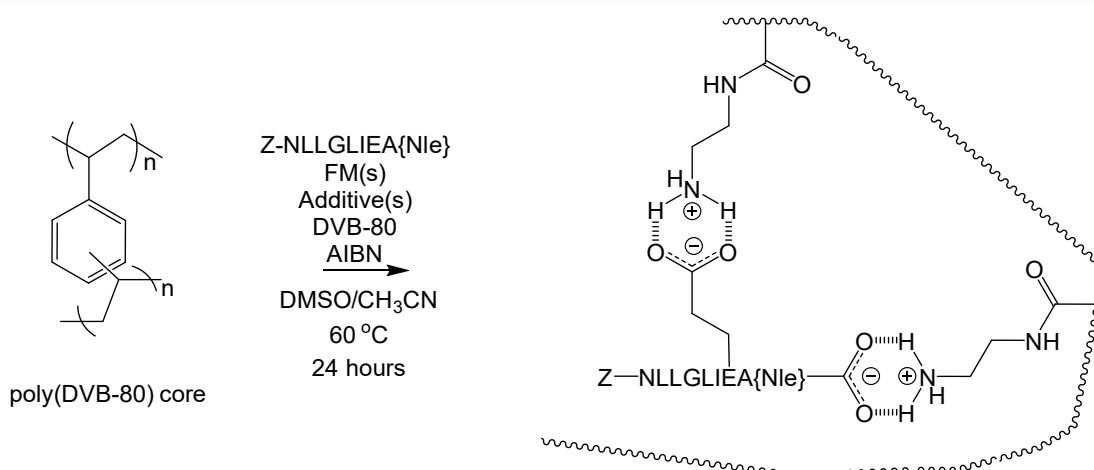


Figure 3.8 Schematic representation of poly(EAMA.HCl-co-DVB-80) core-shell microspheres by the non-covalent molecular imprinting of Z-NLLGLIEA{Nle}, a structural analogue of the ProGRP signature peptide. The carboxylic acid groups in the glutamic acid (E) residue and C-terminus of Z-NLLGLIEA{Nle} are drawn explicitly for emphasis, since these functional groups are involved in the self-assembly of the Z-NLLGLIEA{Nle} with functional monomers (FMs). The complexed synthetic receptor (right hand side) depicts a molecularly imprinted binding site formed upon the free radical copolymerisation of a 1:2 molecular complex of Z-NLLGLIEA{Nle} and N-(2-aminoethyl)methacrylamide hydrochloride with crosslinker (DVB-80).

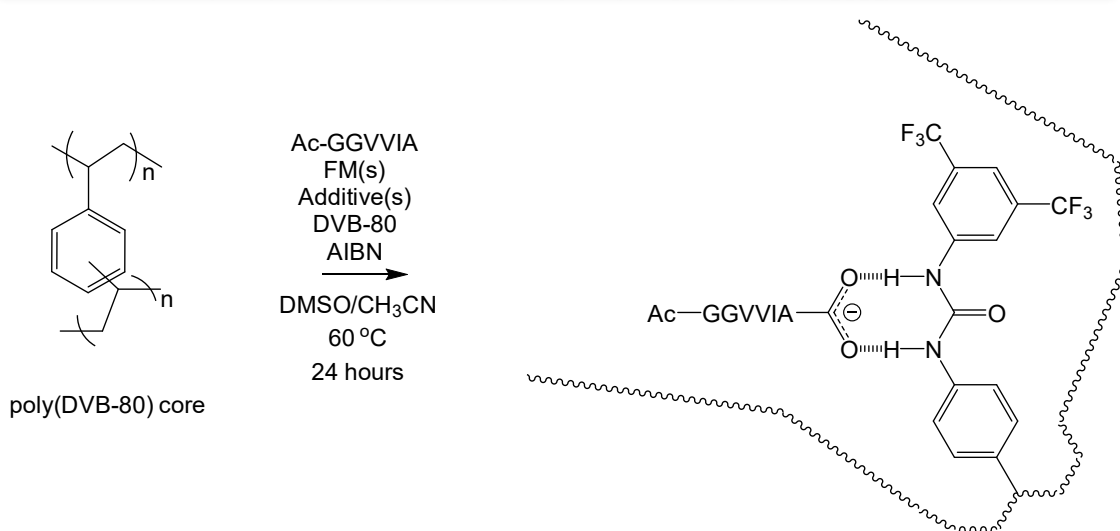


Figure 3.9 Schematic representation of the synthesis of molecularly imprinted poly(NTPVU-co-EAMA.HCl-co-DVB-80) core-shell microspheres by the non-covalent molecular imprinting of Ac-GGVVIA, a structural analogue of the  $\beta$ -amyloid epitope peptide. The carboxylic acid group in the C-terminus of Ac-GGVVIA is drawn explicitly for emphasis, since this functional group is involved in the self-assembly of the Ac-GGVVIA with functional monomers. The complexed synthetic receptor (right hand side) depicts a molecularly imprinted binding site formed upon the free radical copolymerisation of a 1:1 molecular complex of Ac-GGVVIA and N-3,5-bis(trifluoromethyl)-phenyl-N'-4-vinylphenylurea with N-(2-aminoethyl)methacrylamide hydrochloride and crosslinker (DVB-80).

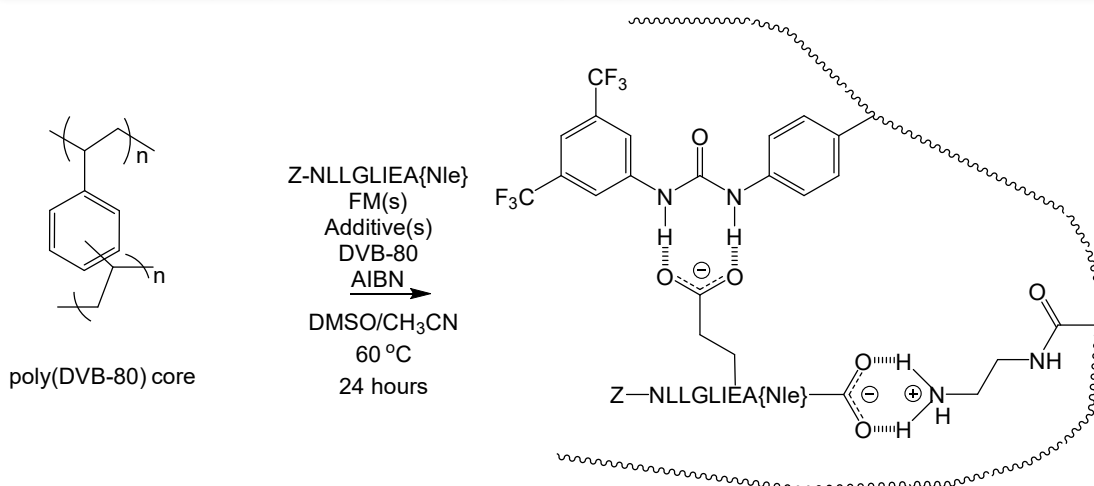


Figure 3.10 Schematic representation of poly(NTPVU-co-EAMA.HCl-co-DVB-80) core-shell microspheres by the non-covalent molecular imprinting of Z-NLLGLIEA{Nle}, a structural analogue of the ProGRP signature peptide. The carboxylic acid groups in the glutamic acid (E) residue and C-terminus of Z-NLLGLIEA{Nle} are drawn explicitly for emphasis, since these functional groups are involved in the self-assembly of the Z-NLLGLIEA{Nle} with functional monomers (FMs). The complexed synthetic receptor (right hand side) depicts a molecularly imprinted binding site formed upon the free radical copolymerisation of a 1:1:1 molecular complex of Z-NLLGLIEA{Nle}, N-(2-aminoethyl)methacrylamide hydrochloride and N-3,5-bis(trifluoromethyl)-phenyl-N'-4-vinylphenylurea with crosslinker (DVB-80).

Table 3.18 Effect of shell compositions on the yield of MIPs and NIPs shells.

Polymer code	Core	Shell description (2:1 Core: Shell)	Template	Yield (%) (shell)
MAS119	MAS91	99.5% DVB-80, 0.5% EAMA.HCl,	-	3
MAS120	MAS91	99.5% DVB-80, 0.5% EAMA.HCl	Z-NLLGLIEA{Nle}	8
MAS121	MAS91	99.3% DVB-80, 0.5% EAMA.HCl, 0.2% NTPVU	Z-NLLGLIEA{Nle}	1
MAS122	MAS91	99.3% DVB-80, 0.5% EAMA.HCl, 0.2% NTPVU	-	2
MAS123	MAS91	99.4% DVB-80; 0.5% EAMA.HCl, 0.1% NTPVU	Ac-GGVVIA-OH	5
MAS124	MAS91	99.4% DVB-80, 0.5% EAMA.HCl, 0.1% NTPVU	-	0

Table 3.19 Microscopic characterisation of core-shell MIPs and their corresponding NIPs.

Polymer code	Optical microscopy observation			Bead average diameter in $\mu\text{m}$ ( $\pm\text{SD}$ ) <sup>b</sup>
	Dispersity (CV%) <sup>a</sup>	Bead size ( $\mu\text{m}$ )	Aggregation	
MAS119	Polydisperse (18.36)	2-3	none	1.97 (0.36)
MAS120	Quasi monodisperse (12.25)	2-3	none	2.06 (0.25)
MAS121	Polydisperse	1-3	Chemical	1-3
MAS122	Polydisperse	1-3	Chemical	1-3
MAS123	Polydisperse (16.71)	2-3	none	1.93 (0.32)
MAS124	Quasi monodisperse (12.78)	2-3	none	1.92 (0.24)

<sup>a</sup> CV% values come from calculations made using SEM images .

<sup>b</sup> A population of 100 microspheres from SEM image was measured for the determination of bead av. diameters. The particle size distribution analysis was performed for MAS119, MAS120, MAS123 and MAS124, as it was not possible to distinguish the exact shapes of the other microparticles: MAS121 and MAS122.

The particle size distribution analysis was performed for the core-shell polymers where secondary nucleation was not observed (example of PSD performed are shown in Figure 3.11). The black and orange bars represent the fraction of particles which are part of the cores and shells, respectively. The fraction of core-shell particles is shifted significantly towards bigger sizes. This analysis clearly shows that the core-shell particles are bigger than their core particles. The yields of shelled products were low (Table 3.18 and Table 3.20). This could be due to the low scale of operation (1.5 g) and to the loss of material during product work-up rather than to polymerisation failure. Delayed addition of template and functional monomer(s) helped to overcome the secondary nucleation problems. After 1.5 h from the polymerisations start, it is expected that more radicals are present in the polymerisation reactions rather than in time 0. Therefore when the template and functional monomer(s) were added, the rate of reagents consumption was faster.

Table 3.20 Effect of shell compositions on the yield of MIP and NIP.

Polymer code	Core	Shell description (2:1 Core: Shell)	Template	Yield (%) (shell)
MAS129	MAS109	99.4% DVB-80, 0.5% EAMA.HCl, 0.1% NTPVU	Z-NLLGLIEA{Nle}	15
MAS130	MAS109	99.4% DVB-80; 0.5% EAMA.HCl, 0.1% NTPVU	-	19

Table 3.21 Microscopic characterisation of core-shell MIPs and their corresponding NIPs.

Polymer code	Optical microscopy observation			Bead average diameter in $\mu\text{m}$ ( $\pm\text{SD}$ ) <sup>b</sup>
	Dispersity (CV%) <sup>a</sup>	Bead size ( $\mu\text{m}$ )	Aggregation	
MAS129	Quasi monodisperse (7.81)	1-2	none	1.92 (0.25)
MAS130	Quasi monodisperse (7.81)	1-2	none	1.87 (0.14)

<sup>a</sup> CV% values come from calculations made using SEM images .

<sup>b</sup> A population of 100 microspheres from SEM image was measured for the determination of bead av. diameters.

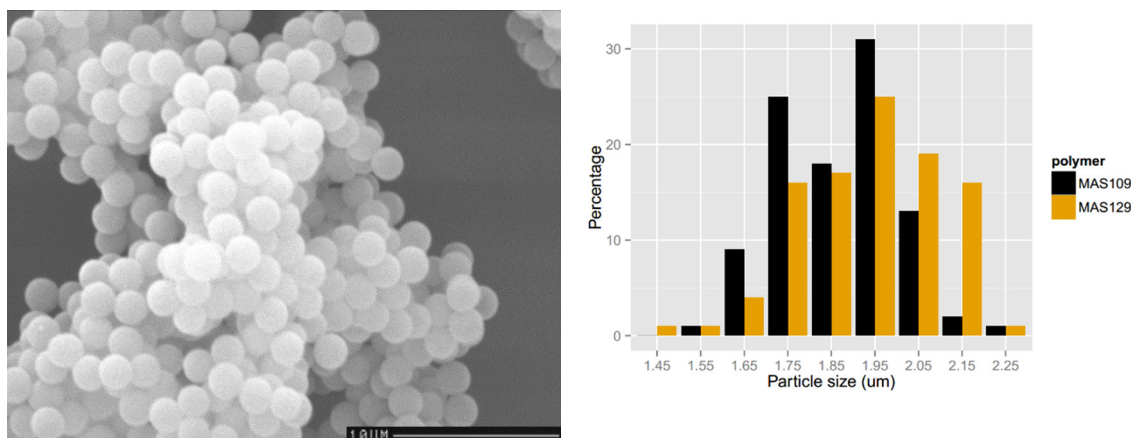


Figure 3.11 SEM of MAS129, core-shells and comparison of particle size distributions of MAS129 ( $n = 100$ ;  $d = 1.92 \mu\text{m} \pm 0.25$ ,  $\text{CV} = 7.81\%$ ) and MAS109, cores ( $n = 100$ ;  $d = 1.87 \mu\text{m} \pm 0.12$ ,  $\text{CV} = 6.85\%$ );  $\times 3200$  magnification for SEM image (scale =  $10 \mu\text{m}$ ).

Selected polymers targeting the ProGRP (MAS120 and MAS129) and  $\beta$ -amyloid (MAS123) targets, and their corresponding NIPs, were sent to PEPMIP partners (Oslo University and Essen University) for off-line Molecularly Imprinted Solid-Phase Extraction (MISPE). These polymers, with the size of microspheres  $\sim 2 \mu\text{m}$  and narrow

particle size distributions, are expected to be easily packed into SPE cartridges. Also, the back pressure is expected to be lower during testing. At the time of writing of this Thesis, the MISPE work was incomplete.

### 3.4 Conclusions and outlook

The scope of the work presented in this chapter spans the design, synthesis and characterisation of the second generation of polymer materials for  $\beta$ -Amyloid and ProGRP targets. The synthesised polymers have been produced in a core-shell format *via* two-step precipitation polymerisations. Although a problem with reproducibility of the core particles arose during the syntheses, core-shell particles were prepared in  $\sim 2 \mu\text{m}$  size which makes them suitable for the packing into SPE cartridges and trap columns. The second generation of polymers prepared were of good quality with narrow particle size distribution. Selected polymers were supplied to PEPMIP partners for testing and evaluation. Although, the materials have been not tested yet, we believe that the core-shell polymers will help to overcome the problems which were reported during the testing of the first generation of materials.

Overall, the successful synthesis and characterisation of the next generation of MIPs can be considered a promising achievement, not least of all because the core-shell approach is generic and can be extended to other targets.



### 3.5 Bibliography

- 1 J. Wang, P. A. G. Cormack, D. C. Sherrington and E. Khoshdel, *Angew. Chem. Int. Ed.*, 2003, **42**, 5336–5338.
- 2 W. Li and H. D. H. Stöver, *Macromolecules*, 2000, **33**, 4354–4360.
- 3 F. Bai, X. Yang, Y. Zhao and W. Huang, *Polym. Int.*, 2005, **54**, 168–174.
- 4 W.-H. Li and H. D. H. Stöver, *J. Polym. Sci. Part A Polym. Chem.*, 1997, **36**, 1543–1551.
- 5 S. E. Shim, S. Yang, H. H. Choi and S. Choe, *J. Polym. Sci. Part A Polym. Chem.*, 2004, **42**, 835–845.
- 6 F. Bai, X. Yang and W. Huang, *J. Appl. Polym. Sci.*, 2006, **100**, 1776–1784.
- 7 F. Barahona, E. Turiel, P. A. G. Cormack and A. Martín-Esteban, *J. Sep. Sci.*, 2011, **34**, 217–24.
- 8 Y. Wang, Q. Liu, F. Rong and D. Fu, *Appl. Surf. Sci.*, 2011, **257**, 6704–6710.

## 4. Magnetic molecularly imprinted polymer microspheres

The synthesis of MIPs in a magnetic format is the focus of the work presented in this Chapter. Through the application of a magnet, magnetic MIPs bond to target analyte can be easily localised. Therefore, MIPs in a magnetic format can help to reduce the testing time and simplify the whole procedure for MIPs in proteomics workflows.

Magnetic particles are a class of particles which can be manipulated using a magnetic field. The magnetic particles possess their magnetic properties thanks to components included in their structure such as: iron, nickel and cobalt.<sup>1</sup>

Magnetite and maghemite include iron in their structures and possess strong magnetic properties, therefore both can be used as the magnetic components for the synthesis of superparamagnetic particles. The co-precipitation of FeCl<sub>3</sub> and FeCl<sub>2</sub> under base condition (at a pH between 8 and 14) results in the formation of either magnetite, Fe<sub>3</sub>O<sub>4</sub>, or maghemite, γFe<sub>2</sub>O<sub>3</sub>. The synthesis of magnetite, as shown in equation 1 in Figure 4.1 requires anaerobic conditions in contrast to the conditions required for the synthesis of maghemite. However, the magnetite is not very stable and can be easily transformed to maghemite under oxidizing conditions, as outlined in equation 2 in Figure 4.1.<sup>2,3</sup>

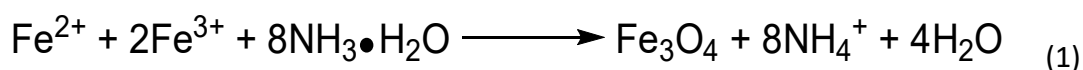


Figure 4.1 Synthesis reactions of magnetite (1) and maghemite (2).

The synthesis of magnetic MIPs usually consist of four steps. The first two steps include the preparation of magnetic particles in which their synthesis and functionalisation take place. These two steps can be skipped if commercially available magnetic particles are purchased. Magnetic particles are widely commercially available and can be easily purchased with different functional groups. In the third step, functionalised magnetic particles are added into the polymerisation solution together with template, functional monomer(s) and crosslinker. These magnetic particles are used as the seed particles for the synthesis of magnetic MIPs. Growth of the MIPs takes place on the surfaces of the functionalised magnetic particles, and magnetic particles are encapsulated inside MIPs. In the last step, the template molecule is extracted and the magnetic MIPs are ready for further characterisation.<sup>4</sup>

Magnetic molecularly imprinted polymers were prepared for the first time by Mosbach and Ansell in the late 90s.<sup>5</sup> They used suspension polymerisation for the incorporation of iron oxide particles into a poly(MAA-co-TRIM) MIP and corresponding NIP. Such a prepared MIP was successfully used in a radioligand assay for the binding of the  $\beta$ -blocker (*S*)-propranolol.<sup>6</sup>

In the literature, there are many examples of magnetic MIPs prepared by different polymerisation methods and used for the detection of compounds in biological or environmental samples. These include: core-shell vinyl-modified silica coated magnetic MIPs and polyethylene glycol-modified MIP particles for herbicide residues<sup>7,8</sup>; nanocomposites with amino-modified magnetic particles for (*S*)-propranolol synthesised by surface-initiated RAFT polymerisation<sup>9</sup>; an acrylamide-based magnetic MIPs for sulfonamide drugs<sup>10</sup>, and others.<sup>11,12,13</sup>

## 4.1 Magnetic MIP with encapsulated magnetite

### 4.1.1 Aim of study

In our syntheses of magnetic macroreticular materials, we hypothesize that

- MIPs have binding sites that have high affinity and selectivity for a given target molecule;
- PP is a useful synthesis method for the preparation of high-quality, MIP microspheres. Near monodisperse and surfactant-free spherical polymer particles in the micron size range can be synthesised by the PP method;
- Modification of the PP protocols: introduction of magnetic particles into PP protocols can result in the synthesis of magnetic polymers;
- $\beta$ -Amyloid is considered as a biomarker which is highly sensitive and specific for Alzheimer's Disease.

Based on this, the aims of the work presented in this section were as follows:

- Introduction of magnetic particles into PP protocols and thereby enable the synthesis of magnetic MIPs for  $\beta$ -Amyloid target;
- Characterisation of the materials produced, including demonstration of magnetic properties;
- Delivery of the first generation of magnetic materials to the PEPMIP partners for evaluation of molecular recognition.

### 4.1.2 Experimental section

#### 4.1.2.1 Materials

The peptide template Ac-GGVVIA-OH (>95% purity), was purchased from LifeTein, *N*-(2-aminoethyl)methacrylamide hydrochloride (EAMA.HCl, purity  $\geq 98\%$ ) was purchased from Polysciences Inc. (Niles, IL, USA), *N*-3,5-*bis*(trifluoromethyl)-phenyl-*N'*-4-vinylphenylurea (NTPVU, purity >95%) is not commercially available and was kindly donated by Dortmund University, 2,2'-azobisisobutyronitrile (AIBN, purity

98%) was purchased from BDH Lab. Supplies (UAE). Divinylbenzene-80 (DVB-80, 80% DVB isomers and 20% ethylvinylbenzene isomers), 1,2,2,6,6-pentamethylpiperidine (PMP, purity >99%), tetrabutylammonium hydroxide solution (TBA.HO, 1.0 M in methanol, 25% ≤ purity < 50%) and hydrochloric acid (37 wt. % in H<sub>2</sub>O) were all purchased from Sigma-Aldrich (St. Louis, MI, USA). FluidMAG-OS with magnetic component concentration 25 mg/mL was purchased from 2B Scientific (UK). All other chemicals used (acetonitrile [ACN], methanol and dimethyl sulfoxide [DMSO, purity ≥99.9%]) were of analytical grade and were purchased from Sigma-Aldrich (St. Louis, MI, USA). DVB-80 was purified by filtration through a short plug of neutral aluminium oxide prior to use. AIBN was recrystallized from acetone at low temperature. The magnetic particles, fluidMAG-OS, were washed with ACN and suspended in ACN before use.

#### *4.1.2.2 Synthesis of magnetic MIP for $\beta$ -Amyloid target*

The first generation of magnetic MIP and their corresponding NIP were synthesised by modification of PP procedure. This modification included: introduction of commercially available magnetic iron oxide nanoparticles into the PP protocol along with the other components which are typical for PP.

Magnetic MIP and their corresponding non-imprinted counterpart were prepared with the feed compositions shown in Table 4.1. Polymers were synthesised on a 0.5 g monomer scale with a monomer and initiator concentration of 2% w/v (with respect to the solvent) and 2 mol% (with respect to the total number of polymerisable double bonds), respectively. The level of magnetic particles used was 25 mg per gram of monomer.

Table 4.1 PP feed for  $\beta$ -Amyloid imprinted magnetic polymer and the corresponding NIP.

Polymer code	Ac-GGVVIA-OH (mmol)	Functional Monomer (mmol)	DVB-80 (mmol)	Solvent (mL)	AIBN (mol%)	TBA.HO (mmol)
MAS14	-	EAMA.HCl (0.07) NTPVU (0.007)	3.71	ACN (19) DMSO (1)	2	0.007
MAS15	0.07	EAMA.HCl (0.07) NTPVU (0.007)	3.71	ACN (19) DMSO (1)	2	0.007

The synthesis of the magnetic MIP with polymer code MAS15 can serve as an example of the PP procedure modified for the synthesis of magnetic polymers. Firstly, the template, Ac-GGVVIA-OH (4.2 mg, 0.07 mmol) was added into a borosilicate Kimax tube. Thereafter, DMSO (1 mL) was added (to dissolve the template) followed by TBA.HO (7.43  $\mu$ L, 0.007 mmol), the functional monomer NTPVU (2.5 mg, 0.007 mmol) and the functional monomer EAMA.HCl (12.3 mg, 0.07 mmol). ACN (14 mL) was then added followed by DVB-80 (0.49 g, 0.53 mL, 3.73 mmol), AIBN (22.3 mg, 0.2 mmol) and ACN (10 mL) with dispersed magnetic particles. (For the synthesis of the corresponding NIP, the template was omitted from the synthetic protocols). The magnetic particles were prepared before use in the PP procedure. The magnetic particles were washed and suspended in ACN. The washing procedure included the following steps: fluidMAG-OS (1 mL) was transferred into a Petri dish and then ACN (10 mL) was added. The magnetic particles were washed with ACN through pipetting (to remove water residues). The separation of ACN from the magnetic particles was achieved through the pipetting and simultaneous application of a magnetic field. The permanent magnet was held against the base of Petri dish while the supernatant was removed. A small volume of ACN was always left covering the magnetic particles placed in the Petri dish. The whole washing procedure of the magnetic particles was repeated four times more until the supernatant became transparent. The magnetic particles were suspended in ACN (10 mL) when added into the PP mixture. When the magnetic particles were added, the PP mixture was then ultrasonicated using a Fisherbrand FB11024 ultrasonic bath for 10 minutes at ambient temperature and then sparged with oxygen-free nitrogen gas for 10 minutes at ice-bath temperature

(to remove dissolved molecular oxygen). Thereafter, the reaction vessel was sealed under nitrogen and transferred to a Stuart Scientific S160 incubator equipped with a Stovall low-profile roller. The incubator temperature was ramped from ambient to 60 °C over a period of around two hours and then maintained at 60 °C for a further 46 hours to yield a milky suspension of polymer microspheres.

A few drops were collected from the polymerisation mixture, and then applied onto a microscope slide and examined by an Olympus Vanox optical microscope. Polymer microspheres were controlled in terms of size, dispersity and their aggregation (if any) by the optical microscopy analysis.

Finally, the polymer microspheres were isolated from the reaction medium by vacuum filtration using a Vacuumbrand Vacuum System (2.0 mbar) on a 0.2 µm nylon membrane filter, washed sequentially with ACN (50 mL), MeOH/0.1 M aq. HCl (90/10, v/v, 50 mL) and MeOH (50 mL). The isolated product was transferred into pre-weighed vial and dried overnight in Townson & Mercer vacuum oven (60 mbar) at 70 °C. The yield of the synthesised material was checked gravimetrically. The yield of MAS15 was 52%.

Magnetic separation was performed to isolate the magnetic polymer particles from non-magnetic particulates. Firstly, dried product was transferred into a clean beaker and washed with ACN (~50 mL). The product dispersed in ACN was mixed with a glass rod. Thereafter, a permanent magnet was held against the base of the beaker, and the beaker with dispersed product was left for 15 s. At this stage, the supernatant was collected. The whole procedure was repeated four times until the supernatant became transparent. The magnetic particles were isolated from the rest of the ACN by vacuum filtration using a Vacuumbrand Vacuum System (2.0 mbar) on a 0.2 µm nylon membrane filter. The isolated product was transferred again into a pre-weighed vial and dried overnight in a Townson & Mercer vacuum oven (60 mbar) at 70 °C. The yield of the synthesised material was again checked gravimetrically. The yield of MAS15 after magnetic separation was 33%.

Polymer microspheres were imaged by scanning electron microscopy (SEM) using a Cambridge Instruments Stereoscan 90. Image analysis of SEM micrographs was done by Image J, as described in in the 2.1.2.2 experimental section. Structural determination of chemical compositions of synthesised polymers were evaluated by using a Shimadzu Fourier Transform Infrared Spectrophotometer. Also, nitrogen sorption analysis and determination of the chemical compositions of the synthesised polymers were evaluated. The evaluation of porosity and specific surface area was done using a micromeritics ASAP 2000 BET Analyzer. The nitrogen sorption analysis and theory which stands behind this analysis were introduced and discussed in detail in Chapter 1 (1.5.1). Additionally, the encapsulation of the magnetic nanoparticles into a MIP for the  $\beta$ -Amyloid target and NIP were evaluated *via* the application of a magnetic field in the vicinity of the nanoparticles. A small amount of product was transferred into a Petri dish and the permanent magnet was applied to the bottom of the Petri dish.

#### 4.1.3 Results and discussion

##### 4.1.3.1 *Synthesis of magnetic MIP and the corresponding NIP*

The synthetic procedure used for the production of the first generation of magnetic polymer microspheres for the  $\beta$ -Amyloid target was analogous to the methodology used for the synthesis of non-magnetic MIPs, discussed in Chapter 2 (2.2.3 and 2.2.4). The MIP and NIP were prepared with the same concentration of template and functional monomer(s) as reported in Chapter 2. The sole difference was the introduction of commercially available magnetic iron oxide nanoparticles. The iron oxide particles were washed five (5) times with ACN prior to their addition to the solutions of monomer. The purpose of the washing procedure was to remove water from the magnetic particles prior to imprinting. The washing and suspension of the magnetic particles in ACN was done immediately before their addition to the solution of monomer. It was done directly prior their addition to avoid a problem which could



arise from instability of the magnetic particles in ACN as this solvent was not their original medium.

The concentration of magnetic particles (25 mg per gram of monomer) was selected based on experience gained in the Cormack Polymer Group. FluidMAG-OS particles at a concentration of 25 mg per gram of monomer were also used for the synthesis of MIPs for a theophylline target.<sup>23</sup> The choice of magnetic particle concentration was done pragmatically. The commercially available magnetic particles, fluidMAG-OS are dispersed in an aqueous solution at a concentration of 25 mg/mL and are stored in a 1 mL vial. This concentration of magnetic particles is exactly the same as required for the synthesis of polymer prepared on 1 g monomer scale. Therefore, there was a good practical reason to select the concentration of 25 mg per gram of monomer for the magnetic polymer synthesis. The magnetic particles at concentration of 25 mg/mL were easy to handle as the whole dispersion of magnetic particles from the vial was poured directly to a Petri dish, where the washing and suspension of the magnetic particles took place. Higher concentrations of magnetic particles (> 5 w/v) was not preferred as the previous examples demonstrated that it was not possible to prepare the polymer microspheres with such a high content of magnetic iron oxide particles.<sup>6</sup>

The first generation of magnetic polymers were prepared in good yields (Table 4.2). The inclusion of magnetic particles did not negatively affect the polymerisation yield. The isolated yields of the polymers were typical for polymerisation of divinylbenzenes under such precipitation polymerisation conditions.

Table 4.2 Effect of feed compositions on the yield of the magnetic polymers.

Polymer code	Template	Polymer name	Yield (%)	
			Before mag. separation	After mag. separation
MAS14	-	poly(NTPVU- <i>co</i> -EAMA.HCl- <i>co</i> -DVB-80)	49	23
MAS15	Ac-GGVVIA-OH	poly(NTPVU- <i>co</i> -EAMA.HCl- <i>co</i> -DVB-80)	52	33

#### 4.1.3.2 Characterisation

The SEM micrographs show that the magnetic MIP and NIP produced are spherical in nature (micrographs shown in Figure 4.2 and Table 4.3). Discrete particles in the micron-sized range were produced, although the microspheres were polydisperse (possibly as a consequence of the presence of magnetic particles and DMSO as a co-solvent). The quality of particles was not ideal as the particles overlap or combine with each other into larger and irregular agglomerates. The SEM observations would suggest that the aggregation of particles was due to chemical bonds formed between the beads. Nevertheless, the particles were suitable for magnetic capture protocols.

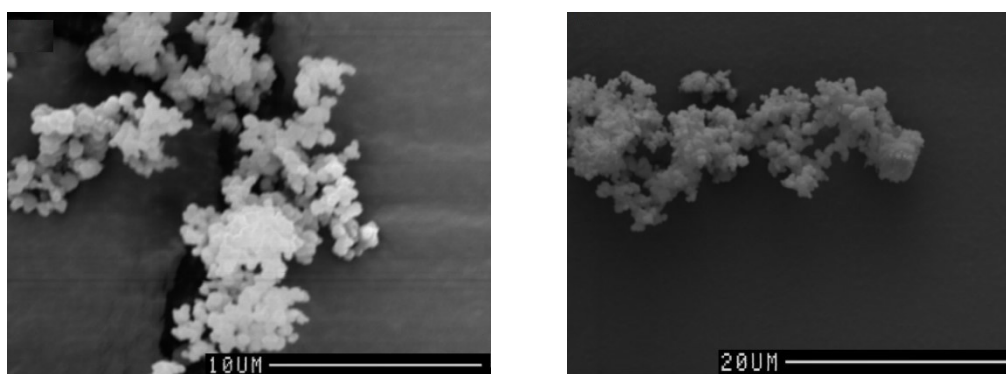


Figure 4.2 SEM of MAS14 (left) and MAS15 (right); magnifications:  $\times 3090$ ,  $\times 1530$  for MAS14 and MAS15, respectively (scales =  $10\ \mu\text{m}$  and  $20\ \mu\text{m}$  for MAS14 and MAS15, respectively).

Table 4.3 Microscopic characterisation of polymer microspheres.

Polymer code	Optical microscopy observation			Bead average diameter in $\mu\text{m}^a$
	Dispersity	Bead size	Aggregation	
MAS14	Polydisperse	Beads? <sup>b</sup>	Chemical	approx. 1
MAS15	Polydisperse	Beads? <sup>b</sup>	Chemical	approx. 1

<sup>a</sup> SEM microscopy observation

<sup>b</sup> Beads? indicates uncertainty whether the observed structures were microspheres.

Incorporation of the magnetic nanoparticles into the MIP and NIP were evaluated *via* the application of a magnetic field in the vicinity of the nanoparticles. Migration of the polymer particles to the magnet was observed when a permanent magnet was applied to the base of a Petri dish containing a certain polymer. This demonstrated

that magnetic nanoparticles were incorporated into MAS14 and MAS15. The colour of the polymers were light brown, which also indicates that magnetic nanoparticles were encapsulated in the polymers. Additionally, during the isolation of products using a 0.2  $\mu\text{m}$  nylon membrane filter, magnetic particles (0.1  $\mu\text{m}$ ) were not detected in the filtrate. These observations indicate that the PP method was successfully extended for the synthesis of magnetic polymers.

In the FT-IR spectra of the magnetic NIP and MIP, the typical peaks associated with poly(-DVB-80) were observed, corresponding with hydroxyl group (Figure 4.3). Due to the presence of these additional peaks, one could conclude that magnetic nanoparticles were not washed sufficiently with ACN (to remove the oil) prior to addition to the polymerisation mixture, but the polymers were dried. These additional peaks could be due to the presence of water permanently entrapped inside the dense polymer network.

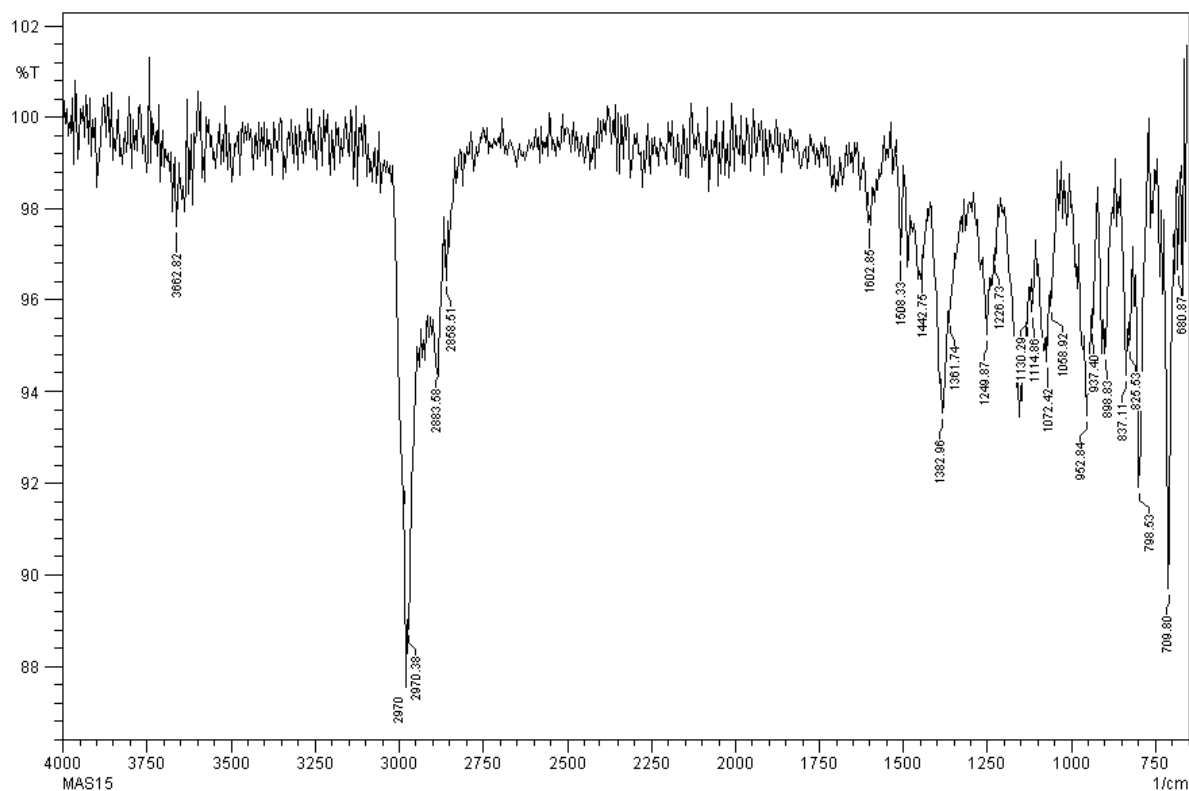


Figure 4.3 FT-IR spectrum of MAS15.

The nitrogen sorption data, shown in Table 4.4, revealed that the MIP and NIP were macroreticular; this was important to establish in view of the need for analyte to access molecularly imprinted binding sites during use of the polymers. The NIP was not identical to the MIP in respect of the porous morphology, again suggestive of the idea that the presence of template during polymerisation influences the polymerisation outcomes.

BET C values for the NIP and MIP were negative, indicating that the data for the tested samples did not fit to the BET isotherm as the nitrogen molecules were absorbed in a single layer onto the surface of the solids (Table 4.4). This change in sorption mode implies that the Langmuir isotherm should be used to describe the specific surface area of the tested polymers for the analysis of the porosimetry data. The nitrogen sorption analysis shows that the average pore size reached a maximum of 2.79 nm (Table 4.4, MAS15). The polymers were highly crosslinked, as DVB-80 constituted more than 97% of the whole polymer network structure, and such a high crosslinking

level usually results in a small pore size. High specific surface areas coupled with the average pore diameters of  $\sim 2$  nm, indicate that the materials tested were microporous. In addition to micropores, there must also be a small percentage of mesopores present within the material (*i.e.*, pores  $> 2$  nm and  $< 50$  nm). These conclusions can be additionally supported by the analysis of nitrogen sorption isotherms. The nitrogen sorption isotherm of type II characteristic for non-porous or macroporous solids with pore width more than 50 nm was generated (MAS14 and MAS15).

Table 4.4 Nitrogen sorption analysis data for the magnetic NIP and MIP for the  $\beta$ -Amyloid target.

Polymer code	BET C value	Specific surface area (m <sup>2</sup> /g)		Specific pore volume (cm <sup>3</sup> /g) <sup>a</sup>	Average pore diameter (nm) <sup>b</sup>
		BET	Langmuir		
MAS14	-75	268	356	0.007	1.66
MAS15	-198	215	287	0.077	2.79

<sup>a</sup> BJH cumulative adsorption pore volume of pores between 1.7 and 300 nm.

<sup>b</sup> Determined by: 4 pore volume/BET surface area.

The MIP for the  $\beta$ -Amyloid target and the corresponding NIP were sent to a PEPMIP partner (Essen University) for off-line Molecularly Imprinted Solid-Phase Extraction (MISPE). Information on the molecular recognition was invaluable in respect of the further optimisation of synthetic protocols.

#### 4.1.3.3 Molecular recognition of the first generation of magnetic polymers

The molecular recognition experiments were performed by Dr Roberto Boi from Essen University. The polymers were tested using SPE coupled with Western Blotting and MALDI-TOF analyses. This subsection contains feedback received from Roberto after testing the first generation of MIPs for the A $\beta$ -Amyloid target.

During the testing procedure, leakage of the polymers was observed. Although, the isolation of magnetic particles from the non-magnetic particulates was performed, a fraction of non-magnetic particles was still present. These particles were present in

almost every collected fraction. In some of the fractions, even though there was no visual sign of polymer particles, their presence was detected in Western Blotting as a massive interference, or in MALDI as an absence of signal.

Both non-imprinted and imprinted magnetic polymers showed affinity to the target peptides. However, further studies were not possible to perform as the polymers lose their magnetic properties after few months, possibly as the result of the storage in MeOH. During testing, the A $\beta$  peptide stuck to everywhere. The peptide adhered to almost every surface, including SPE tubes which are even a little hydrophobic in nature. The hydrophobic nature and susceptibility to aggregation were the main challenges in the analytical chemistry procedures applied to this biomarker.

## 4.2 Magnetic core-shell MIP with encapsulated magnetite

### 4.2.1 Aim of study

In our studies on the design and synthesis of magnetic core-shell materials for peptide imprinting, we hypothesize that

- MIPs have binding sites that have high affinity and selectivity for a given target molecule;
- Two-step PP can be a useful synthesis method for the preparation of high-quality magnetic core-shell microspheres. Near monodisperse and surfactant-free magnetic core-shell spherical polymer particles in the micron size range can be synthesised by the two-step PP method;
- Preformed poly(DVB-80) and/or poly(DVB-55) with incorporated magnetic particles can be used as the magnetic seed particles for the synthesis of magnetic core-shell particles;
- $\beta$ -Amyloid is considered as a biomarker which is highly sensitive and specific for Alzheimer's Disease.

Based on this, the aims of the work presented in this section were as follows:

- Identification of the PP conditions that can be used for the synthesis of magnetic core and magnetic core-shell microspheres;
- Synthesis of magnetic core-shell MIP for  $\beta$ -Amyloid target;
- Characterisation of the materials produced, including demonstration of magnetic properties;
- Delivery of the next generation of magnetic materials to the PEPMIP partners for evaluation of molecular recognition.

## 4.2.2 Experimental section

### 4.2.2.1 Materials

The peptide template Ac-GGVVIA-OH (>95% purity), was purchased from LifeTein, *N*-(2-aminoethyl)methacrylamide hydrochloride (EAMA.HCl, purity  $\geq 98\%$ ) was purchased from Polysciences Inc. (Niles, IL, USA), *N*-3,5-*bis*(trifluoromethyl)-phenyl-*N'*-4-vinylphenylurea (NTPVU, purity >95%) is not commercially available and was kindly donated by Dortmund University, 2,2'-azobisisobutyronitrile (AIBN, purity 98%) was purchased from BDH Lab. Supplies (UAE). Divinylbenzene-80 (DVB-80, 80% DVB isomers and 20% ethylvinylbenzene isomers), divinylbenzene-55 (DVB-55, 55% DVB isomers and 45% ethylvinylbenzene isomers), 1,2,2,6,6-pentamethylpiperidine (PMP, purity >99%), tetrabutylammonium hydroxide solution (TBA.HO, 1.0 M in methanol, 25%  $\leq$  purity <50%) and hydrochloric acid (37 wt. % in H<sub>2</sub>O) were all purchased from Sigma-Aldrich (St. Louis, MI, USA). FluidMAG-OS with magnetic component concentration 25 mg/mL was purchased from 2B Scientific (UK). All other chemicals used (acetonitrile [ACN], methanol and dimethyl sulfoxide [DMSO, purity  $\geq 99.9\%$ ], toluene) were of analytical grade and all purchased from Sigma-Aldrich (St. Louis, MI, USA). DVB-80 and DVB-55 were purified by filtration through a short plug of neutral aluminium oxide prior to use. AIBN was recrystallized from acetone at low

temperature. The magnetic particles, fluidMAG-OS were washed with ACN and suspended in ACN before use.

#### *4.2.2.2 Synthesis and characterisation of magnetic core and core-shell polymers*

Magnetic core-shell particles were synthesised by a two-step PP as described elsewhere by Stöver.<sup>14</sup> Magnetic cores and the magnetic core-shell particles were prepared in two separate and successive reactions. The first step included the synthesis of crosslinked magnetic core particles by a typical PP. The incorporation of magnetic particles into core particles was performed as described in the previous subsection. The preformed magnetic core particles were used as the seed microspheres for the synthesis of magnetic core-shell particles, and the magnetic core-shell polymer particles were prepared in the second PP.

##### *4.2.2.2.1 Synthesis of magnetic core particles*

The first step in our synthetic design for the synthesis of the next generation polymer magnetic core-shell MIPs, included identification of the conditions for the synthesis of the magnetic core particles which could be used further as the seed particles for the synthesis of magnetic core-shell particles. A series of magnetic polymers was prepared with the feed compositions shown in Table 4.5. The concentration of magnetic particles were 12 or 25 mg per one gram of monomer. DVB-80 or DVB-55 were evaluated as the crosslinker. Polymers were synthesised on a 1 g or a 2 g monomer scale. The monomer concentrations were 2% and 4% w/v (respect to the solvent). The initiator concentration was 2 mol%, relative to the number of moles of polymerisable double bonds. Polymers were synthesised in borosilicate glass Kimax tubes. 72 h was the precipitation polymerisation time.



Table 4.5 List of PP conditions tested for the synthesis of magnetic core particles.

Polymer code	Crosslinker (mmol)	Mag. particles (mg/g)	Monomer conc. (% w/v)	Initiator conc. (mol%)	Solvent (v/v)	Incubation time (h)	Scale (g)
MAS60	DVB-55 (7.63)	25	4	2	ACN	72	1
MAS61	DVB-80 (7.66)	25	4	2	ACN	72	1
MAS67	DVB-55 (7.63)	25	2	2	ACN/Tol (60/40)	72	1
MAS71	DVB-55 (7.63)	12.5	4	2	ACN	72	1

The synthesis of the magnetic core particles with polymer code MAS61 can serve as an example of the synthetic procedure used for the synthesis of magnetic core particles. DVB-80 (1.011 g, 1.094 mL, 7.69 mmol) was dissolved in ACN (15 mL). Then, AIBN (45 mg, 0.4 mmol) and ACN (10 mL) with washed magnetic particles were added into the polymerisation mixture. The PP mixture was then ultrasonicated using a Fisherbrand FB11024 ultrasonic bath for 10 minutes at ambient temperature and then sparged with oxygen-free nitrogen gas for 10 minutes at ice-bath temperature (to remove dissolved molecular oxygen). The reaction vessel was sealed under nitrogen. Thereafter, the reaction vessel was transferred to a Stuart Scientific S160 incubator equipped with a Stovall low-profile roller. The incubator temperature was ramped from ambient to 60 °C over a period of around two hours and then maintained at 60 °C for a further 70 hours to yield a milk suspension of polymer microspheres.

The magnetic particles were prepared before use in the PP procedure. The magnetic particles were washed and suspended in ACN. The washing procedure included the following steps: fluidMAG-OS (1 mL or 0.5 mL, depending on the concentration of magnetic particles on one gram monomer scale) was transferred into a Petri dish and then ACN (10 mL) added. The magnetic particles were washed with ACN through the pipetting (to remove water residues). The separation of ACN from the magnetic

particles was achieved through the pipetting and simultaneous application of a magnetic field. A permanent magnet was held against the base of Petri dish while the supernatant was removed. A small volume of ACN was always left covering the magnetic particles in the Petri dish. The whole washing procedure of the magnetic particles was repeated four times more until the supernatant became transparent. The magnetic particles were suspended in ACN (10 mL) and then added into the PP solution.

A few drops were collected from the reaction product, and applied onto a microscope slide and examined by an Olympus Vanox optical microscope. Polymer microspheres were controlled in terms of size, dispersity and their aggregation (if any) by the optical microscopy analysis.

Finally, the polymer microspheres were isolated from the reaction medium by vacuum filtration using a Vacuumbrand Vacuum System (2.0 mbar) on a 0.2  $\mu\text{m}$  nylon membrane filter, washed sequentially with ACN (50 mL) and MeOH (50 mL). The isolated product was transferred into a pre-weighed vial and dried overnight in a Townson & Mercer vacuum oven (60 mbar) at 70 °C. The yield of the synthesised material was checked gravimetrically. The yield of MAS61 was 87%.

Magnetic separation was performed to isolate the magnetic polymer particles from non-magnetic particulates. Firstly, dried product was transferred into a clean beaker and washed with ACN (~50 mL). The product dispersed in ACN was mixed with a glass rod. Thereafter, a permanent magnet was held against the base of the beaker, and the beaker with dispersed product was left for 15 s. At this stage, the supernatant was collected. The whole procedure was repeated four times until the supernatant became transparent. The magnetic particles were isolated from the rest of the ACN by vacuum filtration using a Vacuumbrand Vacuum System (2.0 mbar) on a 0.2  $\mu\text{m}$  nylon membrane filter. The isolated product was transferred again into pre-weighed vial and dried overnight in a Townson & Mercer vacuum oven (60 mbar) at 70 °C. The yield of the synthesised material was again checked gravimetrically. The yield of MAS61 after magnetic separation was 6%.

Polymer microspheres were imaged by scanning electron microscopy (SEM) using a Cambridge Instruments Stereoscan 90. Polymer microspheres were evaluated in terms of size, dispersity and their aggregation (if any). Image analysis of SEM micrographs was done by Image J, as described in Chapter 2 (2.1.2.2). Structural determination of the chemical compositions of the synthesised polymers was evaluated by using an Agilent 5500a FT-IR Spectrophotometer. Additionally, the encapsulation of the magnetic nanoparticles into core particles was evaluated *via* the application of a magnetic field in the vicinity of the nanoparticles. A small amount of product was transferred into a Petri dish and a permanent magnet was applied to the bottom of the Petri dish.

#### *4.2.2.2.2 Reproducibility of magnetic core particles*

The conditions used for the synthesis of MAS61, magnetic core particles prepared with a 4% w/v concentration of DVB-80 (with respect to the solvent) and a 2 mol% concentration of AIBN (with respect to the total number of polymerisable double bonds), were reproduced. Polymer was produced on a 2 g monomer scale. Polymers were synthesised in borosilicate glass Kimax tubes. 72 hours was the precipitation polymerisation time.

Polymers were characterised by the same methods as the magnetic core particles presented in the previous subsection (4.2.2.2.1).

#### *4.2.2.2.3 Synthesis of magnetic core-shell MIP and corresponding NIP*

Magnetic core-shell MIP and its corresponding NIP were synthesised by a typical two-step PP as described elsewhere.<sup>14</sup> The magnetic core and magnetic core-shell particles were prepared in two separate and successive reactions. The first step included the synthesis of crosslinked magnetic core particles by typical PP. The preformed magnetic core particles were then used as the seed microspheres for the

synthesis of magnetic core-shell particles, and the magnetic core-shell polymer particles were prepared in the second PP.

Magnetic core-shell MIP and its corresponding non-imprinted counterpart were prepared. The feed composition is shown in Table 4.6. MAS125 and MAS126 are a pair of a magnetic core-shell MIP and NIP for the Ac-GGVVIA-OH target. The magnetic particles with the code MAS89, the synthesis of which was reported in the previous subsection, were used as the core particles. 76 mg of MAS89 was used as the magnetic core particles for each prepared polymer, and the magnetic core-shell polymers were produced on a 0.1 g scale. A 2:1 w/w ratio of magnetic core particles to monomer scale was used for the syntheses. The shells for the MIP and the NIP for Ac-GGVVIA-OH target included 99.4% of DVB-80, 0.5% of EAMA.HCl and 0.1% of NTPVU, which corresponds to a mole ratio of NTPVU: EAMA.HCl: DVB-80 of 0.001:0.02:5. The mole ratio of template: NTPVU: EAMA.HCl for the synthesis of the shell in MAS125 was kept at 1:1:10. This mole ratio was the same as used in the previous syntheses presented in Chapter 3, for the syntheses of core-shell polymers. The conditions identified in Chapter 3 (3.1.2.5 and 3.1.2.6) for the syntheses of particle cores and particle shells were applied. The monomer and initiator concentration were 4% w/v (with respect to the solvent) and 2 mol% (with respect to the total number of polymerisable double bonds), respectively. Addition of template and functional monomer(s) was timed 1.5 h after the polymerisation started. 24 h was the polymerisation time.

Table 4.6 Feed conditions for  $\beta$ -Amyloid imprinted core-shell magnetic polymer and the corresponding NIP. The scale relates to the mass of the core-shell polymers.

Polymer code	Core	Shell description (2:1 Core: Shell)	Template	Monomer conc. (%w/v)	Initiator conc. (mol%)	Scale (g)
MAS125	MAS89	99.4% DVB-80 0.5% EAMA.HCl 0.1% NTPVU	Ac-GGVVIA-OH	4	2	0.1
MAS126	MAS89	99.4% DVB-80 0.5% EAMA.HCl 0.1% NTPVU	-	4	2	0.1

The synthesis of the MIP with polymer code MAS125 can serve as an example of the PP procedure for the synthesis of magnetic core-shell polymers by delayed addition of template and functional monomer(s).

Firstly, MAS89 (76 mg) magnetic core particles were placed into a borosilicate Kimax culture tube. Then, ACN (2.81 mL) was added into the polymerisation mixture, followed by the addition of DVB-80 (37 mg, 40  $\mu$ L, 0.28 mmol) and AIBN (1.65 mg, 14  $\mu$ mol). The mixture was then ultrasonicated for 10 minutes at ambient temperature and sparged with oxygen-free nitrogen gas for 10 minutes at ice-bath temperature, to remove dissolved molecular oxygen. Thereafter, the reaction vessel was sealed under nitrogen and transferred to a Stuart Scientific S160 incubator equipped with a Stovall low-profile roller. The incubator temperature was ramped from ambient to 60 °C over a period of one and a half hour (1h 30 min). In the meantime, a solution of template and functional monomers was prepared. The template, Ac-GGVVIA-OH (62  $\mu$ g, 1  $\mu$ mol) was added into an Eppendorf tube as a solution in DMSO. (For the synthesis of the corresponding NIP, the template was omitted from the synthetic protocol). In order to measure such a small amount of the template, template (5000  $\mu$ g, 80.6  $\mu$ mol) was dissolved in 0.5 mL of DMSO and 6.2  $\mu$ L of this solution was transferred into an Eppendorf tube. Thereafter, TBA.OH (0.1  $\mu$ mol) was added, for this TBA.OH in methanol (2  $\mu$ L) was dissolved in 40  $\mu$ L of DMSO and 2.3  $\mu$ L of this solution was added into the Eppendorf tube. In order to add

the functional monomer, NTPVU (39  $\mu\text{g}$ , 0.11  $\mu\text{mol}$ ) into the mixture, NTPVU (5000  $\mu\text{g}$ , 14  $\mu\text{mol}$ ) was dissolved in 0.5 ml of DMSO and 3.9  $\mu\text{L}$  of this solution was transferred into the Eppendorf tube. Thereafter, the second functional monomer, EAMA.HCl (184  $\mu\text{g}$ , 1  $\mu\text{mol}$ ) was added, for this 40 mg of EAMA.HCl was dissolved in 0.5 mL of DMSO, and 2.3  $\mu\text{L}$  of this solution was transferred into the Eppendorf tube. The solution with all the components in the Eppendorf tube was mixed through repeated pipetting to ensure that all components added were dissolved. When the temperature in the incubator reached 60 °C after 1.5, the solution of template and functional monomer was transferred into the borosilicate Kimax culture tube. The borosilicate Kimax culture tube was shaken gently and placed back into the incubator. The temperature was maintained at 60 °C for a further 24 hours to yield a milky suspension of polymer microspheres.

A few drops were collected from the polymerisation mixture, and then applied onto a microscope slide and examined by an Olympus Vanox optical microscope. Polymer microspheres were controlled in terms of size, dispersity and their aggregation (if any) by the optical microscopy analysis.

Finally, the polymer microspheres were isolated from the reaction medium by filtration on a 0.45  $\mu\text{m}$  nylon membrane filter using a Vacuumbrand Vacuum System (2.0 mbar), washed sequentially with ACN (10 mL), MeOH/0.1 M aq. HCl (90/10, v/v, 10 mL) and MeOH (10 mL). The isolated product was transferred into a pre-weighed vial and dried overnight in a Townson & Mercer vacuum oven (60 mbar) at 70 °C. The yields of the synthesised material was checked gravimetrically. The yield of MAS125 was 11%.

Magnetic separation was performed to isolate the magnetic polymer particles from non-magnetic particulates. Firstly, dried product was transferred into a clean beaker and washed with ACN (~5 mL). The product dispersed in ACN was mixed with a glass rod. Thereafter, a permanent magnet was held against the base of the beaker, and the beaker with dispersed product was left for 15 s. At this stage, the supernatant was collected. The whole procedure was repeated four times until the supernatant

became transparent. The magnetic particles were isolated from the rest of the ACN by vacuum filtration using a Vacuumbrand Vacuum System (2.0 mbar) on a 0.2  $\mu\text{m}$  nylon membrane filter. The isolated product was transferred again into a pre-weighed vial and dried overnight in a Townson & Mercer vacuum oven (60 mbar) at 70 °C. The yield of the synthesised material was again checked gravimetrically. The yield of MAS125 after magnetic separation was 0% (it could be due work in small scale).

Polymers were characterised by the same methods as the magnetic core particles presented in the previous subsection (4.2.2.2.1).

### 4.2.3 Results and discussion

#### *4.2.3.1 Synthesis and characterisation of magnetic core particles*

Five (5) different conditions were screened in order to identify the PP conditions which can be used for the synthesis of magnetic core particles which were to be used subsequently for the synthesis of magnetic core-shell MIPs. DVB-80 and DVB-55 were both evaluated as crosslinkers. Two different concentrations of magnetic particles were tested: 25 mg and 12.5 mg per one gram of monomer. The first magnetic particle concentration was the same as used for the synthesis of the first generation of magnetic MIPs. When the concentration of commercially available magnetic particles was reduced to half (12.5 mg per one gram of monomer) the polymer microspheres were prepared in good quality with narrow particle size distribution, and the particles were classified as quasi monodisperse. However, this synthesis resulted in a very low yield of magnetic particles (3%, Table 4.7). When DVB-55 was used as the crosslinker with a concentration of magnetic particles at 25 mg per one gram of monomer, the syntheses resulted in a high yield of polymer particles with encapsulated magnetite. However, these reactions resulted in the production of polydisperse microspheres (MAS60 and MAS67, Table 4.8). The monomer concentration in most PP conditions tested was set at 4% w/v as in the previous study for the synthesis of core-shell polymer, as this concentration resulted in the synthesis

of good quality microspheres (Chapter 3). Before magnetic separation, the yields of the prepared particles were high (~60%, Table 4.7), and were typical for the polymerisation of divinylbenzenes under such precipitation polymerisation conditions. When the magnetic separation was performed and non-magnetic particles were extracted, the fraction of particles with the magnetic properties represented a significantly small amount. The PP conditions used for the synthesis of MAS61 was selected for further synthesis of magnetic core-shell polymers. The particles of MAS61 were highly regular in size and shape; the CV value reached 9.23%, which classified them as quasi monodisperse microspheres (Table 4.8 and Figure 4.4).

Table 4.7 Effect of the PP monomer feed on the yield of the magnetic cores.

Polymer code	Crosslinker (mmol)	Mag. particles (mg/g) <sup>a</sup>	Monomer conc. (% w/v)	Initiator conc. (mol%)	Solvent (v/v)	Yield (%)	
						Before mag. sep.	After mag. sep.
MAS60	DVB-55 (7.63)	25	4	2	ACN	83	32
MAS61	DVB-80 (7.66)	25	4	2	ACN	87	6
MAS67	DVB-55 (7.63)	25	2	2	ACN/Tol (60/40)	55	46
MAS71	DVB-55 (7.63)	12.5	4	2	ACN	19	3

<sup>a</sup> Concentration of magnetic particles in mg per one gram of monomer.



Table 4.8 Microscopic characterisation of polymer microsphere morphology.

Polymer code	Optical microscopy observation			Bead average diameter in $\mu\text{m}$ ( $\pm\text{SD}$ ) <sup>c</sup>
	Dispersity (%CV) <sup>a</sup>	Bead size ( $\mu\text{m}$ )	Aggregation	
MAS60	Polydisperse (76)	1-11	Physical	2.63 (2.00)
MAS61	Quasi monodisperse (9.23)	approx. 1	none	1.05 (0.12)
MAS67	Polydisperse	Beads? <sup>b</sup>	Chemical	Beads? <sup>b</sup>
MAS71	Quasi monodisperse (14.10)	approx. 1	none	1.04 (0.14)

a CV% values come from calculations made using SEM images .

b Beads? indicates uncertainty whether the observed structures were microspheres.

c A population of 100 microspheres from SEM image was measured for the determination of bead av. diameters

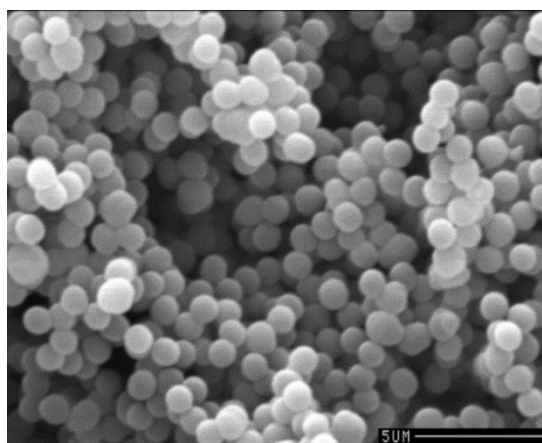


Figure 4.4 SEM of MAS61;  $\times 5440$  magnification (scale =  $5 \mu\text{m}$ ).

#### 4.2.3.2 Synthesis and characterisation of reproduced magnetic core particles

The particles of MAS61 were highly regular in size and shape, and classified as quasi monodisperse spheres (CV = 9.23%). Therefore, this material was selected as the magnetic core for the synthesis of magnetic core-shell polymers. More material of this type was required for further research. However, the next batch of magnetic core particles (MAS89) were produced on a 2 g monomer scale only, as it was not possible to reproduce this material on a bigger scale as the limitation was the fluidMAG-OS magnetic particles, which were expensive to use. The yield of synthesised polymer (MAS89) was high (78%, Table 4.9), but the fraction of particles with magnetic

properties represented only a small amount (10% out of 100%). In fact, 0.2 g of magnetic core particles was available for further research only. Even although the particles were classified as the polydisperse (Table 4.10), the quality of the particles was good as the MAS89 magnetic particles were highly regular in size and shape with relatively narrow particle size distribution. The value of the coefficient of variance (%CV) was 17.01% for MAS89. This value sets MAS89 at the boundary of transition from quasi monodisperse to polydisperse particles. The microscopic characterisation showed that the average diameter of the reproduced magnetic particles was smaller ( $\sim 0.48 \mu\text{m}$ ) than the size of MAS61 ( $\sim 1.05 \mu\text{m}$ ). This difference in the size of particles may be a result of the change in the polymerisation scale from 1 g to 2 g monomer scale.

Table 4.9 Effect of the PP feed on the yield of the magnetic core products.

Polymer code	Crosslinker (mmol)	Mag. particles (mg/g) <sup>a</sup>	Monomer conc. (% w/v)	Initiator conc. (mol%)	Solvent	Yield (%)	
						Before mag. sep.	After mag. sep.
MAS89	DVB-80 (15.32)	25	4	2	ACN	78	10

<sup>a</sup> Concentration of magnetic particles in mg per one gram of monomer.

Table 4.10 Microscopic characterisation of polymer microsphere morphology.

Polymer code	Optical microscopy observation			Bead average diameter in $\mu\text{m}$ ( $\pm\text{SD}$ ) <sup>b</sup>
	Dispersity (%CV) <sup>a</sup>	Bead size ( $\mu\text{m}$ )	Aggregation	
MAS89	Polydisperse (17.01)	approx.1	none	0.48 (008)

<sup>a</sup> CV% values come from calculations made using SEM images .

<sup>b</sup> A population of 100 microspheres from SEM image was measured for the determination of bead av. diameters.

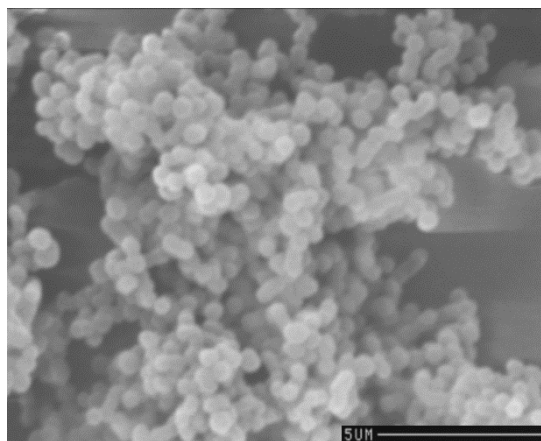


Figure 4.5 SEM of MAS89;  $\times 6840$  magnification (scale = 5  $\mu\text{m}$ ).

#### 4.2.3.3 Synthesis and characterisation of magnetic core-shell MIP and corresponding NIP

The studies presented in this subsection involved the synthesis of the second generation of magnetic materials for the Ac-GGVVIA-OH target: magnetic core-shell polymers. Two-step PP was the synthetic method used. Magnetic core particles with non-magnetic shells were prepared in two separate reactions. Firstly, the magnetic core particles, MAS89, with encapsulated commercially available magnetic particles, fluidMAG-OS, were prepared and then these particles were used as the seed particles for the synthesis of magnetic core-shell particles. Non-magnetic shells were formed around the poly(DVB-80) magnetic particles. The conditions identified in the test studies presented in Chapter 3 (3.1.2.5 and 3.1.2.6), for the synthesis of cores and shells by a two-step PP were applied. A 2:1 w/w ratio of magnetic core particles to monomer was used for the synthesis of the core-shell particles. Such a ratio allowed for the synthesis of core-shell polymer microspheres with a shell thickness of  $\sim 0.1 \mu\text{m}$ . Non-magnetic shells grown on the surface of the magnetic cores were prepared with monomer and initiator concentrations at 4% w/v (with respect to the solvent) and 2 mol% (with respect to the total number of polymerisable double bonds), respectively. 24 h was the polymerisation time used for the synthesis of magnetic core-shell particles.

A MIP, MAS125, and a corresponding NIP, MAS126, were prepared with the same concentrations of template and functional monomer(s) as in the previous syntheses

reported in Chapter 3. A five-fold reduction in the concentrations of template and functional monomers(s) together with addition of template and functional monomer(s) timed 1.5 h after the polymerisations had started were again applied. The yields of the shelled products were low (Table 4.11). In the case of MAS126, the yield was 0%. It could be due to the low scale of operation (0.1 g) and/ or to the loss of material during product work-up rather than to polymerisation failure. A schematic representation of a binding site in a successfully prepared magnetic core-shell MIP for a  $\beta$ -Amyloid target is shown in Figure 4.7 .

Secondary nucleation was not observed for either of the products (SEM of MAS125 shown in Figure 4.7). The particle size distribution analysis revealed magnetic core-shell particles with 0.02  $\mu\text{m}$  and 0.06  $\mu\text{m}$  shell thickness for the MIP and NIP, respectively (PSD of MAS125 shown in Figure 4.7). The black and orange bars represent the fraction of particles which are part of the magnetic cores and shells, respectively. The fraction of magnetic core-shell particles are significantly shifted towards bigger sizes (orange colour). This clearly shows that the magnetic core-shell particles are bigger than their corresponding magnetic cores. Both magnetic core-shell MIP and NIP particles were of significantly small size, 0.50  $\mu\text{m}$  and 0.54  $\mu\text{m}$  for the MIP and NIP, respectively. However, the size of particles is less important during testing if the manipulation of the particles can be done using a magnet.

Table 4.11 Effect of shell compositions on the yield of magnetic core-shell MIP and NIP.

Polymer code	Core	Shell description (2:1 Core: Shell)	Template	Yield (%) (shell) (before and after mag. separation)
MAS125	MAS89	99.4% DVB-80 0.5% EAMA.HCl 0.1% NTPVU	Ac-GGVVIA-OH	11; 0
MAS126	MAS89	99.4% DVB-80 0.5% EAMA.HCl 0.1% NTPVU	-	0; 0

Table 4.12 Microscopic characterisation of magnetic core-shell MIP and NIP.

Polymer code	Optical microscopy observation			Bead average diameter in $\mu\text{m}$ ( $\pm\text{SD}$ ) <sup>b</sup>
	Dispersity (CV%) <sup>a</sup>	Bead size ( $\mu\text{m}$ )	Aggregation	
MAS125	Polydisperse (17.97)	approx. 1	none	0.50 (0.08)
MAS126	Polydisperse (18.67)	approx. 1	none	0.54 (0.1)

a CV% values come from calculations made using SEM images .

b A population of 100 microspheres from SEM image was measured for the determination of bead av. Diameters.

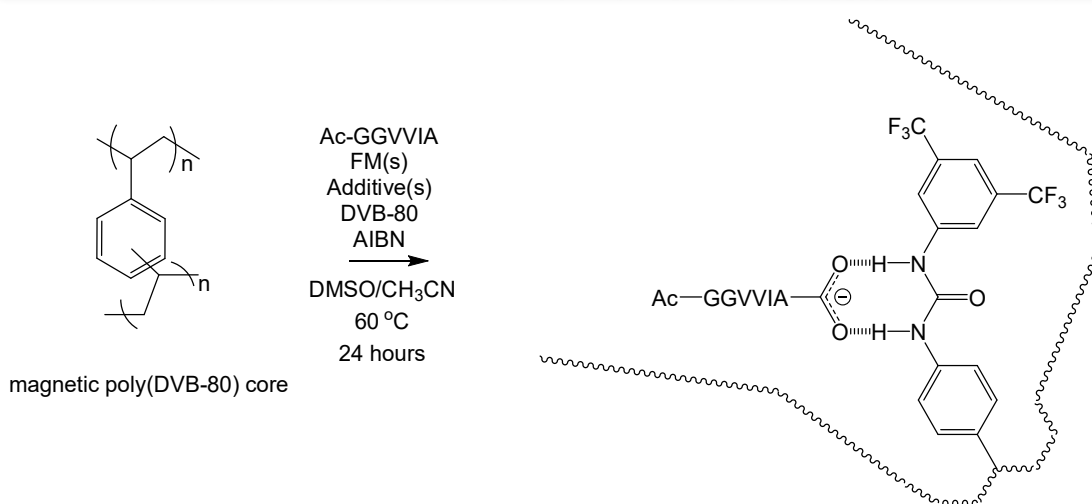


Figure 4.6 Schematic representation of the synthesis of molecularly imprinted poly(NTPVU-co-EAMA.HCl-co-DVB-80) magnetic core-shell microspheres by the non-covalent molecular imprinting of Ac-GGVVIA, a structural analogue of the  $\beta$ -Amyloid peptide. The carboxylic acid group in the C-terminus of Ac-GGVVIA is drawn explicitly for emphasis, since this functional group is involved in the self-assembly of the Ac-GGVVIA with functional monomers. The complexed synthetic receptor (right hand side) depicts a molecularly imprinted binding site formed upon the free radical copolymerisation of a 1:1 molecular complex of Ac-GGVVIA and *N*-3,5-bis(trifluoromethyl)-phenyl-*N'*-4-vinylphenylurea with *N*-(2-aminoethyl)methacrylamide hydrochloride and crosslinker (DVB-80).

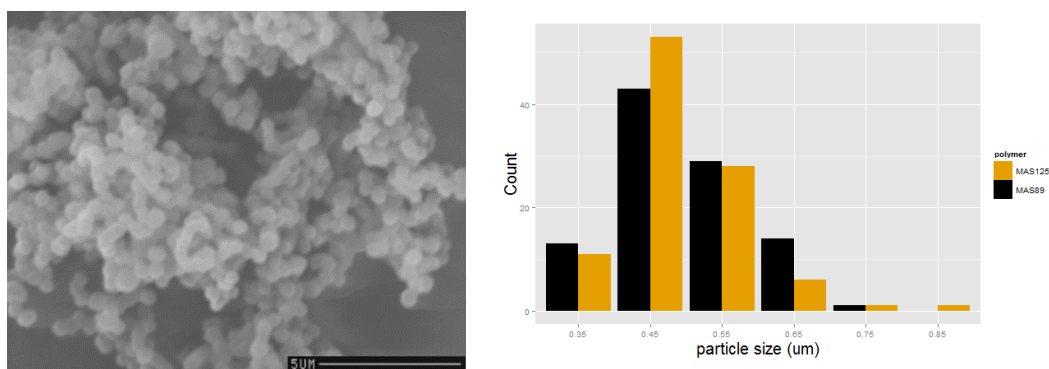


Figure 4.7 SEM of MAS125, and comparison of particle size distributions of MAS125, magnetic core-shell ( $n = 100$ ;  $d = 0.50 \mu\text{m} \pm 0.08$ ,  $CV = 17.97\%$ ) and MAS89, magnetic core ( $n = 100$ ;  $d = 0.48 \mu\text{m} \pm 0.08$ ,  $CV = 17.01\%$ );  $\times 6760$  magnification for SEM image (scale =  $5 \mu\text{m}$ ).

The second generation of magnetic polymers: core-shell MIP for a  $\beta$ -Amyloid target and the corresponding NIP, were sent to a PEPMIP partner (Essen University) for off-line Molecularly Imprinted Solid-Phase. At the time of writing of this Thesis, neither

the magnetic MIP nor the NIP showed any affinity for  $\beta$ -Amyloid isoforms: A $\beta$ 42 and A $\beta$ 40. However, this conclusion was drawn based upon on single experiment (conducted by Dr Roberto Boi, from Essen University), thus further conditions need to be evaluated to establish conditions under which affinity and selectivity can be revealed.

### 4.3 Magnetic core-shell MIPs with incorporated magnetite

#### 4.3.1 Aim of study

In our design and synthesis studies of magnetic core-shell polymers for the ProGRP target, we hypothesize that

- MIPs as the synthetic materials have binding sites that have high affinity and selectivity for a given target molecule;
- PP is a useful synthesis method for the preparation of high-quality, MIP microspheres. Near monodisperse and surfactant-free spherical polymer particles in the micron size range can be synthesised by the PP method;
- The co-precipitation of FeCl<sub>3</sub> and FeCl<sub>2</sub> can take place on the surfaces of the preformed polymers and inside the pores of the polymers in the vicinity of COOH functional groups and it will result in the permanent incorporation of magnetic particles into the preformed polymers;
- ProGRP is considered as a biomarker which is highly sensitive and specific for Small Cell Lung Cancer.

Based on this, the aims of the work presented in this section were as follows:

- Design a method for the incorporation of magnetic particles inside preformed polymers;
- Synthesis of magnetic core-shell MIPs for ProGRP target;
- Characterisation of materials produced, including demonstration of magnetic properties;

- Delivery of the next generation materials to PEPMIP partners for evaluation of molecular recognition.

### 4.3.2 Experimental section

#### 4.3.2.1 Materials

The peptide template Z-NLLGLIEA{Nle} (96.58% purity) was purchased from LifeTein. *N*-(2-Aminoethyl)methacrylamide hydrochloride (EAMA.HCl, purity >98%) was purchased from Polysciences, Inc. *N*-3,5-bis(Trifluoromethyl)-phenyl-*N'*-4-vinylphenylurea (NTPVU, purity >95%) is not commercially available and was kindly donated by Dortmund University. 2-2'-Azobisisobutyronitrile (AIBN, purity 98%) was purchased from BDH Lab. Supplies (UAE). Divinylbenzene-80 (DVB-80, 80% DVB isomers and 20% ethyl vinylbenzene isomers), methacrylic acid (MAA, purity  $\geq 98.0\%$ ), 1,2,2,6,6-pentamethylpiperidine (PMP, purity  $\geq 99\%$ ), tetrabutylammonium hydroxide solution (TBA.HO, 1.0 M in methanol,  $25\% \leq$  purity  $< 50\%$ ), hydrochloric acid (37 wt. % in H<sub>2</sub>O), Tween 20, sodium hydroxide (NaOH, purity  $\geq 97$ ), iron (III) chloride (FeCl<sub>3</sub>, purity 97%), iron (II) chloride (FeCl<sub>2</sub>, purity 98%) and 28%-30% ammonium hydroxide solution (NH<sub>4</sub>OH) were all purchased from Sigma-Aldrich. DVB-80 was purified by filtration through a short plug of neutral aluminium oxide prior to use. AIBN was recrystallized from acetone at low temperature. All other chemicals used (acetonitrile [ACN], methanol [MeOH], ethanol [EtOH] (purity  $\geq 99.5$ ) and dimethyl sulfoxide (DMSO, purity  $\geq 99.9\%$ ) were of analytical grade.

#### 4.3.2.2 Magnetisation procedure

The steps involved in the magnetisation of polymers were as followed: firstly, preformed polymer particles (1 – 10 g) were dispersed in 0.5 M NaOH solution (40 mL; 0.8 g of solid NaOH and 40 mL of distilled water) in a 50 mL polystyrene centrifuge tube followed by 10 min incubation in a Fisherbrand FB11024 ultrasonication bath. If the polymer particles were not sufficiently dispersed, the incubation process in a Fisherbrand FB11024 ultrasonication bath was extended for up to 30 min. In the next step, the polymer particles were isolated from the basic



solution by filtration using a Vacuumbrand Vacuum System (2.0 mbar) on a 0.45  $\mu\text{m}$  nylon membrane filter. Following the isolation step, the material was washed with 0.05% Tween 20 (100 mL; 0.05:99.95 Tween 20: distilled water (w/w)). Further steps included dispersion of the isolated material in a solution of  $\text{FeCl}_3$  and  $\text{FeCl}_2$  (40 mL) consisting of a 1:75 ratio of  $\text{Fe}^{3+}:\text{Fe}^{2+}$  ions followed by a 30 min incubation in a Fisherbrand FB11024 ultrasonication bath. To improve the chelation process, the material could also be left at this stage for overnight incubation. In the next step, the material was centrifuged in an Eppendorf Centrifuge 5804 for 10 min at 12000 rpm. After centrifugation, the upper portion of solution was removed by decanting and distilled water (20 mL) was added to the mixture. The material was again centrifuged in an Eppendorf Centrifuge 5804 for 10 min at 12000 rpm. The upper portion of solution was decanted again. The next step involved placing a sample with the precipitate in warm surroundings, such as an oil bath heated to 60 °C or in a Stuart Scientific S160 incubator heated to 60 °C (to improve the chelation process). The centrifuge tube with the precipitate was incubated until the polymer particles were dry. After the polymer particles became dry, 28%-30% aqueous  $\text{NH}_4\text{OH}$  (20 mL) was added. The basic reaction mixture was incubated either in an oil bath or incubator for 10 min. Next, the magnetic polymer particles were isolated from the basic solution by filtration using a Vacuumbrand Vacuum System (2.0 mbar) on a 0.45  $\mu\text{m}$  nylon membrane filter. Following the isolation step, the material was washed with 0.05% Tween 20 (100 mL, 0.05:99.95 Tween 20: distilled water (w/w)). The isolated material was dried overnight in a Townson & Mercer vacuum oven (60 mbar) at 70 °C, prior to magnetic separation. The whole procedure was repeated two or three times until the polymer particles changed to a dark brown colour. A highly schematic representation of this procedure is shown in Figure 4.8.

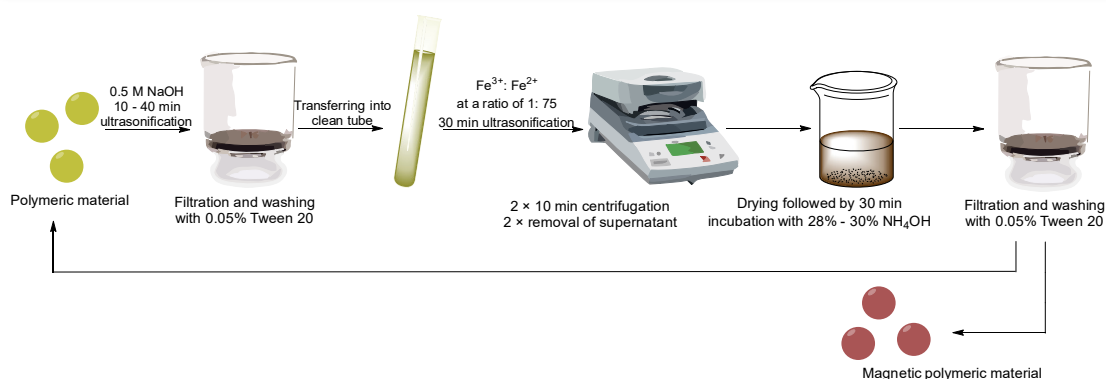


Figure 4.8 Schematic workflow representing the magnetisation procedure. Images were taken from ref. <sup>15</sup> for the purpose of drawing this scheme.

The steps followed for the preparation of the iron chloride solution with the desired ferrous ratio, 1:75 ratio of  $\text{Fe}^{3+}:\text{Fe}^{2+}$ , were as follows: two separate solutions were prepared in 50 mL polystyrene centrifuge tubes. The first solution contained 0.2 M  $\text{FeCl}_3$  in 1:1 EtOH/ distilled water solution (40 mL; 20 mL of EtOH, 20 mL of distilled water and 1.33 g of  $\text{FeCl}_3$ ) and the second one included 1 M  $\text{FeCl}_2$  in 1:1 EtOH/ distilled water solution (40 mL; 20 mL of ethanol, 20 mL of distilled water and 5.17 g of  $\text{FeCl}_2$ ). The iron chloride solutions were then purged with nitrogen for 10 min (to remove oxygen). To prepare the iron chloride solution with the desired iron ions ratio, 1:75 ratio of  $\text{Fe}^{3+}:\text{Fe}^{2+}$  ions, 0.2 M  $\text{FeCl}_3$  (2.5 mL) and 1 M  $\text{FeCl}_2$  (37.5 mL) were transferred into clean a 50 ml polystyrene centrifuge tube. The iron chloride solution was mixed well before the addition of polymer material.

Prior to magnetisation procedure, a stock solution of 0.5 M sodium hydroxide (100 mL; 2 g of solid NaOH in 100 mL deionised water) and a stock solution of 0.05% Tween 20 (1 L; 0.05:99.95 Tween 20: distilled water (w/w)) were prepared.

#### 4.3.2.3 Synthesis of magnetic core particles

Magnetic core particles were prepared by magnetisation of poly(MAA-co-DVB-80). Therefore, the first step was synthesis of the non-magnetic polymer MAS135, which was subsequently subjected to the magnetisation procedure. MAS135 was prepared by typical PP as described elsewhere.<sup>16</sup> The feed composition of MAS135 is shown in Table 4.13. The polymer was synthesised on a 10 g monomer scale, with a monomer

and initiator concentration of 3.28% w/v (with respect to the solvent) and 3.35 mol% (with respect to the total number of polymerisable double bonds), respectively.

Table 4.13 Feed composition of non-magnetic core particles.

Polymer code	Components (mmol)	Monomer conc. (% w/v)	Initiator conc. (mol%)	Solvent (v/v)	Incubation time (h)	Scale (g)
MAS135	DVB-80 (67.16) MAA (14.29)	3.28	3.35	ACN/toluene (75:25)	72	10

The steps for the synthesis of MAS135 were: MAA (1.21 mL, 14.29 mmol) was dissolved in a 75:25 (v/v) mixture of ACN (228 mL) and toluene (76 mL), followed by the addition of purified DVB-80 (9.59 mL, 67.16 mmol) and AIBN (0.74 g, 4.53 mmol). The monomer solution was then ultrasonicated using a Fisherbrand FB11024 ultrasonic bath for 10 minutes at ambient temperature and then sparged with oxygen-free nitrogen gas for 10 minutes at ice-bath temperature (to remove dissolved molecular oxygen). Thereafter, the reaction vessel was transferred to a Stuart Scientific S160 incubator equipped with a Stovall low-profile roller. The incubator temperature was ramped from ambient to 60 °C over a period of around two hours and then maintained at 60 °C for a further 70 hours to yield a milky suspension of polymer microspheres.

A few drops of the reaction product were collected from the polymerisation solution, and then applied onto a microscope slide and examined by an Olympus Vanox optical microscope. Polymer microspheres were controlled in terms of size, dispersity and their aggregation (if any) by the optical microscopy analysis.

Finally, the polymer microspheres were isolated from the reaction media by vacuum filtration using a Vacuumbrand Vacuum System (2.0 mbar) on a 0.45 µm nylon membrane filter and washed sequentially with ACN (100 mL), toluene (100 mL) and MeOH (100 mL). The isolated product was transferred into a pre-weighed vial and dried overnight in a Townson & Mercer vacuum oven (60 mbar) at 70 °C. The yield of synthesised material was checked gravimetrically. The yield of MAS135 was 68%.

The entire mass of MAS135 prepared was subjected to the magnetisation procedure, as described in the previous section. The procedure was applied twice in order to convert non-magnetic MAS135 into magnetic MAS136. The magnetic core particles, MAS136, obtained after the isolation from magnetisation solution, were transferred into a pre-weighed vial and dried overnight in Townson & Mercer vacuum oven (60 mbar) at 70 °C. The yield of synthesised material was checked gravimetrically. The yield of MAS136 was 80%.

The entire mass of MAS136 was also subjected to magnetic separation. Magnetic separation was performed to isolate the magnetic polymer particles from non-magnetic particulates. Firstly, dried product was transferred into a clean beaker and washed with EtOH (~50 mL). The product dispersed in EtOH was mixed with a glass rod. Thereafter, a permanent magnet was held against the base of the beaker, and the beaker with dispersed product was left for 15 s. At this stage, the supernatant was collected. The whole procedure was repeated at least four times until the supernatant became clear. The magnetic particles were separated from the EtOH by vacuum filtration using a Vacuumbrand Vacuum System (2.0 mbar) on a 0.45 µm nylon membrane filter. The isolated product was transferred again into a pre-weighed vial and dried overnight in a Townson & Mercer vacuum oven (60 mbar) at 70 °C. The yield of the isolated magnetic particles was again checked gravimetrically. The yield of MAS136 after magnetic separation was 51%.

Polymer microspheres were evaluated in terms of size, dispersity and their aggregation (if any). Polymer microspheres were imaged by scanning electron microscopy (SEM) using a Cambridge Instruments Stereoscan 90. The steps involved in microscopic analysis and image analysis carried out by Image J, were introduced and discussed in detail in the 1.5.2 subsection and the 2.1.2.2 experimental section.

#### *4.3.2.4 Synthesis of magnetic core-shell MIPs and their corresponding NIPs*

The magnetic core-shell MIPs and their corresponding NIPs were synthesised by a two-step PP with delayed addition of template and functional monomer(s). The

two-step PP method for the synthesis of core-shell polymers has been presented and discussed in detail in Chapter 3 (3.2).

Two magnetic core-shell MIPs and their corresponding non-imprinted counterparts were prepared. The feed compositions of the next generation of magnetic materials is shown in Table 4.14. MAS137 and MAS138, and MAS139 and MAS140, are pairs of MIPs and NIPs for the Z-NLLGLIEA{Nle} target. The magnetic core particles with the code MAS136, the synthesis of which was reported in the previous subsection, were used as the cores for the synthesis of magnetic core-shell microspheres. 1 g of MAS136 was used as the core particles for each polymer prepared, and the magnetic core-shell polymers were produced on a 1.5 g scale. A 2:1 w/w ratio of core particles to monomer was used for the synthesis of each polymer prepared. The shells for the first prepared magnetic core-shell MIP and NIP for the Z-NLLGLIEA{Nle} target included 99.4% of DVB-80, 0.5% of EAMA.HCl and 0.1% of NTPVU which corresponds to a mole ratio of NTPVU: EAMA.HCl: DVB-80 of 0.001:0.02:5. The mole ratio of template: NTPVU: EAMA.HCl for the synthesis of the shell in MAS102 was set at 1:1:10. These molar ratios were the same as in the previous syntheses presented in Chapter 3, for the syntheses of core-shell polymers. The shells for the second prepared magnetic core-shell MIP and NIP for the Z-NLLGLIEA{Nle} target included 99.4% of DVB-80 and 0.5% of EAMA.HCl, which corresponds to a mole ratio of EAMA.HCl: DVB-80 of 0.02: 5. The mole ratio of template: EAMA.HCl for the synthesis of the shell in MAS139 was set at 1:10. These molar ratios were the same as in the previous syntheses presented in Chapter 3, for the syntheses of core-shell polymers. The conditions reported in Chapter 3 for the synthesis of particle cores and shells were applied. The monomer and initiator concentration were 4% w/v (with respect to the solvent) and 2 mol% (with respect to the total number of polymerisable double bonds), respectively. Addition of template and functional monomer(s) was timed 1.5 h after the polymerisation started. 24 h was the polymerisation time.

Table 4.14 Feed composition of core-shell magnetic MIPs and their corresponding NIPs.

Polymer code	Shell description (2:1 core: shell)	Template	Monomer conc. (% w/v)	Initiator conc. (mol%)
MAS137	99.4% DVB-80, 0.5% EAMA.HCl, 0.1% NTPVU	Z-NLLGLIEA{Nle}	4	2
MAS138	99.4% DVB-80, 0.5% EAMA.HCl, 0.1% NTPVU	-	4	2
MAS139	99.4% DVB-80, 0.5% EAMA.HCl	Z-NLLGLIEA{Nle}	4	2
MAS140	99.4% DVB-80, 0.5% EAMA.HCl	-	4	2

### 4.3.3 Results and discussion

The procedure for the synthesis of magnetic microspheres with encapsulated magnetite was developed as reported in previous subsections. Although the method allowed for the synthesis of magnetic microspheres in good quality with narrow particle size distribution, these polymers were prepared in low yield, and the scale-up success of the process was limited. The method required the use of commercially available magnetic particles fluidMAG-Os, which are expensive to use. Therefore, there was a need for the development of a new protocol for the synthesis of next generation of magnetic particles.

A new procedure used for polymer magnetisation was developed through modification of a protocol developed by a collaborator, Dr Taifur Rahman, from Queen's University Belfast. The magnetisation procedure starts with neutralisation of the carboxylic acid groups present in the polymer material using aqueous  $\text{NH}_4\text{OH}$  solution. The neutralised carboxylic acid groups are accessible to ferrous and ferric ions. The ratio of  $\text{Fe}^{3+}:\text{Fe}^{2+}$  ions originally proposed by Dr Taifur Rahman did not allow for the transition of polymer materials into magnetic variants (attempts shown in Grant McCance's Bachelor thesis).<sup>17</sup> Therefore, it was required to revise the ratio of  $\text{Fe}^{3+}:\text{Fe}^{2+}$  and a new ratio used was 1:75. This ratio was the same as in the synthesis of magnetic microgels prepared *via* stop-flow lithography reported by Hatton and

others.<sup>18</sup> The co-precipitation of  $\text{FeCl}_3$  and  $\text{FeCl}_2$  under basic conditions results in the formation of either magnetite,  $\text{Fe}_3\text{O}_4$  or maghemite,  $\gamma\text{-Fe}_2\text{O}_3$ . Magnetite reacts more strongly to the carboxylic acid groups present in the polymers rather than maghemite.<sup>18,19</sup> Also, the  $\text{Fe}^{3+}$  ions have stronger affinity to carboxylate groups than the ions of  $\text{Fe}^{2+}$ .<sup>18</sup> Therefore, the desired product of the coprecipitation of  $\text{FeCl}_3$  and  $\text{FeCl}_2$  was magnetite, and the reaction was required to be carried out under anaerobic conditions. In the magnetisation process, firstly the ions of  $\text{Fe}^{3+}$  diffuse to the carboxylate groups and then are chelated by them, followed by the co-precipitation of  $\text{Fe}^{3+}:\text{Fe}^{2+}$  and the formation of magnetite within and on the surfaces of the microspheres. During the test studies (results not shown), it was observed that insufficient removal of oxygen led to synthesis of maghemite. When the solution in which the polymer particles were incubated changed colour to red, it indicated the formation of maghemite and an unsuccessful magnetisation procedure and, as the consequence the polymer product did not show magnetic properties. When the solution in which the polymer particles were incubated change a color into dark brown, it indicated on successful magnetisation. The formation of the magnetite phase is affected by the temperature. Higher temperature allows for the formation of a greater amount of the magnetite phase.<sup>20</sup> Therefore, the iron chloride solution together with polymer sample was incubated at 60 °C.

#### *4.3.3.1 Synthesis and characterisation of magnetic core particles*

Polymer core particles with carboxylic acid groups were required for the successful growth of magnetic particles. Therefore, the first step in the synthetic design was synthesis of polymers that possess carboxylic acid groups. The copolymerisation of DVB-80 and MAA results in desired products. The PP conditions for the synthesis of MAS135 were the same as described elsewhere.<sup>20</sup> 3.28% w/v (with respect to the solvent) and 3.35 mol% (with respect to the total number of polymerisable double bonds) concentrations of monomer and initiator together with a solvent mixture of acetonitrile and toluene (75:25 (v/v)) allowed for the synthesis of monodisperse microspheres with diameter  $\sim 5 \mu\text{m}$ . The poly(MAA-co-DVB) was synthesised in good

yield (Table 4.15). Microscopic characterisation revealed that good quality particles were prepared (SEM of MAS135 shown in Figure 4.9). Bimodal particle size distributions were observed, because although most of the particles were of size  $\sim 5 \mu\text{m}$ , a fraction of particles with size  $\sim 1 \mu\text{m}$  was also detected (Table 4.16). The entire mass of MAS135 was subjected to magnetisation procedure. The polymer incubated in base solution changed the colour into dark brown, what indicated on the presence of magnetite formed within and on the surface of microspheres. After the magnetisation process, 80% of MAS135, further named as MAS136, was recovered. The whole amount of MAS136 was subjected to magnetic separation. The fraction of magnetic particles constituted 51% of the total MAS136. Incorporation of magnetite into MAS136 was evaluated *via* the application of a magnetic field in the vicinity of the polymer particles. Migration of the polymer particles to and along the magnet were observed when a permanent magnet was applied to the base of a Petri dish containing the polymer. This demonstrates that magnetite was incorporated into MAS136. The colour of the polymer was brown, which also suggests that magnetite was formed. Microscopic characterisation shows that the application of the magnetisation procedure did not change the morphology of the polymer (Table 4.16; SEM of MAS136 shown in Figure 4.9).

Table 4.15 Effect of the PP feed on the yield of non-magnetic core particles.

Polymer code	Components (mmol)	Monomer conc. (% w/v)	Initiator conc. (mol%)	Solvent (v/v)	Incubation time (h)	Scale (g)	Yield (%)
MAS135	DVB-80 (67.16) MAA (14.29)	3.28	3.35	ACN/toluene (75:25)	72	10	68



Table 4.16 Microscopic characterisation of MAS135 and MAS136.

Polymer	Optical microscopy observation			Beads average diameters in $\mu\text{m}^a$
	Dispersity	Bead size ( $\mu\text{m}$ )	Aggregation	
MAS135	Polydisperse	4-5	none	1 and 5
MAS136	Polydisperse	4-5	none	1 and 5

<sup>a</sup> SEM microscopy observation.

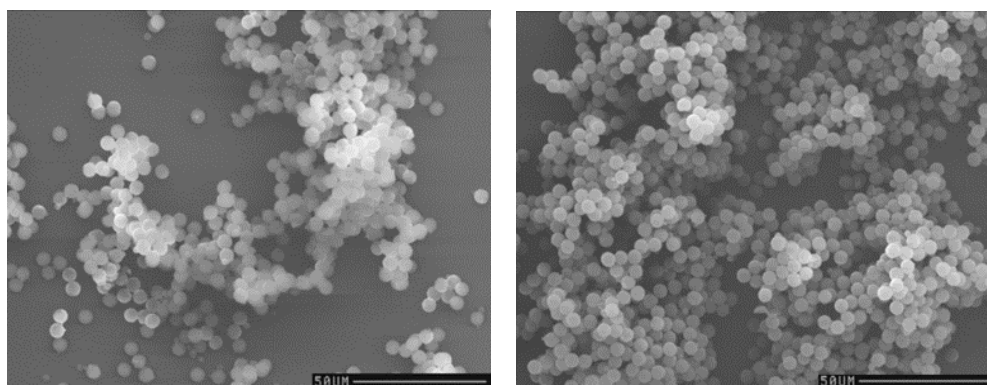


Figure 4.9 SEMs of MAS135 (left) and magnetic MAS136 (right);  $\times 604$  magnification (scale =  $50 \mu\text{m}$ ).

A FT-IR spectrum of MAS135 is presented in Figure 4.10. The following characteristic peaks were observed: aliphatic C-H stretches at  $2922 \text{ cm}^{-1}$ , carboxylic acid C=O stretch at  $1701 \text{ cm}^{-1}$ , aromatic C=C stretch at  $1604 \text{ cm}^{-1}$ , alkene stretches at  $992 \text{ cm}^{-1}$  and  $904 \text{ cm}^{-1}$ , and three stretches at  $832 \text{ cm}^{-1}$ ,  $796 \text{ cm}^{-1}$  and  $711 \text{ cm}^{-1}$ , corresponding to *para*- and *meta*-di-substituted benzene rings. The FT-IR analysis shows that MAA was successfully copolymerised with DVB-80.

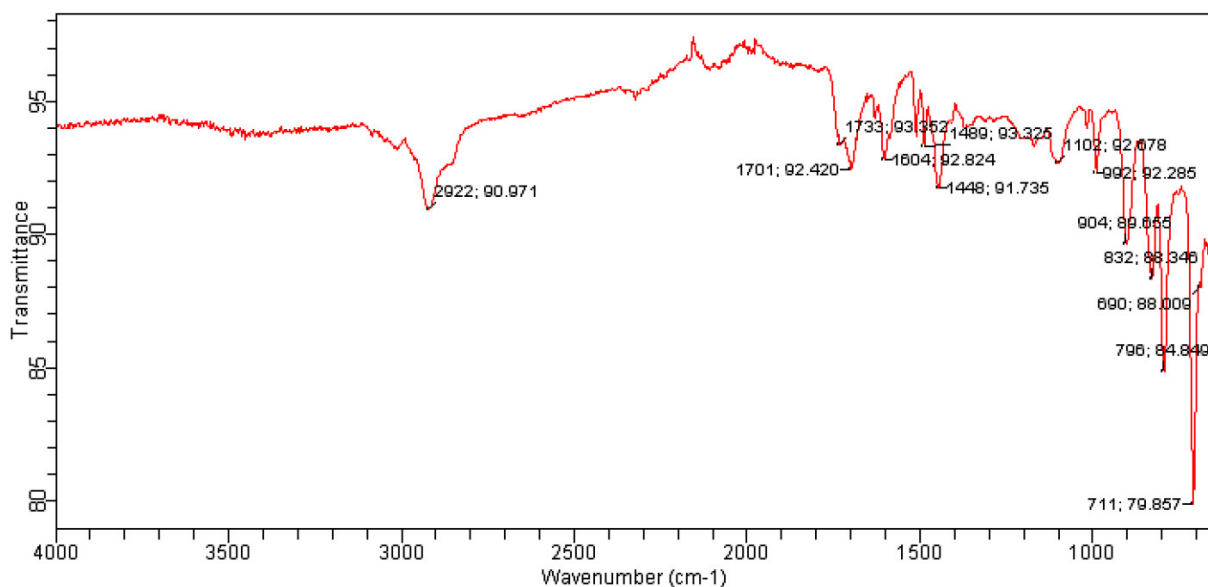


Figure 4.10 FT-IR spectrum of MAS135.

#### 4.3.3.2 Synthesis and characterisation of magnetic core-shell MIPs and their corresponding NIPs

The studies presented in this subsection involved the synthesis of the first generation of magnetic polymers for the Z-NLLGLIEA{Nle} target: magnetic core-shell polymers. A two-step PP was the synthetic method used. Magnetic core particles and non-magnetic shells were prepared in two separate reactions. Firstly, the magnetic core particles, MAS136, with incorporated magnetite were prepared and then these particles were used as the seed particles for the synthesis of magnetic core-shell particles. Non-magnetic shells were formed around the magnetic core particles. The conditions identified in the test studies presented in Chapter 3, for the synthesis of cores and shells by a two-step PP, were applied. A 2:1 w/w ratio of magnetic core particles to monomer was used for the synthesis of the core-shell particles. Such a ratio allowed for the synthesis of core-shell microspheres with a shell thickness  $\sim 0.1 \mu\text{m}$  (Chapter 3). Non-magnetic shells grown on the surfaces of the magnetic cores were prepared with monomer and initiator concentrations at 4% w/v (with respect to the solvent) and 2 mol% (with respect to the total number of polymerisable

double bonds), respectively. 24 h was the polymerisation time used for the synthesis of the magnetic core-shell particles.

MIPs (MAS137 and MAS139) and the corresponding NIPs (MAS138 and MAS140) were prepared with the same concentrations of template and functional monomer(s) as in the previous syntheses reported in Chapter 3. A five-fold reduction in the concentrations of template and functional monomers(s), together with addition of template and functional monomer(s) timed 1.5 h after the polymerisations had started, were again applied. The yields of shelled products were low, ~10% (Table 4.17). This could be due to the low scale of operation (1.5 g) and/or to the loss of material during product work-up, rather than to the failure polymerisation. Microscopic characterisation revealed that good quality particles were prepared (example of SEM shown in Figure 4.11). Most of the particles were of diameter ~5  $\mu\text{m}$ , however a fraction of particles with diameter of ~1  $\mu\text{m}$  were also observed (Table 4.18). This is consistent, as the magnetic core particles used also had a bimodal size distribution. A schematic representation of a molecularly imprinted binding site in the magnetic core-shell MIPs for the ProGRP target is shown in Figure 4.12 and Figure 4.13.

Table 4.17 Effect of shell compositions on the yield of magnetic MIPs and NIPs.

Polymer code	Shell description (2:1 core: shell)	Template	Yield (shell) (before and after mag. sep.) (%)
MAS137	99.4% DVB-80, 0.5% EAMA.HCl, 0.1% NTPVU	Z-NLLGLIEA{Nle}	12; 0
MAS138	99.4% DVB-80, 0.5% EAMA.HCl, 0.1% NTPVU	-	3; 0
MAS139	99.4% DVB-80, 0.5% EAMA.HCl	Z-NLLGLIEA{Nle}	12; 0
MAS140	99.4% DVB-80, 0.5% EAMA.HCl	-	15; 2

Table 4.18 Microscopic characterisation of magnetic core-shell MIPs and NIPs.

Polymer	Optical microscopy observation			Beads average diameters in $\mu\text{m}^a$
	Dispersity	Bead size ( $\mu\text{m}$ )	Aggregation	
MAS137	Polydisperse	4-5	none	1 and 5
MAS138	Polydisperse	4-5	none	1 and 5
MAS139	Polydisperse	4-5	none	1 and 5
MAS140	Polydisperse	4-5	none	1 and 5

<sup>a</sup> SEM microscopy observation

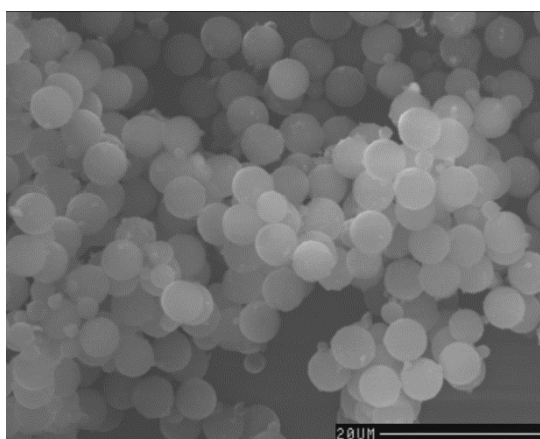


Figure 4.11 SEM of magnetic core-shell MAS137;  $\times 1560$  magnification (scale = 20  $\mu\text{m}$ ).

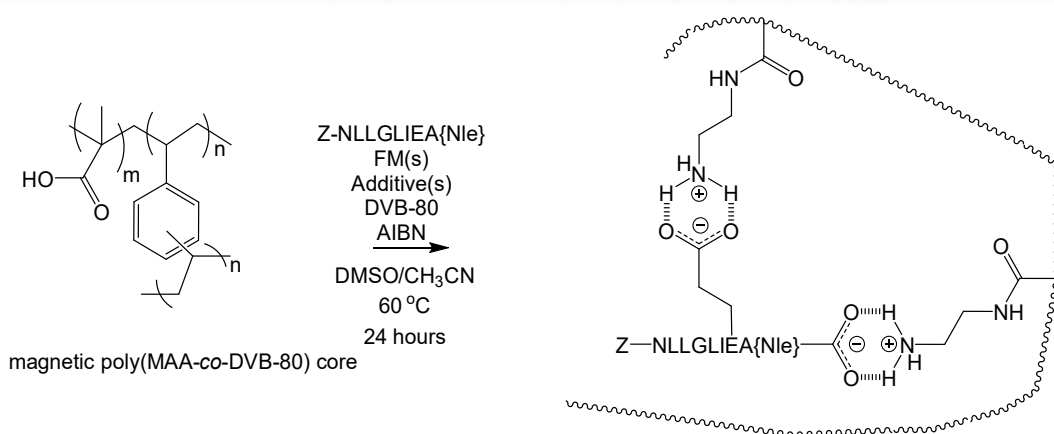


Figure 4.12 Schematic representation of poly(EAMA.HCl-co-DVB-80) magnetic core-shell microspheres by the non-covalent molecular imprinting of Z-NLLGLIEA{Nle}, a structural analogue of the ProGRP signature peptide. The carboxylic acid groups in the glutamic acid (E) residue and C-terminus of Z-NLLGLIEA{Nle} are drawn explicitly for emphasis, since these functional groups are involved in the self-assembly of the Z-NLLGLIEA{Nle} with functional monomers. The complexed synthetic receptor (right hand side) depicts a molecularly imprinted binding site formed upon the free radical copolymerisation of a 1:2 molecular complex of Z-NLLGLIEA{Nle} and N-(2-aminoethyl)methacrylamide hydrochloride with crosslinker (DVB-80).

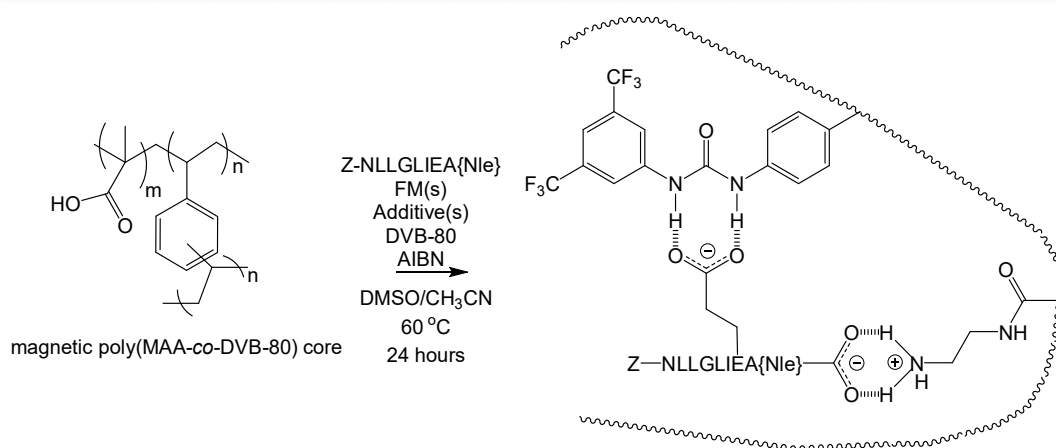


Figure 4.13 Schematic representation of poly(NTPVU-co-EAMA.HCl-co-DVB-80) magnetic core-shell microspheres by the non-covalent molecular imprinting of Z-NLLGLIEA{Nle}, a structural analogue of the ProGRP signature peptide. The carboxylic acid groups in the glutamic acid (E) residue and C-terminus of Z-NLLGLIEA{Nle} are drawn explicitly for emphasis, since these functional groups are involved in the self-assembly of the Z-NLLGLIEA{Nle} with functional monomers (FMs). The complexed synthetic receptor (right hand side) depicts a molecularly imprinted binding site formed upon the free radical copolymerisation of a 1:1:1 molecular complex of Z-NLLGLIEA{Nle}, N-(2-aminoethyl)methacrylamide hydrochloride and N-3,5-bis(trifluoromethyl)-phenyl-N'-4-vinylphenylurea with crosslinker (DVB-80).

The nitrogen sorption data, shown in Table 4.19, revealed that the MIPs and NIPs were macroreticular; this was important to establish in view of the need for analyte to access molecularly imprinted binding sites during MISPE. The NIPs were similar to the MIPs in respect of their porous morphologies, suggestive of the idea this time that the presence of template during polymerisation does not influence significantly the polymerisation outcomes.

Table 4.19 Nitrogen sorption porosimetry data for magnetic core-shell MIPs and NIPs.

Polymer code	BET C value	Specific surface area (m <sup>2</sup> /g)		Specific pore volume (cm <sup>3</sup> /g) <sup>a</sup>	Average pore diameter (nm) <sup>b</sup>
		BET	Langmuir		
MAS137	-136	468	670	0.27	2.96
MAS138	-152	472	702	0.27	3.03
MAS139	-267	369	549	0.21	3.03
MAS140	-266	348	519	0.20	3.11

<sup>a</sup> respect to the solvent; <sup>b</sup> respect to the total number of polymerisable double bonds.

The BET C values for the NIPs and MIPs were negative, indicating that the data for the tested samples did not fit to the BET isotherm as the nitrogen molecules were absorbed in a single layer onto the surfaces of the solids. (Table 4.19). This change in sorption mode implies that the Langmuir isotherm should be used to describe the specific surface area of the tested polymers for the analysis of the nitrogen sorption data. The analysis shows that the average pore size reached a maximum of 3.11 nm (Table 4.19, MAS140). Tested polymers were highly crosslinked as poly(DVB-80) constituted more than 97% of the whole polymer network structure and such high crosslinking level usually results in small pore size. High specific surface areas indicated that the materials tested contained many micropores. These conclusions can be additionally supported by the analysis of nitrogen sorption isotherms. Type I isotherms were generated (MAS139 and MAS140). This isotherm is obtained when a single layer of nitrogen molecules is absorbed on the solid and is typical for materials with microporous structure. In addition to the presence of micropores, there can be a small percentage of mesopores within the materials tested (*i.e.*, pores > 2 nm > 50 nm). A nitrogen sorption isotherm which resembles a type II isotherm, characteristic for non-porous or macroporous solids with pore width more than 50 nm was also generated (MAS137). In this isotherm generated during the analysis, some divergence was observed: the desorption path was not exactly the same as the adsorption path. This divergence indicated the presence of mesoporous in the

polymer network structures.<sup>21</sup> A nitrogen sorption isotherm which does not resemble any known isotherm was generated (MAS138). A sharp initial region, which is related to very strong adsorption, followed by gradual decrease and sharp rise in nitrogen adsorption were observed. The gradual decrease in adsorption could be related to insufficient drying of the samples.<sup>21</sup> The nitrogen sorption analysis together with drying procedure was repeated three times, although the same nitrogen sorption isotherms were obtained. It could be due insufficient amount of the materials used for this analysis.

All prepared core-shell magnetic polymers targeting the ProGRP target, and their corresponding NIPs, were sent to PEPMIP partner (Oslo University) for magnetic capture work.

At the time of writing of this Thesis, Nick McKittrick, a PhD student from Oslo University, was still working on the characterisation of the molecular recognition properties of the core-shell magnetic polymers. The MIPs and NIPs have affinity for the ProGRP signature peptide, and the focus is on establishing robust conditions under which the MIP shows selectivity binding.

## 4.4 Macroreticular polymers converted into magnetic MIPs for ProGP target

### 4.4.1 Aim of study

In our design and synthesis studies of magnetic macroreticular polymers for the ProGRP target, we hypothesize that:

- MIPs as the synthetic materials have binding sites that have high affinity and selectivity for a given target molecule;
- PP is a useful synthesis method for the preparation of high-quality, MIP microspheres. Near monodisperse and surfactant-free spherical polymer particles in the micron size range can be synthesised by the PP method;



- The co-precipitation of FeCl<sub>3</sub> and FeCl<sub>2</sub> can take place inside the pores of the polymers and it can result in the permanent incorporation of magnetic particles into the preformed polymers;
- The first generation of macroreticular MIPs for the ProGRP target can be transferred into magnetic variants through incorporation of magnetite into polymer pores;
- ProGRP is considered as a biomarker which is highly sensitive and specific for Small Cell Lung Cancer.

Based on this, the aims of the work presented in this section were as follows:

- Design a method for the incorporation of magnetic particles inside the preformed polymers;
- Synthesis of magnetic macroreticular MIPs for ProGRP target;
- Characterisation of materials produced, including demonstration of magnetic properties;
- Delivery of the next generation materials to the PEPMIP partners for evaluation of molecular recognition.

#### 4.4.2 Experimental section

##### 4.4.2.1 Materials

The peptide template Z-NLLGLIEA{Nle} (96.58% purity) was purchased from LifeTein. *N*-(2-Aminoethyl)methacrylamide hydrochloride (EAMA.HCl, purity >98%) was purchased from Polysciences, Inc. *N*-3,5-bis(Trifluoromethyl)-phenyl-*N'*-4-vinylphenylurea (NTPVU, purity >95%) is not commercially available and was kindly donated by Dortmund University. 2-2'-Azobisisobutyronitrile (AIBN, purity 98%) was purchased from BDH Lab. Supplies (UAE). Divinylbenzene-80 (DVB-80, 80% DVB isomers and 20% ethyl vinylbenzene isomers), 1,2,2,6,6-pentamethylpiperidine (PMP, purity ≥99%), tetrabutylammonium hydroxide solution (TBA.HO, 1.0 M in methanol, 25% ≤ purity <50%), hydrochloric acid (37 wt. % in H<sub>2</sub>O), Tween 20, sodium hydroxide (NaOH, purity ≥97), iron (III) chloride (FeCl<sub>3</sub>, purity 97%), iron (II)

chloride ( $\text{FeCl}_2$ , purity 98%) and 28%-30% ammonium hydroxide solution ( $\text{NH}_4\text{OH}$ ) were all purchased from Sigma-Aldrich. DVB-80 was purified by filtration through a short plug of neutral aluminium oxide prior to use. AIBN was recrystallized from acetone at low temperature. All other chemicals used (acetonitrile [ACN], methanol [MeOH], ethanol [EtOH] (purity  $\geq 99.5$ ) and dimethyl sulfoxide (DMSO, purity  $\geq 99.9\%$ ) were of analytical grade.

#### *4.4.2.2 Test study: conversion of non-magnetic MAS100 into magnetic variant*

The entire mass of MAS100, poly(EAMA.HCl-co-DVB), 1.12 g, was subjected to the magnetisation procedure as described in the previous section. The procedure was applied twice in order to transfer the non-magnetic polymer into a magnetic format. After two magnetisation cycles, magnetic separation was performed and then the yield of the magnetisation process was checked gravimetrically.

#### *4.4.2.3 Synthesis of magnetic macroreticular MIPs and their corresponding NIPs*

The next generation of magnetic MIPs and NIPs were prepared by the application of the magnetisation procedure to the first generation of materials, which the syntheses of which are reported in Chapter 2 (2.3). Therefore, the first step in the synthesis of the next generation of magnetic polymers was to reproduce the synthesis of the first generation of macroreticular MIPs and NIPs for the Z-NLLGLIEA{Nle} target, which were then subjected to magnetisation.

MIPs and their corresponding NIPs were synthesised by typical a PP as described elsewhere.<sup>16</sup> The feed compositions of the reproduced first generation materials are shown in Table 4.20. Two distinct pair of polymers were synthesised: two MIPs (MAS142 and MAS144) and two NIPs (MAS141 and MAS143). The polymers were produced on a 1 g monomer scale, with a monomer and initiator concentration of 2% w/v (with respect to the solvent) and 2 mol% (with respect to the total number of polymerisable double bonds), respectively. 24 h was the polymerisation time.

Table 4.20 Feed composition of macroreticular MIPs and their corresponding NIPs.

Polymer code	Template (mmol)	Functional Monomer (mmol)	DVB-80 (mmol)	Solvent (mL)	AIBN (mol%)	PMP or/and TBA.OH (mmol)
MAS141	-	EAMA.HCl (0.28)	14.92	ACN (48) DMSO (2)	2	PMP (0.024)
MAS142	Z-NLLGLIEA{Nle} (0.028)	EAMA.HCl (0.28)	14.92	ACN (48) DMSO (2)	2	PMP (0.024)
MAS143	-	EAMA.HCl (0.28) NTPVU (0.04)	14.92	ACN (48) DMSO (2)	2	TBA.OH (0.04), PMP (0.024)
MAS144	Z-NLLGLIEA{Nle} (0.028)	EAMA.HCl (0.28) NTPVU (0.04)	14.92	ACN (48) DMSO (2)	2	TBA.OH (0.04), PMP (0.024)

The entire mass of each prepared polymer was subjected to the magnetisation procedure described in the previous section (4.3.2.2). The procedure was applied twice in order to convert the non-magnetic polymers into magnetic formats. The polymers in the magnetic format, after their isolation from the magnetisation solution, were transferred into pre-weighed vials and dried overnight in a Townson & Mercer vacuum oven (60 mbar) at 70 °C. The yields of polymers were checked gravimetrically. The yields of MAS141, MAS142, MAS143 and MAS144 were 2%, 28%, 8% and 22%, respectively.

Magnetic separations were performed to separate the magnetic polymer particles from any non-magnetic particulates. Firstly, dried products were transferred into clean beakers and washed with EtOH (~50 mL). The products dispersed in EtOH were mixed with a glass rod. Thereafter, a permanent magnet was held against the base of the beakers, and the beakers with dispersed products left for 15 s. At this stage, the supernatants were collected. The whole procedure was repeated at least four times until the supernatants became clear. The magnetic particles were isolated from the rest of EtOH by vacuum filtration using a Vacuumbrand Vacuum System (2.0 mbar) on 0.45 µm nylon membrane filters. The isolated products were transferred again into pre-weighed vials and dried overnight in a Townson & Mercer vacuum oven

(60 mbar) at 70 °C. The yields of the isolated magnetic particles were again checked gravimetrically. The yields of MAS142, MAS143 and MAS144 were 26%, 6% and 20%, respectively. The yield of MAS141 was 0%.

Polymer microspheres were evaluated in terms of size, dispersity and their aggregation (if any). Polymer microspheres were imaged by scanning electron microscopy (SEM) using a Cambridge Instruments Stereoscan 90. The steps involved in microscopic analysis and image analysis carried out by Image J, were introduced and discussed in detail in the 1.5.2 subsection and the 2.1.2.2 experimental section.

#### 4.4.3 Results and discussion

##### *4.4.3.1 Test study: conversion of non-magnetic poly(EAMA.HCl-co-DVB-80) into magnetic variant*

This test study was performed in order to determine if the magnetisation procedure can be applicable to other porous polymers which do not contain carboxylic acid groups in their structure. Two cycles of the magnetisation procedure were enough in order to convert 1.12 g of MAS100, poly(EAMA.HCl-co-DVB-80) into a magnetic variant. The polymer incubated in basic solution changed colour to dark brown, which indicated the presence of magnetite formed within and on the surfaces of the polymer microspheres. The yield of the magnetisation process was moderate, and reached 25% after magnetic separation. Additionally, incorporation of magnetite into MAS100 was evaluated *via* the application of a magnetic field in the vicinity of the polymer particles. Migration of the polymer particles to and along the magnet were observed when a permanent magnet was applied to the base of a Petri dish containing the polymer. This demonstrates that magnetite was incorporated into MAS100. This test study showed that carboxylic acid groups are not required for the successful production of magnetic particles. It can be suggested that apart from by carboxylics, iron ions can bind to the polymer in other ways too. Non-covalent interactions could be involved in this process. The co-precipitation of Fe<sup>3+</sup> and Fe<sup>2+</sup> ions results in the synthesis of magnetite nanoparticles with size from 3 nm up to

20 nm.<sup>22</sup> This size range is bigger than the size of the pores in the materials prepared, as the BET analysis performed so far did not reveal the polymers with the size of pores bigger than 3 nm. The magnetisation mechanism could be as follows: the ions of  $\text{Fe}^{3+}$  and  $\text{Fe}^{2+}$  simply diffuse into the polymer pores during their incubation with porous polymer.  $\text{Fe}^{3+}$  and  $\text{Fe}^{2+}$  can easily get into the polymer pores as their size is significantly smaller than the size of the polymer pores. When the polymer is incubated with the basic solution, the growth of magnetite is initiated inside the polymer pores. It would be that the magnetite particles grow until the pores are filled and the magnetite particles become entrapped inside the polymer pores. Therefore, magnetite particles become closely and permanently trapped inside the polymer pores and the structure of the polymer network does not allow for the diffusion of magnetite particles outside the pores.

#### *4.4.3.2 Synthesis of magnetic macroreticular MIPs and their corresponding NIPs*

The non-imprinted and imprinted polymers for the Z-NLLGLIEA{Nle} target were reproduced in good yields; the average yield of particles was 55% (Table 4.21).

The SEM micrographs of the MIP and NIP microspheres (Table 4.22, example of SEM shown in Figure 4.14) revealed that discrete particles in the micron-sized range had been produced, although the microspheres were polydisperse (possibly as a consequence of the presence of DMSO as a co-solvent). Particles overlap or combine with each other into larger and irregular agglomerates. Microscopic characterisation shows that the application of magnetisation procedure did not noticeably change the morphology of the polymer (Table 4.22, example of SEM shown in Figure 4.14).

Table 4.21 Effect of polymer compositions on the yield of the polymer products.

Polymer code	Polymer name	Template	Yield (%)
MAS141	poly(EAMA.HCl-co-DVB-80)	-	55
MAS142	poly(EAMA.HCl-co-DVB-80)	Z-NLLGLIEA{Nle}	56
MAS143	poly(NTPVU-co-EAMA.HCl-co-DVB-80)	-	53
MAS144	poly(NTPVU-co-EAMA.HCl-co-DVB-80)	Z-NLLGLIEA{Nle}	57

Table 4.22 Microscopic characterisation of macroreticular MIPs and NIPs and their magnetic variants.

Polymer code	Optical microscopy observation			Bead average diameter in $\mu\text{m}^a$
	Dispersity	Bead size ( $\mu\text{m}$ )	Aggregation	
MAS141	Polydisperse	4-5	Chemical	1 and 6
MAS142	Polydisperse	1-5	Chemical	1-5
MAS143	Polydisperse	approx. 1	Chemical	approx. 1
MAS144	Polydisperse	approx. 1	Chemical	approx. 1

<sup>a</sup> SEM microscopy observation.

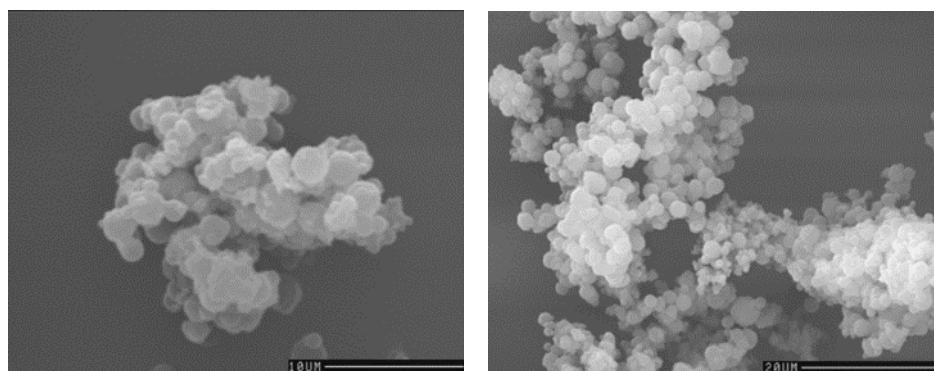


Figure 4.14 SEMs of macroreticular MAS142 (left) and magnetic MAS142 (right); magnifications:  $\times 1680$  and  $\times 3380$  (scales =  $10 \mu\text{m}$  and  $20 \mu\text{m}$  for left and right SEM images, respectively).

The entire mass of each reproduced polymer was subjected to the magnetisation procedure. The polymers incubated in basic solution changed colour into dark brown,

which indicated the presence of magnetite formed within and on the surfaces of the microspheres. After the magnetisation process, the entire mass of each prepared magnetic polymer was subjected to magnetic separation. The yields of the magnetisation process were significantly higher for MIPs (~23%) than for NIPs (~3%). These differences were due to variable loss of material during development of NIPs and MIPs by two different persons. MIPs were prepared by the author of this Thesis, NIPs were prepared by Mingquan Liu, a PhD student from Umeå University, during his secondment at Strathclyde University. Incorporation of magnetite into MAS141, MAS142, MAS143 and MAS144 was evaluated *via* the application of a magnetic field in the vicinity of the polymer particles. Migration of the polymer particles to and along the magnet were observed when a permanent magnet was applied to the base of a Petri dish containing the polymer. This demonstrates that magnetite was successfully incorporated into the porous polymer network structures of MIPs and NIPs.

Table 4.23 Effect of polymer compositions on the yield of the polymer products.

Polymer code	Components (mmol)	Template (mmol)	Yield (%) Before and after mag. sep.
MAS141	DVB-80 (14.92), EAMA.HCl (0.28), PMP (0.024)	-	2; 0
MAS142	DVB-80 (14.92), EAMA.HCl (0.28), PMP (0.024)	Z-NLLGLIEA{Nle} (0.028)	28; 26
MAS143	DVB-80 (14.92), TBA.OH (0.04), NTPVU (0.04), PMP (0.024), EAMA.HCl (0.28)	-	8; 6
MAS144	DVB-80 (14.92), TBA.OH (0.04), NTPVU (0.04), PMP (0.024), EAMA.HCl (0.28)	Z-NLLGLIEA{Nle} (0.028)	22; 20

All prepared magnetic polymers targeting the ProGRP target, and their corresponding NIPs, were sent to PEPMIP partner (Oslo University) for magnetic capture work.

At the time of writing of this Thesis, Nick McKitterick, a PhD student from Oslo University, was still working on the characterisation of the molecular recognition

properties of the macroreticular magnetic polymers. The MIPs and NIPs have affinity for the ProGRP signature peptide, and the focus is on establishing robust conditions under which the MIP shows selectivity binding.

#### 4.5 Conclusions and outlook

The scope of the work presented in this chapter spans the design, synthesis and characterisation of the next generation of magnetic imprinted polymers for  $\beta$ -Amyloid and ProGRP targets. The polymers have been produced in a magnetic microsphere format and a magnetic core-shell formats *via* precipitation polymerisation and a two-step precipitation polymerisation, respectively. The magnetic component, magnetite was either encapsulated or incorporated inside the polymer network structures post-polymerisation. Although, the polymers with encapsulated magnetic component were prepared in low yield and the particles were of relatively small size, these drawbacks were overcome by the application of the magnetisation procedure. The magnetic particles were incorporated either by growth close to the vicinity of carboxylic acid groups present in the polymer network structure and/or through their growth inside the polymer pores. Selected polymers were supplied to PEPMIP partners for testing and evaluation. Although, the materials have not been fully tested yet at the time of writing, we believe that the magnetic core-shell polymers can help to overcome the problems which were reported during the testing of the first generation of materials.

Overall, the successful synthesis and characterisation of the next generation of MIPs can be considered a promising achievement, not least of all because the magnetic approach is generic and can be extended to other targets.



## 4.6 Bibliography

- 1 A. Aseri, S. K. Garg, A. Nayak, S. K. Trivedi and J. Ahsan, *Int. J. Pharm. Sci. Rev. Res.*, 2015, **31**, 119–131.
- 2 S. Laurent, D. Forge, M. Port, A. Roch, C. Robic, L. Vander Elst and R. N. Muller, *Chem. Rev.*, 2008, **108**, 2064–2110.
- 3 R. Massart, *IEEE*, 1981, **17**, 1247–1248.
- 4 L. Chen and B. Li, *Anal. Methods*, 2012, **4**, 2613–2621.
- 5 EP0879063 (A1), 1998, 1–9.
- 6 R. J. Ansell and K. Mosbach, *Analyst*, 1998, **123**, 1611–6.
- 7 S. S. Miao, M. S. Wu, H. G. Zuo, C. Jiang, S. F. Jin, Y. C. Lu and H. Yang, *J. Agric. Food Chem.*, 2015, **63**, 3634–3645.
- 8 Y. Hu, R. Liu, Y. Zhang and G. Li, *Talanta*, 2009, **79**, 576–82.
- 9 C. Gonzato, M. Courty, P. Pasetto and K. Haupt, *Adv. Funct. Mater.*, 2011, **21**, 3947–3953.
- 10 L. Chen, Y. K. Lee, Y. Manmana, K. S. Tay, V. S. Lee and N. A. Rahman, *e-Polymers*, 2015, **15**, 141–150.
- 11 M. Gümüşderelioglu, A. S. Kahraman and A. Tuncel, *Polym. Bull.*, 2012, **69**, 323–335.
- 12 H. Macková, V. Proks, D. Horák, J. Kučka and M. Trchová, *J. Polym. Sci. Part A Polym. Chem.*, 2011, **49**, 4820–4829.
- 13 C. Rodriguez, E. Castro, A. Martin, J. R. Marín, J. Berganza and J. M. Cuevas, *Micro Nano Lett.*, 2011, **6**, 349–352.
- 14 W. Li and H. D. H. Stöver, *Macromolecules*, 2000, **33**, 4354–4360.

- 15 *Google Images* [www.images.google.com](http://www.images.google.com), 2016.
- 16 J. Wang, P. A. G. Cormack, D. C. Sherrington and E. Khoshdel, *Angew. Chem. Int. Ed.*, 2003, **42**, 5336–5338.
- 17 G. McCance, Bachelor Thesis, University of Strathclyde, 2015.
- 18 S. K. Suh, K. Yuet, D. K. Hwang, K. W. Bong, P. S. Doyle and T. A. Hatton, *J. Am. Chem. Soc.*, 2012, **134**, 7337–7343.
- 19 J. Huang, S. Wan, M. Guo and H. Yan, *J. Mater. Chem*, 2006, **16**, 4535–4541.
- 20 S. N. Lavrynenko, V. A. Chebanov and D. S. Sofronov, *Int. J. Env. Sus.*, 2016, **5**, 71–75.
- 21 S. Lowell and J. E. Shields, *Powder Surface Area and Porosity*, Chapman & Hall, London, 3rd edn., 1991.
- 22 S. Sun and H. Zeng, *J. Am. Chem. Soc.*, 2002, **124**, 8204–8205.
- 23 H. G. Imlay, MChem Thesis, University of Strathclyde, 2013.

# 5. Molecularly imprinted polymer hydrogels

The synthesis of MIPs in a hydrogel format was also of interest in the current work. MIPs in this format were suitable for targeting  $\alpha$ -Synuclein.  $\alpha$ -Synuclein protein normally occurs in the presynaptic terminals of the central nervous system, and in unhealthy bodies it forms aggregates in the Lewy bodies and neurites which are considered as the main source of Parkinson's Disease (PD).<sup>1</sup> Nowadays, the early detection of PD is still challenging and, in fact, there is no straightforward and cheap diagnosis tool that can detect the disorder before irreversible changes appear in the brain. MIPs for  $\alpha$ -Synuclein target could be promising diagnosis tools. However, the synthesis of MIPs for the  $\alpha$ -Synuclein target involves use of template molecules which are hydrophilic in nature, thus the conditions which are applied for the synthesis of hydrogels should be conditions under which the templates are soluble.

Hydrogels are defined as polymeric materials with three-dimensional network structures which are swellable in water. They can absorb and retain water up to thousands of times their dry state.<sup>2,3</sup>

Chemically crosslinked hydrogels can be prepared by either  $\gamma$ -ray radiation, small molecule crosslinking, or condensation reactions.<sup>4</sup> Redox polymerisation is one of the methods for the synthesis of the chemically crosslinked hydrogels. Low-molecular weight monomers, *e.g.*, acrylamide, polymerises in the presence of crosslinking agent, *e.g.*, *N,N'*-methylene bis(acrylamide) (BIS). The reaction is initiated by a redox initiator, *e.g.*, ammonium persulfate (APS) and additive catalyst such as *N,N,N',N'*-tetramethylethylenediamine (TEMED). The rate of formation of free radicals from APS is accelerated by TEMED, as it promotes decomposition of APS to form radicals. TEMED decreases almost three-fold the activation energy required for

polymerisation, and hence allows the synthesis to proceed rapidly and at low temperatures.<sup>5</sup>

The Hjertén method is a well-known technique for the synthesis of molecularly imprinted hydrogels.<sup>6</sup> The method involves the synthesis of polyacrylamide-based hydrogels in the presence of protein targets. Acrylamide and BIS were used alone as the monomers in the formation of three-dimensional imprinted gel network structures. In this method, apart from acrylamide no other functional monomer(s) were included in the polymerisation solution. Proteins (ribonuclease, haemoglobin, lysozyme, myoglobin and human growth factor) were imprinted in the polyacrylamide-based hydrogels. The hydrogels showed preferential recognition for their targets. In addition to this, a further study performed by Hjertén revealed that this type of polymeric material could be perfectly used for the discrimination of different forms of the same protein iron-free and iron-containing transferrin, and for the discrimination of the same proteins which came from different species, such as human and bovine haemoglobin.<sup>7,8</sup> More than 20 years have passed since the method was first disclosed, however the mechanism of imprinting is still unclear. It would seem that hydrogen bonds were involved in the process of imprinting, but the molecular recognition took place in aqueous solution, in an environment which is unfavourable for the formation of hydrogen bonds between target proteins and hydrogels as the water molecules compete with target molecules for the binding sites present in the hydrogels. According to the method's author, the properties of this type of gel are mainly dependent on degree of crosslinking, pH and ionic strength.<sup>6</sup> Further modification of the Hjertén method involved inclusion of functional monomers (acrylic acid and/or *N,N*-dimethyl-aminopropylacrylamide) into hydrogel network(s).<sup>9</sup> Lysozyme imprinted hydrogels were grafted onto silica beads and exhibited high selective recognition for the target protein. This type of hydrogel was used successfully as the polymeric film in a quartz crystal microbalance sensor for the recognition of lysozyme.<sup>9</sup> Ou and others also used lysozyme for the synthesis of imprinted polyacrylamide-based hydrogels. In their study, methacrylic acid was used as the functional monomer and 2-(dimethylamino)ethyl methacrylate. However,

discrimination between the proteins tested (albumin and lysozyme) was not observed. In addition, template removal was a problem, as 25% of the lysozyme remained entrapped in the hydrogels.<sup>10</sup> On the other hand, another study showed high selectivity for haemoglobin by polyacrylamide-based imprinted hydrogels.<sup>11,12</sup> In addition, the mechanical stability of the polyacrylamide-based imprinted hydrogels was improved by the entrapment of the gel network structure into porous chitosan beads.<sup>11,12</sup> The problem with the template removal from the gel network structure was studied extensively by Hawkins and others. The combination of surfactant, sodium dodecyl sulfate, and acetic acid allowed for the extraction of 90% of the template from the imprinted hydrogels.<sup>13</sup> As is described above, there were some successfully reported imprinted polyacrylamide-based hydrogels, however this type of polymeric material still suffers from some limitations. The stability of hydrogels is highly affected by the changes in the environment.<sup>14,15,16</sup> Hydrogel-based imprinted polymers suffer from low mechanical robustness. Another problem discussed already is lack of complete extraction of the template from the imprinted gel network structure.

## 5.1 Aim of study

In our design and synthesis studies of molecularly imprinted hydrogels, we hypothesize that:

- polyacrylamide-based gels copolymerized with functional monomers can be used effectively for the synthesis of MIPs for an  $\alpha$ -Synuclein target;
- *N*-(2-Aminoethyl)methacrylamide hydrochloride and *N*-(3-aminopropyl)methacrylamide hydrochloride are functional monomers which would be copolymerized with acrylamide and further involved in the formation of non-covalent interactions with peptide templates for the synthesis of molecularly imprinted hydrogels.

Based on this, the aims of the work presented in this section were as follows:

- Design and synthesis of imprinted and non-imprinted polyacrylamide-based hydrogels for peptide target;
- Delivery of the next generation of materials to the PEPMIP partners for evaluation of molecular recognition.

## 5.2 Experimental section

### 5.2.1 Materials

The peptide templates Ac-DYEPEA (>95% purity) and Ac-EGYQDYEPEA (>95% purity) were purchased from ChinaPeptides. *N*-(2-Aminoethyl)methacrylamide hydrochloride (EAMA.HCl, >98% purity) and *N*-(3-aminopropyl)methacrylamide hydrochloride (APM, >98% purity) were purchased from Polysciences, Inc (Niles, IL, USA). Acrylamide ( $\geq 99\%$  purity), *N,N'*-methylene bis(acrylamide) (BIS, ~99% purity), ammonium persulfate (APS,  $\geq 98\%$  purity), *N,N,N',N'*-tetramethylethylenediamine (TEMED, ~99% purity), sodium phosphate monobasic ( $\geq 99\%$  purity), sodium phosphate dibasic ( $\geq 99\%$  purity), acetic acid ( $\geq 99.7\%$  purity), hydrochloric acid (37 wt. % in H<sub>2</sub>O) and sodium hydroxide (NaOH, purity  $\geq 97$ ) were all purchased from Sigma Aldrich (St. Louis, MI, USA).

### 5.2.2 Synthesis of molecularly imprinted hydrogels for $\alpha$ -Synuclein target

Hydrogel MIPs and their corresponding NIPs were synthesised by implementation of the synthetic method reported by Stellan Hjertén for the production of acrylamide-based insoluble hydrogels<sup>6</sup>.

A series of hydrogel MIPs and NIPs were prepared. The feed compositions of the first and second generation materials are shown in Table 5.1 and Table 5.2. The first generation of hydrogels included either *N*-(2-aminoethyl)methacrylamide hydrochloride or *N*-(3-aminopropyl)methacrylamide hydrochloride as the functional monomer (Table 5.1). Also, Ac-DYEPEA and Ac-EGYQDYEPEA were used as the peptide templates. The first generation of hydrogels were prepared with the mole ratios of template to functional monomer(s) set at 1:4 and 1:320. The second

generation of hydrogels included *N*-(3-aminopropyl)methacrylamide hydrochloride as the functional monomer only (Table 5.2). Ac-EGYQDYEEPA was used as the template. The second generation of hydrogels was prepared with the mole ratios of template to functional monomer, *N*-(3-aminopropyl)methacrylamide hydrochloride set at 1:16 and 1:32. Common components used for both generations of hydrogels were *N,N'*-methylene *bis*(acrylamide) (BIS), used as the crosslinker, ammonium persulfate (APS) and *N,N,N',N'*-tetramethylethylenediamine (TEMED) used as the initiation system. Also, the concentrations of gel components and crosslinker were 6% (w/v) and 3% (w/w), respectively. Each MIP prepared had its corresponding non-imprinted counterpart. Polymers were synthesised on ~10 g monomer scale.

Table 5.1 Feed compositions of the first generation of imprinted hydrogels and their corresponding non-imprinted counterparts.

Polymer code	Mole ratio of T:FM	Template ( $\mu\text{mol}$ )	Functional Monomer (mmol)	Crosslinker (mmol)	Initiation system ( $\mu\text{mol}$ )	Solvent	Others (mmol)
MAS29	1:4	-	EAMA.HCl (0.007)	BIS (0.12)	APS (0.09), TEMED (0.07)	0.01 M sodium phosphate buffer at pH 7.4	Acrylamide (8.19)
MAS30	1:4	-	APM (0.007)	BIS (0.12)	APS (0.09), TEMED (0.07)	0.01 M sodium phosphate buffer at pH 7.4	Acrylamide (8.19)
MAS35	1:4	Ac-EGYQDYEP EA-OH (1.76)	EAMA.HCl (0.007)	BIS (0.12)	APS (0.09), TEMED (0.07)	0.01 M sodium phosphate buffer at pH 7.4	Acrylamide (8.19)
MAS36	1:4	Ac-EGYQDYEP EA-OH (1.76)	APM (0.007)	BIS (0.12)	APS (0.09), TEMED (0.07)	0.01 M sodium phosphate buffer at pH 7.4	Acrylamide (8.19)
MAS37	1:4	Ac-DYEP EA-OH (1.76)	EAMA.HCl (0.007)	BIS (0.12)	APS (0.09), TEMED (0.07)	0.01 M sodium phosphate buffer at pH 7.4	Acrylamide (8.19)
MAS38	1:4	Ac-DYEP EA-OH (1.76)	APM (0.007)	BIS (0.12)	APS (0.09), TEMED (0.07)	0.01 M sodium phosphate buffer at pH 7.4	Acrylamide (8.19)



Cont. Table 5.1 Feed compositions of the first generation of imprinted hydrogels and their corresponding non-imprinted counterparts.

Polymer code	Mole ratio of T:FM	Template ( $\mu\text{mol}$ )	Functional Monomer (mmol)	Crosslinker (mmol)	Initiation system ( $\mu\text{mol}$ )	Solvent	Others (mmol)
MAS45	1:320	-	APM (0.56)	BIS (0.12)	APS (0.09), TEMED (0.07)	0.01 M sodium phosphate buffer at pH 7.4	Acrylamide (8.08)
MAS46	1:320	Ac-EGYQDYEPEA-OH (1.76)	APM (0.56)	BIS (0.12)	APS (0.09), TEMED (0.07)	0.01 M sodium phosphate buffer at pH 7.4	Acrylamide (8.08)
MAS47	1:320	Ac-DYEPEA-OH (1.76)	APM (0.56)	BIS (0.12)	APS (0.09), TEMED (0.07)	0.01 M sodium phosphate buffer at pH 7.4	Acrylamide (8.08)
MAS48	1:320	-	EAMA.HCl (0.56)	BIS (0.12)	APS (0.09), TEMED (0.07)	0.01 M sodium phosphate buffer at pH 7.4	Acrylamide (8.08)
MAS49	1:320	Ac-EGYQDYEPEA-OH (1.76)	EAMA.HCl (0.56)	BIS (0.12)	APS (0.09), TEMED (0.07)	0.01 M sodium phosphate buffer at pH 7.4	Acrylamide (8.08)
MAS50	1:320	Ac-DYEPEA-OH (1.76)	EAMA.HCl (0.56)	BIS (0.12)	APS (0.09), TEMED (0.07)	0.01 M sodium phosphate buffer at pH 7.4	Acrylamide (8.08)

Table 5.2 Feed compositions of the second generation of imprinted hydrogels and their corresponding non-imprinted counterparts.

Polymer code	Mole ratio of T:FM	Template ( $\mu\text{mol}$ )	Functional Monomer (mmol)	Crosslinker (mmol)	Initiation system ( $\mu\text{mol}$ )	Solvent	Others (mmol)
MAS131	1:16	Ac-EGYQDYEP EA-OH (1.76)	APM (0.029)	BIS (0.12)	APS (0.09), TEMED (0.07)	0.01 M sodium phosphate buffer at pH 7.4	Acrylamide (8.17)
MAS132	1:16	-	APM (0.029)	BIS (0.12)	APS (0.09), TEMED (0.07)	0.01 M sodium phosphate buffer at pH 7.4	Acrylamide (8.17)
MAS133	1:32	Ac-EGYQDYEP EA-OH (1.76)	APM (0.056)	BIS (0.12)	APS (0.09) TEMED (0.07)	0.01 M sodium phosphate buffer at pH 7.4	Acrylamide (8.14)
MAS134	1:32	-	APM (0.056)	BIS (0.12)	APS (0.09), TEMED (0.07)	0.01 M sodium phosphate buffer at pH 7.4	Acrylamide (8.14)

The synthesis of the hydrogel with polymer code MAS35, for the imprinting of Ac-EGYQDYEEPA-OH, can serve as an illustrative example of the synthetic procedure. Firstly, Ac-EGYQDYEEPA (2.18 mg, 1.76  $\mu\text{mol}$ ), EAMA.HCl (1.15 mg, 0.007 mmol), acrylamide (0.58 g, 8.19 mmol), BIS (18 mg, 0.12 mmol) and APS (200  $\mu\text{L}$ , 0.09  $\mu\text{mol}$ , 10% (w/v) (aq.)) were dissolved in 0.01 M sodium phosphate buffer at 7.4 pH (10 mL) in a borosilicate culture Kimax tube. (For the synthesis of the corresponding NIP, the template was omitted from the synthetic protocol). The polymerisation solution was ultrasonicated for 10 min and purged with nitrogen for another 10 min. After the degassing step, TEMED (200  $\mu\text{L}$ , 0.07  $\mu\text{mol}$ , 5% (v/v) (aq.)) was added to polymerisation solution. The polymerisation time was 30 min, and resulted in the synthesis of an insoluble hydrogel. After 30 min, the hydrogel was crushed and mashed with spatula, and washed with acetic acid (20 mL, 10% (v/v) (aq.)) (to remove the template). The insoluble hydrogel was left for 24 h in contact with washing solvent. After 24 h, the insoluble polymeric product was isolated from the acetic acid by filtration using a 0.2  $\mu\text{m}$  nylon membrane filter using a Vacuumbrand Vacuum System (2.0 mbar).

Prior to synthesis of hydrogels, 1 L of 0.01 M sodium phosphate buffer at pH 7.4 was prepared. To prepare the buffer, 800 mL of distilled water was poured into a measuring cylinder followed by addition of sodium phosphate dibasic (20.21 g, 0.14 mol) and sodium phosphate monobasic (3.40 g, 0.03 mol). The buffer was mixed using a magnetic stirrer. The pH of the buffer was adjusted to 7.4 using hydrochloric acid or sodium hydroxide. Lastly, distilled water was added until volume of the buffer was 1 L.

## 5.3 Results and discussion

### 5.3.1 Synthesis of molecularly imprinted hydrogels for $\alpha$ -Synuclein target

The hydrogels considered as the first generation included eight (8) distinct hydrogel MIPs and four (4) corresponding non-imprinted counterparts (NIPs) (Table 5.1). Four (4) of the MIPs were imprinted with a decapeptide, Ac-EGYQDYEEPA, and the other

four (4) were imprinted with a hexapeptide, Ac-DYEPEA. During the syntheses, the peptide templates dissolved well in the buffer selected, as the templates used were highly hydrophilic in nature. Also, it was observed that when the polymerisation initiation components were added into the polymerisation mixture, the solution turned quickly into gel. The first generation of hydrogels were prepared with the mole ratios of template to functional monomer(s) set at 1:4 and 1:320. While the mole ratio of template to functional monomer(s) was increased from 1:4 to 1:320, the amount of the acrylamide was decreased at the same time. This was required in order to keep the concentrations of the gel components and crosslinker at 6% (w/v) and 3% (w/w), respectively. All the hydrogels prepared were sent and supplied to Ruhr-Universität Bochum, Germany, and the molecular recognition of polymers were tested by Prabal Subedi, a PhD student in Bochum.

The hydrogels considered as the second generation included two (2) distinct hydrogel MIPs and two (2) corresponding non-imprinted counterparts (NIPs) (Table 5.2). MIPs were imprinted with a decapeptide, Ac-EGYQDYEPEA, and *N*-(3-aminopropyl)methacrylamide hydrochloride was used as the sole functional monomer. During testing of the first generation of hydrogels, the highest enrichment of  $\alpha$ -Synuclein was observed when the decapeptide together with *N*-(3-aminopropyl)methacrylamide hydrochloride were used for the synthesis of the hydrogels. The second generation of hydrogels was prepared with the mole ratios of template to functional monomer set at 1:16 and 1:32 (Table 5.2). During testing, both the non-imprinted and imprinted hydrogels prepared with high functional monomers content, prepared with a ratio of template: functional monomer set at 1:320, gave the best bindings to the target peptides. However, low recoveries of  $\alpha$ -Synuclein were observed, which reached a max. value of 30 %. It would suggest that the most of the  $\alpha$ -Synuclein remained entrapped inside the gel network through non-specific interactions. Therefore, in order to minimise this random incorporation of functional monomer into the gel networks, which contributes to the formation of non-specific binding sites, smaller amounts of functional monomer should be used. However, the mole ratio of template: functional monomer(s) should be higher than 1:4, as it was

observed during testing that none of the hydrogels with the mole ratio of 1:4 were able to enrich  $\alpha$ -Synuclein. The concentrations of gel components (T) and crosslinker (C) were kept at 6% (w/v) and 3% (w/w), respectively.

The second generation of hydrogels was sent to Prabal Subedi, a PhD student from Ruhr-Universität Bochum, Germany.

#### 5.3.1.1 Selection of the templates

The epitope approach<sup>17-20</sup>, as described elsewhere in the Thesis, was used for the design of molecularly imprinted hydrogels. Sequences of six and ten amino acids (DYEPEA and EGYQDYEPEA), corresponding to the C-terminal sequence of  $\alpha$ -Synuclein peptide, were selected as the target analytes for the absolute quantification of  $\alpha$ -Synuclein protein in cerebrospinal fluid samples. Close structural analogues of the peptides were used as templates for the synthesis of MIPs, rather than using the DYEPEA or EGYQDYEPEA as templates, to avoid the possibility of template bleeding interfering with the quantification of the biomarker. The templates used were Ac-DYEPEA and Ac-EGYQDYEPEA, where the N-terminus of the C-terminal of  $\alpha$ -Synuclein peptides have been acetylated.

#### 5.3.1.2 Selection of the functional monomer(s)

*N*-(2-Aminoethyl)methacrylamide hydrochloride (EAMA.HCl) and *N*-(3-aminopropyl)methacrylamide (AMP) hydrochloride were both selected as functional monomers since the carboxylic acid groups in the glutamic acid (E) and aspartic acid (D) residues, and C-terminus of the templates were targeted *via* a non-covalent molecular imprinting approach. Indeed, *N*-(2-aminoethyl)methacrylamide hydrochloride has been shown to be useful for the targeting of oxy-anions.<sup>21-23</sup> *N*-(3-Aminopropyl)methacrylamide hydrochloride was used successfully as the positively charged functional monomer for the synthesis of imprinted soluble nanoparticles, known as “plastic antibodies”.<sup>24</sup> Also, acrylamide itself, apart from

functioning as the backbone monomer in the formation of insoluble gel, was involved in the self-assembly with the templates (Ac-DYEPEA and Ac-EGYQDYEPEA).

### 5.3.1.3 Selection of the mole ratio of template: functional monomer(s)

An important consideration in the molecular imprinting design process was the ratio of template to functional monomer(s). The mole ratios of template to EAMA.HCl and APM were set at 1:4, 1:320, 1:16 and 1:32. These ratios were selected based on the experience gained in the Cormack Polymer Group.

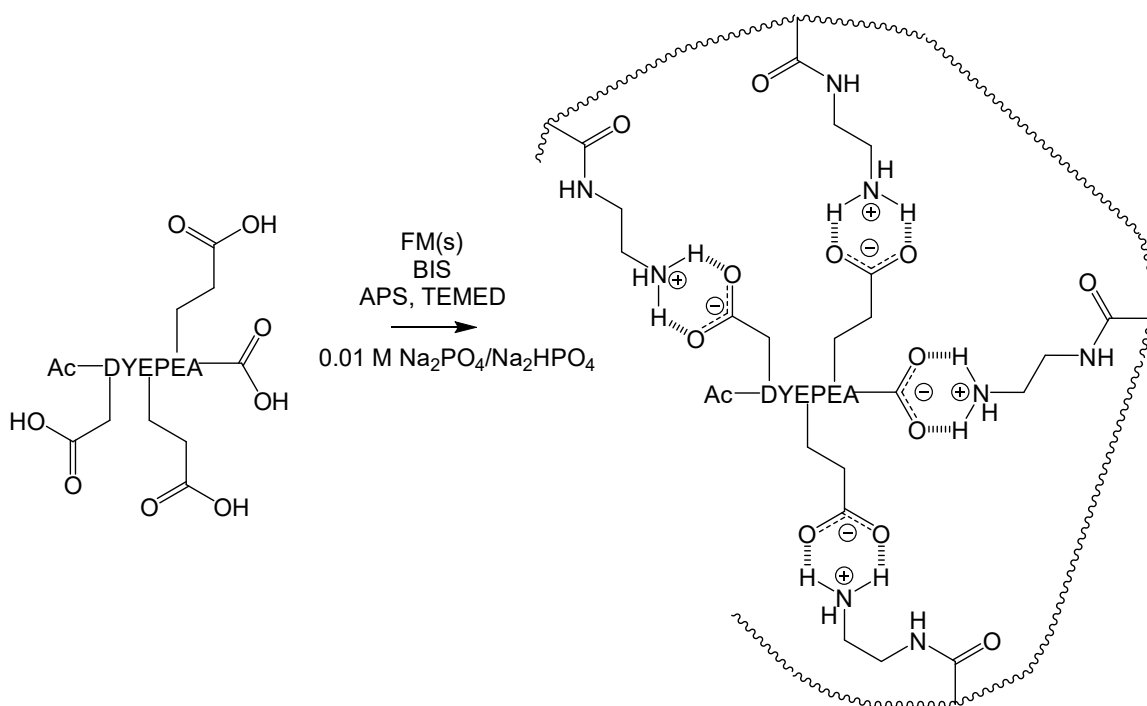


Figure 5.1 Schematic representation of the non-covalent molecular imprinting of a structural analogue of the  $\alpha$ -Synuclein peptide. The carboxylic acid groups in the glutamic acid (E) and aspartic acid (D) residues, and C-terminus of Ac-DYEPEA are drawn explicitly for emphasis, since these functional groups are involved in the self-assembly of the Ac-DYEPEA with functional monomers. The complexed synthetic receptor (right hand side) depicts a molecularly imprinted binding site formed upon the free radical copolymerisation of a 1:1:3 molecular complex of Ac-DYEPEA, acrylamide and N-(2-aminoethyl)methacrylamide hydrochloride.

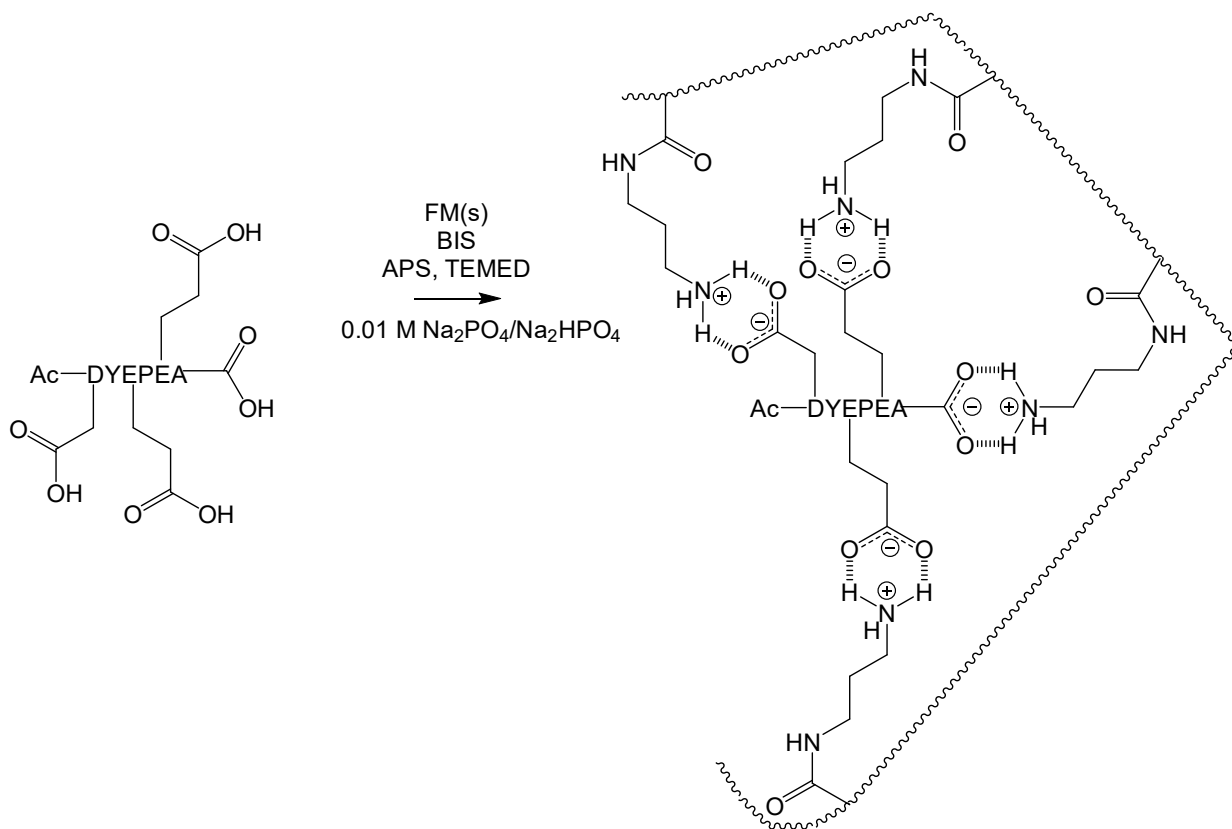


Figure 5.2 Schematic representation of the non-covalent molecular imprinting of a structural analogue of the  $\alpha$ -Synuclein peptide. The carboxylic acid groups in the glutamic acid (E) and aspartic acid (D) residues, and C-terminus of Ac-DYEPEA are drawn explicitly for emphasis, since these functional groups are involved in the self-assembly of the Ac-DYEPEA with functional monomers. The complexed synthetic receptor (right hand side) depicts a molecularly imprinted binding site formed upon the free radical copolymerisation of a 1:1:3 molecular complex of Ac-DYEPEA, acrylamide and N-(3-aminopropyl)methacrylamide hydrochloride.

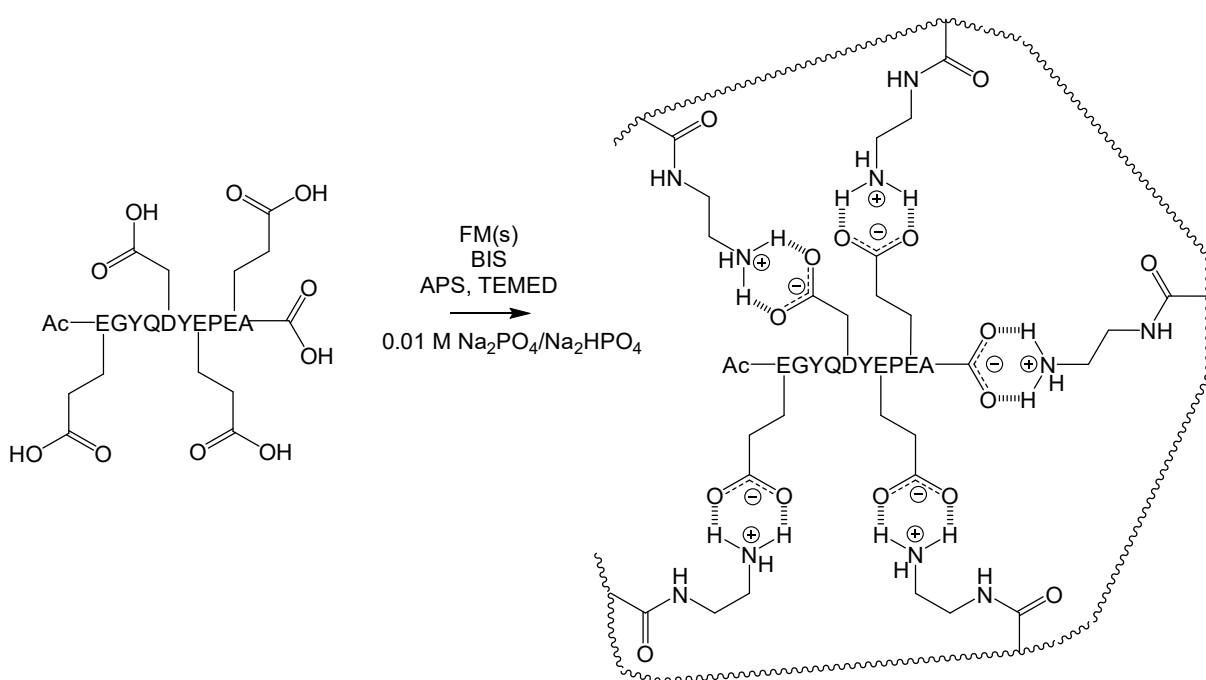


Figure 5.3 Schematic representation of the non-covalent molecular imprinting of a structural analogue of the  $\alpha$ -Synuclein peptide. The carboxylic acid groups in the glutamic acid (E) and aspartic acid (D) residues, and C-terminus of Ac-EGYQDYEPEA are drawn explicitly for emphasis, since these functional groups are involved in the self-assembly of Ac-EGYQDYEPEA with functional monomers. The complexed synthetic receptor (right hand side) depicts a molecularly imprinted binding site formed upon the free radical copolymerisation of a 1:1:4 molecular complex of Ac-EGYQDYEPEA, acrylamide and N-(2-aminoethyl)methacrylamide hydrochloride.



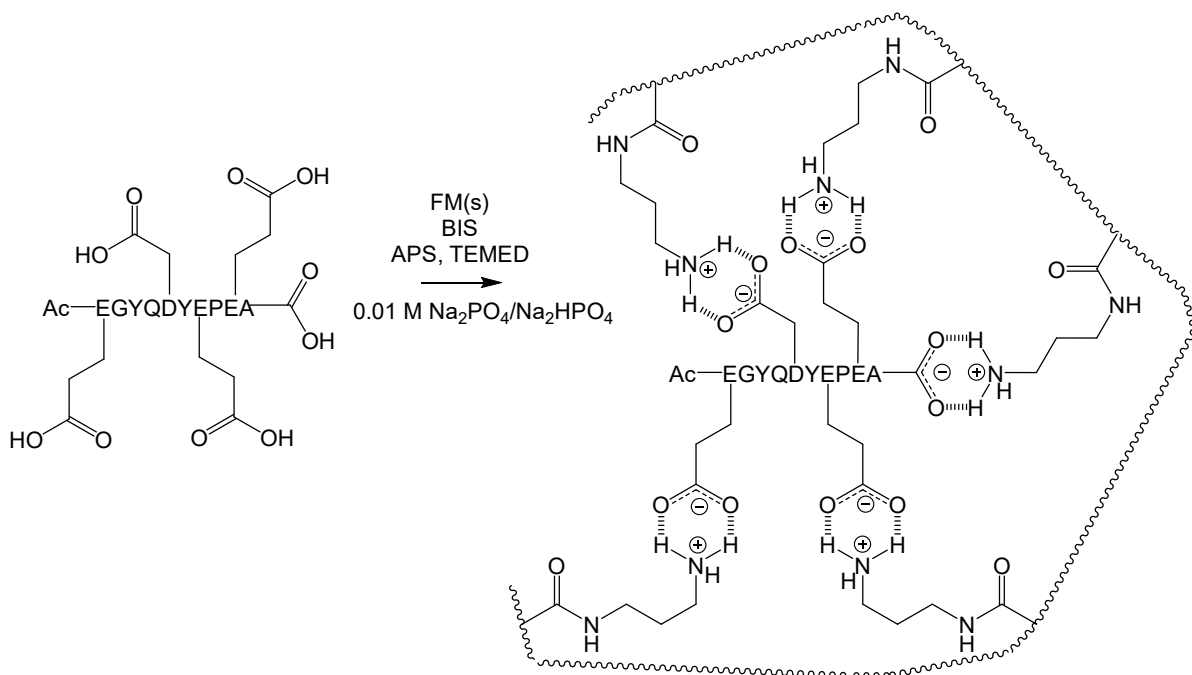


Figure 5.4 Schematic representation of the non-covalent molecular imprinting of a structural analogue of the  $\alpha$ -Synuclein peptide. The carboxylic acid groups in the glutamic acid (E) and aspartic acid (D) residues, and C-terminus of Ac-EGYQDYEEPA are drawn explicitly for emphasis, since these functional groups are involved in the self-assembly of the Ac-EGYQDYEEPA with functional monomers. The complexed synthetic receptor (right hand side) depicts a molecularly imprinted binding site formed upon the free radical copolymerisation of a 1:1:4 molecular complex of Ac-EGYQDYEEPA, acrylamide and N-(3-aminopropyl)methacrylamide hydrochloride.

### 5.3.2 Molecular recognition of the first generation of hydrogels

The molecular recognition characteristics of the hydrogels were interrogated by Prabal Subedi, a PhD student from Ruhr-Universität Bochum, Germany. The feedback from Prabal was valuable and allowed optimisation further steps for the synthesis of the second generation of hydrogels for the  $\alpha$ -Synuclein target.

The analytical work presented below was performed by Prabal Subedi, a PhD student from Ruhr-Universität Bochum, Germany and published in his PhD thesis.<sup>25</sup> The following two and half (2.5) pages of text is abstracted from the thesis.

In order to check if hydrogels could capture  $\alpha$ -Synuclein protein from a real complex sample, HEK cell lysate was used. In a 5  $\mu$ g HEK cell lysate in 0.01 M sodium phosphate buffer, 35 ng  $\alpha$ -Synuclein was spiked in and an enrichment procedure followed by western blot applied. A typical capture of  $\alpha$ -Synuclein protein can be observed in Figure 5.5 where the non-bound and elution fractions were dried, redissolved in lithium dodecyl sulfate buffer and one dimensional gel electrophoresis followed by a western blot was performed. 35 ng  $\alpha$ Syn was denatured by heating at 95  $^{\circ}$ C for 10 min and loaded on the same gel as control. The non-bound fraction was the supernatant collected after the hydrogels were incubated with the HEK lysate. The elution fraction was the supernatant that was collected and pooled after three consecutive elutions of the hydrogels with 0.1 % trifluoroacetic acid.<sup>25</sup>

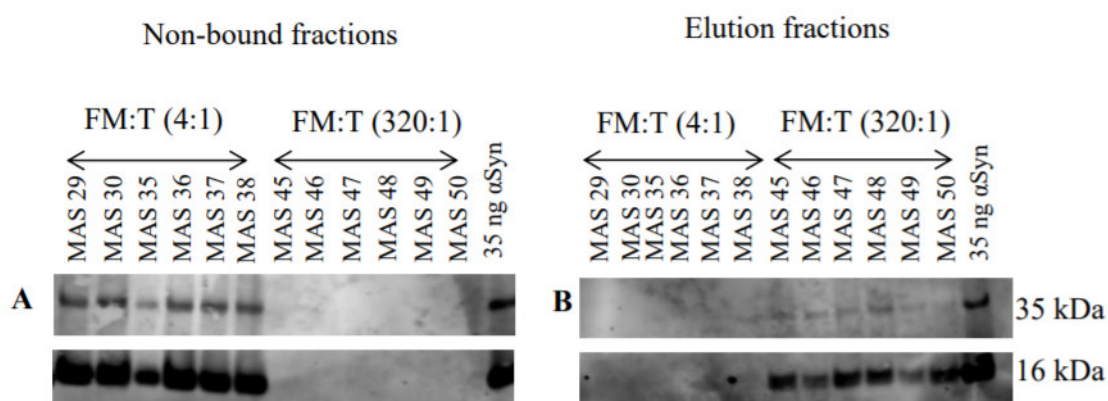


*Figure 5.5 The enrichment of  $\alpha$ -Synuclein by hydrogels with a functional monomer to template (FM:T) ratio of 320:1 (MAS45 - MAS50) revealed by the absence of bands in the (A) non-bound fractions and a presence of bands in the (B) elution fractions when the hydrogels were incubated with a mixture of 5 $\mu$ g HEK lysate containing 35 ng  $\alpha$ -Synuclein. The western blot was performed using anti-  $\alpha$ -Synuclein antibody and the  $\alpha$ -Synuclein monomers can be observed at 16 kDa whereas the dimers at 35 kDa. The hydrogels with FM:T ratio of 4:1 did not enrich  $\alpha$ -Synuclein as revealed by the presence of  $\alpha$ -Synuclein bands only in the non-bound fractions.<sup>25</sup>*

A densitometric quantification was performed for three experiments to determine the efficiency of the enrichment procedure. The enrichment of  $\alpha$ -Synuclein was determined by the ratio of the amount of  $\alpha$ -Synuclein in elution fraction compared

to the initial starting material (35 ng  $\alpha$ -Synuclein). Only the hydrogels that could enrich  $\alpha$ -Synuclein (*i.e.*, MAS45- MAS50) were taken for such quantifications and can be seen in Figure 5.6.<sup>25</sup>

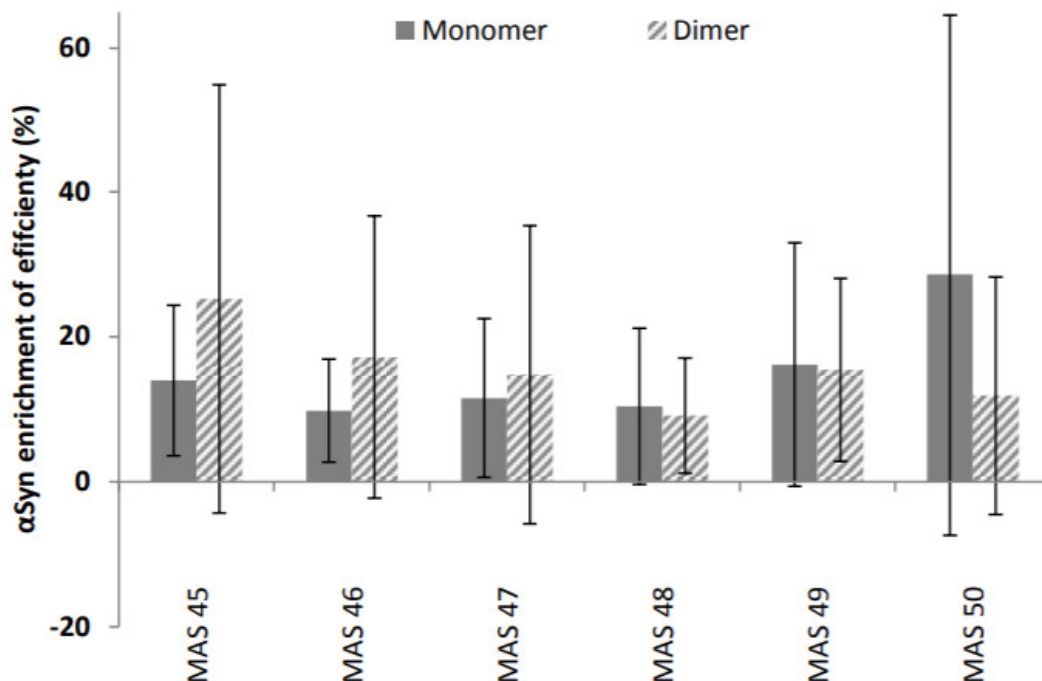


Figure 5.6 The enrichment efficiency of  $\alpha$ -Synuclein with the polymers MAS45 - MAS50 via densitometry ( $n=3$ ). The 'eluted' fractions after three western blot experiments (example of western blot shown in Figure 5.5) were quantified via Odyssey software. The efficiency in percentage is provided in the y-axis and the different polymers in the x-axis. In best cases, only  $\sim 30\%$  monomeric  $\alpha$ -Synuclein was recovered.<sup>25</sup>

Both non-imprinted and imprinted hydrogels prepared with high functional monomer content, made with a ratio of template: functional monomer set at 1:320, performed best in binding to target protein, regardless of the functional monomer used (Figure 5.5). These observations could be attributed to the fact that with an increasing amount of functional monomers, the chances that more high fidelity binding sites are formed is higher, assuming that all the functional monomers take part in the formation of binding sites. Also, the hydrogels synthesised with the longer template showed better binding than those prepared with the shorter one. It could

be explained by the fact that the binding sites were better accessible for the bindings of the target peptide when the hydrogels were formed with decapeptide as the template. Another issue was the low recoveries of  $\alpha$ -Synuclein, which reached a max. of 30 % (Figure 5.6). It means that most of the  $\alpha$ -Synuclein remained entrapped inside the gel network through non-specific interactions. Also, it was observed that NIPs bound more target peptide than the MIPs. This was not the results which was expected, however, this phenomenon is not new in the imprinting field.<sup>26</sup>

The molecular recognition of the second generation of hydrogels for the  $\alpha$ -Synuclein target have not been tested yet. Information on molecular recognition would be invaluable in respect of the further optimisation of synthetic protocols.

## 5.4 Conclusions and outlook

The scope of the work presented in this chapter spans the design, synthesis and molecular characterisation of a first and second generation of imprinted polymers for the  $\alpha$ -Synuclein target. The synthesised polymers have been produced in a hydrogel format *via* redox polymerisation. All hydrogels were supplied to PEPMIP partners for testing and evaluation. Although the second generation of hydrogels has not yet been tested, the first generation of materials (both imprinted and non-imprinted hydrogels) prepared with high content *N*-(3-aminopropyl)methacrylamide and imprinted with longer template (decapeptide), show affinity for  $\alpha$ -Synuclein. However, low recoveries of  $\alpha$ -Synuclein were observed, which reached a max. value of 30 %. It would suggest that most of the  $\alpha$ -Synuclein remained entrapped inside the gel network through non-specific interactions. Therefore, in order to minimise this random incorporation of functional monomer into gel network, the ratio of template: functional monomer(s) was revised during the synthesis of the second generation of hydrogels for the  $\alpha$ -Synuclein target.

Overall, the Hjertén procedure was implemented successfully for the synthesis of the next generation of MIPs for the  $\alpha$ -Synuclein target. The second generation of

hydrogels needs to be tested extensive in order to lead conclusions and eventually further optimisation of the synthesis of the hydrogel MIPs.

## 5.5 Bibliography

- 1 V. M. Y. Lee and J. Q. Trojanowski, *Neuron*, 2006, **52**, 33–38.
- 2 J. M. Rosiak and F. Yoshii, *NIM B*, 1999, **151**, 56–64.
- 3 R. Barbucci, *Hydrogels Biological Properties and Applications*, Springer-Verlag, Milan, 2009.
- 4 M. Ebara, Y. Kotsuchibashu, R. Narain, N. Idota, Y.-J. Kim, J. M. Hoffman, K. Uto and T. Aoyagi, *Smart Biomaterials*, Springer Japan, 1st edn., 2014.
- 5 B. Strachota, L. Matejka, A. Zhigunov, R. Konefał, J. Spevacek, J. Dybal and R. Puffr, *Soft Matter*, 2015, **11**, 9291–9306.
- 6 S. Hjertén, J.-L. Liao, K. Nakazato, Y. Wang, G. Zamaratskaia and H.-X. Zhang, *Chromatographia*, 1997, **44**, 227–234.
- 7 A. Takátsy, Á. Végvári, S. Hjertén and F. Kilár, *Electrophoresis*, 2007, **28**, 2345–2350.
- 8 A. Takátsy, A. Kilár, F. Kilár and S. Hjerten, *J. Sep. Sci.*, 2006, **29**, 2802–2809.
- 9 K. Hirayama, Y. Sakai and K. Kameoka, *J. Appl. Polym. Sci.*, 2001, **81**, 3378–3387.
- 10 S. H. Ou, M. C. Wu, T. C. Chou and C. C. Liu, *Anal. Chim. Acta*, 2004, **504**, 163–166.
- 11 T. Y. Guo, Y. Q. Xia, G. J. Hao, M. D. Song and B. H. Zhang, *Biomaterials*, 2004, **25**, 5905–5912.
- 12 T.-Y. Guo, Y.-Q. Xia, J. Wang, M.-D. Song and B.-H. Zhang, *Biomaterials*, 2005, **26**, 5737–5745.
- 13 D. M. Hawkins, D. Stevenson and S. M. Reddy, *Anal. Chim. Acta*, 2005, **542**, 61–65.
- 14 M. Yan and O. Ramström, Eds., *Molecularly Imprinted Materials: Science and Technology*, Taylor & Francis Group Ltd, LLC, New York, 2004.
- 15 N. W. Turner, C. W. Jeans, K. R. Brain, C. J. Allender, V. Hlady and D. W. Britt, *Biotechnol Prog.*, 2006, **22**, 1474–1489.
- 16 A. Bossi, F. Bonini, A. P. F. Turner and S. A. Piletsky, *Biosens. Bioelectron.*, 2007, **22**, 1131–1137.
- 17 A. Rachkov and N. Minoura, *Biochim. Biophys. Acta*, 2001, **1544**, 255–266.

18 A. Rachkov and N. Minoura, *J. Chromatogr. A*, 2000, **889**, 111–118.

## 6. General conclusions and future work

In this Thesis, a generic synthetic protocol for the synthesis of protein-imprinted polymers has been developed. We can identify immediately the great advantage of using this approach, since it allows for the rapid production of peptide imprinted polymers in a convenient microsphere format with bead diameters around  $\sim 2 \mu\text{m}$ . Particles of such a size are highly desirable in the separation science. When they are used as stationary phase in analytical column, they are packaged more efficiently than their non-microsphere counterparts giving better flow properties and higher efficiencies, thus providing better separation. Last but not least, MIPs in the format of microspheres provide significantly faster binding kinetics, better accessibility of binding sites, higher binding affinity and specificity to target analytes than irregular particulates.<sup>1</sup>

It is essential to stress the importance of the methodology developed in the Thesis work, as the synthesis of protein-imprinted polymers has always been challenging. Proteins are large and complex molecules with conformational flexibility along their backbones. They are typically insoluble in organic solvents, which makes them even more tricky to imprint.<sup>2</sup> The mobility of large molecules such as proteins are limited within highly crosslinked polymer networks, and this may prevent efficient protein template removal.<sup>3</sup> Also, the conditions that are used for the removal of the protein template from the prepared polymer have to be chosen carefully. There is a risk that the binding sites created in the polymer network can interact with the components that are present in the washing solvent, for instance with sodium dodecyl sulfate (SDS), resulting in creation of polymeric sorbents with non-specific binding sites known as artefacts.<sup>4</sup> The synthetic approach developed in the Thesis work was successfully applied for the synthesis of peptide imprinted polymers for three



different targets: ProGrp for Small Cell Lung Cancer (SCLC), A $\beta$ -Amyloid for Alzheimer's Disease (AD) and  $\alpha$ -Synuclein for Parkinson's Disease (PD). There is a huge demand in the market for cheap and fast diagnostic tools that could allow for the reliable detection of peptide-based biomarkers for SCLC, AD and PD in their early stages. The developed approach allows for cheap production of peptide imprinted polymers with outstanding affinity and selectivity in an optimal way, as it was revealed in new analytical protocol developed for the diagnosis of SCLC using serum samples. Therefore, we believe that the peptide imprinted polymers targeting ProGRP, A $\beta$ -Amyloid and  $\alpha$ -Synuclein produced in the Thesis work are attractive alternatives to the diagnostic methods currently available.

In fact, in this Thesis four different formats of MIPs for the peptide-based biomarkers have been developed and described.

The first generation of MIPs was polymers produced in a microsphere format *via* precipitation polymerisation. Macroreticular, discrete particles in the micron-sized range have been produced, although the microspheres were polydisperse. Nevertheless, the particles were suitable for packing into trap columns. Although not all materials have been completely tested, the MIPs prepared, especially those relevant to SCLC, show a promising degree of imprinting-related selectivity. In fact, a new sensitive analytical protocol for SCLC has been developed using these materials.

The second generation of MIPs was produced in a core-shell format *via* a two-step precipitation polymerisation process. The core-shell particles were prepared with diameters  $\sim 2 \mu\text{m}$  which makes them suitable for the packing into SPE cartridges. The second generation of polymers were prepared in good quality with narrow particle size distribution. Selected polymers were supplied to PEPMIP partners for testing and evaluation. Although, the materials have been not tested yet, we believe that the core-shell format will help to overcome the problems which were reported during the testing of the first generation of materials.

The third generation of MIPs was produced in a magnetic microsphere and magnetic core-shell formats *via* precipitation polymerisation and two-step precipitation polymerisation. The magnetic component, magnetite, was either encapsulated or incorporated inside the polymer network structures. Although the polymers with encapsulated magnetic components were prepared in low yield, and the particles were relatively small in size, these drawbacks were overcome by the application of the magnetisation procedure for the incorporation of magnetite into the non-magnetic polymer network. The procedure allows magnetic polymers to be prepared in relatively good yield, in some cases the yield even reached 22% or 28%. Also, the method revealed an interesting magnetisation mechanism; magnetite can grow efficiently inside the polymer pores providing permanent magnetic properties.

Selected polymers were supplied to PEPMIP partners for testing and evaluation. Although the materials have not yet been tested fully, the initial results are promising, we believe that the magnetic core-shell polymers would help to overcome the problems which were reported during the testing of the first generation of materials.

MIPs were also prepared in the form of hydrogels. MIPs for the  $\alpha$ -Synuclein target were prepared by redox polymerisation through implementation of the Hjertén procedure. All hydrogels were supplied to PEPMIP partners for testing and evaluation. Although, the second generation of hydrogels has not been tested yet, the first generation of materials (both imprinted and non-imprinted hydrogels prepared with high content of *N*-(3-aminopropyl)methacrylamide and imprinted with longer template; a decapeptide), show affinity for  $\alpha$ -Synuclein. However, low recoveries of  $\alpha$ -Synuclein were obtained, which reached a max. of 30%. The second generation of hydrogels needs to be extensively tested in order to lead to conclusions and eventually further optimisation of the synthesis for the hydrogel MIPs.

Overall, four different formats of MIPs for the peptide-based biomarkers were synthesised and characterised, and sent to PEPMIP partners for testing and evaluation. A new analytical protocol has been developed for the diagnosis of SCLC

using serum samples, and significant progress made towards the development of MIPs suitable for the detection of AD and PD.

## Bibliography

- 1 B. Sellergren, Ed., *Molecularly Imprinted Polymers—Man-Made Mimics of Antibodies and Their Application in Analytical Chemistry*, Elsevier, Amsterdam, 2001.
- 2 K. Haupt, A. V Linares, M. Bompert and B. Tse Sum Bui, *Top. Curr. Chem.*, 2012, **325**, 1–28.
- 3 L. Chen, S. Xu and J. Li, *Chem. Soc. Rev.*, 2011, **40**, 2922–2942.
- 4 E. Verheyen, J. P. Schillemans, M. van Wijk, M.-A. Demeniex, W. E. Hennink and C. F. van Nostrum, *Biomaterials*, 2011, **32**, 3008–3020.

# Appendix 1 BET isotherms

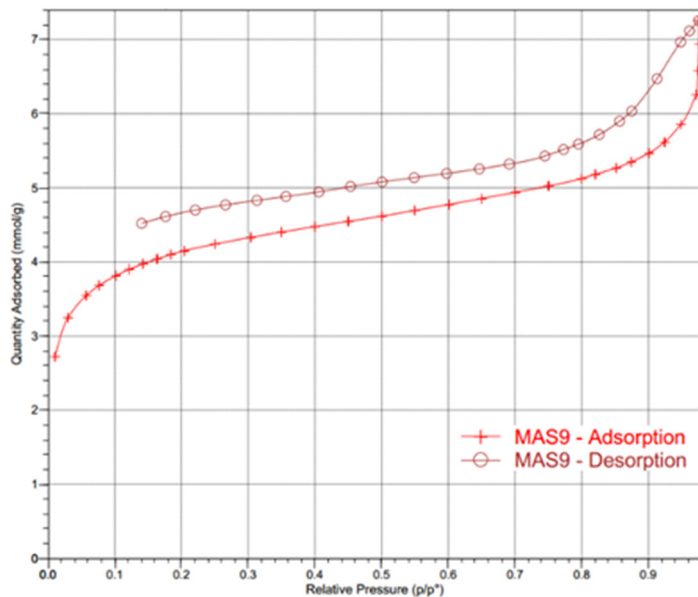


Figure I  $N_2$  sorption for isotherm MAS9, poly(N-3,5-bis(Trifluoromethyl)-phenyl-N'-4-vinylphenylurea-co-EAMA.HCl-co-DVB-80) at 77.58 K.

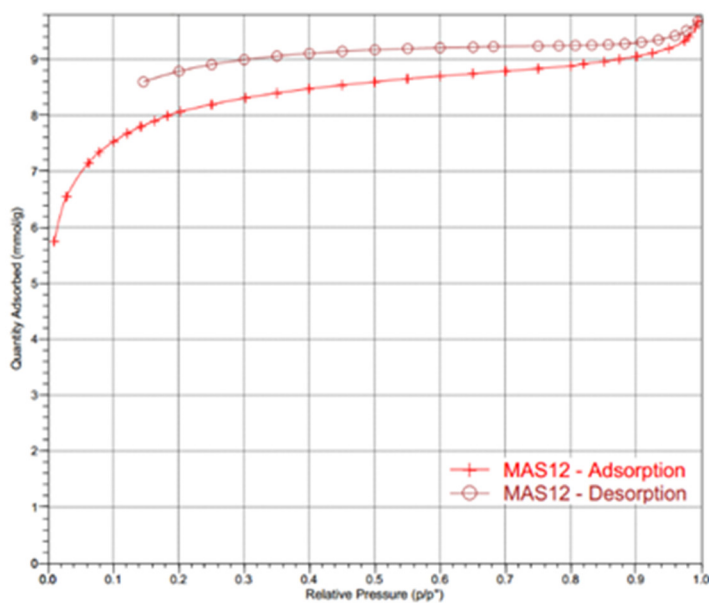


Figure II  $N_2$  sorption isotherm for MAS12, poly(N-3,5-bis(Trifluoromethyl)-phenyl-N'-4-vinylphenylurea-co-EAMA.HCl-co-DVB-80) at 77.47 K.

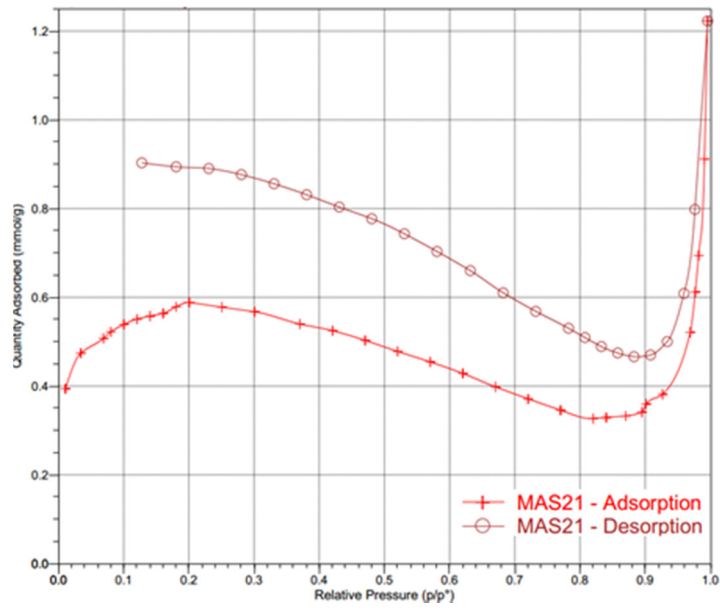
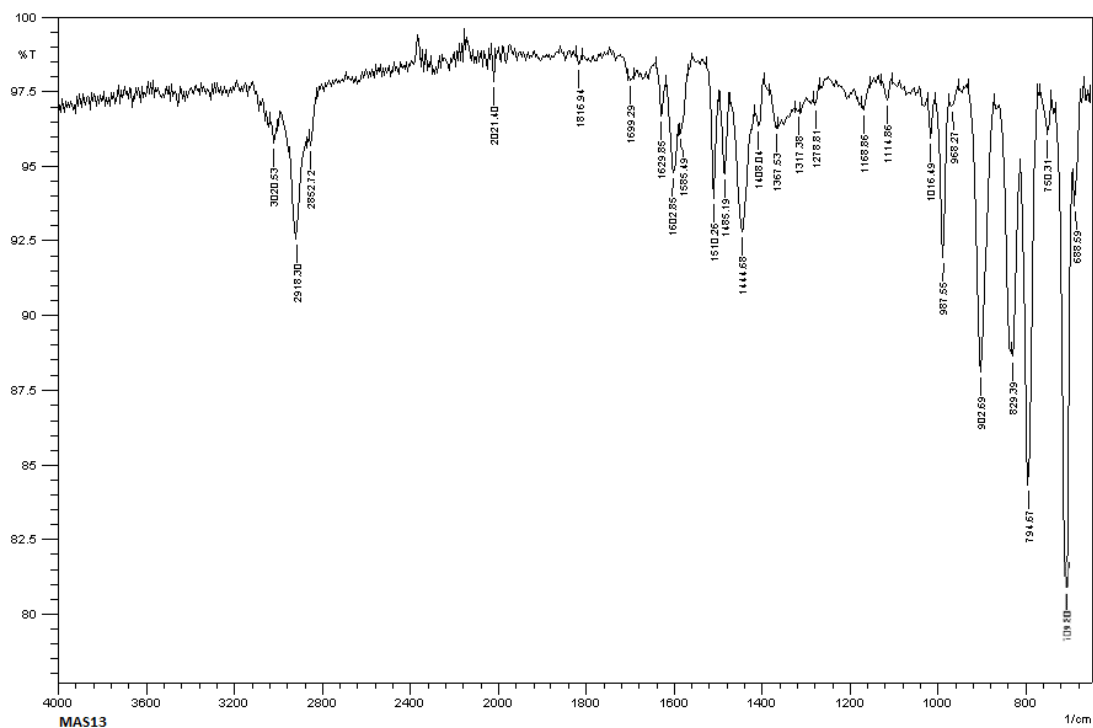


Figure III N<sub>2</sub> sorption isotherm for MAS21, poly(EAMA.HCl-co-DVB-80) at 77.31 K.

# Appendix 2 FT-IR spectra



Approximate stretching frequency (cm <sup>-1</sup> )	Group
3020	Aromatic C-H
2918	Aliphatic C-H
1602, 1510 and 1485	Aromatic C=C
987 and 902	Aliphatic C=C
829	<i>para</i> -di- substituted benzene
794 and 709	<i>meta</i> -di- substituted benzene

Figure 1 FT-IR spectrum of MAS13 and assignments of FT-IR peaks.

# Appendix 3 Manuscript

## **Automated Protein Biomarker Analysis: on-line extraction of clinical samples by Molecularly Imprinted Polymers**

Cecilia Rossetti<sup>1</sup>, Magdalena A. Świtnicka-Plak<sup>2</sup>, TrineGrønhaug Halvorsen<sup>1</sup>, Peter A. G. Cormack<sup>2</sup>, Börje Sällergren<sup>3</sup> & Léon Reubsæet<sup>1</sup>

Manuscript published in March 2017 at *Scientific Reports*

<sup>1</sup>Department of Pharmaceutical Chemistry, University of Oslo, School of Pharmacy, Postbox 1068 Blindern, 0316 Oslo, Norway. <sup>2</sup>WestCHEM, Department of Pure and Applied Chemistry, University of Strathclyde, Thomas Graham Building, 295 Cathedral Street, Glasgow, G1 1XL, United Kingdom. <sup>3</sup>Department of Biomedical Sciences, Faculty of Health and Society, Malmö University, SE20506 Malmö, Sweden. Correspondence and requests for materials should be addressed to L.R. (email: leon.reubsæet@farmasi.uio.no).



# SCIENTIFIC REPORTS



OPEN

## Automated Protein Biomarker Analysis: on-line extraction of clinical samples by Molecularly Imprinted Polymers

Received: 22 August 2016

Accepted: 26 January 2017

Published: 17 March 2017

Cecilia Rossetti<sup>1</sup>, Magdalena A. Świtnicka-Plak<sup>2</sup>, Trine Grønhaug Halvorsen<sup>1</sup>, Peter A.G. Cormack<sup>2</sup>, Börje Sellergren<sup>3</sup> & Léon Reubsaet<sup>1</sup>

Robust biomarker quantification is essential for the accurate diagnosis of diseases and is of great value in cancer management. In this paper, an innovative diagnostic platform is presented which provides automated molecularly imprinted solid-phase extraction (MISPE) followed by liquid chromatography-mass spectrometry (LC-MS) for biomarker determination using ProGastrin Releasing Peptide (ProGRP), a highly sensitive biomarker for Small Cell Lung Cancer, as a model. Molecularly imprinted polymer microspheres were synthesized by precipitation polymerization and analytical optimization of the most promising material led to the development of an automated quantification method for ProGRP. The method enabled analysis of patient serum samples with elevated ProGRP levels. Particularly low sample volumes were permitted using the automated extraction within a method which was time-efficient, thereby demonstrating the potential of such a strategy in a clinical setting.

Automated biomarker analysis is attracting significant attention in the field of proteomics<sup>1</sup>. Furthermore, biomarker analyses which require low sample volumes and minimal sample handling steps are of particular interest in clinics. Very often, it is the limited availability of sample together with the need for a reliable, cost- and time-effective method which leads to “conventional” immunoassays being preferred over innovative mass spectrometry (MS) assays<sup>2</sup>. In recent years, there has been an intense focus upon automated systems directly integrating sample preparation with MS bioanalysis to satisfy clinical requirements<sup>3–5</sup>. Within this context, many efforts have been made to develop reliable and sensitive MS alternatives to immunoassays for biomarker quantification, including MS assays for the low abundant biomarker ProGastrin Releasing Peptide (ProGRP) which has been studied widely as model biomarker<sup>6–12</sup>.

ProGRP is a sensitive (reference level of 7.6 pM in serum) and specific biomarker with diagnostic and prognostic value for Small Cell Lung Cancer (SCLC)<sup>13–18</sup>. Hence, quantitative information on its abundance in serum will strongly impact SCLC management.

Currently, ProGRP is analysed in the clinics by ELISA with a time-resolved immunofluorometric assay (TR-IFMA)<sup>19</sup>. However, targeted proteomic immuno-MS assays<sup>10,11</sup> have also been developed, allowing the quantification of ProGRP through a bottom-up approach. The use of immunoextraction prior to the MS analysis was shown to be essential for the realization of low detection limits, to enable discrimination between healthy and patient donors according to ProGRP expression. Other studies have focused on ProGRP extraction with the aim of replacing antibodies with synthetic receptors<sup>20,21</sup>. In this regard, molecularly imprinted polymers (MIPs) were developed and used as “plastic antibodies” for the off-line enrichment of the ProGRP signature peptide (NLLGLIEAK) from serum. This method was well-suited for coupling with the MS assays developed previously<sup>11</sup> and represented a fast and economical alternative to immunocapture. However, the off-line MIP extraction was unable to determine ProGRP concentrations close to the reference level due to the high detection limits of the off-line method<sup>21</sup>. The MIPs used in the aforementioned study were synthesized *via* a template analogue

<sup>1</sup>Department of Pharmaceutical Chemistry, University of Oslo, School of Pharmacy, Postbox 1068 Blindern, 0316 Oslo, Norway. <sup>2</sup>WestCHEM, Department of Pure and Applied Chemistry, University of Strathclyde, Thomas Graham Building, 295 Cathedral Street, Glasgow, G1 1XL, United Kingdom. <sup>3</sup>Department of Biomedical Sciences, Faculty of Health and Society, Malmö University, SE20506 Malmö, Sweden. Correspondence and requests for materials should be addressed to L.R. (email: leon.reubsaet@farmasi.uio.no)

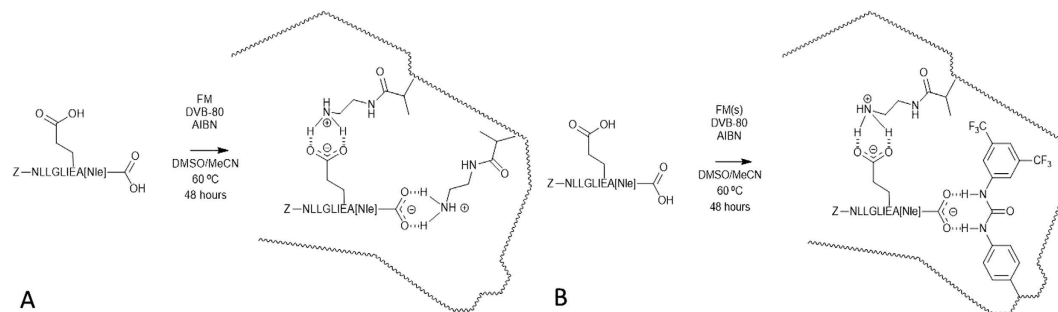


**Figure 1. Representation of the non-covalent molecular imprinting of Z-NLLGLIEA[Nle] for MIP A (A) and MIP B (B).** The carboxylic acid groups in the glutamic acid (E) residue and C-terminus of Z-NLLGLIEA[Nle] are drawn explicitly for emphasis, since these functional groups are involved in the self-assembly of the Z-NLLGLIEA[Nle] with the functional monomers (FMs). The complexed synthetic receptors depict the hypothetical molecularly imprinted binding sites formed upon the free radical copolymerisation of a molecular complex of Z-NLLGLIEA[Nle] and FM(s) with crosslinker (DVB-80).

imprinting strategy, a powerful approach reported previously by Manesiotis *et al.*<sup>22</sup>. In the case of ProGRP, an analogue of the signature peptide was used as template in the production of thin MIP films on silica beads surfaces *via* a non-covalent molecular imprinting protocol, giving core-shell RAFT-beaded particles.

The use of uniform, beaded MIPs is particularly desirable in challenging separation science applications since beads are physically robust and can be easily and reproducibly packed into solid-phase extraction (SPE) cartridges and chromatographic columns, circumventing any fluid flow problems arising from high back pressures<sup>23–25</sup>. Uniform, beaded MIPs with low mean particle sizes offer yet further advantages since the low particle size leads to high separation efficiencies thanks to the fast binding kinetics arising from improved accessibility of binding sites<sup>26</sup>.

Precipitation polymerization is a very attractive synthetic method for the synthesis of MIP microspheres<sup>27–33</sup>. MIP microspheres of controlled size and porosity are obtained easily by the tuning of polymerization conditions<sup>34–36</sup> without the need for surfactants or stabilizers, delivering clean products with narrow particle size distributions. Typically, the microspheres are obtained in one synthetic step and the particle diameters are normally in the range 0.1–10  $\mu\text{m}$ <sup>37</sup>. MIP microspheres are thus particularly well-suited as molecularly selective packings in trap columns for integration with MS systems, as will be demonstrated in this study.

Within this context, molecularly selective polymeric sorbents were prepared by precipitation polymerization to develop an innovative diagnostic approach for ProGRP quantification, involving automated MIP-based extraction coupled with liquid chromatography-MS (LC-MS). The main goal was to evaluate the performance of the new, automated MIP extraction method on patient serum samples containing clinically relevant concentrations of ProGRP.

## Results and Discussion

**Synthesis of MIPs: template, functional monomers and crosslinker selection.** The template used was Z-NLLGLIEA[Nle]; in effect, the N-terminus of the signature peptide has been protected with a benzyloxy-carbonyl group (Cbz; Z) to enhance the solubility of the template in the porogenic solvents used for the polymerization, and the C-terminal lysine has been replaced by norleucine (Nle)<sup>21</sup>. The latter modification was introduced in order to overcome the intramolecular competition for the anionic sites caused by the lysine side.

Two different functional monomers were used, N-(2-aminoethyl)methacrylamide hydrochloride (EAMA.HCl), solely for MIP A, and N-3,5-bis(trifluoromethyl)-phenyl-N'-4-vinylphenylurea, together with EAMA.HCl for MIP B, since the carboxylic acid groups in the glutamic acid (E) residue and C-terminus of the template were targeted *via* a non-covalent molecular imprinting approach. Indeed, both monomers have been shown to be useful for the targeting of oxy-anions<sup>20,38,39</sup>. A representation of the Z-NLLGLIEA[Nle]-imprinted binding sites in MIP A and MIP B is shown in Fig. 1A and B, respectively. For success, precipitation polymerizations must involve the polymerization of monomers in dilute solution (typically <5% w/v monomer in solvent) in a near- $\ominus$  solvent, therefore DVB-80 was selected as crosslinker, the porogen was MeCN and the monomer concentration was fixed at 2% w/v. DMSO was required to promote solubility of the template, but the use of this dipolar aprotic solvent was kept to a minimum (Supplementary Table S-1).

High crosslinker levels were used to ensure good yields of mechanically robust polymer microspheres with well-developed and permanent porous morphology. The mole ratio of template to FMs was set at 1:10 (Supplementary Table S-3). This small excess promotes template-FM self-assembly, minimizing the possibility of non-specific binding events arising from the random incorporation of a large excess of FMs into the polymer networks, as reported previously<sup>39</sup>. Moreover, the choice of precipitation polymerization as synthetic protocol yielded uniform, porous, particles with low mean particle diameters (as shown below) suitable for packing into the trap columns, without any need for the silica-core which was the inner component of the larger RAFT-MIPs for ProGRP (20  $\mu\text{m}$  silica-core particles) reported earlier<sup>20,21</sup>.

**Characterization of the polymers.** The SEM micrographs of the polymers (Supplementary Fig. S-2) revealed the production of discrete particles in the low micron-sized range (diameters  $\leq 5 \mu\text{m}$ ), although the

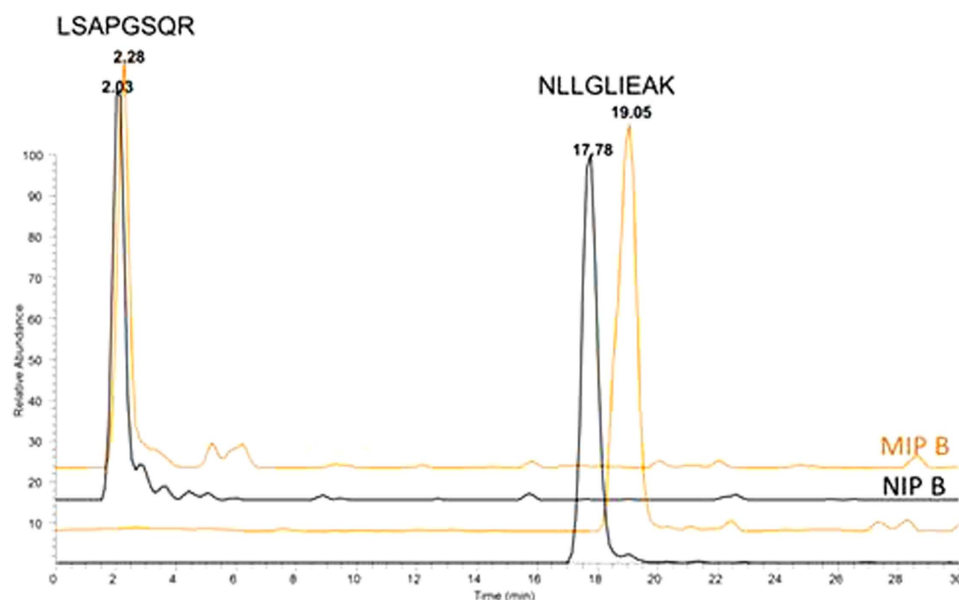


**Figure 2.** MS/MS Chromatograms of 10 nM digested ProGRP isoform 1 obtained by using MIP B (orange) and NIP B (black) coupled directly to the MS detector without analytical column.

microspheres were polydisperse (possibly as a consequence of the presence of DMSO as a co-solvent). The nitrogen sorption data (Supplementary Table S-4) revealed that the MIPs and NIPs were porous, but mean pore diameters placing them at the boundary between microporous and mesoporous solids; this was important to establish in view of the need for analyte to access molecularly imprinted binding sites during the SPE. The NIPs were not identical to the MIPs in respect of their porous morphologies, indicating an influence of the template on the timing of the phase separation<sup>40</sup>. Although this is often the case for MIP/NIP pairs, since by definition a NIP is synthesised in the absence of any template whatsoever and there can be no template influence upon the polymerization, the differences are probably accentuated here because we are operating close to the solubility limit of the template. Irrespective of the morphology differences, however, through careful optimisation binding conditions which enabled binding affinity and selectivity could be established.

**Peptide retention on MIP and corresponding NIP by direct injection of ProGRP isoform 1.** All four polymers were packed into stainless steel columns and evaluated for peptide retention by direct injection of protein digests containing the target peptide NLLGLIEAK. Thus, ProGRP isoform 1 was trypsinated and loaded on the MIP and NIP columns which were, at this stage, used as analytical columns coupled directly with the ESI source of the MS detector (Fig. 2). The SRM transitions corresponding to the ProGRP peptides (LSAPGSQR and the target peptide NLLGLIEAK) were acquired from the moment of the injection to the end of the gradient. No retention was seen for the signature peptide of isoform 1 of ProGRP (LSAPGSQR) on both MIP and NIP columns. The target peptide, NLLGLIEAK, was retained longer on the MIP (19.05 minutes), and this was reassuring given the intention to use the MIP as a trap column in a later part of the study.

The corresponding NIP B also showed affinity for NLLGLIEAK and this can be ascribed to non-covalent interactions between this peptide and the polymer. Similar retention differences and trends were observed when MIP A and NIP A were tested.

**Effect of the loading pH.** The optimal pH to promote non-covalent interactions between the target peptide and the binding sites of the MIPs was assessed by testing MIP A and B solely. Figure 3 shows the retention time and the intensities obtained on both MIPs upon loading the heavy labelled target peptide NLLGLIEA[K<sub>13</sub>C<sub>6</sub><sup>15</sup>N<sub>2</sub>] at three different pH values (3.0, 7.6 and 8.6). Loading with 20 mM FA (pH 3.0) for 10 minutes gave peptide high intensity and retention times above 27 minutes on both MIPs. Upon increasing the pH of the loading solution using 50 mM ammonium bicarbonate buffer adjusted to pH 7.6 and pH 8.6, the retention time of the peptide rises until 29.5 minutes, but a drop in signal intensity is observed simultaneously for both MIPs. The increase in peptide retention at higher pH can be rationalized as the progressive strengthening of the interactions between the positively charged EAMA residues in both polymers (pKa 9.6) and the negatively charges of the glutamic acid residue (pKa 4.2) and the C-terminal carboxylic acid (pKa 2.2) of the peptide. At pH 3.0 only 10% of the glutamic acid residues are charged while for pH >6.2 more than 99% of them are available to establish ionic interactions with the FM<sup>41</sup>. Likewise, 90% of the C-terminal carboxylic acid is charged at pH 3.0 contributing to the peptide retention which increases at higher pH.

In addition to these interactions, a combined effect of the peptide negative charges (pI 6.44) is feasible when the pH is basic. The drop in signal intensities can be ascribed to incomplete positive ionization of the peptide in the MS detector when the pH is >7. This was confirmed by direct injection in the TSQ analyzer of the peptide solutions (1 nM) with three different pH values (3.0, 7.6 and 8.6) (Supplementary Fig. S-5). Since the increase in

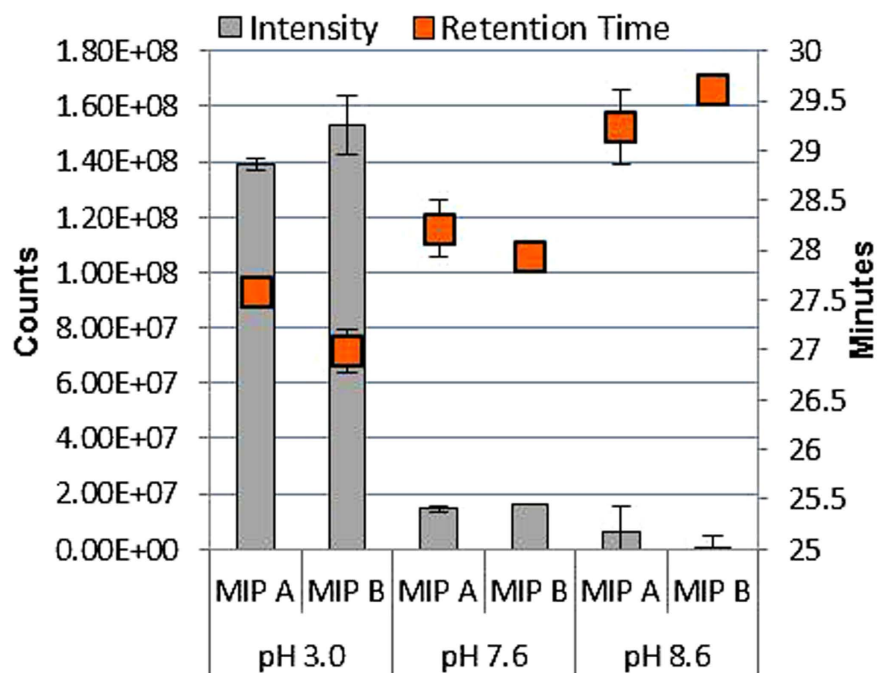


**Figure 3.** Effect of loading pH on retention times and peak areas of NLLGLIEA[K-<sup>13</sup>C<sub>6</sub><sup>15</sup>N<sub>2</sub>] (5 nM) extracted on both MIPs.

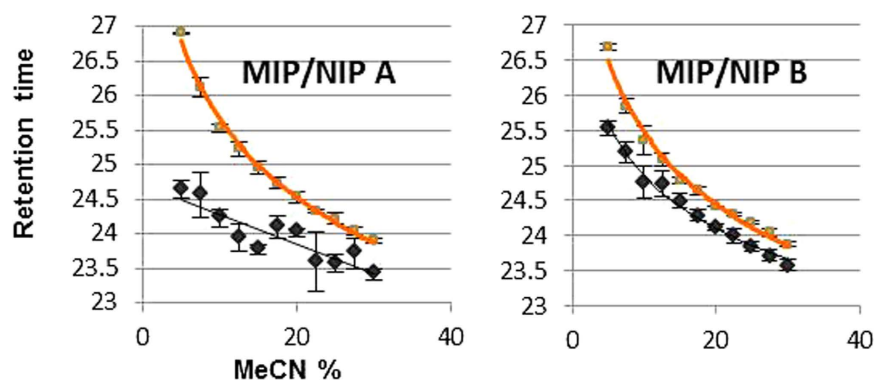


**Figure 4.** Differences in retention times of NLLGLIEA[K-<sup>13</sup>C<sub>6</sub><sup>15</sup>N<sub>2</sub>] (1 nM) on the MIPs (orange) and corresponding NIPs (black) for both polymer pairs (A and B).

retention time at higher pH was of less significance than the increase in signal intensity at low pH, 20 mM FA was used for the loading of the samples on the columns.

**Evaluation of MIP/NIP pairs and MIP selection.** The imprinting effects were evaluated by comparison of the NLLGLIEAK retention times on the two MIP/NIP pairs. Retention times of NLLGLIEA[K-<sup>13</sup>C<sub>6</sub><sup>15</sup>N<sub>2</sub>] were recorded upon its loading onto all the columns with 10 column volumes of 20 mM FA and subsequent isocratic elution directed to the MS detector, using small MeCN increments (Fig. 4). The differences in NLLGLIEA[K-<sup>13</sup>C<sub>6</sub><sup>15</sup>N<sub>2</sub>] retention of the MIP/NIP pairs appears to be highest when EAMA.HCl was used as sole functional monomer (MIP A). Any significant differences in peptide retention among the polymers batches can be ascribed uniquely to differences in the structures of the binding sites, since the columns were checked for complete packing by optical control of the transversal section of the cartridges (Fig. 5D) and measurement of backpressures gave similar results for all columns (7 PSI for MIP A and NIP A and 10 PSI for MIP B and NIP B).

The MIP A column was selected as trap column for further automatization and coupled with the analytical column. The MIP A column gave longer analyte retention, which is desirable for highly specific enrichment of the peptide when it is in the presence of many different interferences occurring in complex matrices such as serum samples. Additionally, MIP A showed a higher imprinting factor (IF) than MIP B (Supplementary Table S-6) under the conditions of use. These MIPs are distinct to many others synthesized by precipitation polymerisation, in that the low solubility of the template in the porogen necessitated the use of low template concentrations and high crosslink ratios (Supplementary Table S-3). Such synthetic constraints lead to MIPs with theoretical binding

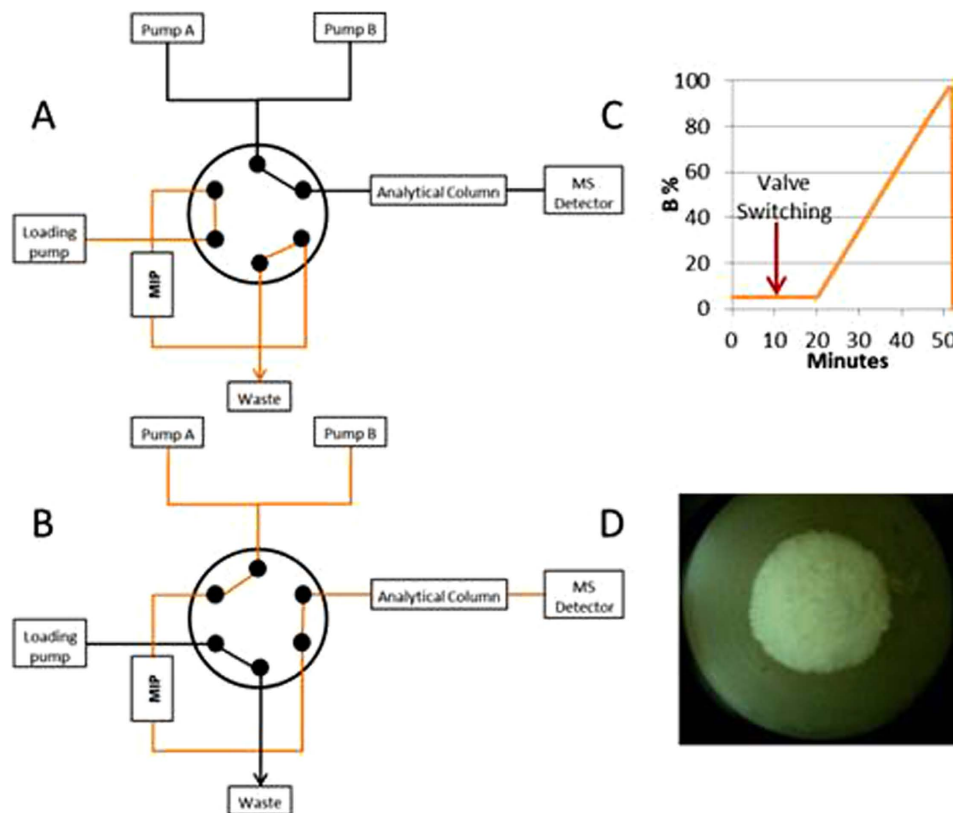


**Figure 5. Schematic representation of on-line extraction using a 6-port-valve:** (A) loading of the sample on MIP column, (B) forward-flushing of the MIP column to the analytical column, (C) analytical gradient applied for NLLGLIEAK determination, (D) transversal section of MIP A after packing in the trap column.

capacities that are considerably lower than MIPs synthesised under traditional conditions, and imprinting factors that are deceptively low when the MIPs are evaluated under normal loading conditions. The modest binding capacity of the MIPs is not a concern given that the concentrations of the target in the clinical samples is in the pM range, since the MIPs will not be over-loaded when in use (under the conditions of use of the MIPs for the clinical samples, a proportion of the highest fidelity binding sites are being exploited) and binding conditions that enabled binding affinity and selectivity could be established.

**Coupling of MIP columns with the analytical column and method optimization.** The arrangement of the 6-port valve when the sample is loaded onto the MIP column and subsequent valve switching is shown in Fig. 5A and B respectively.

Optimization of the wash and loading duration (Fig. 6A and B) provided 10 minutes for loading and washing for 5 minutes, whilst keeping the flow constant at  $30 \mu\text{L}/\text{min}$ . The capacity of the columns determined the serum volume to be extracted (Fig. 6C). The extraction of  $50 \mu\text{L}$  of serum performed remarkably well in terms of peptide signal intensity (for comparison, the present gold standard method TR-IFMA requires  $100 \mu\text{L}$ ) and was judged to be optimal. This result was very promising indeed for the management of clinical samples which are often available in very limited volumes only. Increasing the injection volume from 5 to  $30 \mu\text{L}$  allowed a linear increase in the peptide signal intensity (Fig. 6D), demonstrating the suitability of the extraction of  $50 \mu\text{L}$  of serum. In order to minimize the sample complexity before the extraction, depletion of the high abundant proteins such as serum albumin was decided to be performed by protein precipitation. This step was optimized by testing different MeCN volumes for the protein precipitation of ProGRP isoform 1 spiked samples. The highest peptide recovery was achieved using a 0.75:1 ratio of MeCN:serum (v/v) and 1:40 trypsin to substrate ratio, without reduction/alkylation (Fig. 6E and F). The enzyme to protein ratios shown in the figure are based on the amount of serum albumin expected to be left in the sample after protein precipitation. The amounts ranged between 1 and 10% in earlier studies which investigated protein precipitation with different acetonitrile concentrations<sup>42,43</sup>. Accordingly, a depletion of at least 90% of serum albumin with 50% of acetonitrile as precipitant agent can be assumed.

The extraction into the on-line system and the chromatographic run were complete within 50 minutes. The overall outcome was an automated and cost-effective method with remarkably low sample volume consumption.

**Linearity, LOD and LOQ.** The linearity of the method was explored over 3 orders of magnitude of ProGRP levels. The regression curve obtained (Supplementary Fig. S-6) upon plotting the ratio of the area of the signature peptide NLLGLIEAK to the area of the IS NLLGLIEA[ $\text{K}_2^{13}\text{C}_6^{15}\text{N}_2$ ] had an acceptable correlation value ( $R^2 > 0.97$ ).

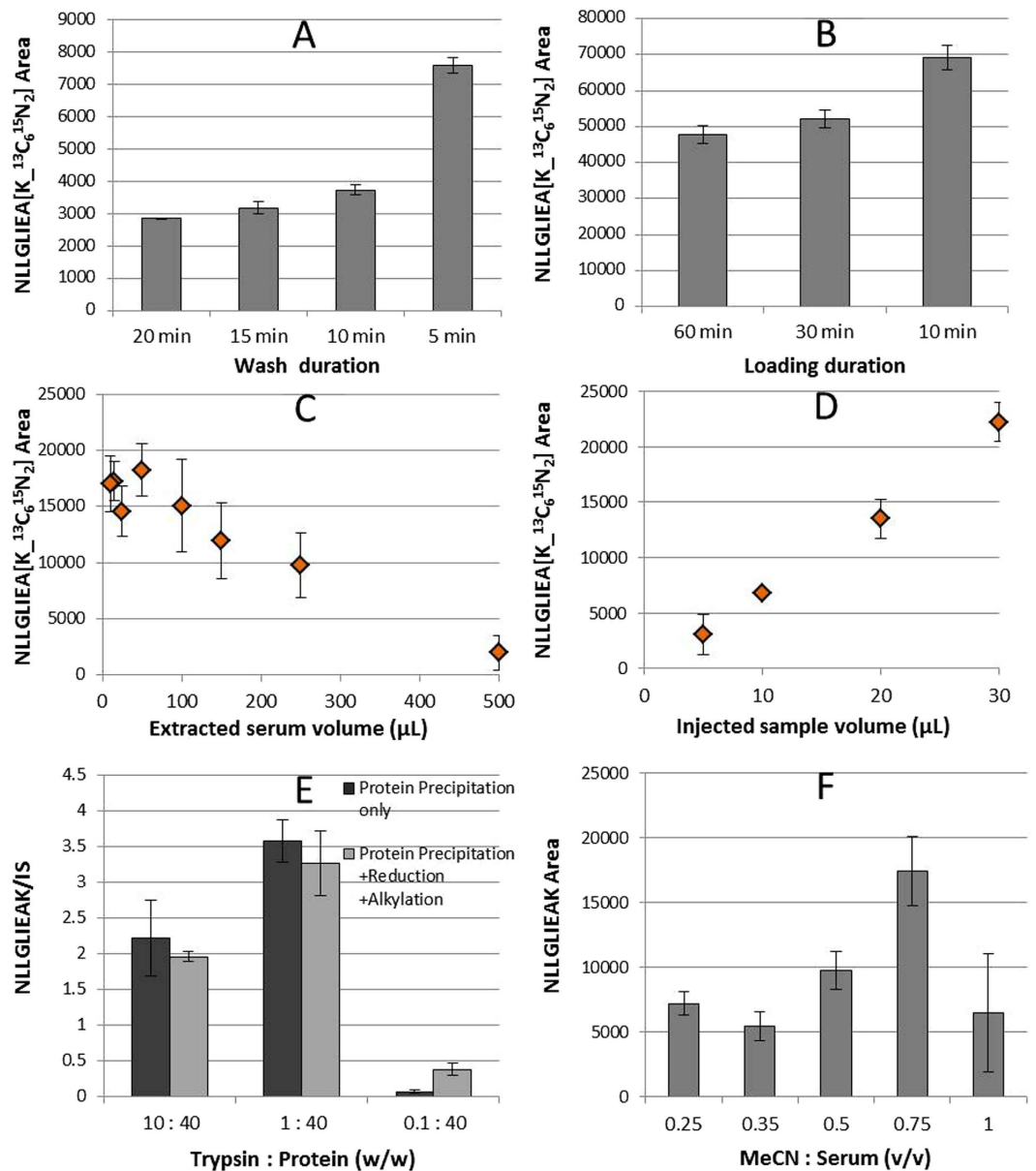


**Figure 6.** Extraction optimization (A–D) by using 1 nM NLLGLIEA[K-<sup>13</sup>C<sub>6</sub><sup>15</sup>N<sub>2</sub>]: (A) duration of the wash step (5% MeCN) on MIP A column; (B) duration of the loading step (20 mM FA) on MIP A column; (C) capacity evaluation by extraction of different serum volumes; (D) injection volume evaluation by extraction of 50 μL of serum. Sample pretreatment optimization (E–F) by using 37 nM ProGRP isoform 1 spiked serum samples: (E) evaluation of trypsin amount and reduction (DTT) and alkylation (IAA) after protein precipitation (PP) on spiked serum; (F) optimization of the MeCN:serum ratio (v/v) in protein precipitation step.

From the signal-to-noise ratio (S/N) of the lowest concentration of the curve, the limit of detection (LOD) was estimated to be 17.2 pM (S/N = 3) corresponding to a lower limit of quantification (LLOQ) of 57.3 pM (S/N = 10). The mass limit of detection (mLOD) on column was estimated to be 425 amol.

The detection limit of this new method is therefore substantially lower than the limit achieved previously by the MIP-based extraction<sup>21</sup> (625 pM) but is still marginally higher than the immunocapture LC-MS<sup>10</sup> (1 pM) and TR-IFMA methods. In the case of extended disease, clinically relevant concentrations of ProGRP are above the LOD achieved with this method<sup>44</sup>. However, the method is not able to discriminate healthy donors close to the reference limit of 7.6 pM.

**Analysis of patient samples and benchmarking with other methods.** Two patient serum samples suffering from SCLC were analyzed to demonstrate the applicability of the method to determine ProGRP in real samples with high levels of endogenous ProGRP (Fig. 7). The monitoring of selected transitions of NLLGLIEAK together with the co-elution of the IS allowed a correct peak identification.

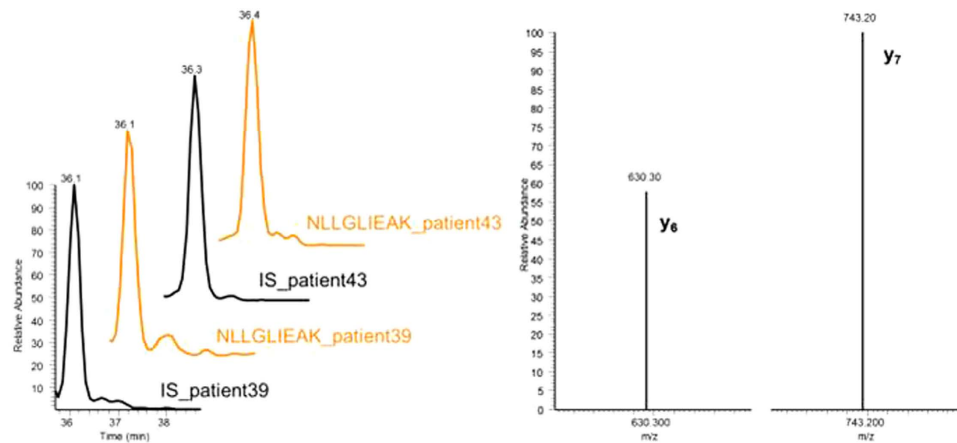


**Figure 7. Analysis of patient serum samples:** chromatograms of NLLGLIEAK (orange) and the Internal Standard (IS) NLLGLIEA[K- $^{13}\text{C}_6$ - $^{15}\text{N}_2$ ] (black) (left side) and corresponding ion spectra for selected reaction monitored (fragments  $y_6$  and  $y_7$ ) for NLLGLIEAK determination (right side).

	MISPE-LC-MS	immuno-LC-MS <sup>45</sup>	TR-IFMA <sup>45</sup>
Patient_39	2402 pM	922 pM	2425 pM
Patient_43	1029 pM	918 pM	1899 pM

**Table 1. Benchmarking of ProGRP concentrations in patient samples measured by the three analytical methods.**

From the calibration curve, the ProGRP concentrations were calculated for both samples; the values are reported in Table 1 together with the ProGRP concentrations determined previously for these samples by the immunocapture LC-MS and TR-IFMA methods<sup>45</sup>. Good accordance among ProGRP values is demonstrated. These results demonstrate very clearly the suitability of the new MISPE-LC-MS/MS method for the extraction and quantification of ProGRP present in clinical serum samples.

## Conclusion

In this paper, a template analogue imprinting strategy was implemented successfully for the design and synthesis of a polymeric synthetic receptor enabling biomarker determination in native serum at the pM level. Precipitation polymerization was used to deliver molecularly imprinted polymer microspheres in a physical format very convenient for their direct packing into trap column and direct integration with an LC-MS system for automated extraction of the ProGRP signature peptide. A MIP synthesized using EAMA.HCl as the sole functional monomer was found to be especially promising for the retention of the target peptide, and so was evaluated in further detail.

Coupling of a MIP trap column with an analytical column and tandem MS detection allowed for the development of the first automated method for the determination of ProGRP in patient samples. The practical combination of a low sample volume (50  $\mu\text{L}$ ) and short analysis time represents a noteworthy breakthrough in ProGRP determination by LC-MS using synthetic receptors. In addition, the low limits of detection and quantification were achieved without the need for antibodies and this is a unique novelty in ProGRP analysis.

Future studies should focus on a rapid and automated protein digestion before the MISPE in order to increase further the clinical advantage of the platform presented in this paper.

## Methods

**Reagents.** The peptide template Z-NLLGLIEA[Nle] (purity 96.58%), was purchased from LifeTein, *N*-(2-aminoethyl)methacrylamide hydrochloride (EAMA.HCl, purity  $\geq 98\%$ ) was purchased from Polysciences Inc. (Niles, IL, USA), *N*-3,5-bis(trifluoromethyl)-phenyl-*N'*-4-vinylphenylurea (purity  $>95\%$ ) is not commercially available and was kindly donated by Dortmund University, 2,2'-Azobisisobutyronitrile (AIBN, purity  $\geq 98\%$ ) was purchased from BDH (UAE). Divinylbenzene-80 (DVB-80, 80% DVB isomers and 20% ethylvinylbenzene isomers), 1,2,2,6,6-pentamethylpiperidine (PMP, purity  $>99\%$ ), tetrabutylammonium hydroxide solution (TBA.HO, 1.0 M in methanol, 25%  $\leq$  purity  $<50\%$ ) and hydrochloric acid (purity  $\geq 37\%$ ) were all purchased from Sigma-Aldrich (St. Louis, MI, USA). DVB-80 was purified by filtration through a short plug of neutral aluminium oxide prior to use. AIBN was recrystallized from acetone at low temperature. All other chemicals used (acetonitrile (MeCN), methanol and dimethyl sulfoxide [DMSO, purity  $\geq 99.9\%$ ]) were of analytical grade.

**Protein and Peptide Standards.** Recombinant ProGRP isoform 1 (AA 1–125 + 8) was cloned from human cDNA (OriGene Technologies, Rockville, MD, USA), expressed in *Escherichia coli* (Promega, Madison, WI, USA) using pGEX-6P-3 constructs (GE Healthcare Little Chalfont, UK) and purified as described elsewhere<sup>46</sup>.

Solutions of ProGRP and the Internal Standard (IS) NLLGLIEA[K-<sup>13</sup>C<sub>6</sub><sup>15</sup>N<sub>2</sub>] (purity >95%, Sigma-Aldrich) were prepared as described elsewhere<sup>21</sup>.

**Serum Samples.** Human serum from healthy subjects was obtained from Ullevål Hospital (Oslo, Norway), and serum samples from cancer patients were supplied by Radiumhospitalet (Oslo, Norway). All serum samples were stored at -30 °C. The use of patient samples for research purposes was approved by the Norwegian Regional Committee for Medical Research Ethics (REK, <http://helseforskning.etikkom.no>). Informed consent was obtained from all subjects. Methods used to analyse all serum samples were in accordance with relevant guidelines and regulations.

**Synthesis, Characterization and Column Packing of MIPs and NIPs.** Four distinct polymers were synthesized after protocol optimization (Supplementary section 1): two MIPs (MIP A and B) and two corresponding non-imprinted polymers (NIPs) (NIP A and B). MIPs were synthesized by firstly adding the template Z-NLLGLIEA[Nle] (8.2 mg, 7 μmol) into a borosilicate Kimax tube. Thereafter, DMSO (1 mL) was added (to dissolve the template), followed by PMP (1.9 mg, 0.01 mmol) and the functional monomer EAMA.HCl (12.3 mg, 0.07 mmol). For the synthesis of MIP B, TBA.HO (3.93 mg, 0.01 mmol) and *N*-3,5-*bis*(trifluoromethyl)-phenyl-*N'*-4-vinylphenylurea (5.25 mg, 0.01 mmol) were also included. MeCN (24 mL) was then added followed by DVB-80 (0.49 g, 0.53 mL, 3.73 mmol) and AIBN (22.3 mg, 0.2 mmol). (For the synthesis of the NIPs, the template was omitted from the synthetic protocols). The four solutions were then ultrasonicated for 10 minutes at ambient temperature and purged with oxygen-free nitrogen gas for 10 minutes at ice-bath temperature, to remove dissolved molecular oxygen. Thereafter, the reaction vessels were sealed under nitrogen and transferred to a Stuart Scientific S160 incubator equipped with a Stovall low-profile roller. The incubator temperature was ramped from ambient to 60 °C over a period of around two hours and then maintained at 60 °C for a further 46 hours to yield milky suspensions of polymer microspheres. Finally, the polymer microspheres were isolated from the reaction media by filtration on 0.45 μm nylon membrane filters, and washed sequentially with MeCN (50 mL), MeOH/0.1 M aq. HCl (90/10, v/v, 50 mL) and MeOH (50 mL), and finally dried overnight in Townson & Mercer vacuum oven at 70 °C.

The microspheres were evaluated in terms of their size and size distribution. Scanning Electron Microscopy (SEM) images were acquired using a Stereoscan 90 (Cambridge Instruments). Polymer microspheres were sputter-coated with gold using a Polar SC500A Sputter Coater Fison Instrument prior to analysis. Image analysis of the SEM micrographs was performed using Image J<sup>47</sup> software, on a population of 100 microspheres.

Brunauer-Emmett-Teller (BET) surface area analysis and Barrett-Joyner-Halenda (BJH) pore size and volume analysis were assessed by using an ASAP 2000 BET Analyzer. For each analysis, around 0.2 g of polymer was dried overnight in a vacuum oven at 70 °C, followed by a degassing step (pressure ~3 mmHg) for 24 h at 100 °C. BET theory was applied for the determination of specific surface areas, BJH cumulative adsorption pore volume was determined for pores between 1.7 and 300 nm, the micropore volume was based on the Harkins and Jura's thickness equation<sup>48</sup>.

Particles were evaluated in terms of binding capacity by plotting of the binding isotherms and the calculation of imprinting factors (Supplementary section 3.2 and 3.3, respectively). For both MIP/NIP pairs, binding isotherms were fitted by Freundlich curves as described by Rampey *et al.*<sup>49</sup> and imprinting factors of the polymers were calculated as described by Manesiotis *et al.*<sup>50</sup>. Packing of the MIPs and NIPs in trap columns (1.4 × 5 mm with 1 μm stainless steel frits) was performed by G&T Septech, Norway, by wet packing around 10 mg of polymer in 1200 μL of MeCN using a flowrate of 500 μL/min. In order to verify the quality of the packing of the columns, transversal microscopy (Dino Capture microscope with × 100 magnification) images were acquired, and back-pressures measured when flowing a mobile phase of 70% MeCN in water at 50 μL/min.

**On-Line MISPE-Liquid Chromatography-Tandem Mass Spectrometry (MISPE-LC-MS/MS) analysis.** The LC system consisted of an LPG-3400 M binary pump with degasser, an ISO-3100 A loading pump, a WPS-3000TRS autosampler and FLM-3000 flow-manager (all Dionex, Sunnyvale, CA, USA). The LC system was controlled by Chromeleon v. 6.80 SR6 (Dionex). The extraction was carried out by using the MIP A trap column. The LC separation was carried out using a Hypersil GOLD aQ, analytical column (Thermo Scientific, 100 Å, 3 μm, 1 × 50 mm) preceded by a Hypersil GOLD aQ Drop-In Guard Cartridge (Thermo Scientific, 100 Å, 3 μm, 1 × 10 mm).

The extraction was performed by loading 25 μL of sample with the loading buffer (20 mM aqueous formic acid [FA]). The isocratic flow (30 μL/min) was directed to the waste *via* the MIP cartridge, as shown in Fig. 5A. After 10 minutes, the system was switched in order to forward-flush the MIP cartridge to the analytical column and thus to the MS detector, as shown in Fig. 5B. The gradient flow (30 μL/min) had an initial ratio of mobile phase A (20 mM FA) to mobile phase B (pure MeCN) of 95:5 (v/v); this was kept constant for 10 minutes before the elution using a 27 minute linear gradient from 5 to 86% of mobile phase B. After the gradient run, the MIP column and the analytical column were washed for 5 minutes with 97% mobile phase B and re-equilibrated with mobile phase A, as shown in Fig. 5C.

The MS system consisted of a TSQ Quantum Access (Thermo Scientific) and was used for quantification of signature peptides by Selected Reaction Monitoring (SRM) experiments. The following transition pairs were monitored (qualifier and quantifier, respectively): for the ProGRP signature peptide NLLGLIEAK (485.8 → 630.3 and 485.8 → 743.4); for its internal standard NLLGLIEA[K-<sup>13</sup>C<sub>6</sub><sup>15</sup>N<sub>2</sub>] (489.9 → 638.3 and 489.9 → 751.4); for the ProGRP isoform 1 signature peptide LSAPGSQR (408.2 → 272.6 and 408.2 → 544.4).

TSQ-data were processed by Xcalibur's™ QualBrowser (Thermo Scientific) and peak areas, automatically processed by the Genesis peak detection algorithm, were used for the evaluation of the MS-responses. Only peaks



with signal-to-noise (S/N) ratios above 10 and retention times and ion ratios corresponding to that of standard samples were considered.

**ProGRP digestion.** ProGRP isoform 1 was diluted to the desired concentration with 50 mM freshly prepared ammonium bicarbonate buffer (ABC), trypsin added at an enzyme-to-substrate ratio of 1:40 (w/w), and then incubated at 37 °C overnight at 800 r.p.m.

**Calibration curve and patient sample analysis.** For the calibration curve, triplicates of human serum (50 µL) were spiked with ProGRP isoform 1 and vortexed for 30 seconds, to give the desired final concentrations: 0.183, 1.83, 3.66, 7.32, 36.6, 73.2 and 110 nM. Protein precipitation was performed by adding a volume of cold MeCN (−32 °C) to the serum (MeCN to serum v/v ratio = 0.75:1) and shaking for 5 minutes. Samples were then centrifuged at 10,000 r.p.m. for 10 minutes and the supernatants evaporated to dryness under a nitrogen stream at 40 °C. 50 µL of the trypsin solution (1 mg/mL in 50 mM ABC buffer) (1:40 protein: enzyme ratio) was used to reconstitute the samples and tryptic digestion was performed at 37 °C overnight. Analysis of patient samples (Oslo University Hospital, Oslo, Norway; approved by the Norwegian Regional Committee for Medical Research Ethics REK, <http://helseforskning.etikkom.no>) was performed by preparing the samples in triplicate as described for the calibration curve without the spiking of ProGRP isoform 1. All the samples were spiked with IS 10 nM before the injection to the chromatographic system.

## References

- Kim, J.-H., Inerowicz, D., Hedrick, V. & Regnier, F. Integrated Sample Preparation Methodology for Proteomics: Analysis of Native Proteins. *Analytical Chemistry* **85**, 8039–8045, doi: doi.org/10.1021/ac401477w (2013).
- Hoofnagle, A. N. & Wener, M. H. The fundamental flaws of immunoassays and potential solutions using tandem mass spectrometry. *Journal of Immunological Methods* **347**, 3–11 (2009).
- Rogeberg, M., Malerod, H., Roberg-Larsen, H., Aass, C. & Wilson, S. R. On-line solid phase extraction-liquid chromatography, with emphasis on modern bioanalysis and miniaturized systems. *Journal of Pharmaceutical and Biomedical Analysis* **87**, 120–129, doi: 10.1016/j.jpba.2013.05.006 (2014).
- Moein, M. M., Said, R. & Abdel-Rehim, M. Microextraction by packed sorbent. *Bioanalysis* **7**, 2155–2161, doi: 10.4155/bio.15.154 (2015).
- Massolini, G. & Calleri, E. Immobilized trypsin systems coupled on-line to separation methods: Recent developments and analytical applications. *Journal of Separation Science* **28**, 7–21, doi: 10.1002/jssc.200401941 (2005).
- Winther, B. & Reubsæet, J. L. Determination of the small cell lung cancer associated biomarker pro-gastrin-releasing peptide (ProGRP) using LC-MS. *Journal of Separation Science* **30**, 234–240, doi: 10.1002/jssc.200600319 (2007).
- Winther, B., Moi, P., Paus, E. & Reubsæet, J. L. E. Targeted determination of the early stage SCLC specific biomarker pro-gastrin-releasing peptide (ProGRP) at clinical concentration levels in human serum using LC-MS. *Journal of Separation Science* **30**, 2638–2646, doi: 10.1002/jssc.200700221 (2007).
- Winther, B., Nordlund, M., Paus, E., Reubsæet, L. & Halvorsen, T. G. Immuno-capture as ultimate sample cleanup in LC-MS/MS determination of the early stage biomarker ProGRP. *Journal of Separation Science* **32**, 2937–2943, doi: 10.1002/jssc.200900233 (2009).
- Winther, B. *et al.* Absolute ProGRP quantification in a clinical relevant concentration range using LC-MS/MS and a comprehensive internal standard. *Journal of Chromatography B: Analytical Technologies in the Biomedical and Life Sciences* **877**, 1359–1365, doi: 10.1016/j.jchromb.2008.12.023 (2009).
- Torsetnes, S. B., Nordlund, M. S., Paus, E., Halvorsen, T. G. & Reubsæet, L. Digging deeper into the field of the small cell lung cancer tumor marker progrp: A method for differentiation of its isoforms. *Journal of Proteome Research* **12**, 412–420, doi: 10.1021/pr300751j (2013).
- Torsetnes, S. B. *et al.* Multiplexing Determination of Small Cell Lung Cancer Biomarkers and Their Isovariants in Serum by Immunocapture LC-MS/MS. *Analytical Chemistry* **86**, 6983–6992, doi: 10.1021/ac500986t (2014).
- Hustoft, H. K. *et al.* Integrated enzyme reactor and high resolving chromatography in “sub-chip” dimensions for sensitive protein mass spectrometry. *Scientific Reports* **3**, 3511, doi: 10.1038/srep03511 (2013).
- Niho, S. *et al.* Significance of serum pro-gastrin-releasing peptide as a predictor of relapse of small cell lung cancer: comparative evaluation with neuron-specific enolase and carcinoembryonic antigen. *Lung Cancer* **27**, 159–167, doi: 10.1016/S0169-5002(99)00100-2 (2000).
- Molina, R., Filella, X. & Augé, J. M. ProGRP: a new biomarker for small cell lung cancer. *Clinical Biochemistry* **37**, 505–511, doi: 10.1016/j.clinbiochem.2004.05.007 (2004).
- Molina, R. *et al.* Usefulness of Serum Tumor Markers, Including Progastrin-Releasing Peptide, in Patients with Lung Cancer: Correlation with Histology. *Tumor Biology* **30**, 121–129, doi: doi.org/10.1159/000224628 (2009).
- Wang, J., Gao, J. & He, J. Diagnostic value of ProGRP and NSE for Small Cell Lung Cancer: A meta-analysis. *Chinese Journal of Lung Cancer* **13**, 1094–1100, doi: 10.3779/j.issn.1009-3419.2010.12.03 (2010).
- Yang, H. J., Gu, Y., Chen, C., Xu, C. & Bao, Y. X. Diagnostic value of pro-gastrin-releasing peptide for small cell lung cancer: A meta-analysis. *Clinical Chemistry and Laboratory Medicine* **49**, 1039–1046, doi: 10.1515/cclm.2011.161 (2011).
- Kim, H. R. *et al.* Plasma proGRP concentration is sensitive and specific for discriminating small cell lung cancer from nonmalignant conditions or non-small cell lung cancer. *Journal of Korean Medical Science* **26**, 625–630, doi: 10.3346/jkms.2011.26.5.625 (2011).
- Nordlund, M. S., Stieber, P., Brustugun, O. T., Warren, D. J. & Paus, E. Characteristics and clinical validity of two immunoassays for ProGRP. *Tumor Biology*, 1–9, doi: 10.1007/s13277-012-0351-1 (2012).
- Qader, A. A. *et al.* Peptide imprinted receptors for the determination of the small cell lung cancer associated biomarker progastrin releasing peptide. *J. Chromatogr. A* **1370**, 56–62, doi: 10.1016/j.chroma.2014.10.023 (2014).
- Rossetti, C., Abdel Qader, A., Halvorsen, T. G., Sellergren, B. & Reubsæet, L. Antibody-free biomarker determination: Exploring molecularly imprinted polymers for pro-gastrin releasing peptide. *Analytical Chemistry* **86**, 12291–12298, doi: 10.1021/ac503559c (2014).
- Manesiotis, P., Hall, A. J., Courtois, J., Irgum, K. & Sellergren, B. An Artificial Riboflavin Receptor Prepared by a Template Analogue Imprinting Strategy. *Angewandte Chemie International Edition* **44**, 3902–3906, doi: 10.1002/anie.200500342 (2005).
- Chen, L., Wang, X., Lu, W., Wu, X. & Li, J. Molecular imprinting: Perspectives and applications. *Chemical Society Reviews* **45**, 2137–2211, doi: 10.1039/c6cs00061d (2016).
- Xu, S., Li, J. & Chen, L. Molecularly imprinted polymers by reversible addition-fragmentation chain transfer precipitation polymerization for preconcentration of atrazine in food matrices. *Talanta* **85**, 282–289, doi: 10.1016/j.talanta.2011.03.060 (2011).
- Wen, Y., Chen, L., Li, J., Liu, D. & Chen, L. Recent advances in solid-phase sorbents for sample preparation prior to chromatographic analysis. *TrAC - Trends in Analytical Chemistry* **59**, 26–41, doi: 10.1016/j.trac.2014.03.011 (2014).

26. Rachkov, A. & Minoura, N. Recognition of oxytocin and oxytocin-related peptides in aqueous media using a molecularly imprinted polymer synthesized by the epitope approach. *Journal of Chromatography A* **889**, 111–118, doi: 10.1016/S0021-9673(00)00568-9 (2000).
27. Cacho, C., Turiel, E., Martín-Esteban, A., Pérez-Conde, C. & Cámara, C. Characterisation and quality assessment of binding sites on a propazine-imprinted polymer prepared by precipitation polymerisation. *Journal of Chromatography B* **802**, 347–353, doi: 10.1016/j.jchromb.2003.12.018 (2004).
28. Turiel, E., Tadeo, J. L., Cormack, P. A. G. & Martín-Esteban, A. HPLC imprinted-stationary phase prepared by precipitation polymerisation for the determination of thiabendazole in fruit. *Analyst* **130**, 1601–1607, doi: 10.1039/B511031A (2005).
29. Beltran, A., Marcé, R. M., Cormack, P. A. G. & Borrull, F. Synthesis by precipitation polymerisation of molecularly imprinted polymer microspheres for the selective extraction of carbamazepine and oxcarbazepine from human urine. *Journal of Chromatography A* **1216**, 2248–2253, doi: 10.1016/j.chroma.2009.01.024 (2009).
30. Sambe, H., Hoshina, K., Moaddel, R., Wainer, I. W. & Haginaka, J. Uniformly-sized, molecularly imprinted polymers for nicotine by precipitation polymerization. *Journal of Chromatography A* **1134**, 88–94, doi: 10.1016/j.chroma.2006.08.073 (2006).
31. Helling, S. *et al.* Ultratrace enrichment of tyrosine phosphorylated peptides on an imprinted polymer. *Analytical Chemistry* **83**, 1862–1865, doi: 10.1021/ac103086v (2011).
32. Valero-Navarro, A. *et al.* Synthesis of caffeic acid molecularly imprinted polymer microspheres and high-performance liquid chromatography evaluation of their sorption properties. *Journal of Chromatography A* **1218**, 7289–7296, doi: 10.1016/j.chroma.2011.08.043 (2011).
33. Beltran, A., Borrull, F., Cormack, P. A. G. & Marcé, R. M. Molecularly imprinted polymer with high-fidelity binding sites for the selective extraction of barbiturates from human urine. *Journal of Chromatography A* **1218**, 4612–4618, doi: 10.1016/j.chroma.2011.05.049 (2011).
34. Ye, L., A. G. Cormack, P. & Mosbach, K. Molecularly imprinted monodisperse microspheres for competitive radioassay. *Analytical Communications* **36**, 35–38, doi: 10.1039/A809014I (1999).
35. Wang, J., Cormack, P. A. G., Sherrington, D. C. & Khoshdel, E. Monodisperse, Molecularly Imprinted Polymer Microspheres Prepared by Precipitation Polymerization for Affinity Separation Applications. *Angewandte Chemie International Edition* **42**, 5336–5338, doi: 10.1002/anie.200352298 (2003).
36. Yoshimatsu, K. *et al.* Uniform molecularly imprinted microspheres and nanoparticles prepared by precipitation polymerization: The control of particle size suitable for different analytical applications. *Analytica Chimica Acta* **584**, 112–121, doi: 10.1016/j.aca.2006.11.004 (2007).
37. Wang, J., Cormack Peter, A. G., Sherrington David, C. & Khoshdel, E. Synthesis and characterization of micrometer-sized molecularly imprinted spherical polymer particulates prepared via precipitation polymerization. *Pure Appl. Chem.* **79**, 1505–1519, doi: 10.1351/pac200779091505 (2007).
38. Urraca, J. L. *et al.* Polymeric complements to the Alzheimer's disease biomarker  $\beta$ -amyloid isoforms A $\beta$ 1–40 and A $\beta$ 1–42 for blood serum analysis under denaturing conditions. *Journal of the American Chemical Society* **133**, 9220–9223, doi: 10.1021/ja202908z (2011).
39. Hall, A. J. *et al.* Urea host monomers for stoichiometric molecular imprinting of oxyanions. *Journal of Organic Chemistry* **70**, 1732–1736, doi: 10.1021/jo048470p (2005).
40. Emgenbroich, M. *et al.* A phosphotyrosine-imprinted polymer receptor for the recognition of tyrosine phosphorylated peptides. *Chemistry - A European Journal* **14**, 9516–9529, doi: 10.1002/chem.200801046 (2008).
41. Csizmadia, J. S. & Szegezdi, J. Chemicalize.com, <https://chemical/#/calculation> (Date of access: 11/11/2015)(2004–2007).
42. Polson, C., Sarkar, P., Inledon, B., Raguvaran, V. & Grant, R. Optimization of protein precipitation based upon effectiveness of protein removal and ionization effect in liquid chromatography–tandem mass spectrometry. *Journal of Chromatography B* **785**, 263–275, doi: 10.1016/S1570-0232(02)00914-5 (2003).
43. Kay, R. *et al.* Enrichment of low molecular weight serum proteins using acetonitrile precipitation for mass spectrometry based proteomic analysis. *Rapid communications in mass spectrometry: RCM* **22**, 3255–3260, doi: 10.1002/rcm.3729 (2008).
44. Aoyagi, K. *et al.* Enzyme immunoassay of immunoreactive progastrin-releasing peptide (31–98) as tumor marker for small-cell lung carcinoma: development and evaluation. *Clinical Chemistry* **41**, 537–543 (1995).
45. Torsetnes, S. B., Broughton, M. N., Paus, E., Halvorsen, T. G. & Reubsaet, L. Determining ProGRP and isoforms in lung and thyroid cancer patient samples: comparing an MS method with a routine clinical immunoassay. *Analytical and Bioanalytical Chemistry* **406**, 2733, doi: 10.1007/s00216-014-7634-x (2014).
46. Nordlund, M. S., Fermer, C., Nilsson, O., Warren, D. J. & Paus, E. Production and characterization of monoclonal antibodies for immunoassay of the lung cancer marker proGRP. *Tumor Biology* **28**, 100–110, doi: 10.1159/000099335 (2007).
47. Rasband, W. S. *ImageJ*. <http://imagej.nih.gov/ij/> (Date of access: 13/06/2013) (1997–2016).
48. Jura, G. & Harkins, W. D. Surfaces of Solids. XI. Determination of the Decrease ( $\pi$ ) of Free Surface Energy of a Solid by an Adsorbed Film. *Journal of the American Chemical Society* **66**, 1356–1362, doi: 10.1021/ja01236a046 (1944).
49. Rampey, A. M. *et al.* Characterization of the Imprint Effect and the Influence of Imprinting Conditions on Affinity, Capacity, and Heterogeneity in Molecularly Imprinted Polymers Using the Freundlich Isotherm-Affinity Distribution Analysis. *Analytical Chemistry* **76**, 1123–1133, doi: 10.1021/ac0345345 (2004).
50. Manesiotis, P., Kashani, S. & McLoughlin, P. Molecularly imprinted polymers for the extraction of imiquimod from biological samples using a template analogue strategy. *Analytical Methods* **5**, 3122–3128, doi: 10.1039/c3ay40239h (2013).

## Acknowledgements

This work was supported by the Seventh Research Framework Programme of the European Commission PEPMIP project (Grant agreement number–264699) and from the Research Council of Norway (Grant agreement number–226654/F11). We thank R. Trones, T. Løvli and C. Huang from G&T Septech AS, Norway, for the packing of the MIPs and NIPs into columns.

## Author Contributions

C.R., T.G.H. and L.R. planned the analytical experiments. M.A.S. and P.A.G.C. designed the polymerization protocols. C.R. and M.A.S. performed the experiments and data analysis on analytical method development and polymeric synthesis. B.S. supervised the PEPMIP project. C.R. wrote the manuscript. All authors reviewed the manuscript.

## Additional Information

**Supplementary information** accompanies this paper at <http://www.nature.com/srep>

**Competing Interests:** The authors declare no competing financial interests.

**How to cite this article:** Rossetti, C. *et al.* Automated Protein Biomarker Analysis: on-line extraction of clinical samples by Molecularly Imprinted Polymers. *Sci. Rep.* **7**, 44298; doi: 10.1038/srep44298 (2017).

**Publisher's note:** Springer Nature remains neutral with regard to jurisdictional claims in published maps and institutional affiliations.



This work is licensed under a Creative Commons Attribution 4.0 International License. The images or other third party material in this article are included in the article's Creative Commons license, unless indicated otherwise in the credit line; if the material is not included under the Creative Commons license, users will need to obtain permission from the license holder to reproduce the material. To view a copy of this license, visit <http://creativecommons.org/licenses/by/4.0/>

© The Author(s) 2017

# SUPPORTING INFORMATION

## Automated Protein Biomarker Analysis: on-line extraction of clinical samples by Molecularly Imprinted Polymers

Cecilia Rossetti<sup>1</sup>, Magdalena A. Świtnicka-Plak<sup>2</sup>, Trine Grønhaug Halvorsen<sup>1</sup>, Peter A.G. Cormack<sup>2</sup>, Börje Sellergren<sup>3</sup> and Léon Reubsæet\*<sup>1</sup>

1. Department of Pharmaceutical Chemistry, University of Oslo, School of Pharmacy, Postbox 1068 Blindern, 0316 Oslo, Norway

2. WestCHEM, Department of Pure and Applied Chemistry, University of Strathclyde, Thomas Graham Building, 295 Cathedral Street, Glasgow, G1 1XL, United Kingdom

3. Department of Biomedical Sciences, Faculty of Health and Society, Malmö University, SE20506 Malmö, Sweden.

### TABLE OF CONTENTS

<b>1. Optimization of the polymer synthesis:</b>	
1.1 Solubility tests.	
Table S-1 Solubility tests for EAMA.HCl	S2
1.2 Choice of reaction vessel and synthesis conditions.	
Table S-2 Synthesis conditions and the yields of the non-imprinted polymers	S2
Figure S-1: Overlap of the FTIR spectra of NIP 1 and NIP 4	S3
<b>2. Synthesis of the polymers:</b>	
Table S-3 Monomer feed conditions and yields of the imprinted polymers	S3
<b>3. Characterization of the polymers:</b>	
3.1 SEM analysis.	
Figure S-2: SEM images of polymers	S4
3.2 BET analysis.	
Table S-4 Nitrogen sorption data	S4
3.3 Binding isotherms.	
Figure S-3 Equilibrium binding isotherms for MIP/NIP A	S5
Figure S-4 Equilibrium binding isotherms for MIP/NIP B	S5
Table S-5: Freundlich fitting parameters for all the polymers	S5
3.4 Imprinting factors.	
Table S-6 Retention coefficients and imprinting factors	S6
<b>4. Method development:</b>	
4.1 Drop of peptide signal intensity due to increased pH.	
Figure S-5: Direct MS infusion TIC chromatogram of 1 nM NLLGLIEA[K- <sup>13</sup> C <sub>6</sub> <sup>15</sup> N <sub>2</sub> ]	S6
4.2 Linearity of the method.	
Figure S-6: Calibration curve	S7
<b>5. Verification of NIP failure:</b>	
Figure S-5: Extraction on NIP A of a serum samples spiked with ProGRP iso1	S7
<b>REFERENCES</b>	<b>S7</b>

# 1. Optimization of the polymer synthesis:

## 1.1 Solubility tests.

In order to adapt the experimental approaches described elsewhere<sup>1</sup> to the precipitation polymerization procedure, solubility tests for the functional monomer EAMA.HCl were performed. Moreover, the solubility tests had the aim to determine the amount of DMSO needed to bring all the precipitation polymerization components into a homogenous solution. Different mole ratio of EAMA.HCl and DVB-80 (crosslinker) together with different combinations of MeCN (solvent) and DMSO (co-solvent) were tested, as presented in Table S-1.

Table S-1 Solubility tests for EAMA.HCl to be co-polymerized with DVB in MeCN and DMSO.

Test #	EAMA.HCl / DVB (mol ratio)	EAMA.HCl (mmol)	MeCN / DMSO (v/v)
1	1 / 5	0.7470	99 / 1
2	1 / 5	0.7470	96 / 4
3	0.1 / 5	0.0747	99 / 1
4	0.1 / 5	0.0747	96 / 4

The use of EAMA.HCl in the same 1 / 5 molar ratio of EAMA.HCl / DVB as used in the synthesis performed in the previous work<sup>1</sup> resulted in monomer insolubility. This problem was overcome by decreasing the functional monomer concentrations. In solubility test #4, the amount of EAMA.HCl was reduced ten times and was dissolved completely in 4 % of DMSO and 96 % of MeCN. Thus the mole ratio of EAMA.HCl to DVB was set at 0.1:5. The mole ratio of DVB to *N*-3,5-*bis*(trifluoromethyl)-phenyl-*N'*-4-vinylphenylurea was set at 5:0.02.

## 1.2 Choice of reaction vessel and synthesis conditions.

In order to optimize the synthetic protocol, polymers without the addition of the template (non-imprinted polymers) were pre-tested as shown in Table S-2. A polymer with only the crosslinker (DVB-80) was prepared as control and polymers providing the use of the selected functional monomers (EAMA.HCl and *N*-3,5-*bis*(trifluoromethyl)-phenyl-*N'*-4-vinylphenylurea) were prepared in two different reaction vessels.

Table S-2 Synthesis conditions and the yields of the non-imprinted polymers prepared in different reaction vessel.

Polymer Code	Reaction vessel	Functional Monomer (mmol)	DVB-80 (mmol)	Solvent (mL)	AIBN (mol%)	Incubation time	Other components (mmol)	Polymer Yield (%)
NIP 1	Borosilicate Kimax tube	-	3.06	MeCN (20)	2	24 h	-	29
NIP 2	Borosilicate Kimax tube	EAMA.HCl (0.07)	3.73	MeCN (24) DMSO (1)	2	24 h	PMP (0.006)	22
NIP 3	Polyethylene Nalgene bottle	EAMA.HCl (0.07)	3.73	MeCN (24) DMSO (1)	2	24 h	PMP (0.006)	19
NIP 4	Borosilicate Kimax tube	EAMA.HCl (0.07) urea monomer* (0.01)	3.73	MeCN (24) DMSO (1)	2	24 h	PMP (0.006) TBA.HO <sup>+</sup> (0.007)	28
NIP 5	Polyethylene Nalgene bottle	EAMA.HCl (0.07) urea monomer* (0.01)	3.73	MeCN (24) DMSO (1)	2	24 h	PMP (0.006) TBA.HO <sup>+</sup> (0.007)	4

\* *N*-3,5-*bis*(trifluoromethyl)-phenyl-*N'*-4-vinylphenylurea.

As the table shows, yields are lower for the polymers synthesized in Polyethylene Nalgene bottles. Thus Borosilicate Kimax tubes were used to perform the syntheses. PMP and TBA.HO were used to bring the various functional groups (of EAMA and *N*-3,5-*bis*(trifluoromethyl)-phenyl-*N'*-4-vinylphenylurea respectively) into appropriate ionization states for non-covalent interactions between functional monomers and the template (which here was not added). Moreover, for the synthesis of Molecularly Imprinted Polymers, where the template will be added at the beginning, it was decided to increase the amount of PMP and TBA.HO<sup>+</sup> from 0.006 mmol to 0.01 mmol since the template has two sites able to bind the functional monomers: the carboxylic acid group in the glutamic acid (E) residue and C-terminus of Z-NLLGLIEA[Nie] as shown in Figure 2 of the main text.

The incubation time was extended to 48 hours in order to increase the yield of the polymerization as Table S-3 demonstrates.

A control polymer made of DVB-80 only gave a reaction yield typical for the polymerization of divinylbenzene under such precipitation polymerization conditions.

For this polymer (NIP 1) as for the polymers NIP 2 and 4, the FTIR spectra were acquired using a Shimadzu IRAffinity-1 Fourier Transform Infrared Spectrophotometer with Attenuated Total Reflection (ATR) Mode.

Figure S-1 shows the Overlap of the FTIR spectra of NIP 1 [poly(EVB-co-DVB-80)] (black solid line) and NIP 4. [poly(*N*-3,5-*bis*(trifluoromethyl)-phenyl-*N'*-4-vinylphenylurea-co-EAMA.HCl-co-DVB-80)] (orange solid line) and presents the characteristic peaks for the polymerization of DVB-80: aromatic C-H stretches at 3018 cm<sup>-1</sup> and 3007 cm<sup>-1</sup>, aliphatic C-H stretches at 2916 cm<sup>-1</sup>, aromatic C=C stretches at 1627 cm<sup>-1</sup>, 1600 cm<sup>-1</sup> and 1510 cm<sup>-1</sup>, alkene stretches at 987 cm<sup>-1</sup> and 902 cm<sup>-1</sup>, and three stretches at 829 cm<sup>-1</sup>, 794 cm<sup>-1</sup> and 709 cm<sup>-1</sup>, corresponding to para- and meta-di-substituted benzene rings.

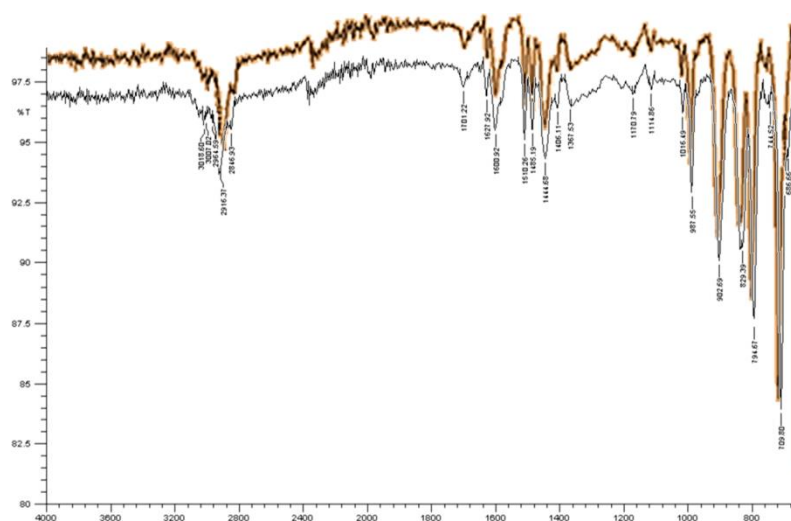


Figure S-1: Overlap of the FTIR spectra of NIP 1 [poly(EVB-co-DVB-80)] (black solid line) and NIP 4. [poly(*N*-3,5-*bis*(*t*Trifluoromethyl)-phenyl-*N'*-4-vinylphenylurea-co-EAMA.HCl-co-DVB-80)] (orange solid line).

Both poly(EVB-co-DVB-80) and NIP 4. [poly(*N*-3,5-*bis*(trifluoromethyl)-phenyl-*N'*-4-vinylphenylurea-co-EAMA.HCl-co-DVB-80)] showed these peaks only. Also, NIP 2 [poly(EAMA.HCl-co-EVB-co-DVB-80)] showed the typical peaks associated with the poly(EVB-co-DVB-80) only. Peaks associated with the presence of EAMA.HCl or *N*-3,5-*bis*(trifluoromethyl)-phenyl-*N'*-4-vinylphenylurea were not observed, as the amount of functional monomers present in the monomer feed was relatively small compared to the level of DVB.

For this reason, elemental microanalysis of the polymers was not performed, since the elemental composition was expected to reflect the poly(EVB-co-DVB-80) composition. However, the theoretical composition of polymers produced could be determined from the composition and the reactivity of the monomers used in the polymerizations performed.

## 2. Synthesis of the polymers:

Table S-3 Monomer feed conditions and the yields of the polymeric products: Z-NLLGLIEA[Nie] imprinted polymers and their corresponding NIPs.

Polymer Code	Template <sup>a</sup> (mmol)	Functional Monomer (mmol)	DVB-80 (mmol)	Solvent (mL)	AIBN (mol%) <sup>#</sup>	PMP or TBA.HO <sup>a</sup> (mmol)	Incubation time (h)	Polymer Yield (%)
NIP A	-	EAMA.HCl (0.07)	3.73	MeCN (24) DMSO (1)	2	PMP (0.01)	48	54
MIP A	0.007	EAMA.HCl (0.07)	3.73	MeCN (24) DMSO (1)	2	PMP (0.01)	48	41
NIP B	-	EAMA.HCl (0.07) urea monomer* (0.01)	3.73	MeCN (24) DMSO (1)	2	PMP (0.01) TBA.HO (0.01)	48	49
MIP B	0.007	EAMA.HCl (0.07) urea monomer* (0.01)	3.73	MeCN (24) DMSO (1)	2	PMP (0.01) TBA.HO (0.01)	48	52

\* *N*-3,5-*bis*(trifluoromethyl)-phenyl-*N'*-4-vinylphenylurea. <sup>#</sup> Relative to polymerizable double bonds.

<sup>a</sup> PMP and TBA.HO were used to bring the various functional groups into appropriate ionization states for non-covalent interaction and to promote template solubility.

### 3. Characterization of the polymers:

#### 3.1 SEM analysis.

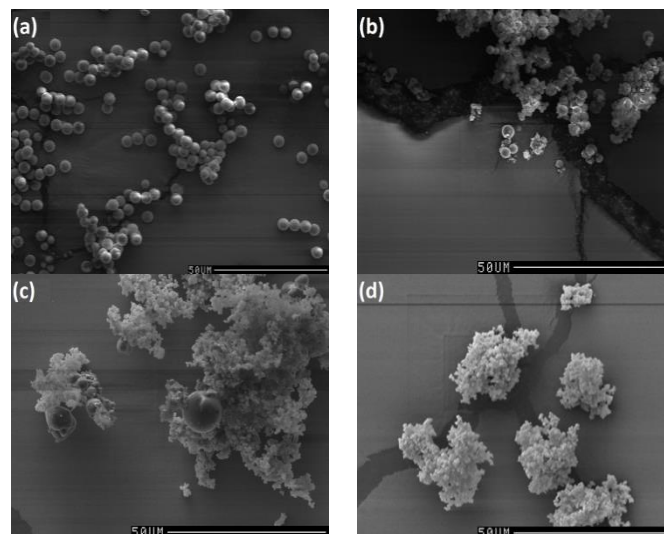


Figure S-2: SEM images of the polymers: (a) NIP A, (b) MIP A, (c) NIP B, (d) MIP B (x 777 magnification).

#### 3.2 BET analysis.

Table S-4 Nitrogen sorption data for the non-imprinted and molecularly imprinted polymers for the Z-NLLGLIEA[Nle] target.

Polymer Code	BET specific surface area (m <sup>2</sup> /g)	Specific pore volume (cm <sup>3</sup> /g)	Average pore diameter <sup>a</sup> (nm)	Micropore volume (cm <sup>3</sup> /g)	Micropore area (m <sup>2</sup> /g)
NIP A	221	0.036	2.10	0.060	137
MIP A	31	n/a	n/a	0.032	76
NIP B	307	0.026	1.96	0.099	218
MIP B	349	0.083	2.34	0.093	205

<sup>a</sup>The average pore diameter was determined by equation : Average pore diameter =  $\frac{4 \text{ pore volume}}{\text{BET surface area}}$

#### 3.3 Binding isotherms.

The polymers (1 mg) were mixed with different solution of NLLGLIEA[K-<sup>13</sup>C<sub>6</sub><sup>15</sup>N<sub>2</sub>] spanning the concentration range of 10 – 220 nM in 700 μL of MeCN: ABC buffer (5:95) (50 mM pH 7.6), and were incubated for 24 h at 20 °C setting the Eppendorf shaker at 800 r.p.m. Afterward the solutions were centrifuged at 10000 r.p.m. for 30 minutes and the supernatants were collected and injected into the LC-MS/MS system.

The chromatographic separation was carried out by using Hypersil GOLD aQ, analytical column (Thermo Scientific, 100 Å, 3 μm, 1 × 50 mm) preceded by a pre-column (Hypersil GOLD aQ Drop-In Guard Cartridge Thermo Scientific, 100 Å, 3 μm, 1 × 10 mm). The 30 min linear gradient ranged from 1 to 85% of mobile phase B (20 mM FA : MeCN 5:95, v/v) and the column was re-equilibrated with 99% of mobile phase A (20 mM FA : MeCN 95:5, v/v). The column temperature was kept constant at 30 °C. A triple quadrupole (TSQ Quantum™ Access, Thermo Fisher Scientific) was used for quantification of the peptide in Selected Reaction Monitoring (SRM) mode, following a transition pair: 489.9 → 638.3 and 489.9 → 751.4. Peak areas, automatically processed by genesis peak detection algorithm, were calculated by Xcalibur's™ QualBrowser (Thermo Scientific).

The amount of peptide bound to the polymer (B) was calculated by subtracting the non-bound analyte (F) from the initial NLLGLIEA[K-<sup>13</sup>C<sub>6</sub><sup>15</sup>N<sub>2</sub>] concentration in the solution. The incubation was performed in duplicate. The curves were obtained by plotting the average of B versus F (Figure S-2 and S-3), and then fitted to the Freundlich model using the following power function:

$$B = aF^m \quad \text{Eq. 1}$$

with  $B$  the concentration of bound analyte and  $F$  the amount of free analyte.  $a$  and  $m$  are parameters which describe the power function and were used to calculate the average affinity constant  $K$  as described from Rampey et al<sup>2</sup>.

$$K = \left( \frac{m}{m-1} \right) \frac{K_1^{1-m} - K_2^{1-m}}{K_1^{-m} - K_2^{-m}} \quad \text{Eq. 2}$$

with  $K_1 = 1/F_{max}$  and  $K_2 = 1/F_{min}$ ;

$$N = a (1 - m^2) (K_1^{-m} - K_2^{-m}) \quad \text{Eq. 3}$$

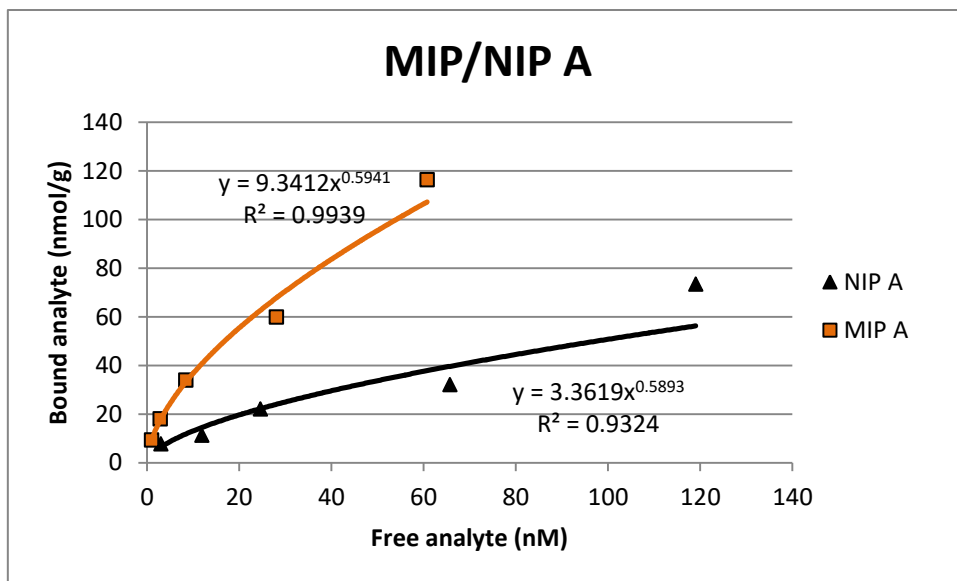


Figure S-3: Equilibrium binding isotherms obtained from Freundlich fitting for the uptake of NLLGLIEA[K-<sup>13</sup>C<sub>6</sub><sup>15</sup>N<sub>2</sub>] by MIP A (squares, orange line) and NIP A (triangles, black line) in ABC/MeCN (95:5, v/v).

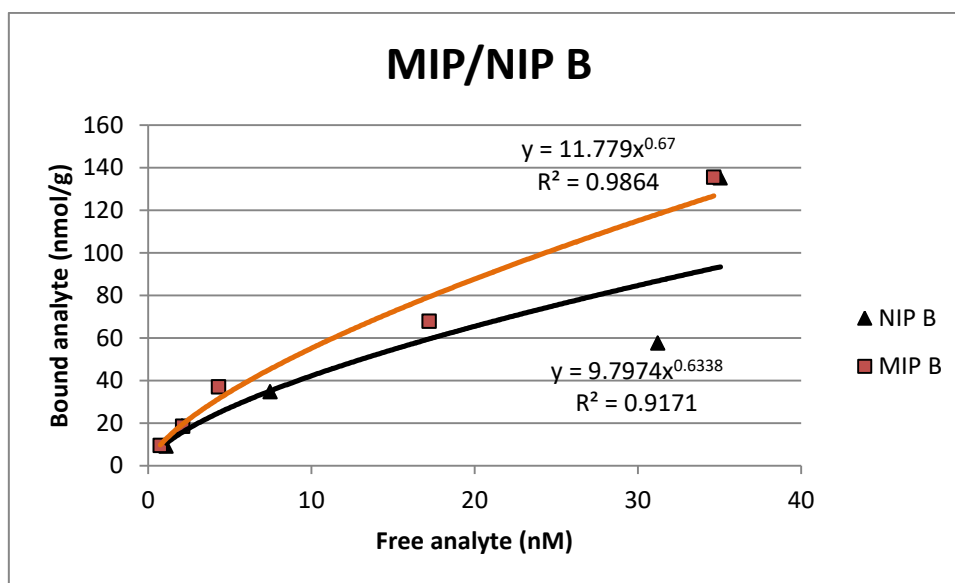


Figure S-4: Equilibrium binding isotherms obtained from Freundlich fitting for the uptake of NLLGLIEA[K-<sup>13</sup>C<sub>6</sub><sup>15</sup>N<sub>2</sub>] by MIP B (squares, orange line) and NIP B (triangles, black line) in ABC/MeCN (95:5, v/v).

Table S-5: Freundlich fitting parameters for all the polymers

	Affinity constant, K (nM <sup>-1</sup> )	Total Number of binding sites, N (μmol g <sup>-1</sup> )	Heterogeneity parameter, m <sup>a</sup>	Binding capacity, a	Regression coefficient, R <sup>2</sup>
MIP A	0.11	6.73	0.59	9.34	0.99
NIP A	0.05	9.00	0.59	3.36	0.93
MIP B	0.16	5.40	0.67	11.78	0.99
NIP B	0.14	4.64	0.63	9.80	0.92

<sup>a</sup> The parameter *m* represents the heterogeneity index of the polymer, ranging from 1 (homogeneous samples) to 0 (heterogeneous samples).



The Freundlich model commonly describes site distributions well in MIPs. The model implies a heterogeneous distribution of sites continuously ranging from low to high binding energies and absence of homogeneous populations of binding sites. The parameter  $m$  is of particular importance and here confirms a heterogeneous population of molecularly imprinted binding sites arising from the non-covalent molecular imprinting strategy adopted.

### 3.3 Imprinting Factors.

Imprinting factors of the polymers were calculated as described by Manesiotis *et al.*<sup>3</sup> for both MIP/NIP pairs based on the retention times of a non-retained peptide (LSAPGSQR) and the target analyte (NLLGLIEAK) after the isocratic elution with 5% MeCN from the cartridges according to the equation 4:

$$IF = k'_{MIP}/k'_{NIP} \quad \text{Eq.4}$$

where  $k'_{MIP}$  and  $k'_{NIP}$  are the respective retention factors defined as:

$$k' = (t_R - t_0)/t_0 \quad \text{Eq.5}$$

with  $t_R$  the retention time of the analyte (NLLGLIEAK) and  $t_0$  the retention time of a not-retained peptide (LSAPGSQR).

**Table S-6: Retention coefficients and imprinting factors of the two polymerisation protocols.**

	Retention factor, $k'$	Imprinting factor, IF
<b>MIP A</b>	14.36	1.11
<b>NIP A</b>	12.91	
<b>MIP B</b>	13.41	1.00
<b>NIP B</b>	13.43	

## 4. Method development:

### 4.1 Drop of peptide signal intensity due to increased pH.

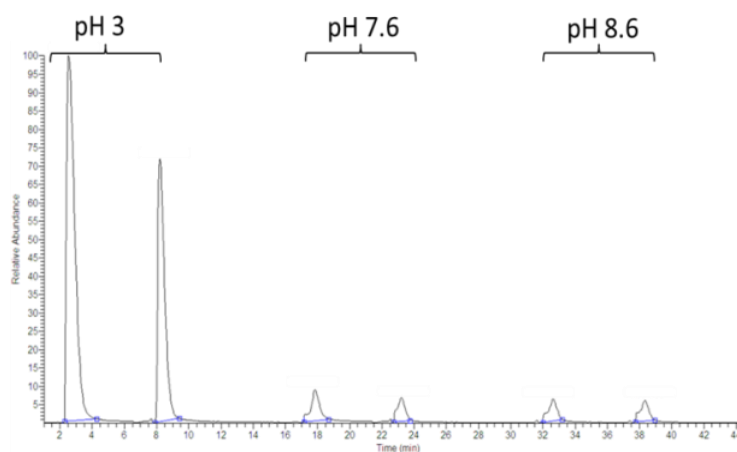


Figure S-5: Direct MS infusion TIC chromatogram of 1 nM NLLGLIEA[K-<sup>13</sup>C<sub>6</sub><sup>15</sup>N<sub>2</sub>] prepared at different pH values and injected at different time points

Figure S-5 shows the peaks obtained when the different peptide solutions were injected in duplicate (no MIP or analytical columns): The highest intensity was registered at pH 3.0, whilst the drop in signal intensity is significant at pH  $\geq 7.6$ .

## 4.2 Linearity of the method.

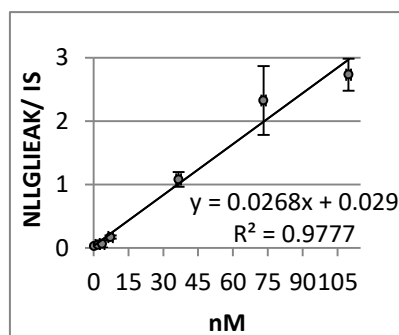


Figure S-6: Calibration curve obtained plotting the ratio of the area of the signature peptide NLLGLIEAK to the area of the internal standard (IS) for different ProGRP isoform 1 concentrations in serum.

## 5. Verification of NIP failure:

The extraction on a NIP cartridge (NIP A) of a serum samples spiked with 1 nM of ProGRP isoform 1 was performed in order to compare the performance with the extracted samples from the calibration curve. Addition of a solution of NLLGLIEA[K-<sup>13</sup>C<sub>6</sub><sup>15</sup>N<sub>2</sub>] 10 nM was performed before the injection in the chromatographic system in order allow a correct peak identification.

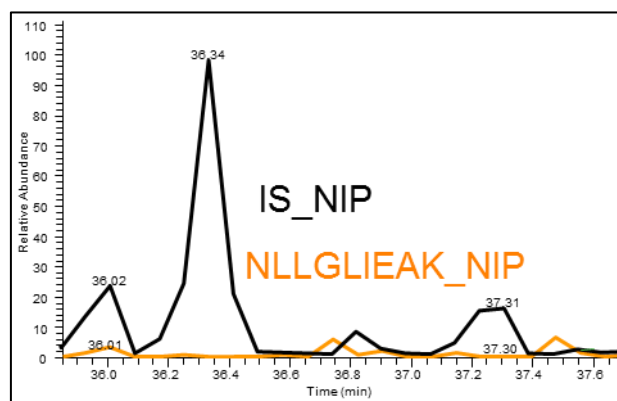


Figure S-7: Extraction on NIP A of a serum samples spiked with of ProGRP iso1 (1 nM) (orange line). Addition of a solution of NLLGLIEA[K-<sup>13</sup>C<sub>6</sub><sup>15</sup>N<sub>2</sub>] 10 nM (black line).

The presence of the internal standard only show the impossibility of the NIP in enriching the targeted peptide within the serum sample after the optimized sample preparation, while the MIP could enrich such concentration with similar intensities for both target peptide and internal standard.

## REFERENCES

- 1 Qader, A. A. *et al.* Peptide imprinted receptors for the determination of the small cell lung cancer associated biomarker progastrin releasing peptide. *Journal of Chromatography A* **1370**, 56-62, doi:10.1016/j.chroma.2014.10.023 (2014).
- 2 Rampey, A. M. *et al.* Characterization of the Imprint Effect and the Influence of Imprinting Conditions on Affinity, Capacity, and Heterogeneity in Molecularly Imprinted Polymers Using the Freundlich Isotherm-Affinity Distribution Analysis. *Analytical Chemistry* **76**, 1123-1133 (2004).
- 3 Manesiotes, P., Kashani, S. & McLoughlin, P. Molecularly imprinted polymers for the extraction of imiquimod from biological samples using a template analogue strategy. *Analytical Methods* **5**, 3122-3128, doi:10.1039/c3ay40239h (2013).